Top-Quark Search in the Dilepton Channel in 1.8-TeV Proton-Antiproton Collisions

Takeshi Chikamatsu

Top-Quark Search in the Dilepton Channel in

Top-Quark Search in the Dilepton Channel in 1.8-TeV Proton-Antiproton Collisions

Takeshi Chikamatsu

A dissertation submitted to the Doctral Program in Physics,
The University of Tsukuba in partial fulfillment of requirements
for the degree of Doctor of Philolosophy (in Physics)

February 1994

Abstract

A search for the top quark (t) in $p\bar{p}$ collisions at $\sqrt{s} = 1.8$ TeV is described. We consider the $t\bar{t}$ pairs, followed by semileptonoic decays via real W bosons: $t\bar{t} \rightarrow W^{+}b\ W^{-}\ \bar{b} \rightarrow l_1 l_2 X$, where l_1 and l_2 are electrons or muons. Analysis is based on data with an integrated luminosity of 21.4 pb^{-1} collected with the CDF detector at Fermilab in the 1992-93 collider run. We observe two $e\mu$ events with the total dilepton backgrounds of 0.56 ± 0.14 events. We also determine the lower bound on the top quark mass to be 120 GeV/c^2 at the 95% CL.

Acknowledgements

My great thanks go to my advisor, Professor Kunitaka Kondo, for giving me the opptunity to participate in this experiment, for his continuous encouragement during my five-year graduate student career.

I would like to express my great appreciation to Drs. G.P. Yeh and Milciades Contreras, who are the co-leaders of the group for this analysis. I learned a lot of physics, techniques, and philosophies which were accumulated in the history of CDF. Their excellent guidance and useful suggestions have been indispensable in the analysis.

I wish to thank Drs. Luc Demortier and Lingfeng Song who devoted much time with me to discuss and checking out this analysis.

I also thank Dr. Alvin Tollestrup, who gave me a lot of useful comments on the analysis and encouraged me personally.

This physics results presented here were obtained in the collaboration of the Collider Detector at Fermilab. I thank all of the physicists, engineers, and technicians of the collaboration who made this work possible. Many people helped with the analysis in one way or another. I want to thank C. Campagnari, A. Gordon, H. Keutelian, S. Kim, J. Konigsberg, S. Kopp, T. Liss, M. Mangano, A. Mukherjee, C. Newman-Holms, J. Romano, Y. Seiya, L. Stanco, J. Wang, Q. Wang, and C. Wendt.

I also want to express my thanks to Carol Picciolo, Kyoko Kunori, and Mutsumi Uenishi for their secretary work.

Finally my best appreciation goes to my family for their hospitality and support throughout my hard days of experiments, analysis, and the work on this thesis. Especially, I would like to dedicate this thesis to my mother, who is facing difficult times in her life.

This work was supported by the U.S. Department of Energy and National Science Foundation; the Italian Istituto Nazionale di Fisica Nucleare; the Ministry of Science, Culture, and Education of Japan; the Natural Sciences and Engineering Research Council of Canada; the A. P. Sloan Foundation; and the Alexander von Humboldt-Stiftung.

Contents

List of Tables

The CDF Collaboration

F. Abe,[13] M. Albrow,[7] D. Amidei,[16] C. Anway-Wiese,[4] G. Apollinari,[26] H. Areti,[7] P. Auchincloss,[25] F. Azfar,[21] P. Azzi,[20] N. Bacchetta,[18] W. Badgett,[16] M. W. Bailey,[24] J. Bao,[33] P. de Barbaro,[25] A. Barbaro-Galtieri,[14] V. E. Barnes,[24] B. A. Barnett,[12] P. Bartalini,[23] G. Bauer,[15] T. Baumann,[9] F. Bedeschi,[23] S. Behrends,[2] S. Belforte,[23] G. Bellettini,[23] J. Bellinger,[32] D. Benjamin,[31] J. Benlloch,[15] D. Benton,[21] A. Beretvas,[7] J. P. Berge,[7] A. Bhatti,[26] K. Biery,[11] M. Binkley,[7] F. Bird,[28] D. Bisello,[20] R. E. Blair,[1] C. Blocker,[28] A. Bodek,[25] V. Bolognesi,[23] D. Bortoletto,[24] C. Boswell,[12] T. Boulos,[14] G. Brandenburg,[9] E. Buckley-Geer,[7] H. S. Budd,[25] K. Burkett,[16] G. Busetto,[20] A. Byon-Wagner,[7] K. L. Byrum,[1] C. Campagnari,[7] M. Campbell,[16] A. Caner,[7] W. Carithers,[14] D. Carlsmith,[32] A. Castro,[20] Y. Cen,[21] F. Cervelli,[23] J. Chapman,[16] G. Chiarelli,[8] T. Chikamatsu,[30] S. Cihangir,[7] A. G. Clark,[23] M. Cobal,[23] M. Contreras,[5] J. Cooper,[7] M. Cordelli,[8] D. P. Coupal,[28] D. Crane,[7] J. D. Cunningham,[2] T. Daniels,[15] F. DeJongh,[7] S. Dell'Agnello,[23] M. Dell'Orso,[23] L. Demortier,[26] B. Denby,[7] M. Deninno,[3] P. F. Derwent,[16] T. Devlin,[27] M. Dickson,[25] S. Donati,[23] J. P. Done,[29] R. B. Drucker,[14] A. Dunn,[16] K. Einsweiler,[14] J. E. Elias,[7] R. Ely,[14] E. Engels, Jr.,[22] S. Eno,[5] D. Errede,[10] S. Errede,[10] A. Etchegoyen,[7a] Q. Fan,[25] B. Farhat,[15] I. Fiori,[3] B. Flaugher,[7] G. W. Foster,[7] M. Franklin,[9] M. Frautschi,[18] J. Freeman,[7] J. Friedman,[15] H. Frisch,[5] A. Fry,[28] T. A. Fuess,[28] Y. Fukui,[13] S. Funaki,[30] G. Gagliardi,[23] M. Gallinaro,[20] A. F. Garfinkel,[24] S. Geer,[7] D. W. Gerdes,[16] P. Giannetti,[23] N. Giokaris,[26] P. Giromini,[8] L. Gladney,[21] D. Glenzinski,[12] M. Gold,[18] J. Gonzalez,[21] A. Gordon,[9] A. T. Goshaw,[6] K. Goulianos,[26] H. Grassmann,[28] A. Grewal,[21] G. Grieco,[23] L. Groer,[27] C. Grosso-Pilcher,[5] C. Haber,[14] S. R. Hahn,[7] R. Hamilton,[9] R. Handler,[32] R. M. Hans,[33] K. Hara,[30] B. Harral,[21] R. M. Harris,[7] S. A. Hauger,[6] J. Hauser,[4] C. Hawk,[27] J. Heinrich,[21] D. Hennessy,[6] R. Hollebeek,[21] L. Holloway,[10] A. Hölscher,[11] S. Hong,[16] G. Houk,[21] P. Hu,[22] B. T. Huffman,[22] R. Hughes,[25] P. Hurst,[9] J. Huston,[17] J. Huth,[7] J. Hylen,[7] M. Incagli,[23] J. Incandela,[7] H. Iso,[30] H. Jensen,[7] C. P. Jessop,[9] U. Joshi,[7] R. W. Kadel,[14] E. Kajfasz,[7] T. Kamon,[29] T. Kaneko,[30] D. A. Kardelis,[10] H. Kasha,[33] Y. Kato,[19] L. Keeble,[29] R. D. Kennedy,[27] R. Kephart,[7] P. Kesten,[14] D. Kestenbaum,[9] R. M. Keup,[10] H. Keutelian,[7] F. Keyvan,[4] D. H. Kim,[7] H. S. Kim,[11] S. B. Kim,[16] S. H. Kim,[30] Y. K. Kim,[14] L. Kirsch,[2] P. Koehn,[25] K. Kondo,[30] J. Konigsberg,[9] S. Kopp,[5] K. Kordas,[11] W. Koska,[7] E. Kovacs,[7a] M. Krasberg,[16] S. E. Kuhlmann,[1] E. Kuns,[27] A. T. Laasanen,[24] S. Lammel,[4] J. I. Lamoureux,[32] T. LeCompte,[10] S. Leone,[23] J. D. Lewis,[7] P. Limon,[7] M. Lindgren,[4] T. M. Liss,[10] N. Lockyer,[21] O. Long,[21] M. Loreti,[20] E. H. Low,[21] D. Lucchesi,[23] C. B. Luchini,[10] P. Lukens,[7] P. Maas,[32] K. Maeshima,[7] A. Maghakian,[26] M. Mangano,[23] J. Mansour,[17] M. Mariotti,[23] J. P. Marriner,[7] A. Martin,[10] J. A. J. Matthews,[18] R. Mattingly,[2] P. McIntyre,[29] P. Melese,[26] A. Menzione,[23] E. Meschi,[23] G. Michail,[9] S. Mikamo,[13] M. Miller,[5] T. Mimashi,[30] S. Miscetti,[8] M. Mishina,[13] H. Mitsushio,[30] S. Miyashita,[30] Y. Morita,[13] S. Moulding,[26] J. Mueller,[27] A. Mukherjee,[7] T. Muller,[4] L. F. Nakae,[28] I. Nakano,[30] C. Nelson,[7]

D. Neuberger,[4] C. Newman-Holmes,[7] L. Nodulman,[1] S. Ogawa,[30] K. E. Ohl,[33] R. Oishi,[30] T. Okusawa,[19] C. Pagliarone,[23] R. Paoletti,[23] V. Papadimitriou,[7] S. Park,[7] J. Patrick,[7] G. Pauletta,[23] L. Pescara,[20] M. D. Peters,[14] T. J. Phillips,[6] G. Piacentino,[3] M. Pillai,[25] R. Plunkett,[7] L. Pondrom,[32] N. Produit,[14] J. Proudfoot,[1] F. Ptohos,[9] G. Punzi,[23] K. Ragan,[11] F. Rimondi,[3] L. Ristori,[23] M. Roach-Bellino,[31] W. J. Robertson,[6] T. Rodrigo,[7] J. Romano,[5] L. Rosenson,[15] W. K. Sakumoto,[25] D. Saltzberg,[5] A. Sansoni,[8] V. Scarpine,[29] A. Schindler,[14] P. Schlabach,[9] E. E. Schmidt,[7] M. P. Schmidt,[33] O. Schneider,[14] G. F. Sciacca,[23] A. Scribano,[23] S. Segler,[7] S. Seidel,[18] Y. Seiya,[30] G. Sganos,[11] M. Shapiro,[14] N. M. Shaw,[24] Q. Shen,[24] P. F. Shepard,[22] M. Shimojima,[30] M. Shochet,[5] J. Siegrist,[28] A. Sill,[7a] P. Sinervo,[11] P. Singh,[22] J. Skarha,[12] K. Sliwa,[31] D. A. Smith,[23] F. D. Snider,[12] L. Song,[7] T. Song,[16] J. Spalding,[7] P. Sphicas,[15] A. Spies,[12] L. Stanco,[20] J. Steele,[32] A. Stefanini,[23] K. Strahl,[11] J. Strait,[7] G. Sullivan,[5] K. Sumorok,[15] R. L. Swartz, Jr.,[10] T. Takahashi,[19] K. Takikawa,[30] F. Tartarelli,[23] Y. Teramoto,[19] S. Tether,[15] D. Theriot,[7] J. Thomas,[28] R. Thun,[16] M. Timko,[31] P. Tipton,[25] A. Titov,[26] S. Tkaczyk,[7] A. Tollestrup,[7] J. Tonnison,[24] J. F. de Troconiz,[9] J. Tseng,[12] M. Turcotte,[28] N. Turini,[3] N. Uemura,[30] F. Ukegawa,[21] G. Unal,[21] S. Vejcik, III,[16] R. Vidal,[7] M. Vondracek,[10] R. G. Wagner,[1] R. L. Wagner,[7] N. Wainer,[7] R. C. Walker,[25] J. Wang,[5] Q. F. Wang,[26] A. Warburton,[11] G. Watts,[25] T. Watts,[27] R. Webb,[29] C. Wendt,[32] H. Wenzel,[14] W. C. Wester, III,[14] T. Westhusing,[10] A. B. Wicklund,[1] E. Wicklund,[7] R. Wilkinson,[21] H. H. Williams,[21] P. Wilson,[5] B. L. Winer,[25] J. Wolinski,[29] D. Y. Wu,[16] X. Wu,[23] J. Wyss,[20] A. Yagil,[7] W. Yao,[14] K. Yasuoka,[30] Y. Ye,[11] G. P. Yeh,[7] M. Yin,[6] J. Yoh,[7] T. Yoshida,[19] D. Yovanovitch,[7] I. Yu,[33] J. C. Yun,[7] A. Zanetti,[23] F. Zetti,[23] S. Zhang,[15] W. Zhang,[21] and S. Zucchelli[3]

(CDF Collaboration)

[1] *Argonne National Laboratory, Argonne, Illinois 60439*

[2] *Brandeis University, Waltham, Massachusetts 02254*

[3] *Istituto Nazionale di Fisica Nucleare, University of Bologna, I-40126 Bologna, Italy*

[4] *University of California at Los Angeles, Los Angeles, California 90024*

[5] *University of Chicago, Chicago, Illinois 60637*

[6] *Duke University, Durham, North Carolina 27708*

[7] *Fermi National Accelerator Laboratory, Batavia, Illinois 60510*

[8] *Laboratori Nazionali di Frascati, Istituto Nazionale di Fisica Nucleare, I-00044 Frascati, Italy*

[9] *Harvard University, Cambridge, Massachusetts 02138*

[10] *University of Illinois, Urbana, Illinois 61801*

[11] *Institute of Particle Physics, McGill University, Montreal H3A 2T8, and University of Toronto, Toronto M5S 1A7, Canada*

[12] *The Johns Hopkins University, Baltimore, Maryland 21218*

[13] *National Laboratory for High Energy Physics (KEK), Tsukuba, Ibaraki 305, Japan*

[14] *Lawrence Berkeley Laboratory, Berkeley, California 94720*

[15] *Massachusetts Institute of Technology, Cambridge, Massachusetts 02139*

[16] University of Michigan, Ann Arbor, Michigan 48109
[17] Michigan State University, East Lansing, Michigan 48824
[18] University of New Mexico, Albuquerque, New Mexico 87131
[19] Osaka City University, Osaka 588, Japan
[20] Universita di Padova, Instituto Nazionale di Fisica Nucleare, Sezione di Padova, I-35131 Padova, Italy
[21] University of Pennsylvania, Philadelphia, Pennsylvania 19104
[22] University of Pittsburgh, Pittsburgh, Pennsylvania 15260
[23] Istituto Nazionale di Fisica Nucleare, University and Scuola Normale Superiore of Pisa, I-56100 Pisa, Italy
[24] Purdue University, West Lafayette, Indiana 47907
[25] University of Rochester, Rochester, New York 14627
[26] Rockefeller University, New York, New York 10021
[27] Rutgers University, Piscataway, New Jersey 08854
[28] Superconducting Super Collider Laboratory, Dallas, Texas 75237
[29] Texas A&M University, College Station, Texas 77843
[30] University of Tsukuba, Tsukuba, Ibaraki 305, Japan
[31] Tufts University, Medford, Massachusetts 02155
[32] University of Wisconsin, Madison, Wisconsin 53706
[33] Yale University, New Haven, Connecticut 06511

Chapter 1

Introduction

Particle physics deals with the study of the fundamental constituents of matter and the nature of the interactions between them. As of today, the Standard Model of particle physics [1] with three generations of quarks and leptons has provided a successful description of known quarks and leptons. Within this model, the quarks occupy 3 left-handed doublets and six right-handed singlets as shown below.

$$\begin{pmatrix} \nu_e \\ e^- \end{pmatrix}_L \begin{pmatrix} \nu_\mu \\ \mu^- \end{pmatrix}_L \begin{pmatrix} \nu_\tau \\ \tau^- \end{pmatrix}_L \quad e_R^- \quad \mu_R^- \quad \tau_R^- \quad \nu_{eR} \quad \nu_{\mu R} \quad \nu_{\tau R}$$

$$\begin{pmatrix} u \\ d' \end{pmatrix}_L \begin{pmatrix} c \\ s' \end{pmatrix}_L \begin{pmatrix} t \\ b' \end{pmatrix}_L \quad d'_R \quad s'_R \quad b'_R \quad u_R \quad c_R \quad t_R$$

The Standard Model predicts the existence of the top quark, but direct searches in the collider experiments have so far failed to yield evidence for the top quark.

We can argue several questions about the top quark:

- Does the top quark really exist?
- How strong is the current evidence for the top quark?
- How do we detect the top quark?

It is reported that the top quark must be more massive than 91 GeV/c^2, at least 18 times heavier than any other quark mass[1] . The most interesting question is why the top quark is so heavy. But we have no idea why it is heavier.

This thesis describes an attempt to search for the top quark, performed on data taken by CDF collaboration during the 1992-93 collider run at Fermilab. The search is made by detecting two high Pt leptons in the event. Th dilepton decay channel is the most promising one to detect top, since the backgrounds are relatively small. The emphasis is placed on how to separate the signal from backgrounds.

The remainder of Chapter 1 is devoted to an overview of theoretical prediction and current status of the top quark searches and to describing the production and decay mechanisms which the Standard Model top quark is anticipated to have. Chapter 2 briefly reviews the Tevatron and the CDF detector. In Chapter 3, we discuss the Monte Carlo data sets to evaluate the accetance for the top quark and to study background processes. Event selection tools are described in Chapter 4. Based on these tools, dilepton event selection criteria to enhance the top signal is studied in Chapter 5. This section also describes the results of the search in our data sample. Chapter 6 is devoted to the determination of the detection efficiency for the top quark. Systematic uncertainties are also estimated. In Chapter 7 we estimate the background contribution to our selection criteria. In Chapter 8 we summarize the top quark search both in the high mass region and in the low mass region. We also derive a lower limit on the top quark mass. Chapter 9 concludes this analysis.

1.1 Theoretical indication for the top quark

The theoretical motivation the top quark must exist is that the complete families are required for the cancellation of anomalies in the current which couple to gauge fields. If the gauge current is anomalous, the gauge theory is not renormalizable. Hence the

[1] Recently, D0 collaboration extended the lower bound on the top mass to 131 GeV/c^2 [2]

partner of the b, τ and ν_τ must exist to complete the third family.

1.2 Indirect evidences for the existence of top quark

The top quark should exist in the framework of the Standard Model. Evidence for its existence is quite strong. Experimentally, there are four pieces of data which indicate the existence of an $SU(2)$ partner of the bottom quark, *i.e.*, top quark.
They all come from measurement of the properties of b measons.

(1) **Forward-backward asymmetry in $e^+e^- \to b\bar{b}$**
In the Standard Model, the bottom quark is produced in e^+e^- annihilation with aforward-backward asymmetry which is given by

$$A^b_{FB} = \frac{\sigma(\theta < \pi/2) - \sigma(\theta > \pi/2)}{\sigma(\theta < \pi/2) + \sigma(\theta > \pi/2)} \simeq \frac{-3T^3_e T^3_b s/M^2_Z}{8\sin^2\theta_W \cos^2\theta_W \cdot Q_b(s/M^2_Z - 1)}$$

With $T^3_e = T^3_b = -1/2$, $Q_b = -1/3$ and the measured M_Z and $\sin^2\theta$, one can expect an asymmetry of about -0.25 at a center of mass energy of $\sqrt{s} \simeq 35$ GeV. The JADE collaboration has observed an asymmetry of -25.0 $\pm$ 6.5 % at the PETRA e^+e^- collider [8]. In the absence of a top quark, the bottom quark would be a singlet of weak isospin($T^3_b = 0$) resulting in zero asymmetry.

(2) **Upper limit on the flavor changing decay $b \to \mu^+\mu^- X$**
At the time when only u, d, s quarks were known, Glashow, Iliopoulas and Maiani pointed out that the existence of a charm quark (in a same doublet with the s quark) would explain the experimentally observed extreme supression of flavor changing neutral current (FCNC) $s \to d$ transitions (GIM mechanism). It is natural to search for flavor-changing neutral currents in the weak decays of the b quark.

Some nonstandard models predict FCNC in the b decay. Kane and Peskin[13] showed that thee ratio $\Gamma(b \to l^+l^- + X)/\Gamma(b \to l\nu X$ must exceed 0.12, if there were no top quark and the bottom quark were a member of a left-handed-singlet. This corresponds to a branching ratio for $b \to l^+l^- X$ of greater than 1.3 $\times 10^{-2}$. No positive evidence for FCNC in the b decay has been observed. Upper limits on the branching ratio for $b \to l^+l^- + X$) have been set by several groups and the most stringent limit is 1.2 $\times 10^{-3}$ from a CLEO search[14], a factor of 10 below the Kane-Peskin limit.

(3) **Observed value of the $B^0\bar{B}^0$ mixing**

It was a surprising results that the observation of nonvanishing amount of $B_d^0\bar{B}_d^0$ mixing was made by the ARGUS collaboration [15]. While the UA1 collaboration [16] had already observed a positive signal of $B^0\bar{B}^0$ mixing the previous year, it could be ascribed to B_s mesons; the ARGUS signal was the first to point to mixing of B_d mesons.

The important contribution to mixing is via the box diagrams of Figure 1.1. The mixing is usually described by the mixing parameter r which is defined as the ratio of the probabilies that an initial B^0 decay as a $\bar{\text{B}}^0$ or as a B^0, r=prob($B^0 \to \bar{B}^0$)/prob($B^0 \to B^0$), where r=0 means no mixing.

The mixing parameter r_d is given by [17]

$$r_d = \frac{(\Delta M/\Gamma)^2}{2 + (\Delta M/\Gamma)^2} = \frac{x^2}{2 + x^2},$$

where ΔM is the mass difference between weak eigen states of B^0 and $\bar{B}^0$ and Γ is their lifetime. ΔM calculated from the matrix element for the B_d transition assuming the box diagram with a virtual top quark exchange is given by [17]

$$\Delta M = 1/6\pi^2\ G_F^2 B_b f_b m_{top}^2 m_b \mid V_{tb} V_{td^*} \mid^2 .$$

Note that ΔM is proportional to square of the top quark mass, m_{top}. The observed large $B^0\bar{B}^0$ mixing actually indicates that the top quark is heavy. ARGUS reported [15] that $r_d = 0.22 \pm 0.08$. This value suggests that the top quark mass is larger than about 50 GeV/c^2.

(4)**Meaurement of $Z \to b\bar{b}$ width**

The last evidence for the existence of the top quark comes from the precision measurrement of $Z \to b\bar{b}$ decay width at LEP by ALEPH and L3 [18] which give

$$\Gamma(Z \to b\bar{b}) = 350 \pm 50 MeV.$$

One can calculate the width including the small QCD corretion to be

$$\Gamma(Z \to b\bar{b}) = \frac{G_F M_Z^3}{\pi\sqrt{2}}(1 + \frac{\alpha_s}{\pi})[(T_b^3 - Q_b \sin^2\theta_W)^2 + (Q_b \sin^2\theta_W)^2],$$

and gets

$$\begin{aligned}\Gamma(Z \to b\bar{b}) &= 381 MeV \text{for } T_b^3 = -1/2; \\ &= 24 MeV \text{for } T_b^3 = 0\end{aligned}$$

corresponding to whether the b quark is accompanied by a SU(2) partner or not. The measured value clearly suggests the presence of a SU(2) partner of b -i.e. the top quark.

1.3 Indirect constraints on the top mass

A number of indirect constraints on the top mass is available.
The ratio of cross sections for W and Z production with subsequent decay into $e\nu$ or ee is related to the W and Z total width through the formula,

$$R = \frac{\sigma_W Br(W \to e\nu)}{\sigma_Z Br(Z \to ee)} = \frac{\sigma_W}{\sigma_Z}\frac{\Gamma(W \to e\nu)}{\Gamma(Z \to ee)}\frac{\Gamma_Z}{\Gamma_W}$$

The measurement of the ratio R allows us to set a lower limit on the top mass, independ of its decay modes. The width of the W (Γ_W), which depends on the top quark mass, can be extracted from the ratio. The first two terms are predicted by QCD, and a large fraction of the uncertainties cancel in taking the ratio of the cross section. The width of the Z is precisely measured by LEP. We find that M_{top} >45(49) GeV/c^2 at 95(90) % confidence level [19].

Measurements of low-energy neutral current parameters and vector boson masses are sensitive to the top mass via one-loop radiative corrections in the Standard Model. The relation between the electroweak parameters can be expressed [20] as

$$sin^2\theta_W = \frac{A^2}{M_W^2(1-\Delta r)},$$

where $A = (\pi\alpha/\sqrt{2}G_\mu)^{1/2}$, $\sin^2\theta_W = 1 - M_W^2/M_Z^2$ and Δr is a radiative ccorrection involving, among other parameters, the unknown top mass and the Higgs mass. The upper bound on the top mass is estimated to be 150-250 GeV/c^2 [9].

We can see that there are a number of parameters within the Standard Model which have some dependence on the top mass. Thus by combining all of the measurements with the theoretical analysis of their dependences on the top mass, it is possible to extract predictions for the allowable range and most likely value for this parameter. Several groups have reported the mass range and global fits to recent precision electroweak measurements yield a favored mass of $M_{top} = 164^{+17+18}_{-16-20}$ GeV/c^2 [11]

1.4 Previous Searches

Direct searches in the collider experiments have so far failed to yield evidence for the top quark. We describe these searches at e^+e^- and $p\bar{p}$ colliders.

1.4.1 Searches at e^+e^- colliders

In e^+e^- colliders, charged particles of mass up to the energy of the beam can be produced in pairs. Thus we would expect to observe charged quarks with mass up to the highest energy available, until recently at LEP.

An electron and a positron annhilate into quark and antiquark pairs. The hadron cross section, relative to the μ-pair cross section given by

$$R = \sigma(e^+e^- \to \text{hadrons})/\sigma(e^+e^- \to \mu\mu) = 3\sum e_i^2,$$

where e_i are the charges of quarks and the factor of three comes from three colored quarks. This R value means just the sum of the squares of the quark charges times the number of colors in the final state. For the center of mass energy >10 GeV, all the known quarks are included in the sum,

$$\begin{aligned} R &= 3\,(e_u^2 + e_d^2 + e_s^2 + e_c^2 + e_b^2) \\ &= 3\,(4/9 + 4/9 + 1/9 + 1/9 + 1/9) = 3.66 \end{aligned}$$

A plot of measured R value is shown in Figure1.9. It is clear from this figure that the ratio is essentially constant in between thresholds for production of new heavy quarks.

An increase in the hadronic cross section at the threshold for production of a new generation of quarks: for top quarks, $e_t = 2/3$ one should observe ΔR=4/3;

The process $Z \to t\bar{t}$ is an excellent way to look for the light top quark, and the large number of Z's allows the LEP experiment to exclude a top quark mass less than 46 GeV/c^2 at 95% confidence level with little dependence on the top decays.

1.4.2 Searches at $p\bar{p}$ colliders

The proton-antiproton collider experiments at CERN and Tevatron give us a unique oppotunity and have played a major role to search for the top quark because of its large center of mass energy.

Searches at $Sp\bar{p}S$

The first hadron collider search was made by UA1 at S$p\bar{p}S$ [21]. UA1 explored a top quark mass range above 40 GeV/c^2, where $p\bar{p} \to W \to t\bar{b}$ is more important than the strong production channel at $\sqrt{s} = 630$ GeV. Top searches by UA1 have been performed using the μ + jets and $\mu\mu$ channels.

The μ + jets selection applied on the 1988-1989 data required an isolated muon with transverse momentum P_T^{μ} >12 GeV/c^2 accompanied by at least two jets with transverse energies E_T^{jet1} >13 GeV and E_T^{jet2} >7 GeV. A transverse mass [2] cut of $M_T^{\mu\nu}$ <60 GeV/c^2 is used to reject backgrounds from $W \to \mu\nu$ produced in association with jets. After selection, the main backgrounds for top are muons from the semileptonic decays of heavy flavors in $b\bar{b}$ and $c\bar{c}$ events, and from the decay in flight of kaons and pions. Four variables are used to distinguish the top signal from from backgrounds. (i) An isolation variable, $I \equiv \sqrt{(\sum E_T/3)^2 + (\sum P_T/2)^2}$, where the sum runs over all calorimeter cells and tracks in a cone of radius R=0.7 [3] surrounding the muon. (ii) The muon transverse momentum, P_T^μ. (iii) The missing transverse energy, $\not{E}_T$. (iv) The azimuthal separation between the muon and the leading jet, $\Delta\phi(\mu - jet1)$.

Muons from $b\bar{b}$ and $c\bar{c}$ are produced inside or near jets and are not isolated while muons from very heavy quark decay are usually well separated from the jets and therefore isolated. No excess of isolated muons is observed in the UA1 data.

For improved sensitivity, all four variables are combined in a 'likelihood' variable :

$$L = \prod_{i=1}^{4} P_{top}(X_i)/P_{bot}(X_i), \tag{1.1}$$

where $P_{top}(X_i)$ and $P_{bot}(X_i)$ are the probability density functions of the variable X_i for top signal events and for $b\bar{b}$ and $c\bar{c}$ background events, respectively. After a final cut of $\ln(L) > 4$, only 2 events remain in the data while 2.8±0.8 events are expected from $b\bar{b}$, $c\bar{c}$ and decays in flight. A total of 6.2 top events (4.1 from $t\bar{b}$ and 2.1 from $t\bar{t}$) are expected for $M_{top} = 50$ GeV/c^2. From the μ + jets analysis , a 95 % CL lower limit of M_{top} >52 GeV/c^2 is obtained.

The UA1 search in the $\mu\mu$ channel required one isolated muon with P_T^μ >8 GeV/c, a second non-isolated muon with P_T^μ >3 GeV/c and at least one jet with E_T^{jet} >10 GeV to search for $W \to t\bar{b}$. Again, no top signal was found and the data were consistent with

[2]The transverse mass variable is defined as $M_T^{\mu\nu} = \sqrt{2P_T^\mu \not{E}_T(1 - \cos\Delta\phi_{\mu\nu})}$, with $\not{E}_T$ the missing transverse energy in the event, and $\Delta\phi_{\mu\nu}$ the azimuthal separation between the muon and missing transverse energy vectors.

[3]R is a distance measured in pseudorapidity-azimuth space (radians). R $\equiv \sqrt{(\Delta\eta)^2 + (\Delta\phi)^2}$. $\eta = -\ln(\tan(\theta/2))$. θ is the angle to the proton direction.

expected backgrounds, predominantly from b-quark and c-quark production and decays in flight. The $\mu\mu$ channel alone excludes $M_{top} > 46$ GeV/c^2 at the 95 % CL.

UA1 has combined the 1988-1989 searches in the μ + jets and $\mu\mu$ channels with previous searches from 1983-1985 in the e + jets, μ + jets, and $\mu\mu$ channels. The combined UA1 limit is $M_{top} > 60$ GeV/c^2 at the 90% CL.

The UA2 collaboration has looked for semileptonic decays of the top quark in the e + jets channel [4]. The UA2 e + jets selection required an electron candidate with $E_T^e > 12$ GeV, missing transverse energy $\not{E}_T < 15$ GeV, and at least one jet with $E_T^{jet} > 10$ GeV. To reduce misidentification backgrounds, events with the electron back-to-back to the leading jet were rejected. The major background after these cuts is from high P_T W events produced in association with jets. The transverse mass of the electron-neutrino system

$$M_T^{e\nu} = \sqrt{2E_T^e \not{E}_T (1 - \cos\Delta\phi_{e\nu})}\ , \tag{1.2}$$

is used to distinguish a possible top signal from the W + jets background. The transverse mass distribution for the UA2 data was found to be consistent with expectations from W boson decay alone. The top quark would manifest itself as an excess of events in the low transverse mass region. The absence of such an excess in the UA2 data implies that $M_{top} > 69$ GeV/c^2 at the 95% CL.

Previous searches at CDF

The first CDF top results came from searches in the e + jets[5] channel and in the $e\mu$[6] channel. The search in e + jets, similar to the UA2 analysis already described, employed the transverse mass variable to discriminate between top events and the dominant W + jets background. A limit of $M_{top} > 77$ GeV/c^2 was obtained. This method is no longer useful when M_{top} approaches M_W, in which case the transverse mass distributions are very similar.

The $e\mu$ signature requires the presence of an electron and a muon with opposite electric charges, each with transverse momentum above the threshold $P_T^{min} = 15$ GeV/c^2.

There is one event in the top quark signal region. Given one candidate event, a 95%-C.L. the lower bound on the top mass of 72 GeV/c^2 was obtained.

A straightforward extension of the $e\mu$ analysis is to also search for top in ee and $\mu\mu$ events[7]. Dielectron and dimuon events were selected by requiring $P_T > 15$ GeV/c^2 for each lepton. A simple mass cut around the Z peak removes most of the background from Z decays. After the mass cut, the signal to background ratio is improved by requiring missing transverse energy $\not{E}_T > 20$ GeV. Also, events with back-to-back or collinear dileptons are eliminated by requiring the azimuthal opening between the leptons to be in the region $\Delta_{l^+l^-} < 160°$. After all cuts, there are no ee or $\mu\mu$ events remaining in the data. With only one $e\mu$ event observed, the limit from the $e\mu$, ee, and $\mu\mu$ channels together is $M_{top} > 85$ GeV/c^2.

Finally, CDF has looked for additional low P_T muons in the e + jets and μ + jets samples. The low P_T muon in the event is employed as a possible tag of the bottom quark in the chain $t \rightarrow b \rightarrow \mu$. No candidates were found. The result of the low P_T muon search combined with the previous dilepton searches extends the CDF top quark mass limit to $M_{top} > 91$ GeV at the 95%-C.L.

1.5 Heavy quark production and decay

1.5.1 Production

The parton model describes succesfully the hadronic cross section involving a large momentum transfer. We assume that any physically observed hadrons are made up of constituent particles, "partons", which we identify with quarks and gluons. At high energy, the masses of partons are neglegible compared to the scale of Q of the hard scattering. A schematic view of a $p\bar{p}$ collision is shown in Figure xx. In this picture the scattering occurs between partons that are treated as quasi free particles inside hadrons.

The parton model cross section is given by the formula

$$\sigma = \sum_{i,j} \int dx_1 dx_2 \hat{\sigma_{ij}}(\hat{s}) f_i(x_1, Q^2)\, f_j(x_2, Q^2)$$

The momentum distributions of the initial partons are represented by a set of parton distribution functions f_i, which gives the probability for finding a parton of type i inside the hadron carrying a fraction x of the hadron's total momentum. The subscript i and j indicate the type of the incoming parton. The sum extends over all parton cross sections $\hat{\sigma_{ij}}$ contributing the process. The parton cross section is evaluated at the parton center of mass energy $\sqrt{\hat{s}}$ through the relation $\hat{s}=x_1 x_2 s$. They are calculable with perturbative QCD and are expressed as an expansion in the coupling constant α_s.

In the lowest oder (α_s^2), the processes are quark-antiquark annihilation and gluon-gluon fusion:

$$\begin{aligned} g + g &\rightarrow Q + \bar{Q} \\ q + \bar{q} &\rightarrow Q + \bar{Q} \end{aligned} \tag{1.3}$$

The Feynman diagrams for these processes are shown in Figure 1.3. Two important kinematic consequences of the leading order processes are (1) the quark and antiquark are produced back-to-back in the parton-parton center of mass frame and remain beck-to-back in the plane transverse to the colliding beam and (2) the heavy quarks are emitted with an average transverse momentum of about the half of the quark mass.

The issue of higher order QCD corrections is important in heavy quark production. The splitting of a final state gluon from $gg \rightarrow gg$, into a pair of heavy quark (g $\rightarrow Q\bar{Q}$) occurs with only a small fraction of oder $\sim \alpha_S(m^2)$ of the time. However, given the large cross section of $gg \rightarrow gg$, it can be a competitive quark production proceess. This process ($gg \rightarrow gQ\bar{Q}$) and other $2 \rightarrow 3$ processes of order α_S^3, as well as the α_S^3 part of the $2 \rightarrow 2$ processes of 1.3 have been calculated by Nason, Dawson and Ellis [25]. The following parton subprocesses are included in the calculation up to order α_S^3:

$$
\begin{aligned}
&q+\bar{q}\rightarrow Q+\bar{Q} && \alpha_S^2, \alpha_S^3 \\
&g+g\rightarrow Q+\bar{Q} && \alpha_S^2, \alpha_S^3 \\
&q+\bar{q}\rightarrow Q+\bar{Q}+g && \alpha_S^3 \\
&g+g\rightarrow Q+\bar{Q}+g && \alpha_S^3 \\
&g+q\rightarrow Q+\bar{Q}+q && \alpha_S^3 \\
&g+\bar{q}\rightarrow Q+\bar{Q}+\bar{q} && \alpha_S^3
\end{aligned} \tag{1.4}
$$

The theoretical cross sections depend on thee different input quantities: parton distribution functions, choice of renormalization and factorization scale μ, the choicee of running coupling α_S (or equivalentlly, the choicee of the QCD parameter Λ, since α_S is a function of μ/Λ), and the mass of the heavy quark.

The corections affect the $t\bar{t}$ production cross section. Due to the large uncertainties in the gluon structure function at small x together with contributions to the total cross section from gluon-gluon diagrams, total cross section is quite uncertain.

Since the top quark is now believed to be heavier than the W, a dominant production process is the $t\bar{t}$ pair creation by gluon-gluon fusion and $q\bar{q}$ annihilation. Above a top mass of about 100 GeV/c^2, $q\bar{q}$ annihilation is expected to be the dominant production source.

In order for the experiment to compute the number of $t\bar{t}$ events expected, or to set the lower bound on the top mass, it is important to have a good central values for the production cross sections as well as estimation of systematic uncertainties. Cross sections have been calculated within QCD at the full NLO [25]. Recent work has extended those results with the inclusion of clases of higher-order diagrams dominated by the emission of multiple soft gluons[26].

1.5.2 Fragmentation of heavy quark

After a heavy quark is produced, it 'fragments' or 'hadronizes' into a hadron containing its flavor, and some softer, light-flavored hadrons.

The fragmentation function D_Q^H of a heavy quark Q into a Q-flavored hadron H describes the probability that the hadron carries away a fraction of the quark's momentum between $z = P_H/P_Q$ and $z + dz$. A softer fragmentation (i.e. the hadron carries away less of the quark's momentum) will result in more accompanying hadrons with higher energies. Heavy quark fragmentation is modeled with the Peterson parametrization [33]:

$$D_Q^H = \frac{N}{z[1-(1/z)-\epsilon_Q/(1-z)]^2} \tag{1.5}$$

where N is a normalization constant and the Peterson parameter ϵ is proportional to $1/M_Q^2$. The Peterson parametrization adequately describes existing c and b quark fragmentation data, as is seen in figure 1.6.

In the spectator approximation, the heavy quark contained in the hadron is assumed to decay independently of the other constituents, since the energy released by the quark is much bigger than the typical quark binding energies.

1.5.3 Decay of heavy quark

The experimental lower limit of 91 GeV/c^2 on the top mass is valid so that the top quark decays into a bottom quark and a charged intermediate vector boson ($t \to Wb$) [4] in the minimal Standard Model. In the limit in which $M_{top} > m_W$ the width is given by

$$\Gamma(t \to bW) = \frac{G_F M_{top}^3}{8\pi\sqrt{2}} \mid V_{tb} \mid^2 \approx 170 \mid V_{tb} \mid^2 (\frac{m_T}{m_W})^3$$

MeV

[4] Decays into a strange quark or a down quark is possible: t $\to$Ws or Wd. But according to the Kobayashi-Maskawa theory, the top decay rate into these two quarks are too small to detect, because KM matrix elements V_{ts} ($\Gamma_s \sim 0.0025$) and V_{td} ($\Gamma_d \sim 10^{-4}$) are very small compared to V_{tb}, which is close to 1.

When the top quark is so heavy that the width becomes bigger than a typical hadronic scale. The top quark decays before its hadronization so that the meson are never formed.

The two W bosons subsequently decay either to a lepton and a neutrino or a quark and an antiquark while the b quarks hadronize to a jet. The branching fractions for the different decay modes are listed in Table 1.1. The $t\bar{t}$ decays can be characterized by the decay mode of the final state W^+W^- pair. The branching ratio is given by counting over the decay modes $e\nu, \mu\nu$ and $\tau\nu$ and three colors of $u\bar{d}$ and $c\bar{s}$. with roughly equal probability for a total of nine possible final states. The brancing ratio for each mode is thus 1/9.

Most often both W bosons will decay to a quark-antiquark pair, leading to a fully hadronic final state. While this happens for about 44% ($6/9\times6/9$) of $t\bar{t}$ decays, there is a huge background from all other QCD multijet production processes, making separation of the $t\bar{t}$ signal from the background extremely difficult. If one requires that at least one of the W^+W^- pair decay leptonically, the backgrounds are substantially reduced. Because of the difficulties associated with identifying τ leptons, the backgrounds are reduced further if the lepton is restricted to be either an electron or a muon. When just one of the W bosons decays to an electron or muon, the final state includes a high transverse momentum charged lepton, a transverse momentum imbalance from the undetected neutrino, referred to as *missing* E_T or $\not{E}_T$, and four or more jets from the hadronized quarks. This 'lepton + jets' mode occurs about 30% ($2/9\times$ $6/9\times2$) of the time and the background comes predominantly from higher-order production of W bosons, where the W is recoiling against significant jet activity. the rate is about 2 to 10 times larger than the $t\bar{t}$ rate, depending on the top mass and the jet selection requirements used.

Dilepton events with leptons coming directly from the decay of the W would have a probability of $1/9 \times 1/9$. Thus $ee, \mu\mu$, and $\tau\tau$ all occur with the same rate. For an $e\mu$ event, since there are two choices for which the W decays to e or μ, a branching fraction is 2/81. Hence, we would expect the branching ratio of dilepton events (ee, $\mu\mu$ or $e\mu$) is

Decay mode	Branching ratio
$t\bar{t} \longrightarrow q\bar{q}'bq\bar{q}'\bar{b}$	36/81
$t\bar{t} \longrightarrow q\bar{q}'be\nu\bar{b}$	12/81
$t\bar{t} \longrightarrow q\bar{q}'b\mu\nu\bar{b}$	12/81
$t\bar{t} \longrightarrow q\bar{q}'b\tau\nu\bar{b}$	12/81
$t\bar{t} \longrightarrow e\nu b\mu\nu\bar{b}$	2/81
$t\bar{t} \longrightarrow e\nu b\tau\nu\bar{b}$	2/81
$t\bar{t} \longrightarrow \mu\nu b\tau\nu\bar{b}$	2/81
$t\bar{t} \longrightarrow e\nu be\nu\bar{b}$	1/81
$t\bar{t} \longrightarrow \mu\nu b\mu\nu\bar{b}$	1/81
$t\bar{t} \longrightarrow \tau\nu b\tau\nu\bar{b}$	1/81

Table 1.1: Decay modes for a $t\bar{t}$ pair and their branching ratios (to lowest order) assuming charged-current decays. The symbol q stands for a light quark: u,d,c,s.

about 5%.

1.5.4 Signature

One expect event configurations consisting of two leptons, missing transverse energy and as many as two additional two jets. The dilepton signal originates from WW, Wb, $b\bar{b}$, Wτ and $\tau\tau$. Here b denotes both b and c quarks, and τ denotes tau-daughters of a W decay. Most of the top acceptance, about 80 % for the top mass in the range of 90-160 GeV/c^2, comes from the WW case. Contributions from other cases, with leptons coming from the decay of b or τ-decays are also included in the acceptance.

Background contribution to the seelected candidates is as follows:

- $b\bar{b}(c\bar{c})$ production followed by semi-leptonic decay of both b(c) quarks;
- $Z \rightarrow \tau\tau$, followed by the decay of τ's into e or μ;
- Drell-Yan production of lepton pairs;
- diboson production; WW and WZ
- lepton misidentification in generic multi-jet QCD events aand in events containing W+jets, conversions and decays in flight.

1.6 Collider Run

The Fermilab Tevatron collider resumed operation on May 12, 1992, when it started delivering $\bar{p}p$ collisions to the CDF detector. Comissioning the detector with beam lasted from May to August in 1992 and we showed that the detector was well on the way to achieving good quality data. With the start of the physics run in August 1992, the attention was turned to obtain the physics results, especially to search for the top quark. The 1992-93 collider run was successfully completed in July 1. During the run, the Fermilab Tevatron achieved a peak luminosity of 9.22×10^{30} (cm · sec) which is nearly a factor of two larger than was planned for this run. For one year operation the Tevatron delivered an integrated luminosity of 25 pb^{-1}, with CDF recording 21.4 pb^{-1}on tape, more than 5 of the data sample from the last run. This was achieved with an average initial luminosity of around xx. The detector operated with almost 80% efficiency during the time.

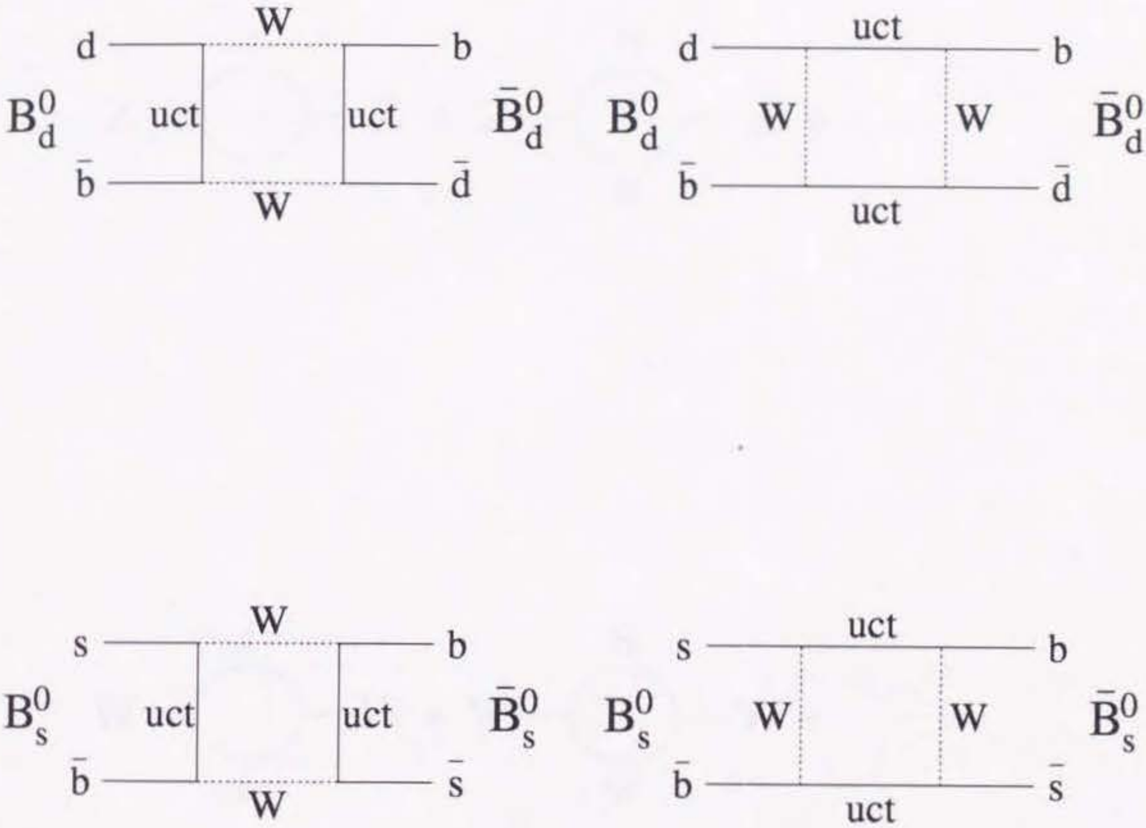

Figure 1.1: Box diagrams for a) $B_d^0\bar{B}_d^0$ and b) $B_d^0\bar{B}_d^0$ mixing.

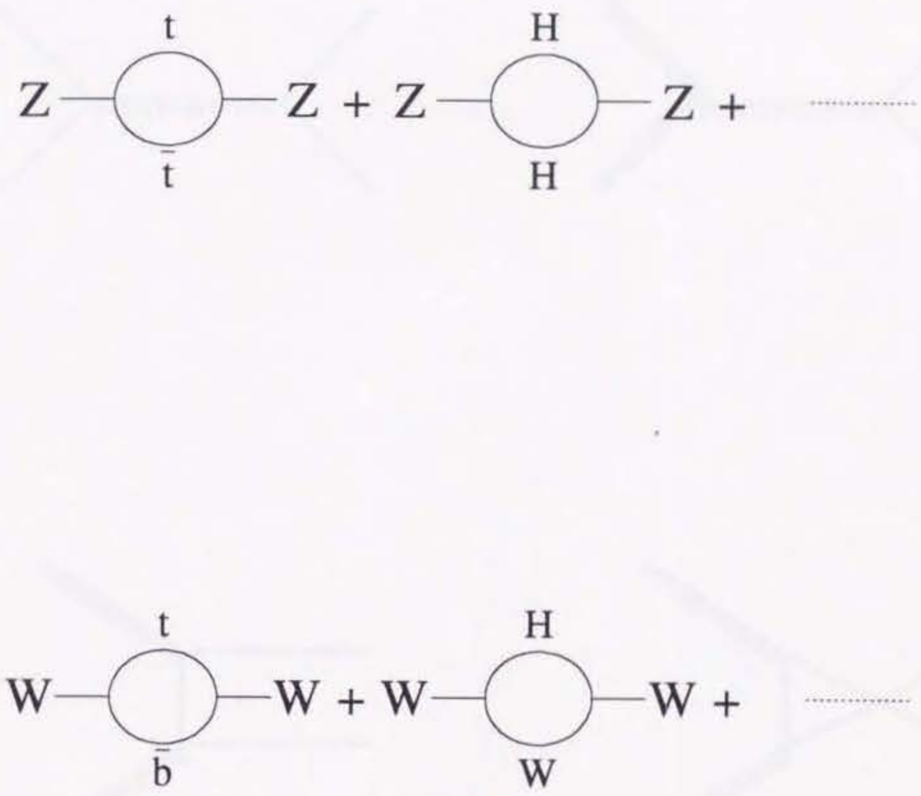

Figure 1.2: Diagrams for one-loop radiative corrections.

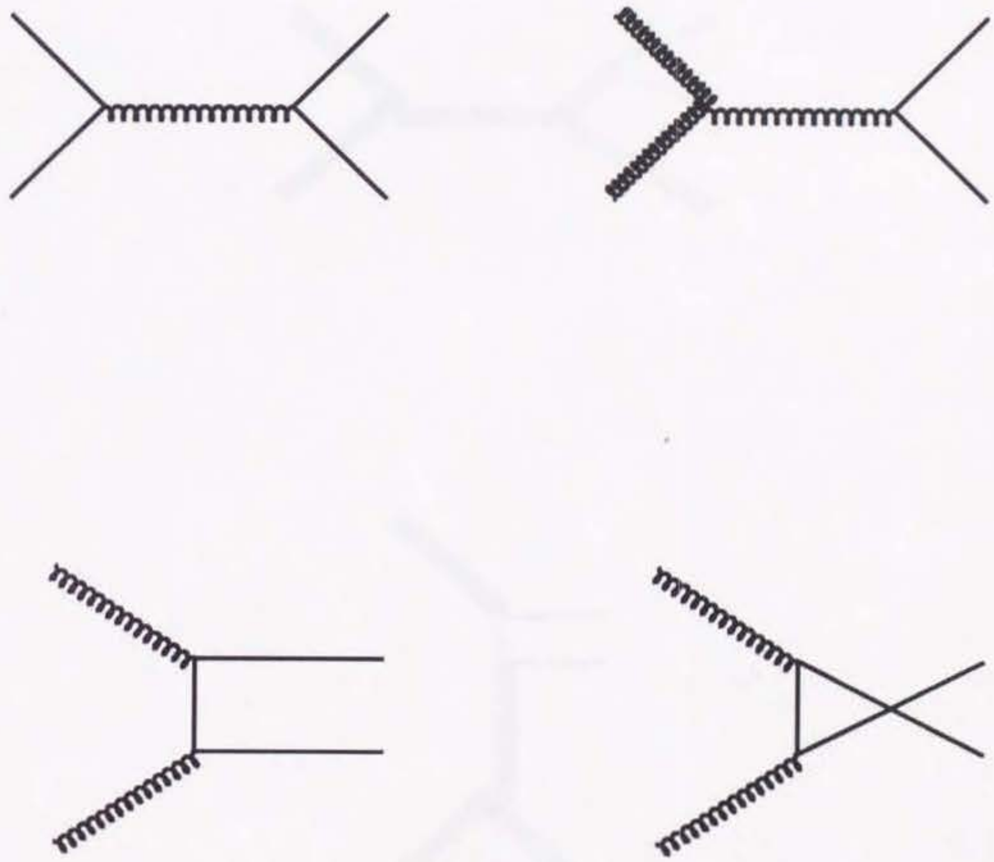

Figure 1.3: Lowest order Feynman diagrams for heavy quark production.

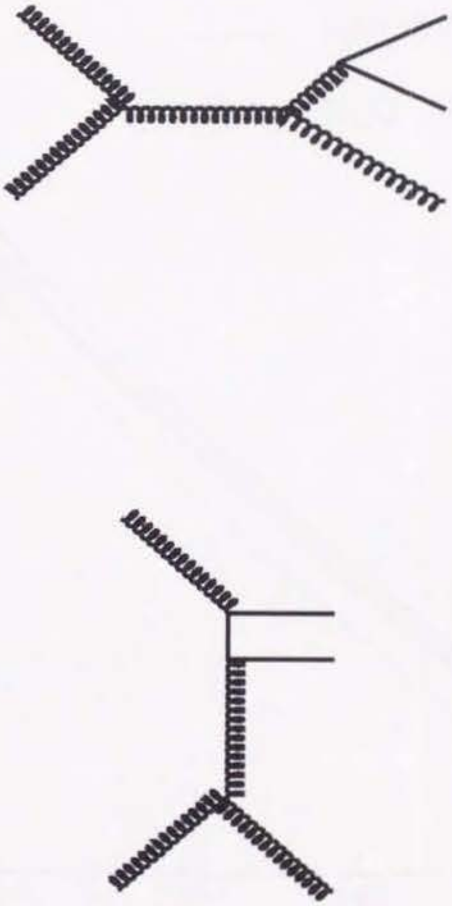

Figure 1.4: Feynman diagrams for a) gluon splitting and b) flavor excitation.

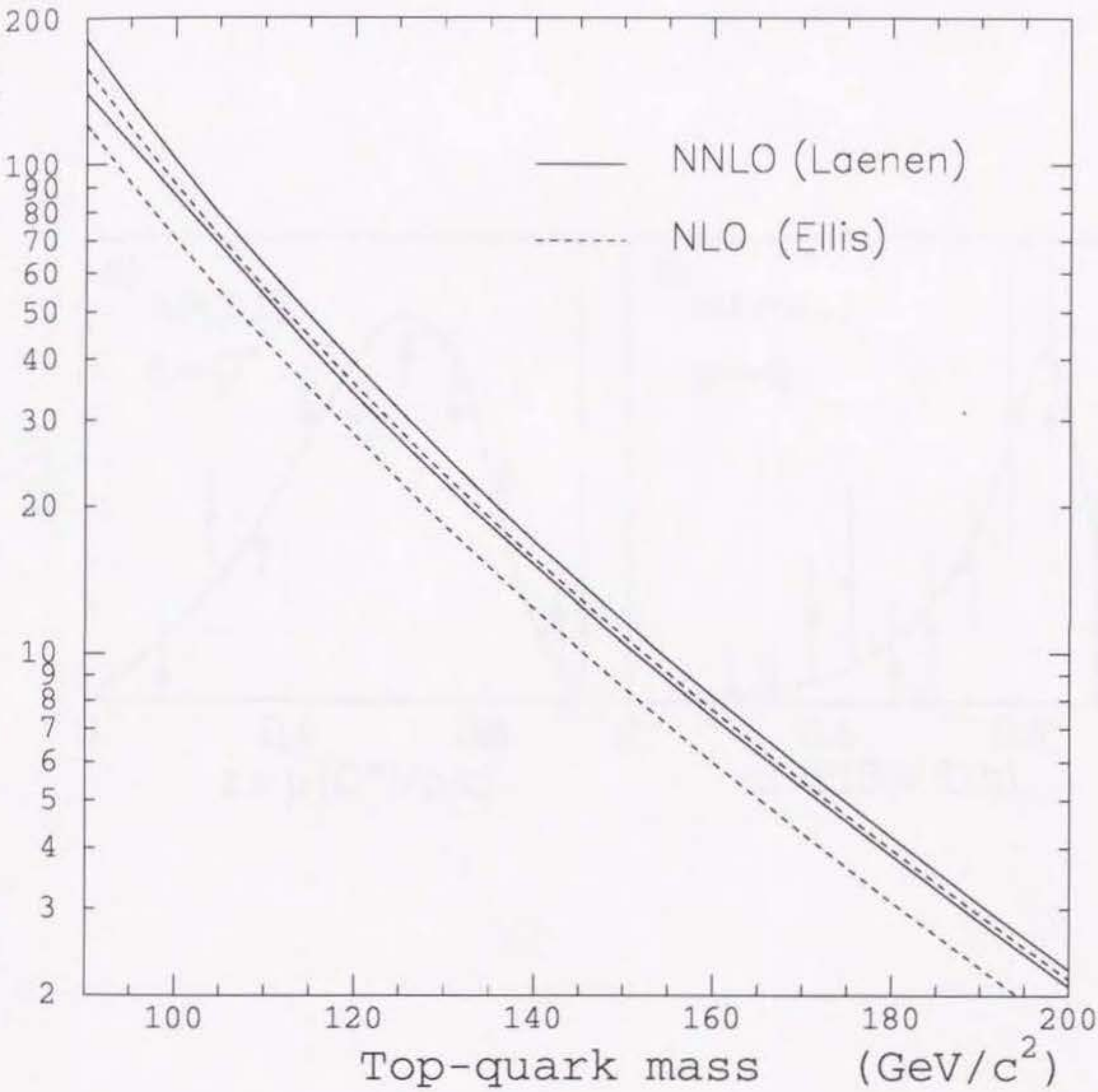

Figure 1.5: The $t\bar{t}$ production cross section by Laenen et al.[26], based on the next–to–next–to–leading order calculation.

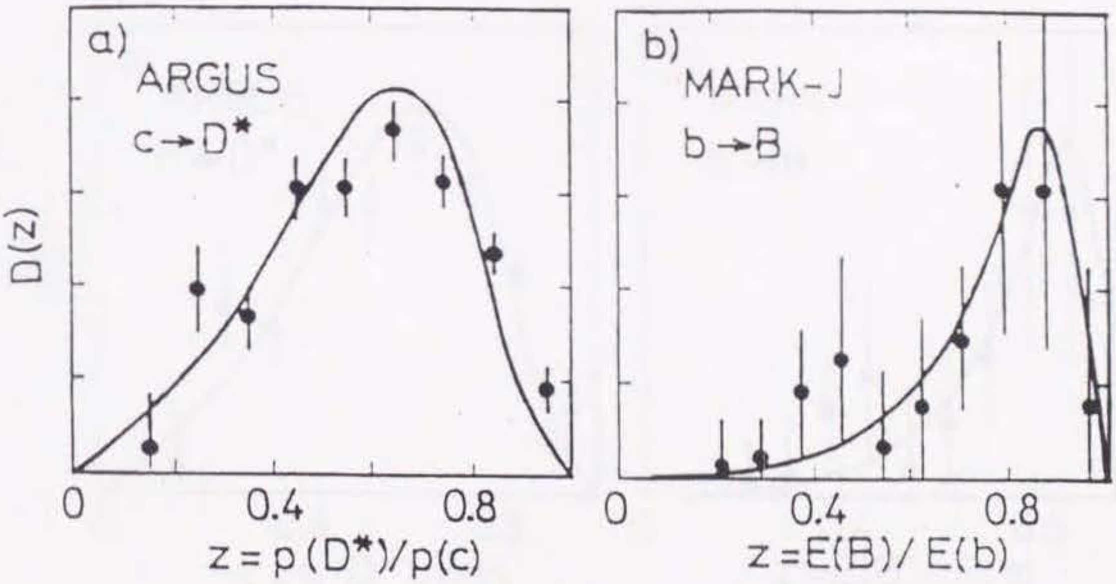

igure 1.6: The fragmentation functions for $c \to D^*$ and $b \to B$ from Argus and Mark-J xperiments, compared to Peterson model for ϵ=0.18 and ϵ=0.018, respectively.

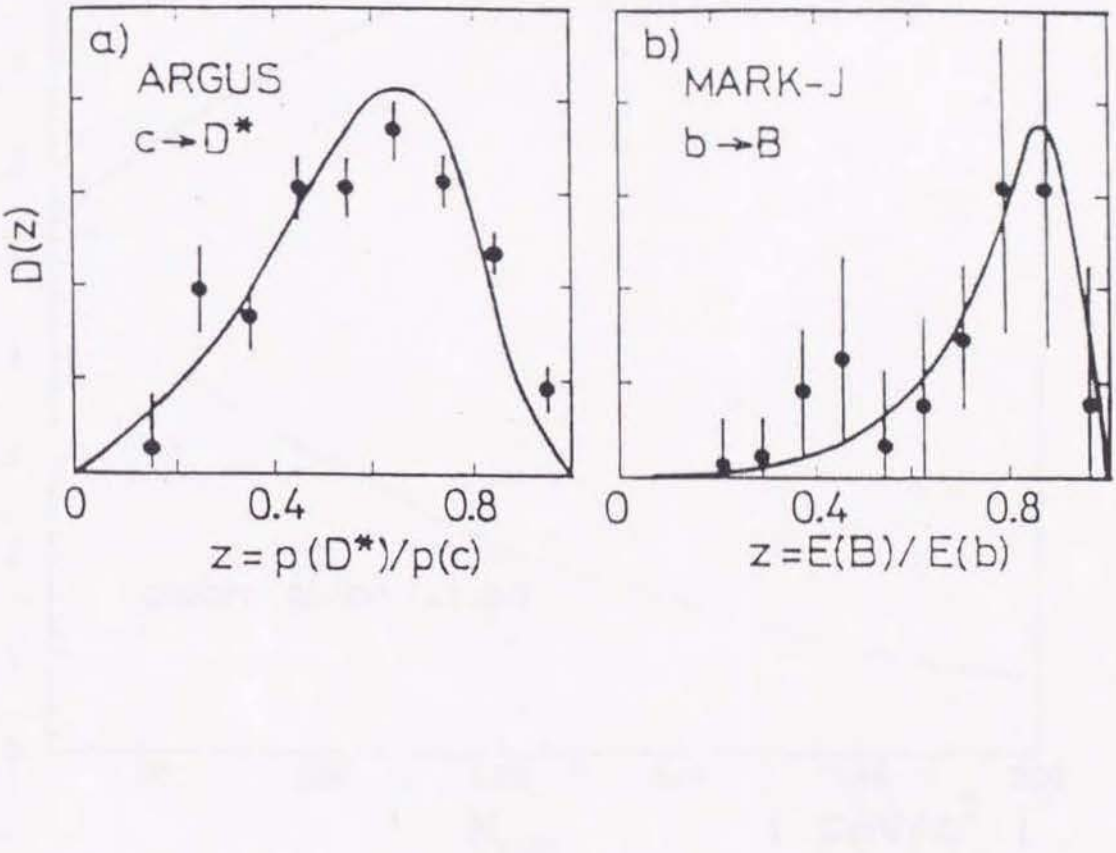

Figure 1.6: The fragmentation functions for $c \to D^*$ and $b \to B$ from Argus and Mark-J experiments, compared to Peterson model for ϵ=0.18 and ϵ=0.018, respectively.

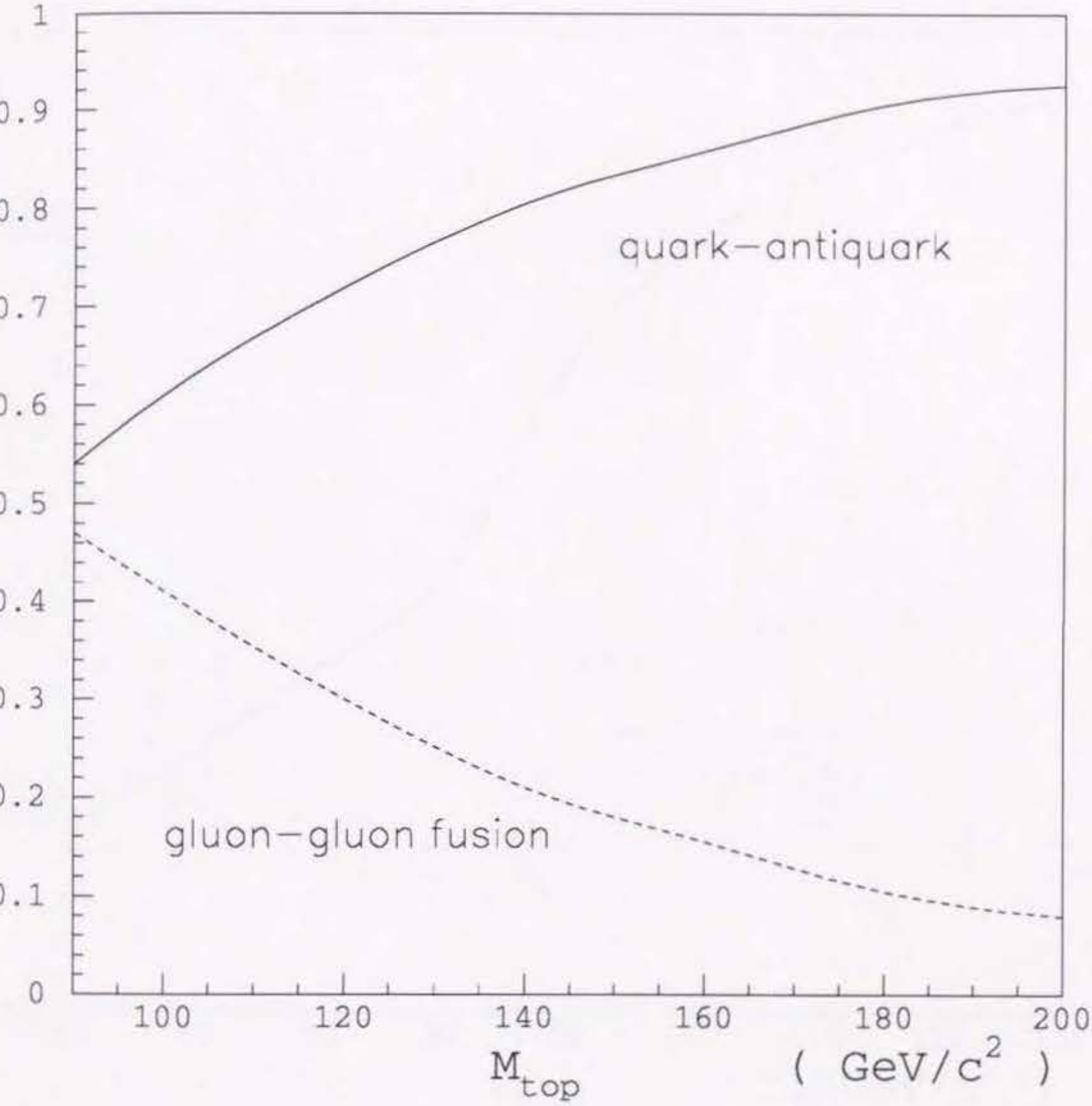

Figure 1.7: Fractions of $q\bar{q}$ channel and gg channel contribution to total next-to-leading-order cross section as a function of the top quark mass at $\sqrt{s}$=1.8 TeV.

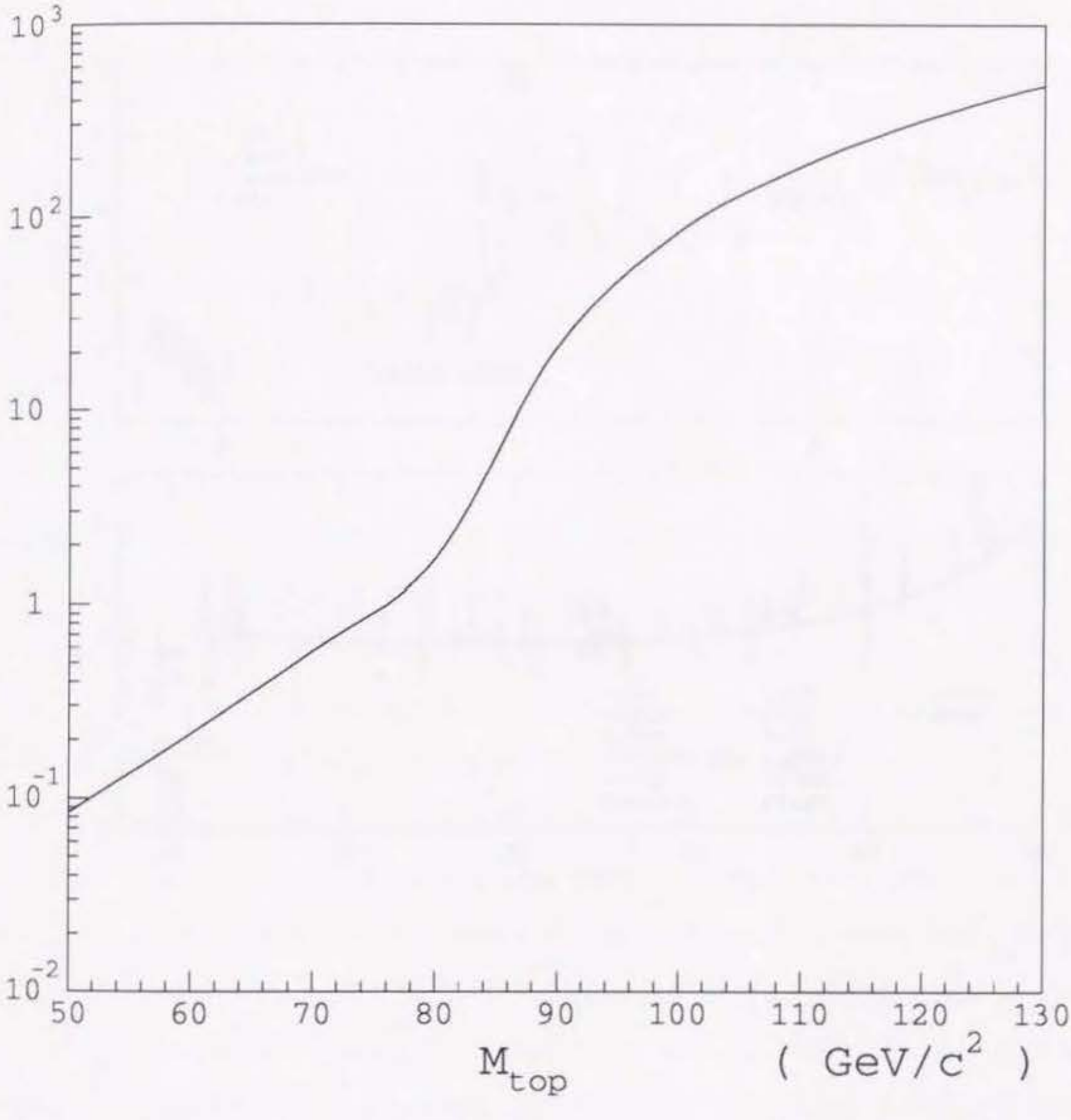

Figure 1.8: Decay width Γ_{top} for the top as a function of the top-quark mass.

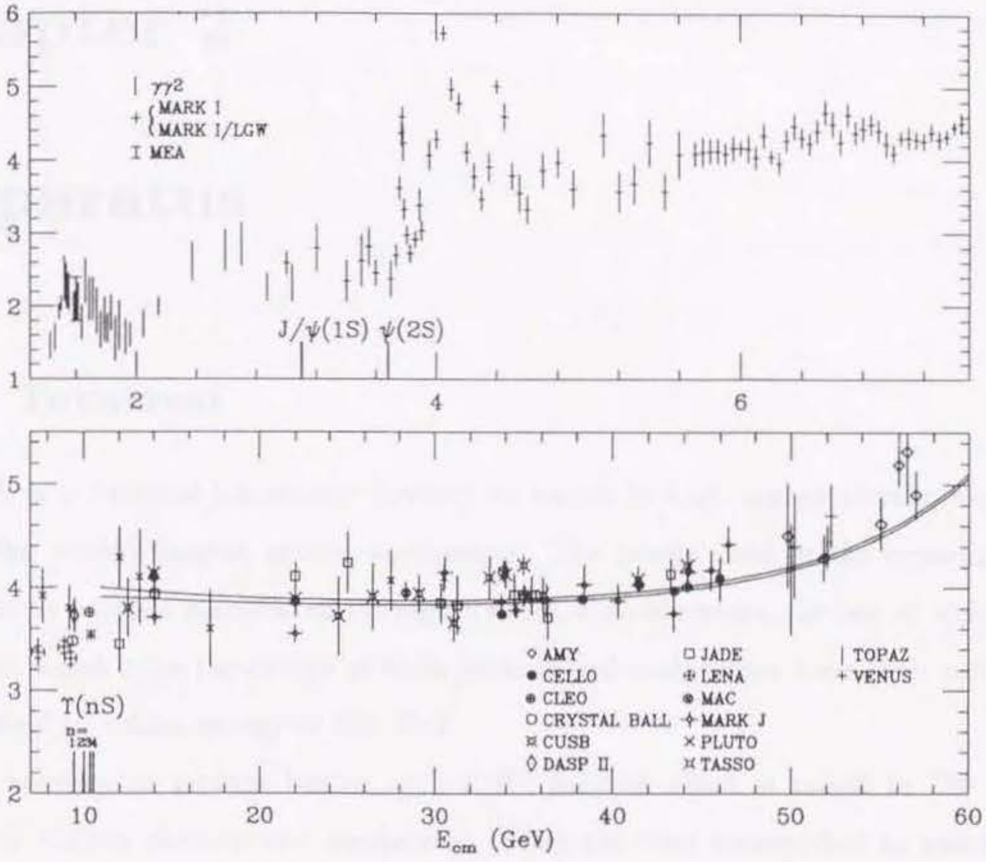

Figure 1.9: Measurements of R $\equiv \sigma(e^+e^- \rightarrow hadrons)/\ \sigma(e^+e^- \rightarrow \mu^+\mu^-)$.

Chapter 2

Apparatus

.1 Tevatron

ermilab is a national laboratory devoted to search in high energy physics and is the te of the world's largest proton accelerator. The beams used in the experiment are roduced by protons accelerated through a series of accelerators, the last of which is the evatron, which raise the energy of both protons and antiprotons from their rest energy 938 MeV to a final energy of 900 GeV.

The accelerator process begins with a H$^-$ sourrce which is raised to 750 keV by ockcroft-Walton electrostatic accelerator. They are then transported to and injected to the Linac which increases the kinetic energy to 200 MeV. Upon entering the booster thin foil is used to strip the two electrons from the H$^-$ ion yielding a bare proton. The rotons are then captured by the magnetic field of the booster. The booster is a rapid cling (15 Hz) alternate gradient synchrotron which raise the proton kinetic energy to GeV. From the Booster the 8 GeV protons are transported to the Main Ring where e energy is raised to 150 GeV total energy. The protons are coalesced into a bunch fore they are extracted from the Main Ring and injeected into the Tevatron. The evatron is a large (radius = 1km, the same as the Main Ring) (anti)proton accelerator nstructed from superconducting magnets. A bunch of protons from the Main Ring is njected into the Tevatron and stored there at 150 GeV.

150 GeV protons are focussed into a beryllium target to produce $\bar{p}$'s of approximately GeV/c momentum. The $\bar{p}$'s are then focussed and collected into an Accumulator at rate of 2 × 10^10 $\bar{p}$'s/hour and cooled to produce a typical monoenergetic $\bar{p}$ stack f approximately 2 × 10^11 particles. In succesive main ring cycles, six proton and x anti-proton bunches are transfered to the Tevatron ring. Finally the bunches are multaneously accelerated to 900 GeV in the Tevatron. The protons and anti-protons re collided at the B0 intersection. To observe processes with small production cross ections, a large number of $\bar{p}p$ collisions must be occur. A useful measure of collider erformance is the luminosity L defined by the relation,

$$N = L\sigma,$$

here N is the number of events produced per second for some final state, σ is the ross section for a given reaction (cm^2) and L is the luminosity in units of $cm^{-2} \cdot sec^{-2}$. he luminosity 'can be expressed in terms of the properties of the colliding proton and nti-proton bunches in the Tevatron.

$$L = f_r \frac{n_{bunch} N_p N_{\bar{p}}}{A},$$

here f_r is the revolution frequency of the beam, N_p($N_{\bar{p}}$) is the number of the protons nti-protons) in each bunch, n is the number of bunches and A is the effective cross ectinal area of beam overlap.

.2 The CDF Detector

he collider detector is expected to perform a wide range of measurement. To begin ith, we briefly describe the feature of the detector at the hadron collider. For a general urpose detector it is necessary to measure leptons and hadrons over a large range of ıomenta. Quarks and gluons are observed as jets, and neutrnos, which escape detec-on, are meaasured as the missing energy. The nature of $p\bar{p}$ collisions places general equirements on the detector design.

The detector should be a calorimetric detector. Good energy resolution, containment f particle showers and the absence of cracks are necessary to eliminate fake sources of issing energy.

The CDF is an azimutaly and forward-backward symmetric detector designed to udy the physics of $p\bar{p}$ collisions at the Fermi National Accelater (FNAL) Tevatron. vent analysis is based on charged-particle tracking, magnetic-momentum analysis, and nely segmented calorimeters.

We expected the higher luminosity for the run, so the detector was upgraded to be ble to tolerant the higher luminosity.

The CDF coordinate systemis shown in figure . Its origin is at the center of the etector. The Z axis is defined as the same direction as motion of the proton beam, om West to East. The y-axis points vertically upward, and the x-axis points radially ıt of the Tevatron ring, so as to make a right handed coordinate system. The azimuthal ıgle phi is set to be 0 on the positive x-axis and increases from positive x to positive The polar angle is measured from the proton beam direction. Instead of theta, we se the peudo-rapidity $\eta = -log(tan(\theta/2))$. The event vertex position can be shiffted ong the beam line and has rms width of approximately 30 cm. We will refer to both s which are detector pseudorapidity η_d for an origin chosen at the geometric center of ie detector and event pseudorapidity η for n origin chosen at the event vertex.

.2.1 Beam-beam counter

he beam-beam counters consist of two planes of scintillating plastic located in front ıd in back of the central calorimeters. Each plane of counters covered the angular gion $0.32° < \theta$ $4.47°$. This provides a monitor of the luminosity.

.2.2 Tracking

he CDF tracking system covers the angular range $\sim 8^{\circ}$ to $\sim 172^{\circ}$ in polar angle ($|\cos\theta|$ 0.99) and is contained within a 1.5 T axial magnetiic field. Three dimensional track construction is available in the range 25 ° to 155 ° in polar angle($|\cos\theta| <0.91$). The acking detectors consist of two separate systems: an inner radius system of

Veretx chamber

ue to space charge distortions in the drift region, the Vertex Time Projection Chamer operated during last run was inoperatble at $L > 3\times 10^{30}$, so it was replaced for this n to able to withstand the higher luminosity and, in addition, to make space for the VX. A vertex chamber(VTX) surrounds the beam pipe and extends $\pm$ 1.4 m along the eam line from the interaction point. This chamber measures charged parrticle tracks the $r - z$ plane to within 3.5° of the beam line. The interaction vertex of of the $p\bar{p}$ llisions is reconstructed with an rms resolution of 1 mm in the z direction. This vertex used as the origin in computing the transverse energy ($E_T = E_T \sin\theta$) deposited in ch calorimeter cell. The distribution in z of reconstructed vertices in dilepton events is own in Figure 2.4 and is well described as a gaussian mean -2.0 cm and width 29.5 cm. his spread in vertices reflect the convolution of of the proton and antiproton buncches the collider. The VTX is also used to detect photon conversions.

Central Tracking Chamber

ie central tracking chamber (CTC) surrounds the VTX. The CTC was designed to easurre charged particle tracks in the $r - \phi$ plane to determine their curvature in e magnetic fieald and thustheir momenta. The CTC has 84 layers of wires grouped gether in nine "superlayers" as shown Figure 2.7. The nine superlayers are subdivided to measurement cells. Five superlayers have 12 sense wires per cell, parallel to the am direction. These axial layerss are used for the preliminary determination of the ack curature. In the other four superlayers, each cell has six sense wires within a stereo angle to provide information necessary to determine the polar angle of the acks. The cells in all suoerlayers are tilted at a 45° angle with respect to the radial rection to compensate for the Lorentz angle of electron drift in the magnetic field. This lows electrons to drift azimuthally(in the ideal case), simplifying the time-to-distance lationship.

The momentum resolution of the CTC is $\delta p_T/\ p_T = 0.0011 p_T$ (p_T in GeV/c) for isoted tracks by requiring that a track intersect the beam at the beam position point(beam nstraint). Complete tracking information is only available for $40^\circ < \theta > 140^\circ$. Tracks itside this angular region do not pass through all laayers of the chamber and conseiently have a poorer momentum resolution.

.2.3 Calorimetry

ie CDF has three calorimeter systems: central, plug and forward regions over the gion $\mid \eta \mid <4.2$. Each section has a tower structure of an electromgnetic calorimeter d a hadoronic calorimeter. In the central region($\mid \eta \mid <1.1$) a lead-scintillator sampling lorimeter 18 radiation lengths deep provides electromagnetic shower detection. This ntral electromagnetic calorimeter (CEM) is segmented into 15° wedges in the azimuthal rection, with each wedge consisting of ten projective read out towers numbered from 0 9, where tower 0 is at 90° polaar angle. The size of a central tower is approximately $\phi \times \Delta\eta = 15^\circ \times 0.11$.

A set of proportional wire chambers is located in the CEM at a depth of six raation lengths to meaasure the position and shape of electromagnetic showers. These ntral strip chambers(CES) have wire and cathode strip readout providing independent construction off showers in the z and azimuthal views.The resolution on the position shower centroids from 25 GeV/c elecrons is ~ 2.5 mm for both views.

Measurement of hadronic energy in the central region is provided by the central and d-wall hadronic calorimeters(CHA/WHA). The CHA/WHA has aapproximately the me geometry and segmentations as the CEM and covers the same region of pseudoradity. The energy resolution is $\sigma(E)/E = 80\%/\sqrt{E_T}$

In this analysis the central and plug calorimeters were used to identify electron ıd jets, and the missing transverse energy (which will be defined in Section 4.5) was ɔmputed using the full calorimeter out to $| \eta | < 3.6$.

System	η range	Energy resolution
CEM	$\mid \eta \mid <1.1$	$13.5\%/\sqrt{E_T} \oplus 2\%$
PEM	$1.1 < \mid \eta \mid <2.4$	$28\%/\sqrt{E_T} \oplus 2\%$
FEM	$2.4 < \mid \eta \mid <4.2$	$25\%/\sqrt{E_T} \oplus 2\%$
CHA	$\mid \eta \mid <1.3$	$75\%/\sqrt{E_T} \oplus 3\%$
PHA	$1.3 < \mid \eta \mid <2.4$	$90\%/\sqrt{E_T}/ \oplus 4\%$
FHA	$2.4 < \mid \eta \mid <4.2$	$130\%/\sqrt{E_T}/ \oplus 4\%$

ıble 2.1: Summary of calorimeter properties. CEM(CHA), PEM(PHA) and EM(FHA) denote the central, plug and forward EM(HAD) calorimeters. The symɔl $\oplus$ signifies that the constant term is added in quadrature in the resolution.

.2.4 Muon chamber

uon chambers are located behind the central calorimeters at a radius of 3.47 m. ere are approximately five hadronic absorption length of material between the muon amn=bers and the interaction point. The chamber covers the rapidity region $| \eta |$).63 ($56° < \theta < 124°$). There is a gap between neiboring chambers at the boundary η=0 of about $\delta\eta$=0.05. A 2.4° gap in ϕ between adjacent 15° calorimeter sections so is not covered. The four layers of drift cells in a muon chamber provide the threemensional reconstruction of tracks via single-hit time-to-digital converters (TDC's) in e transverse direction and charge division in the longitudinal direction. A drift resotion of 250 μ (ϕ) and a charge division resolution of 1.2 mm (z) are determined from smic-ray studies.

Central Muon Upgrade

ıe original CDF Central Muon detector(CMU), which covers the pesudorapidity re-on | η | <0.6, has been complemented by the addition of the 4 layers of drift tubes ehind 2 feet of steel resulting in a total of 8 absorption lengths. Only muon candidates ith P_T above 2.5 GeV/c^2 are expected to be able to reach the CMP chambers. As a sult, hadronic punch-through backgrounds to the muon signal have been considerably duced by requiring hits in the CMP chamber.

Central Muon Extension (CMX)

e have added layers of drift tubes outside the calorimeter in the pseudorapidity region 0.6 <| η | <1.0. The coverage in ϕ is 80 % and the chambers are located behind 6 sorption length of calorimeter. This increases the muon coverage in CDF by 50 %.

.3 Trigger

vents are selected in several stages. The first two levels are used to reduce the rate events to a manageable level before writing to tape. Level 3 reduces the number of ents to be reconstructed in order to economize on computing time.

The CDF trigger system has three levels of hardware triggers followed by a softre(Level 3) trigger that utilizes a farm of processors running offline-like algorithms. ese triggers require the presence of an inelastic $\bar{p}p$ collision, signaled by a coincince between two scintillator counters located along the beam pipe at the forward and ckward regions.

Scintillation counter arranged in a rectangle around the beam pipe and covering e angular interval from 0.3° to 4.5 ° and from 355.5° to 359.7° provide a "minimum as" trigger, which is satisfied if at least one scintillation counter on each side of the eraction region is above threshold within a 15-ns window centered on the beam-beam ossing time. Events satisfying this trigger are then considered by the higher level gger logic.

At Level 1, a simple but fast decision to reject the majority of events are made

fore the next beam crossing. For Level 2 a more complex decision based on identifying
hysics" objects. The detector is dead for several crossing while this decision is being
ade. The Level 3 trigger is a software filter that is part of the online data decision
th and runs a subset of the event reconstruction code and physics algorithms. Events
at survive the Level 1 and Level 2 hardware triggeres are passed to Level 3 for a more
tailed analysis before being accepted or rejected. The decision was made with Silicon
raphics processors using the UNIX operating system. The final stage after the trigger
lection is the offline reconstruction.

Level 3 was running the equivalent of offline production, therefore all the information
electron objects(ELES) and muon objects (CMUO) are available at level 3. At Level
Detector is read out completely.

3.1 Electron trigger

e hardware trigger system is designed to use the projective nature of the calorimeter
wers along with a fast two-dimensional hardware track finder, called the ceentral fast
icker (CFT). Trigger towers have a width of 0.2 in pseudorapidity and 15° in azimuth,
apping the detector into an array of 42 (in η) by 24 (in ϕ) in both electromagnetic
d hadronic calorimeters. Electron candidates are triggered on using calorimeter in-
rmation that requires a significant localized deposite of energy in the electromagnetic
lorimeter with little leakage into the hadron compartment behind it. Further rejection
n be obtained by requiring a stiff track pointing at the cluster.

Level 1

e first level trigger used information exclusively from the calorimeters and required a
gle trigger tower with E_T more than 6 GeV for the CEM, or E_T more than 8 GeV in
y region of the calorimeter.

Level 2

e central electron trigger requires an energy cluster with E_T >9.2 GeV, together with
aassociated CTC track with transverse momentum P_T >9.2 GeV/c as measured by

e CFT. The plug electron trigger simply requires either an energy cluster with E_T 20 GeV or E_T >15 GeV and $\not{E}_T$ >15 GeV. The ratio of hadronic to electromagnetic ergy in the cluster (HAD/EM) is required to be less than 0.125.

Level 3

ie central electron trigger at level 3 requires that the reconstructed cluster energy E_T above 18 GeV and that there be a reconstructed track with P_T >13 GeV/c pointing the cluster. The plug trigger requires the reconstructed E_T is required to be above GeV with $\not{E}_T$ >20 GeV.

3.2 Muon trigger

evel 1

ie level 1 trigger ws based solely on the muon chamber information. condition requires at hits from a track form coincidence in two of the four layers of the chamber within time window determined by the P_T threshold, as shown in the following equation: $in(\mid t_4 - t_2 \mid, \mid t_3 - t_1 \mid) < t_{max}$, where $\mid t_4 - t_2 \mid$ and $\mid t_3 - t_1 \mid$ are the time difference uivalent to the P_T threshold preset. The P_T is measured by using the constraint aat the track had to originated at the beam line and knowing the line integral of the agnetic field traversed by the particle. P_T of the muon track segment in the CMU th P_T >6 GeV/c in coincidence with hits in the CMP was required.

Level 2

ie level 2 trigger condition is that a match between a CFT track in the $r - \phi$ plane th P_T >9.2 GeV/c and a track segment in the muon chambers which is defined as a el 1 trigger. The hits in the CMP chambers is used to confirm a trigger in the CMU ambers if the CMP chambers are available.

Level 3

ie level 3 muon requires a match better than 10 cm in $r - \phi$ between a reconstructed ick with P_T >18 GeV/c which is extrapolated to the radius of the muon chambers and rack segment in those chambers. In addition, the energy deposited in the associated

HA tower must be less than 6 GeV.

3.3 Offline reconstruction

nce the last run(1988-89), all of CDF's offline reconstruction codes was ported to NIX(both Silicon Graphics and IBM), enabling us to run the offline code as part of e level 3 trigger.

Large fraction of the 1992 code is new for new detectors and many changes to the construction code for existing detectors were made based on the data collected in the t run. A data compression scheme is introduced to accomodate the laarge size of the ta set.

Full reconstruction of all CDF data is completed within two days of data taking, ing 1000 MIPS from a Silicon Graphics farm , while approximately 5-10 % of the ta, including the most interesting events, are reconstructed and available within a few urs of data taking.

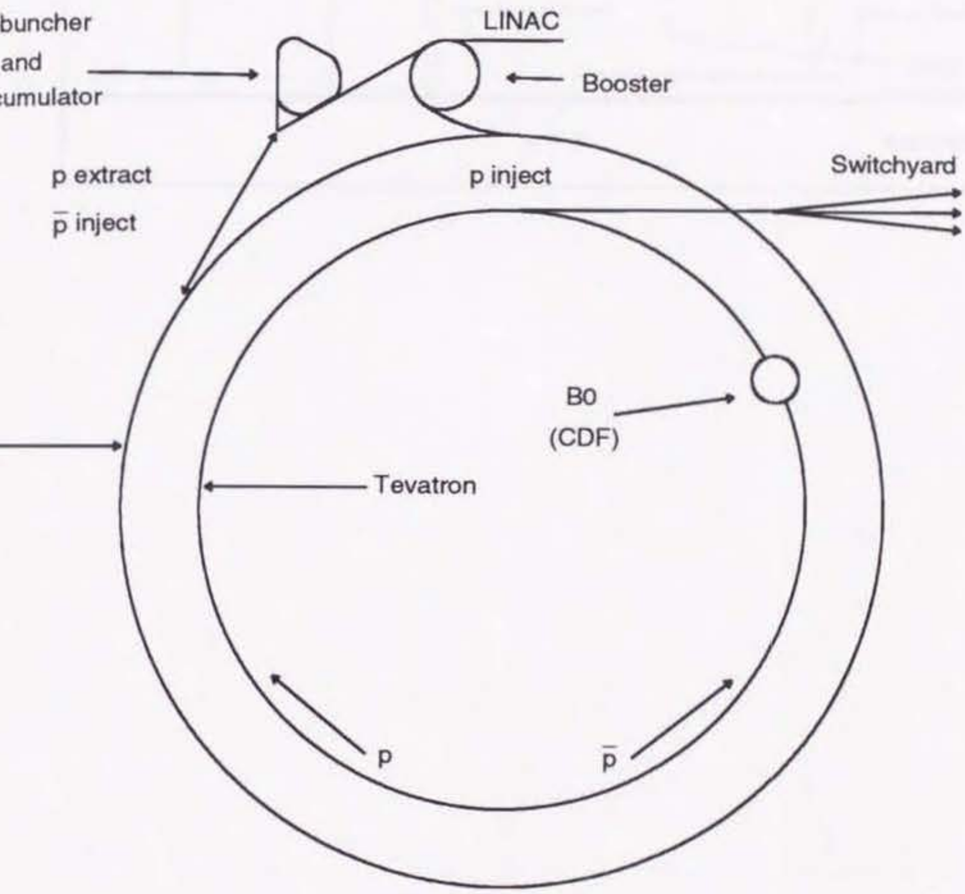

Figure 2.1: The Fermilab accelerator complex

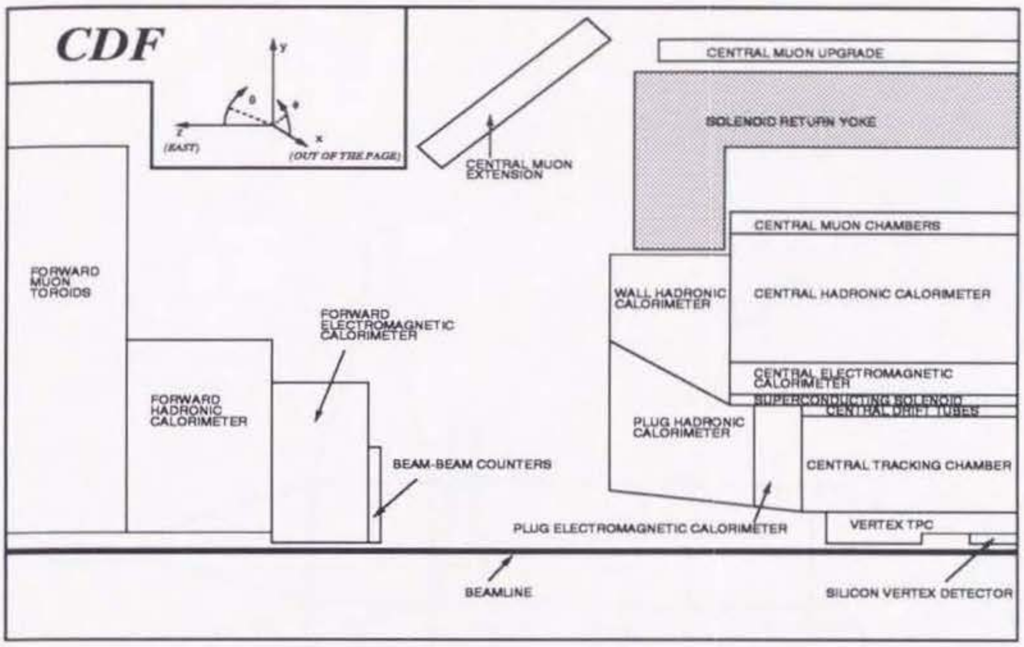

gure 2.2: A cut-away view of onee qudrant of the CDF detector. The detector is ward-backward symmetric about the interaction point.

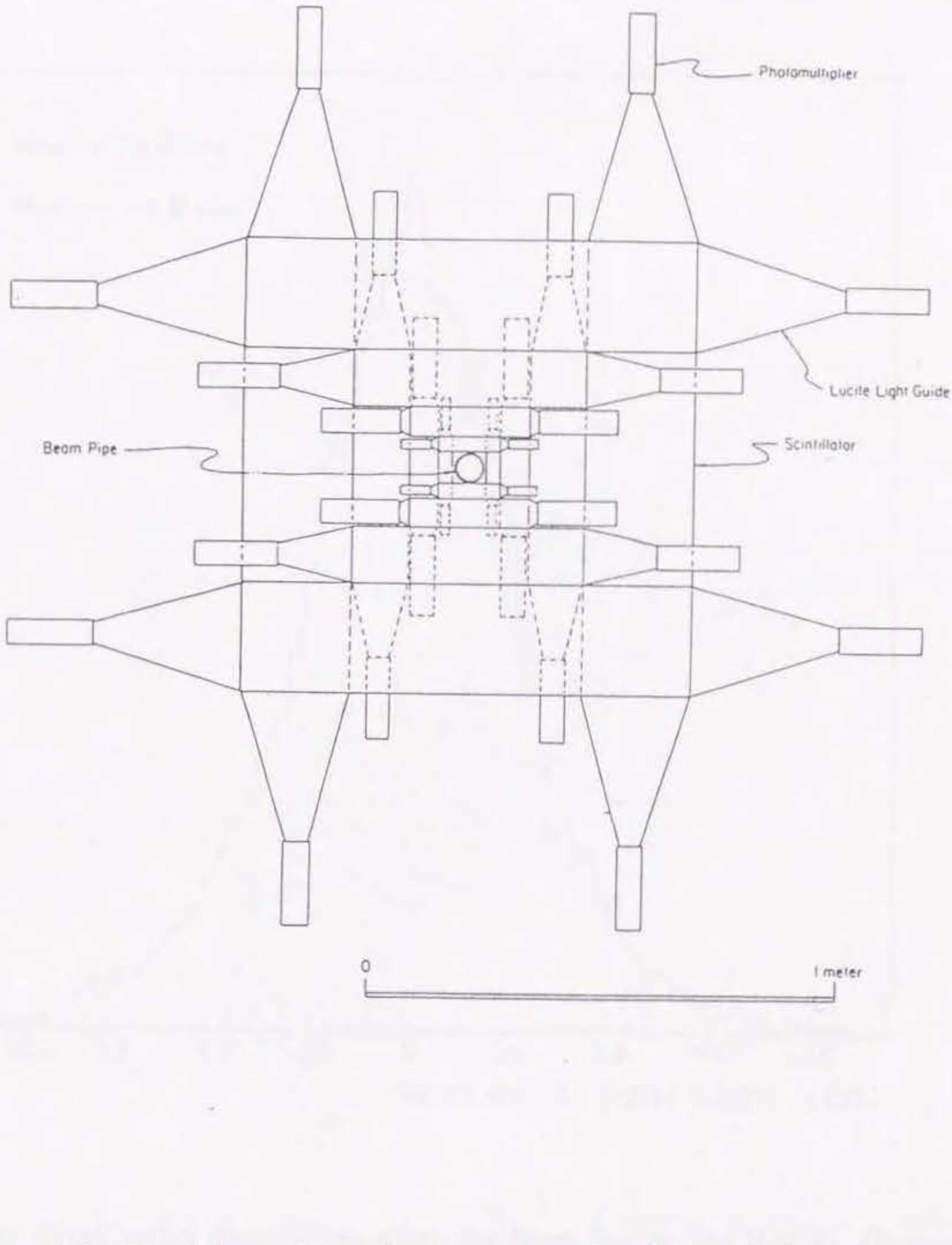

Figure 2.3: One of plane of beam-beam counters viewed from the beam-line

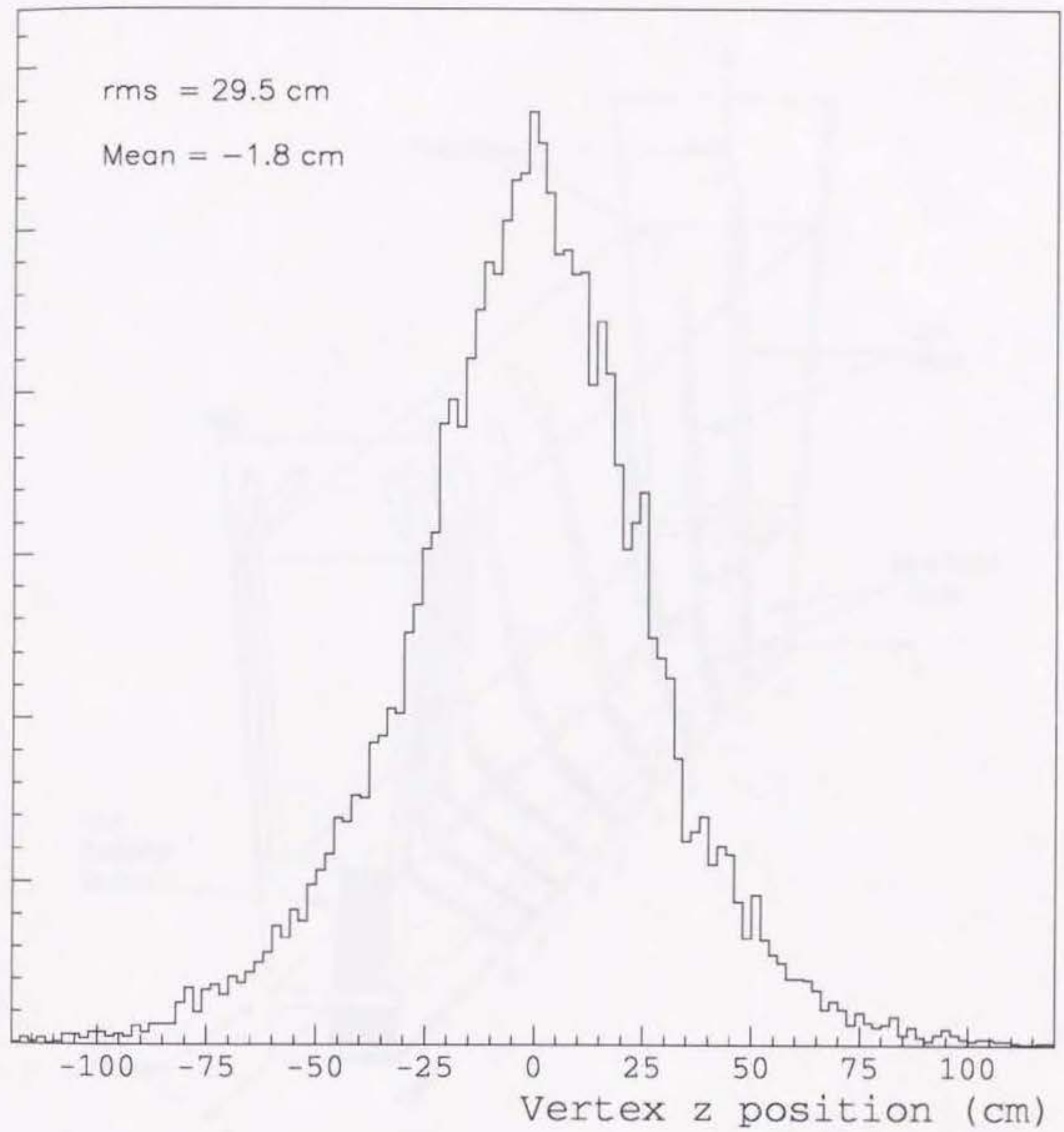

gure 2.4: Event vertex distributions along the beam line for the high P_T dilepton
ents.

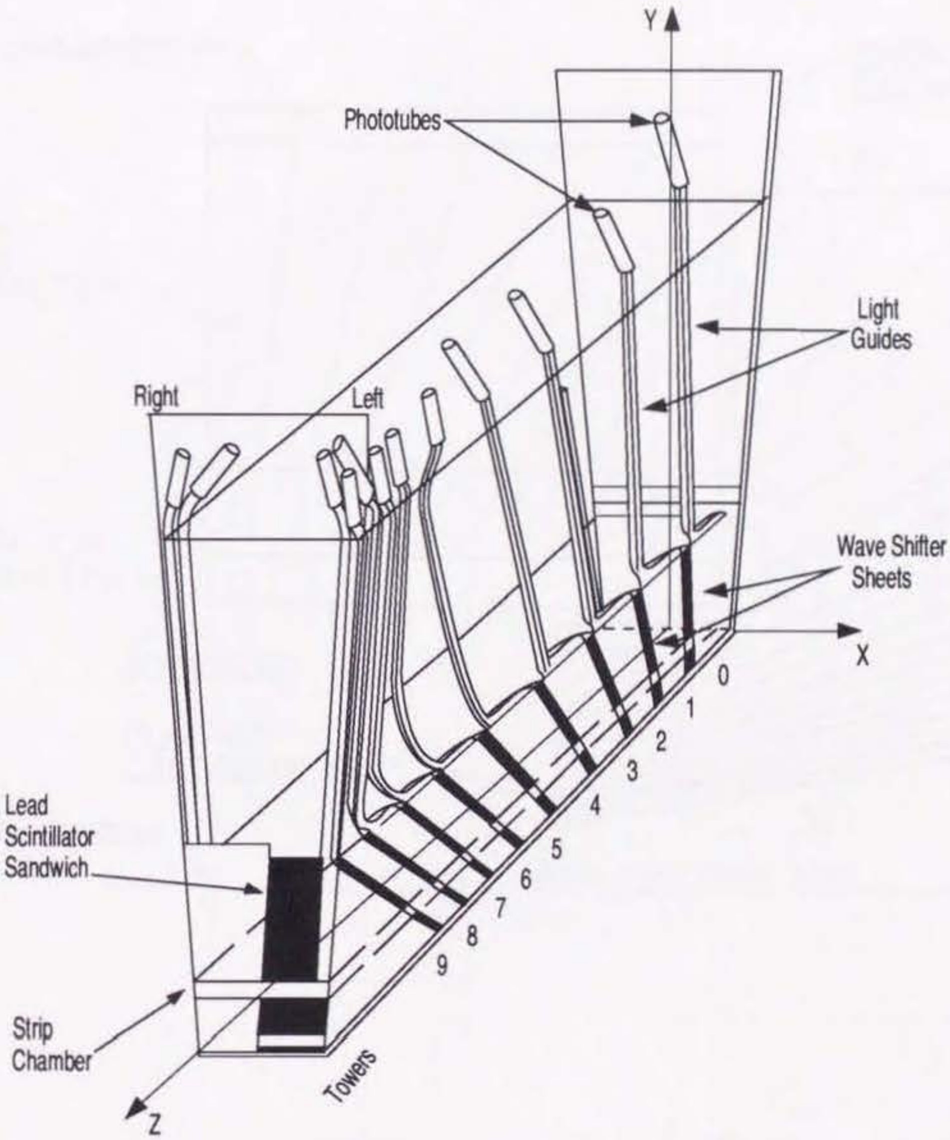

ure 2.5: Cutaway view of a central electromagnetic calorimeter module. The wave-
gth shifters collect the light from the layers of scintillators and indicate the cell
ucture in η. Each wedge subtends 15∘ in ϕ.

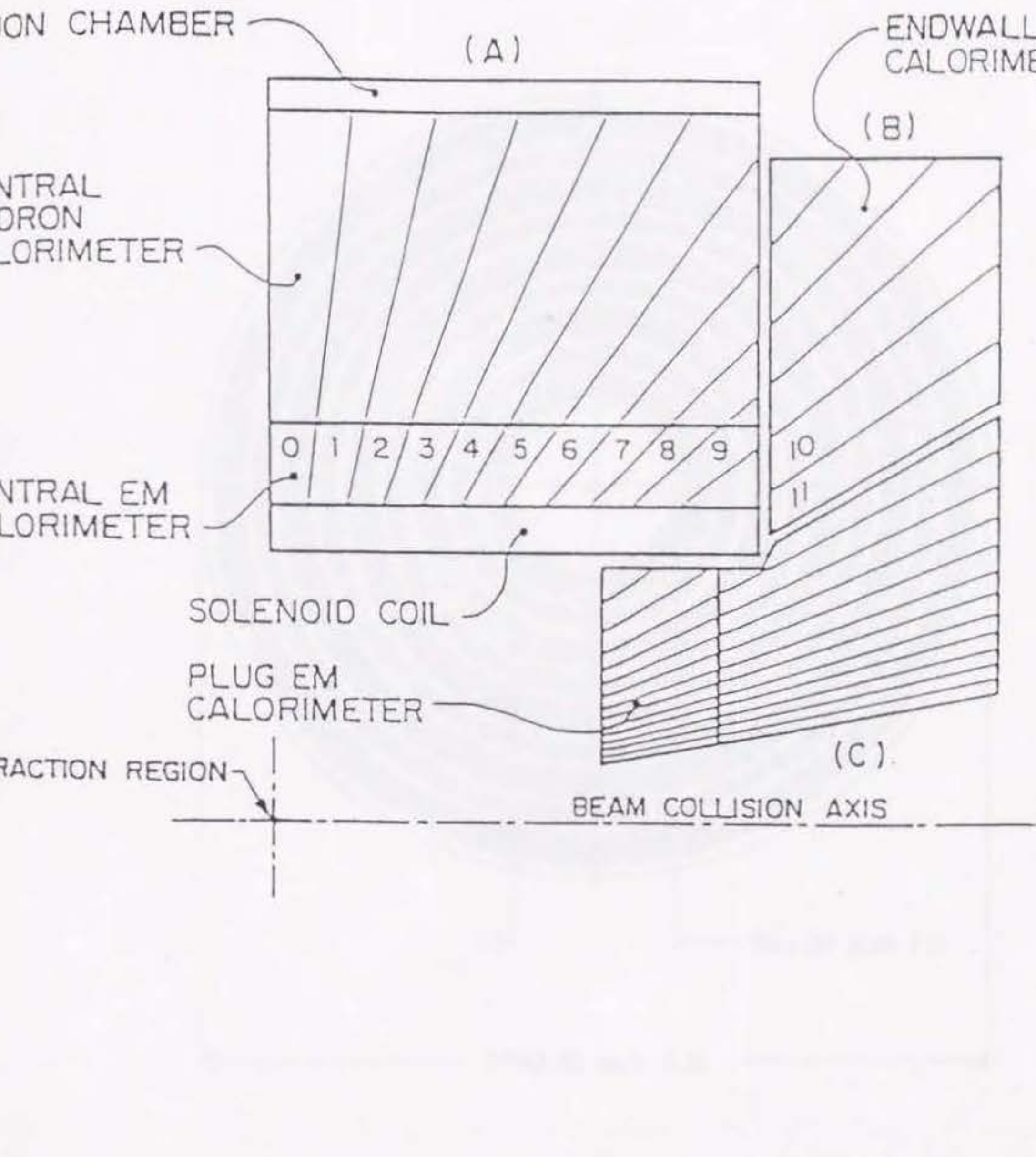

gure 2.6: Quadrant of the calorimeter where A, B and C show the central, endwall
d plug, respectively.

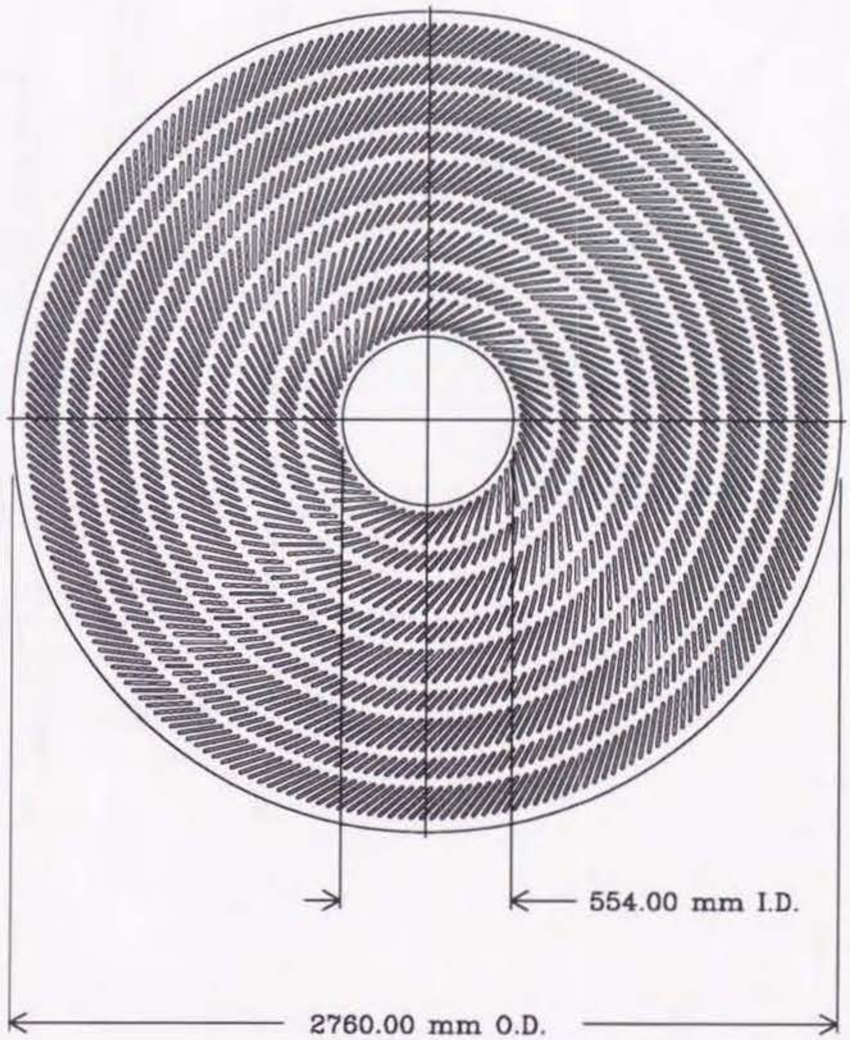

ure 2.7: Layout of wires at the end of the central tracking chamber (CTC) showing
disposition of the superlayers and cells within the superlayers.

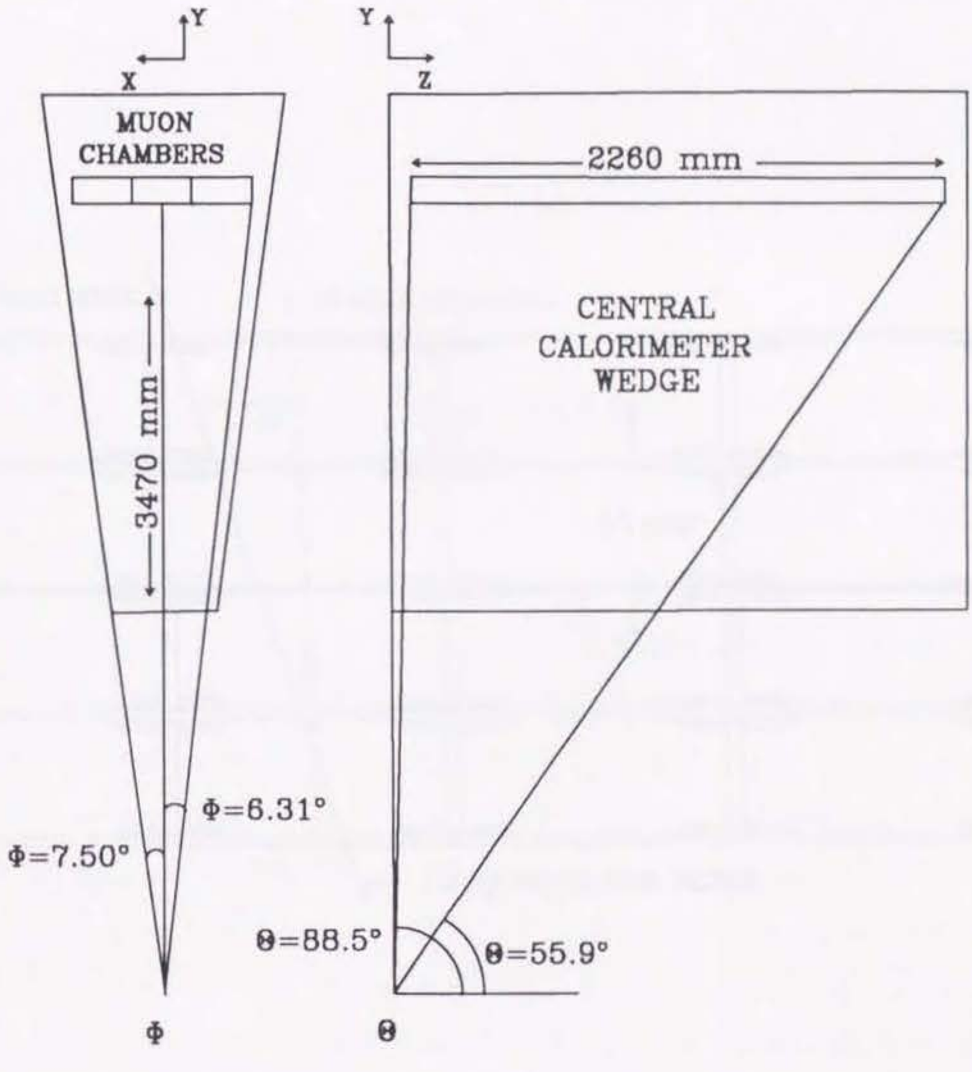

gure 2.8: Central muon chamber location with respect to a central calorimeter wedge.

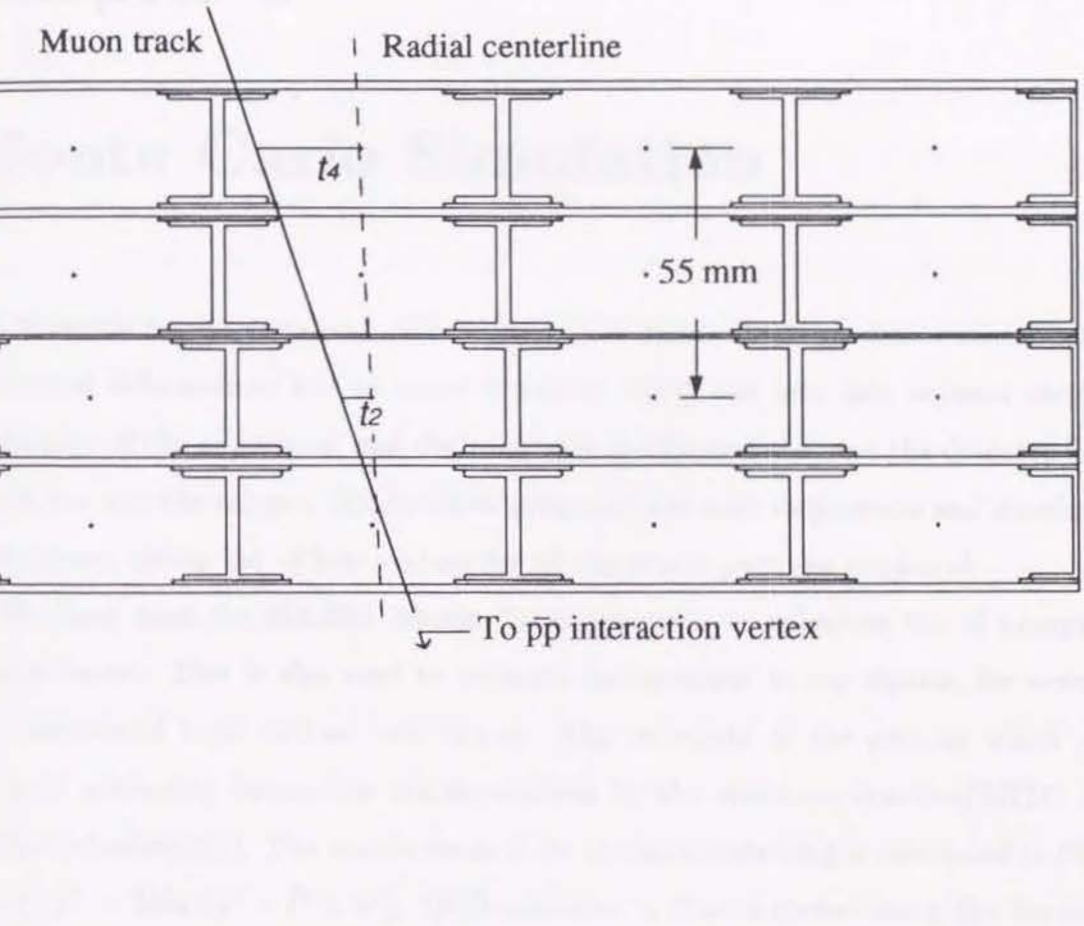

gure 2.9: The arrangement of the four plates of central muon chambers in a view along
e beam direction. The drift times t_2 and t_4 are used at the trigger level to determine
muon momentum cutoff.

hapter 3

Ionte Carlo Simulation

: $t\bar{t}$ events must be analized with a help of the Monte Carlo generator containing the oretical information, and an event simulator which can take into account the finite eptance of the apparatus, and the variations in efficiencies across the detector due to device and the trigger. Monte Carlo programs are used to generate and simulate $p\bar{p}$ eractions, giving list of four-vectors for all the stable particles produced.

We have used the ISAJET Monte Carlo generator to calculate the $t\bar{t}$ acceptance xperiment. This is also used to estimate backgrounds to top signals, for example, background from bottom and charm. The momenta of the partons which enter hard scattering interaction are determined by the structure function(EHLQ set 1 ameterization[31]). The matrix element for the hard scattering is calculated to $O(\alpha_s^2)$, ing $Q^2 = 2\hat{s}\hat{t}\hat{u}/(\hat{s}^2 + \hat{t}^2 + \hat{u}^2)$. QCD radiation is then included using the branching roximation[32]. QCD radiation from the incoming and outgoing partons is simulated atively, so that parton showers are generated. The partons which originate from the d scattering diagram are generally off-shell. At each branching point, the partons ve closer to their on-shell masses. A cut-off parameter is used to truncate the shower elopment; for instance, for gluons, the branching process is stopped when the virtual ss of the gluon falls below 6 GeV/c^2.

owiing the QCD shower simulation, the outgoing heavy quarks are fragmented indedently, using the Peterson parameteriztion [33] with ϵ_c=0.08 for charm and ϵ_b=0.5 bottom. For top, the Peterson variable is scaled according to $1/M_{top}^2$, giving a very d fragmentation function. Light partons are fragmented using a purely phenomel- cal parametrization. The unstable particles produced in the fragmentation process decayed based on the measured branching ratios if possible and estimated branching os otherwise.

The "underlying event", all the particles unrelated to the hard scattering process, are P_T hadrons which are approximately uniformly distributed in rapidity and azimuth. ISAJET program, the underlying has two components: (1) QCD radiation from oming partons described above, and (2) beam-jet fragmentationsimulated using a nomelogical model. The average level activity from the underlying event is adjusted s to match the measurement.

In addition to simulating QCD-induced heavy flavor production as described, ISAJET generate a variety of process such as Drell-Yan and W processes.

1 Monte Carlo Data Sets

s section describes the Monte Carlo data sets to which we will refer in subsequent ions. The primary Monte Carlo generator used to evaluate acceptance and back- unds is ISAJET[1] All Monte Carlo events were passed through a simulation of the F detector. The detector simulation program extrapolates the final-state particle jectories through the magnetic field to the calorimeter cells. The average calorimeter ponses and resolutions for charged pions, photons, electrons, and muons have param- rized and tuned to reproduce (1) test-beam measurements for paticles with momenta n a few GeV/c up to about 200 GeV/c, and (2) isolated track data collected with a imum-bias trigger at low P_T. The simulation also includes effects of response across ndaries between calorimeter cells, zero responce in uninstrumented regions, photon

[1] Unless otherwise stated, we used version 6.43 of ISAJET Monte Carlo program.

versions and the observed distribution of vertex positions about the mean position at center of the detector. After simulation, the events were passed through the offline nstruction in the same way as the CDF data. The effects on the trigger efficiencies small differences of lepton detection efficiencies between data and Monte Carlo re-struction were corrected. Corrections were also applied for muon acceptance, since e of CMU wedges have been completely dead, throughout the run so far.

We have checked the validities of the Monte Carlo simulation, especially on the lepton tification, isolation variables and the missing E_T.

- $t\bar{t}$

ISAJET Monte Carlo program was used to generate $t\bar{t}$ events for the top quark sses of 100, 120, 140, 160 and 180 GeV/c^2. The integrated luminosity of these gener-d samples were 1127, 2953, 6780, 14194 and 27768 pb^{-1}, respectively. We have used $t\bar{t}$ production cross section calculated by Laenen et al. [26] which was used for the malization of the expected $t\bar{t}$ events.

- $b\bar{b}$ and $c\bar{c}$

JET program was also used to generate a sample of $b\bar{b}$ and $c\bar{c}$ events. Production of uarks via the mechanisms of (a) direct $b\bar{b}$ production ($gg \rightarrow b\bar{b}$), (b) gluon splitting $\rightarrow gg, g \rightarrow b\bar{b}$), and (c) flavor excitation ($gb \rightarrow gb$) are included in the calculation. have required that there was at least one b quark with P_T more than 25 GeV/c^2. s P_T threshold was chosen to keep 90 % of the daughter leptons with P_T more than GeV/c^2. The sample was then passed through the CLEO Monte Carlo to decay b rks. It is known from the CLEO and CDF experiences that the CLEO program dels them better than that in the naive ISAJET program. This changes the average rged particle multiplicity and the energy flow around the lepton.

- WW and WZ

ISAJET was also used to model WW and WZ backgrounds. The integrated luminos- of WW and WZ samples are 16790 pb^{-1} and 94100 pb^{-1}, respectively. The ISAJET dicts WW cross section to be 6 pb, but we use the theoretical predictions of 9.5 pb :ulated by Ohnemus[47].

• $Z \rightarrow \tau\tau$

used $Z \rightarrow e^+e^-$ in data to make $Z \rightarrow \tau\tau$ simulation sample. The two electrons in $Z \rightarrow e^+e^-$ event were removed and then replace each elecron with a tau. The tau hen allowed to decay semileptonically and simulated with the full simulation of the F detector. The reeconstructed tau's were merged to the original event. In order to much statistics, we have repeated this process 80 times for every Z event.

hapter 4

vent Selection

e top-quark search in this analysis is based on a signature with high transverse mo-
ntum leptons, large missing transverse energy, and jets. We begin with the techniques
lepton detection in the hadron collider environment in section 4.1 and 4.2, respec-
ly. Each section presents a set of lepton identification variables used in the analysis.
tons coming from the top-decays are expected to be isolated, and we present the
on isolation in the follwing section. The last two sections of the chapter explain jet
onstruction and the neutrino detection in CDF.

1 Electron Identification in CDF

s section describes the electron variables used to identify electrons and gives the cut
ies used.

.1 Offline clustering

e electron identification algorithms begin with the formation of electromagnetic clus-
using an array of seed towers with transverse electromagnetic energy >3.0 GeV.
boring towers with E_T >0.1 GeV are added to the cluster until the maximum cluster
is reached. The maximum cluster size is limited to three towers in pseudorapidity

≈ 0.3) by 1 tower in azimuth ($\delta\phi$=15° in the central region, and 5 towers in pseu-
apidity ($\delta\eta \approx 0.5$) by 5 towers in azimuth ($\delta\phi$=25° in the plug region. The cluster used for the different calorimeters reflect the variation of shower size and cell size . For clustering purposes, we define the transverse energy $E_T \equiv E \sin\theta$ using the sured energy E in the calorimeter and the polar angle θ given by the tower center tion in the detector and the event vertex. As a cluster candidate, offline software shold is required that the electromagnetic E_T of the cluster be >5.0 GeV and that ratio of hadronic E_T(for towers in the electromagnetic cluster) to electromagnetic (HAD/EM) be less than 0.125.

.2 Electron responce corrections

central calorimeter modules were calibrated in a test beam. These calibrations were ntained with radioactive sources and light flushers. However, the ultimate calibra- of the electromagnetic detector was performed using the CDF data itself. First, energy deposited in the calorimeter was compared to the momentum measured in central tracking chamber for a large sample of low energy electrons. This E/p mea- ement was used to set the relative calibration of the individual calorimeter modules ver-to-tower responce). Then, the overall energy scale was determined by requiring the E/p as measured using electrons in $W \to e\nu$ events agree with the predictions radiative W Monte Carlo [35].

.3 Central Electron Identification Variables

er the trigger selections, a sample contains significant backgrounds from $\pi^0, \pi^\pm$ over- early showering charged pions, conversions, and Dalitz pairs. At CDF, electron tification requires both calorimeter and tracking information. We have used the wing variables to define electrons [36]:

Track momentum

require the three-dimensional track associated to the EM cluster to distinguish elecis from photons. This track is used to determine the electron's three momentum :or. The direction is much better determined using this track than using calorimeter ables which has a coarse granuarity.

HAD/EM

re must be minimal shower "leakage" into the hadronic calorimeter. We define the o between the hadronic and electromagnetic energy in the cluster. The electron/pion ration has been studied in the test beam and verified taken at the collider using unbiused sample of electrons, i.e., the $W \rightarrow e\nu$ sample obtained by triggering on neutrino. The offline analysis required a missing E_T >30 GeV in the event, and entral EM cluster with E_T >30 GeV matched to a reconstructed track; thus this ple provides an unbiused electron sample. Figure 4.2 shows the hadronic fraction ribution for the electron candidate cluster. Test beam data for electrons and pions shown, as well as electrons from the sample mentioned above. Both distributions e fairly well and HAD/EM has good pion rejection.

Lateral shower profile

shower development in the electromagnetic calorimeter must be characteristic of an tromagnetic process. We define the Lshare variable, which is a chisquare-like lateral ver profile measuring the energy deposition in towers adjacent to the seed tower of electromagnetic cluster. The lateral shower profile in the calorimeter is equivalent to cal isolation requirement of electron candidates, since the EM cluster is essentially % contained in a single tower. This variable is defined as

$$Lshr = 0.14 \sum_k \frac{M_k - P_k}{\sqrt{0.14^2 E + (\Delta P_K)^2}}$$

re the sum is over the towers adjacent to the seed tower, M_k is the measured energy he adjacent tower, P_k is the expected energy in the adjacent tower predicted using impact point z in the proportional chamber(CES), the event vertex and a shower file parametrization obtained from testbeam measurements, E is the electromagnetic rgy in the 3-tower segment and δP_k is the error in P associated with a 1 cm variation he impact point. The factor 0.14 $\sqrt{E}$ is chosen to normaliize the energy difference P_k relative to the statistical fluctuation inherent in the energy measurement of elecnagnetic showers. For most events δP_k is small since the CEM has full containment 9%) for showers more than 2 cm away from a boundary.

Strip chamber variables

lescribed in section 2.2.3, a gas proportional chamber (CES) is located close to shower imum in the central electromagnetic calorimeter. This chamber is used to determine shower center and to quantify the cleanliness of the electron signal. The shower iles across the strips and across the wires are separately fitted to parameterizations ved from 50 GeV/c testbeam electron data[37]. In the strip view for instance, the ng procedure obtains the z-coordinate of the shower center, Z_{CES}, and the strip ter energy E_s by minimizing the function:

$$X^2(z, E) \stackrel{\text{def}}{=} \sum_{i=1}^{n} \frac{(E_i^{meas} - E\, q_i^{pred}(z))^2}{\sigma_i^2(z)} \tag{4.1}$$

re the sum extends over $n = 11$ channels. The E_i^{meas} represent measured channel rgies, whereas the $q_i^{pred}(z)$ are predicted energies normalized to 1 and corresponding given z-coordinate of the shower center. Fluctuations in a single channel response taken as

$$\sigma_i^2(z) = (0.026)^2 + (0.096)^2\, q_i^{pred}(z) \tag{4.2}$$

ation 4.2 has been obtained from 10 GeV/c testbeam electron data. Since shower tuations and the location of shower maximum both vary with energy, the variance of annel response can also be expected to depend on energy. However, this dependence ommon to all channels and hence does not affect the fitting.

To test a single electron or single photon hypothesis, one introduces the variable:

$$\chi^2_{Strips} \stackrel{\text{def}}{=} \frac{1}{4}\left(\frac{E_{CEM}}{10}\right)^{0.747} \sum_{i=1}^{n} \frac{(q_i^{meas} - q_i^{pred}(Z_{CES}))^2}{\sigma_i^2(Z_{CES})} \tag{4.3}$$

re $\{q_i^{meas}\}_{i=1}^n$ is the measured strip profile normalized to 1. The E_{CEM}-dependent or in front of the sum sign compensates for the aforementioned energy dependence χ_i^2 (E_{CEM} is the electron energy measured from the CEM cluster, which has better lution than the CES measurement E_s).

The treatment of the wire view is entirely analogous to that of the strip view consists in calculating the local x-coordinate X_{CES} of the shower center and the esponding goodness of fit variable χ^2_{Wires}. A plot of the average CES chisquare $_{rips} + \chi^2_{Wires})/2$ is shown in figure 4.2 for 50 GeV testbeam electrons and pions, and electrons from $W \rightarrow e\nu$. The χ^2 cut is made to remove a potential contamination n pion overlap backgrounds in a sample.

We also require a match between the EM cluster position as measured by the strip mbers and the extraplated track coordinates.

$$\Delta X = X_{extrap} - X_{CES} \quad (4.4)$$

$$\Delta Z = Z_{extrap} - Z_{CES} \quad (4.5)$$

re X_{extrap} and Z_{extrap} are the coordinates of the electron track extrapolated to the us of the strip chamber. These variables help reject fake electron signals caused by a ged pion track which overlaps with a neutral pion showering in the electromagnetic rimeter.

Energy-momentum ratio

trons are expected to have a good agreement between the electromagnetic energy a track in the central tracking chamber. We use the ratio of the calorimeter energy he electron track momentum of the highest momentum track associated with the cluster, $E/P = E_T/P_T$, in order to verify the matching between the EM custer and CTC measuement of the electron energy. This ratio is calculated from the corrected gy and beam constrained momentum.

The presence of a small tail at higher E/p due to hard synchrotron radiation which ers the value of the momentum(p) detected in the central tracking chamber, while ing a smaller effect on the energy E because most of the radiated energy is deposited he same calorimeter cell with the electron shower.

ause high energy electrons tend to radiate in the detector, and since the CTC only sures the charged track momenta wheres the calorimeter caputures most of the ated energy, we expect the mean of the E/p distribution to be slightly above 1.

Variable	Tight	Loose
E_T	$>$ 20 GeV	$>$ 20 GeV
P_T	$>$ 10 GeV/c	$>$ 10 GeV/c
HAD/EM	$<$ 0.05	$<$ 0.055+0.045E_T/100
E/P	$<$ 1.5	$<$ 4.0
L_{shr}	$<$ 0.2	$<$ 0.2
Δ_x	$<$ 1.5 cm	$<$ 1.5 cm
Δ_z	$<$ 3.0 cm	$<$ 3.0 cm
χ^2_{strip}	<15	

Table 4.1: Central electron selection requirement

Isolation

require that an absence of additional particles around the electron, since electrons ing from the top-decay are expected to be isolated. We require that at least one ral lepton in the event be isolated in the central tracking chamber. This will be ribed in section 4.3 of this chapter.

Table 4.1 summarizes the central electron selection criteria. The distributions of the tification variables before cuts are shown in Figure 4.3, 4.4, 4.5, 4.6, 4.7, and 4.8 electrons from a sample of $Z \rightarrow ee$ events. In the same figures, we also show the ribution for electrons coming from $W-$ and b-decays from top Monte Carlo. The ral electron detection efficiency determined from $Z \rightarrow ee$ events is 87% and 94%, ectively for the tight and loose selection cuts, as we see in Section 6.2.1.

Conversion removal

reject electrons from photon conversions and π^0 decays by requiring that the electron lidate has a VTX track and that the second oppositely charged track forming an ctive e^-e^+ mass less than 0.5 GeV is not present. The number of nonconversion trons mistakenly rejected by the algorithm depends on the density of tracks near the tron. It is estimated that approximately 4 % of prompt electrons are rejected by e requirement. We have taken into this correction in the acceptance calculations.

Fiducial cuts

following regions are excluded in order to ensure the quality of electrons.

- The seed tower of the electron cluster must be one of towers 0-8 of the central electromagnetic calorimeter.The tower 9 has a different shape from other central calorimeter towers and the electron responce varies significantly with the z position in the tower.

- The shower position in the strip chamber must be at least 9 cm away from the Z=0 plane in order to exclude the 90° crack region.

- The extrapolated track position at the strip chamber(=184 cm) must be at least 2.5 cm away from azimuthal boundaries between central calorimeter wedges(15° boundaries).

.4 Plug Electron Identification Variables

plug electrons must satisfy the following requirement:

HAD/EM

use the same quantity as the central electron's as stated above.

Lateral shower shape: $\chi^2_{3\times3}$

teral shower distribution variable ($\chi^2_{3\times3}$) measures the deviation of the shower from predicted shower shape obtained from test beam. We use a 3×3 array of calorimeter since most of electron shower is confined in this size.

VTX hit occupancy

use the position information in the VTX, which gives good position in the θ coordi-, but poor position resolution in ϕ. Given the cluster position and the event vertex, define a road where we would expect the electron go through the VTX active region look for hits on the wires along this road. The fraction of actual hits to expected is used to distinguish electrons from photons and required to be greter than 0.5.

Table 4.2: Plug electron selection requirement

Variable	Cut
E_T	$>$ 20 GeV
HAD/EM	$<$ 0.05
$\chi^2_{3\times3}$	$<$ 3.0
χ^2_{depth}	$<$ 15.0
N_{VTX}	$>$ 0.5
Track	one and only one CTC track
$N_{\mathrm{axialsuperlayer}}$	$>$ 3
Isolation	$<$ 0.1

Track requirement

and only one track associated to the EM cluster is required to be well reconstructed hree CTC by demanding a minimum number of hits above 3. There must be no tional three-dimensional track with P_T >1.5 GeV/c within a cone of radius 0.25 nd the electron track. This is required because we see some plug electrons with a ch of tracks pointing to an EM cluster, which identifies to be a jet. Figure 4.11 shows track finding efficiencies which satisfy track quality cuts. In the region $1.2 <| \eta |$ 4 fewer CTC layers are available for pattern recognition as shown in Figure 4.11.

Isolation

$(E_C - E_T)/E_T$, where E_C is the total transverse energy within a cone of radius 0.4

$- \phi$ space centered on the cluster and require I <0.1.

Fiducial region

- The position of the seed tower of the electron cluster must not be in three outer tower annuli nor in two inner tower annuli. This means that it should be within a psudo-rapidity range of 1.32 $<\eta_d<$2.22.
- The posiition of the cluster centroid must be at least 5° away from azimuthal boundaries between the quadrants.

Table4.2 summarizes the plug electron selection cuts. The efficiency of these require-ts are calculated from $Z \rightarrow ee$ events and it is 85% (See Section 6.2.1).

2 Muon Identification in CDF

ns are identified by their ability to penetrate many hadronic interaction lengths of rber with minimal energy loss. Both carlorimeter and tracking information are used lentify muons by requiring that the tower to which a track extrapolates has energy gy deposition consistent with that of a minimum ionizing particle. This requirement rress backgrounds from hadrons that interact in the calorimeters. High P_T muons be efficiently found in the rapidity region $| \eta |$ <1.2, covered by the central and vall calorimeters, and where the tracking information is available from the CTC. If track goes into the region $| \eta |$ <1.0 where the muon chambers are instrumented, atch between the CTC track and the muon chamber segment can be used to re- backgrounds. The confirmation by additional CMP chambers also make possible educe the backgrounds. The presence of a muon chamber segment is also useful online-triggering of muons. If the muon has no associated muon segment track, the tion cut is imposed in order to reject backgrounds instead of using the muon seg- t information. We call muons with and without a muon chamber track as CMUOs tral muon objects) and CMIOs (central minimum ionizing objects), respectively.

Fiducial Region

ensure the energy deposited is well measured, fiducial cuts are imposed. The same cial cuts defined for electrons are applied on CMIOs to avoid cracks between calorime- modules. No explicit fiducial cuts are applied on the muon-chamber muons, since ks going through cracks are naturally avoided. This requirement defines a muon cial volume that covers 85 % of solid angle for $|\eta| < 1.2$.

.1 Identification variables

describe the parameters which characterize muons in this section.

Minimum ionization requirement

demand that the energy deposite to calorimeter be consistent with that of a minimum- ing particle. Energy deposite of the muon to the calorimeter tower must be less 2.0 GeV in the EM compartments and less than 6 GeV in the hadronic compart- ts. We also require that a sum of EM and hadronic energy deposite must be above GeV. Figure 4.12 shows energy deposited to the EM and HAD compartments for eV/c test-beam muons. On the average a minimum ionizing particle deposites 0.3 in the EM and 2 GeV in the HAD calorimeters.

Track requirement

CTC track for the muon candidate must have an impact parameter $|d_0| < 0.3$ cm re $|d_0|$ is the distance of the extrapolated track trajectory from the beam axis at point of closest approach. A match between the CTC track and the primary vertex g the beamline must also be less than 5 cm. These cuts are placed to reject occa- al tracks from cosmic rays and from muons coming from decays in flight of kaons pions. In addition, we require at least 3 axial and 2 superlayers and the sum of both reater or equal to 6 to ensure the quality of tracks.

Match between the CTC track and the muon chamber track

the CMUO, an additional requirement of matching between CTC track and muon nent track in $R-\phi$ plane(Δ x) is imposed. Muons must satisfy either of $\Delta x(CMU)$ cm or $\Delta x(CMP)$ <20 cm or $\Delta x(CMX)$ <20 cm.

solation

require that at least one central lepton in the event be isolated in the central tracking nber. This will be described in section 5.3. We require the absence of additional icles around CMIOs. The transverse energy in the towers within a cone of 0.4 uding the muon energy must be less than 5 GeV.

Table 4.3: Central muon selection requirement

Variable	CMUO cuts	CMIO cuts
P_T	> 20 GeV	>20 GeV
η range	< 1.0	<1.2
EM energy	< 2 GeV	<2 GeV
HAD energy	<6 GeV	<6 GeV
Impact parameter	<3 mm	<3 mm
Z-vertex match	<5 cm	<5 cm
Δx (CMU)	<10 cm	
Δx (CMP)	<20 cm	
Δx (CMX)	<20 cm	

Cosmic ray removal

cosmic ray events have tracks which are back-to-back in three dimensions in the cen- tracking chamber. Also, they do not normally pass close to the interaction region, e their impact parameter distribution is relatively flat. Reconstruction of the cosmic racks as it goes towards the CTC center is generally worse than for tracks emanating the center, because the time-of-flight corrections are wrong. By looking for a poor ty tracks back-to-back with the muon candidate rejects the majority of cosmic rays.

classify CMUOs into two classes: 'tight' and 'loose' muons. The difference be-
n them is that tight muons are required to match to a CMU or CMP track segment, e loose ones are allowed to that the muon type is CMU or CMP or CMX.

3 Lepton Isolation

energy surrounding a lepton depends on the lepton source. Leptons coming from l-Yan process, W's and Z's are said to be isolated in contrast to the nonisolated ons coming from the decay of charm and bottom hadrons which are accompanied uark hadronization and decay products. Leptons from the decay of top quark are cted to be isolated. In the semi-leptonic decay of a W from a top quark will be ted at a large angle with respect to the other decay and hadronization products. on isolation is a powerful tool in detecting leptons from top quark decay in the ence of botom and charm leptonic decays. We define a measure to quantify the nce of the additional particles around the lepton. In the CDF detector the activity nd leptons can be measured both in calorimeter and in the central tracking chamber, ely carolimeter isolation and track isolation.

n the following we show that a track isolation cut will be more efficient for top and ast as good at rejecting background.

ooking at $t\bar{t}$ Monte Carlo with M_{top}=120 GeV/c^2, we see that the calorimeter tion cut keeps 89% of 'direct' ($t \rightarrow W \rightarrow e$) 20 GeV central electrons which pass the dard set of electron identification requirement (figure 4.17 (c)). A track isolation requiring less than 3 GeV of P_T in a cone of 0.25 about the electron does better, ing 94% of the 'direct' electrons (figure 4.17 (a)). These are efficiencies per lepton. uiring both legs in the event to be isolated will double the inefficiency.

ooking at the same Monte Carlo, we can also find the efficiency for all the electrons e event, direct or indirect. Figure 4.17 (b) shows the sum P_T of CTC tracks inside ne of 0.25 for central electrons, and Figure 4.17 (b) shows the calorimeter E_T in a of 0.4 for all central electrons in the $t\bar{t}$ events In both cases, the lepton energy is uded from the sum. Cutting on calorimeter isolation on a single electron keeps 85% hem, cutting on track isolation keeps 91%.

Electrons passing tight cuts, selected inclusively from the high-P_T dilepton sample y loose selection cuts on the second lepton), are enriched in $b \to e$ decays and also ain fakes and, to a much lesser extent, electrons from Drell-Yan and Z. Looking hese electrons, we see that the calorimeter isolation cut rejects 39% of the central tron with E_T above 20 GeV which pass a set of tight electron cuts, while the track tion cut rejects 51% of them. This gives us some indication of how well the two reject background. The track isolation cut is favorable over the isolation cut. rnatively, we can look at EM clusters which have HAD/EM greater than 6%, so we know we are looking at 'junk', and we see that the calorimeter isolation cut ts 82% and the track isolation cut rejects 83%.

Cut	Cone	$t \to W \to e$	$t \to X \to e$	'good' EM cluster	HAD/EM > 0.06
$_T < 5$	0.40	.89	.85	.39	.82
$_T < 3$	0.20	.96	.93	.49	.80
$_T < 3$	0.25	.94	.91	.51	.83
$_T < 3$	0.30	.92	.88	.53	.84

le 4.4: Comparison of tracking and calorimeter isolation variables. The efficiencies rst two columns are from Monte Carlo. The second two, are from data. See text for ils.

We also checked that the cuts did not throw away good electrons by looking at $\to ee$. Putting tight cuts listed in Table 4.1 on both legs of the Z leaves us with 415 ral-central events, or 830 electrons. The track isolation cut keeps 828/830 electrons, e the calorimeter isolation cut keeps 822/830.

Finally, we varied the cone size for the track isolation cut. A summary is given in e 4.4. The numbers are fractions of electrons with E_T >20 GeV which passed the tion cut of given cone size.

We use sum of track P_T in a cone of R=0.25 around the muon, excluding the muon k, <3.0 GeV/c (See Section 5.3).

4 Jets

are characterized by an extended cluster of hadronic and electromagnetic deposition. are reconstructed using an algorithm which forms clusters from the recorded energies osited in the calorimeter towers. In CDF it is an iterative fixed cone algorithm begins by looking for cintiguous clumps of energy, called "pre-clusters", and then ers all the energy within a fixed distance from these pre-clusters. The pre-clustering e begins by combining contigous towers with Et >1 GeV. This relatively high tower shold is designed to eliminate clusters formed from fluctuations in the soft underlying t. Any pre-cluster with Et >3GeV is considered a "seed" for the cluster finder. A e in eta-phi space is drawn around each seed. The radius of this circle is a parameter e algorithm; the default is 0.7. Now, all towers inside the circle and with Et above MeV are included in the cluster. (Once a good seed has been found, a lower threshold ed to allow the algorithm to gather the maximum fraction of the jet energy and efore have the best possible energy resolution. The 100 MeV threshold is well above electronic noise level for the calorimeter in CDF.) The position off each cluster is lculated using the Et weighted centroid of all towers in the cluster. A new circle is ted until stable. If two clusters have more than 75 % of their towers in common, the ers are merged. When a tower is shared by two unmerged clusters, it is uniquely ned to the cluster that is closest in $\eta - \phi$ space.

From the towers associated with the cluster, the quantities (p_x, p_y, p_z, E) are calted. The electromagnetic and hadronic compartments of each tower are assingned sless four-vector with magnitude equal to the energy deposited in the tower and the direction defined by a unit vector pointing from the event origin to the center e face of the calorimeter tower(calculated at the depth that corresponds to shower imum). E is the scalar sum of tower energies; p_x is the sum of $p_{x,i}$ where i is the er index. The transverse energy is deined as $E_T \equiv E \sin\theta$.

5 Missing transverse energy

ays of $t\bar{t}$ events produces neutrinos. Since these particles can not be detected directly, r presence must be inferred by the presence of a large momentum imbalance in the t. The missing transverse energy($\not{E}_T$) is defined to be the negative of the vector of the transverse energy in all calorimeter towers with $|\eta| <3.6$.

$$\not{E}_T = - | \sum_{|\eta|<3.6} \vec{E} |$$

η range is restricted because the low-β quadrupoles of the Tevatron cover part of azimuthal regions for $3.6 < \eta < 4.2$. To be included in the sum, towers must pass nergy threshold requirement of 0.1 GeV for all the carolimeters (This is the same shold as the one used for the jet clustering). Missing E_T measurement is sensitive all s of detector imperfections. Mismeasurement of jets due to finite detector resolution, of energy in cracks and loss of jet down the beamline is the primary source of the ing E_T.

We compute the missing E_T from the 'raw' missing transverse energy $\vec{\not{E}}_{\mathrm{T,uncorrected}}$ as

$$\vec{\not{E}}_{\mathrm{T}} = \vec{\not{E}}_{\mathrm{T,uncorrected}} + \sum_{\mathrm{muons}} (\vec{\mathrm{E}}_{\mathrm{T}}^{\mathrm{muon-tower}} - \vec{\mathrm{p}}_{\mathrm{T}}^{\mu}) + \sum_{\mathrm{jets}} (\vec{\mathrm{E}}_{\mathrm{T,uncorrected}}^{\mathrm{jet}} - \vec{\mathrm{E}}_{\mathrm{T,corrected}}^{\mathrm{jet}}), \quad (4.6)$$

re $\vec{\mathrm{p}}_{\mathrm{T}}^{\mu}$ is the transverse component of the muon momentum vector, $\vec{\mathrm{E}}_{\mathrm{T}}^{\mathrm{muon-tower}}$ is transverse energy measured in the calorimeter tower crossed by the muon. Note we also correct the missing E_T for jets with observed E_T >10 GeV and $|\eta| <2.4$. second sum on the right-hand side is the difference between the corrected jet E_T $_{\mathrm{orrected}}$) and the observed(uncorrected) jet E_T ($\vec{\mathrm{E}}_{\mathrm{T,uncorrected}}^{\mathrm{jet}}$). We will show that the ing E_T corrected for jet energy scale has a better rejection for the backgrounds than g uncorrected quantity in Section 5.6.

The resolution on the $\not{E}_T$ measurement depends on the amount of energy in the t. For minimum-bias events, the resolution for thee two components $\not{E}_{T_x}$ and $\not{E}_{T_y}$ ne $\not{E}_T$ vector can be parametrized as $\sigma(\not{E}_T) = 0.47\sqrt{\sum E_T}$, where

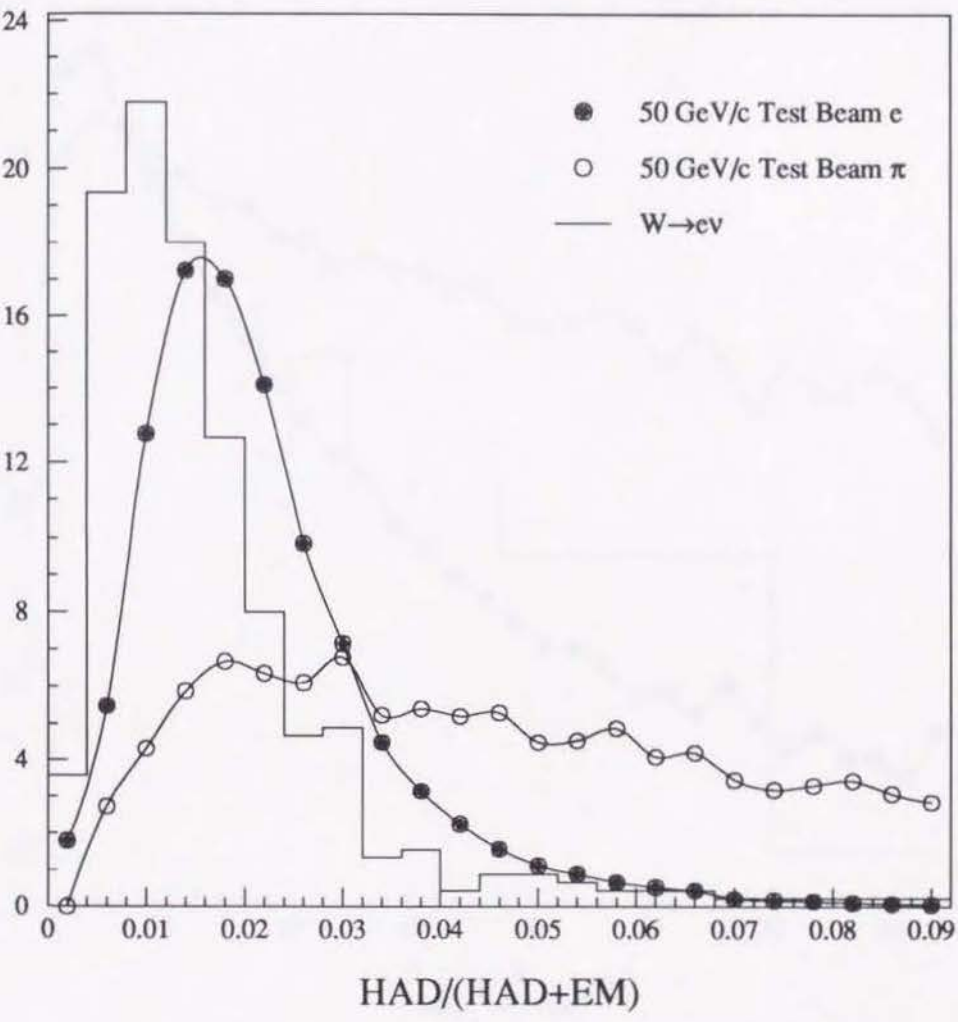

re 4.1: The HAD/(HAD+EM) distribution for 50 GeV testbeam eleectrons and for
rons from W decays. From

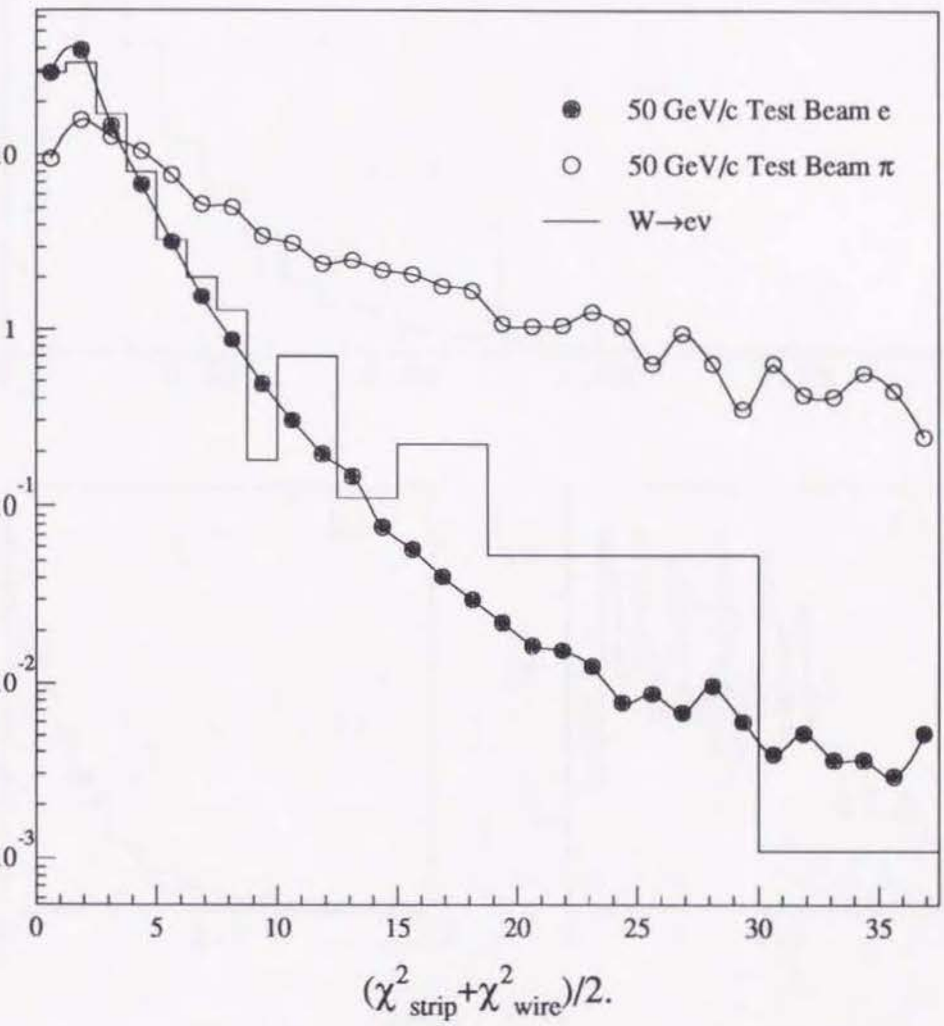

re 4.2: The average CES chisquare distribution for 50 GeV testbeam electrons and ged pions, and for electrons from W decays. From

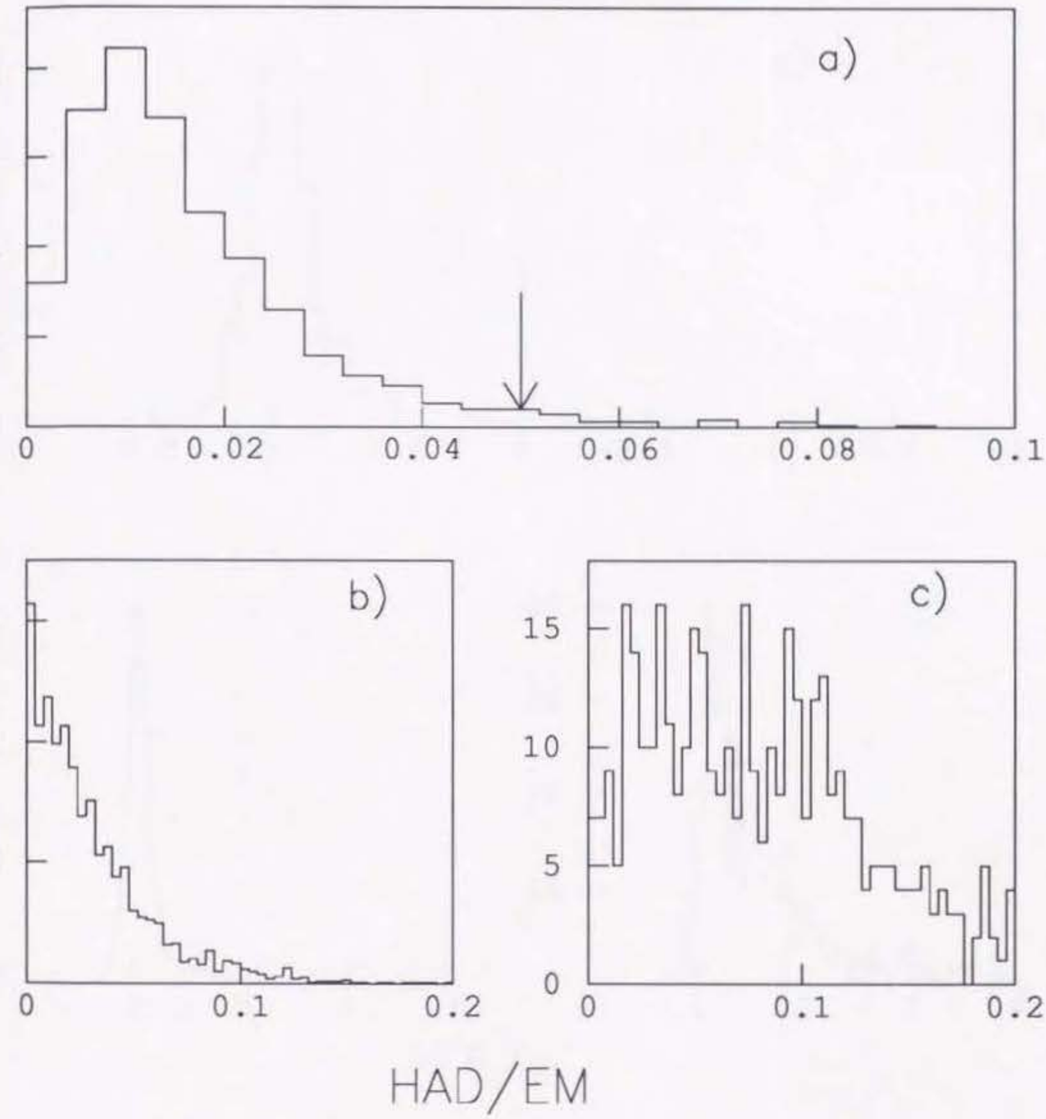

re 4.3: Ratio of hadronic and electromagnetic energy deposition (HAD/EM) for rons from a) $Z \to ee$ decays. Also shown are the values of the cuts for the selection e dilepton analysis. b) and c) are the same variables for electrons from the decays / and from the decays of b, respectively from the $t\bar{t}$ Monte Carlo.

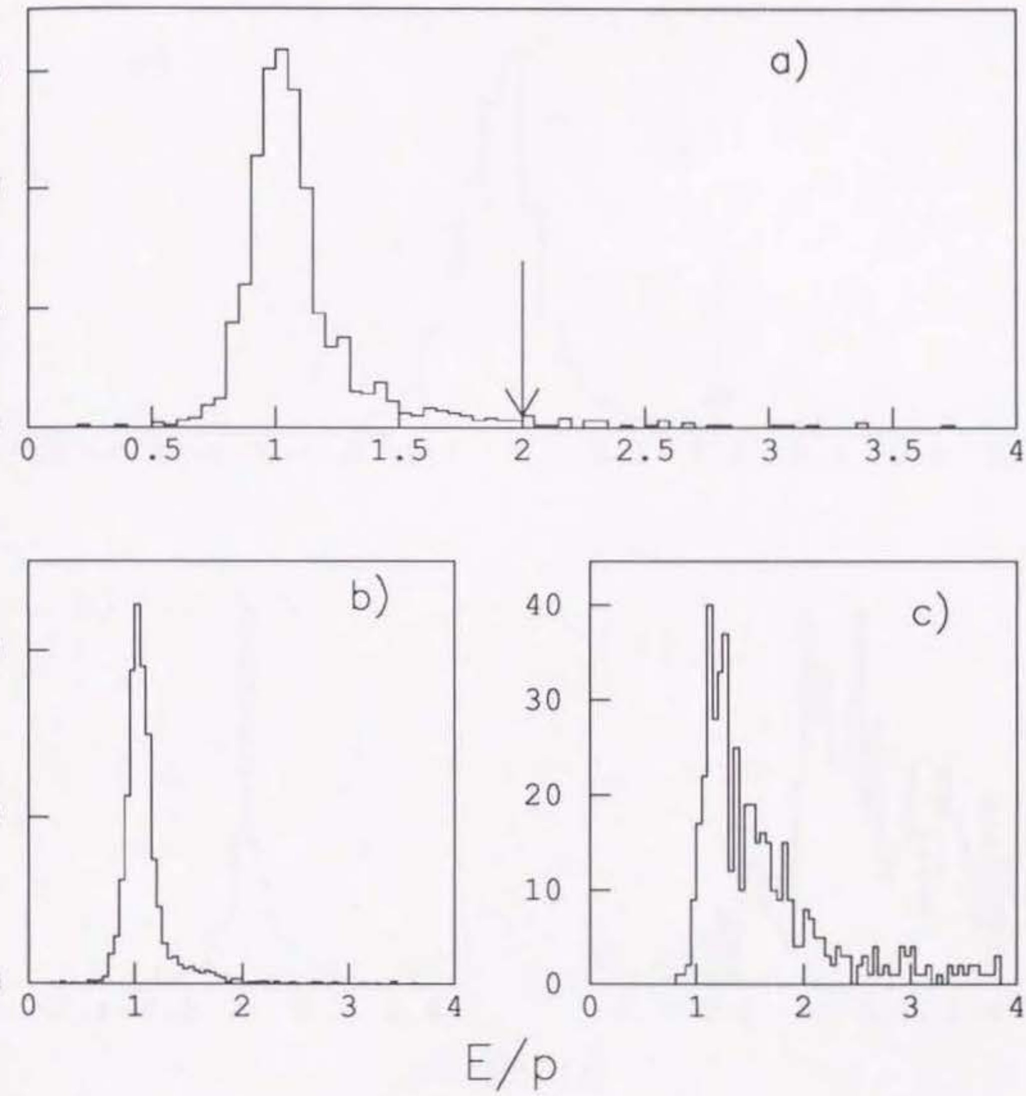

re 4.4: Ratio of calorimeter energy and momentum for electrons from a) $Z \rightarrow ee$ ys. Also shown are the values of the cuts for the selection in the dilepton analysis. nd c) are the HAD/EM distributions for electrons from the decays of W and from decays of b, respectively in the Monte Carlo $t\bar{t}$ events.

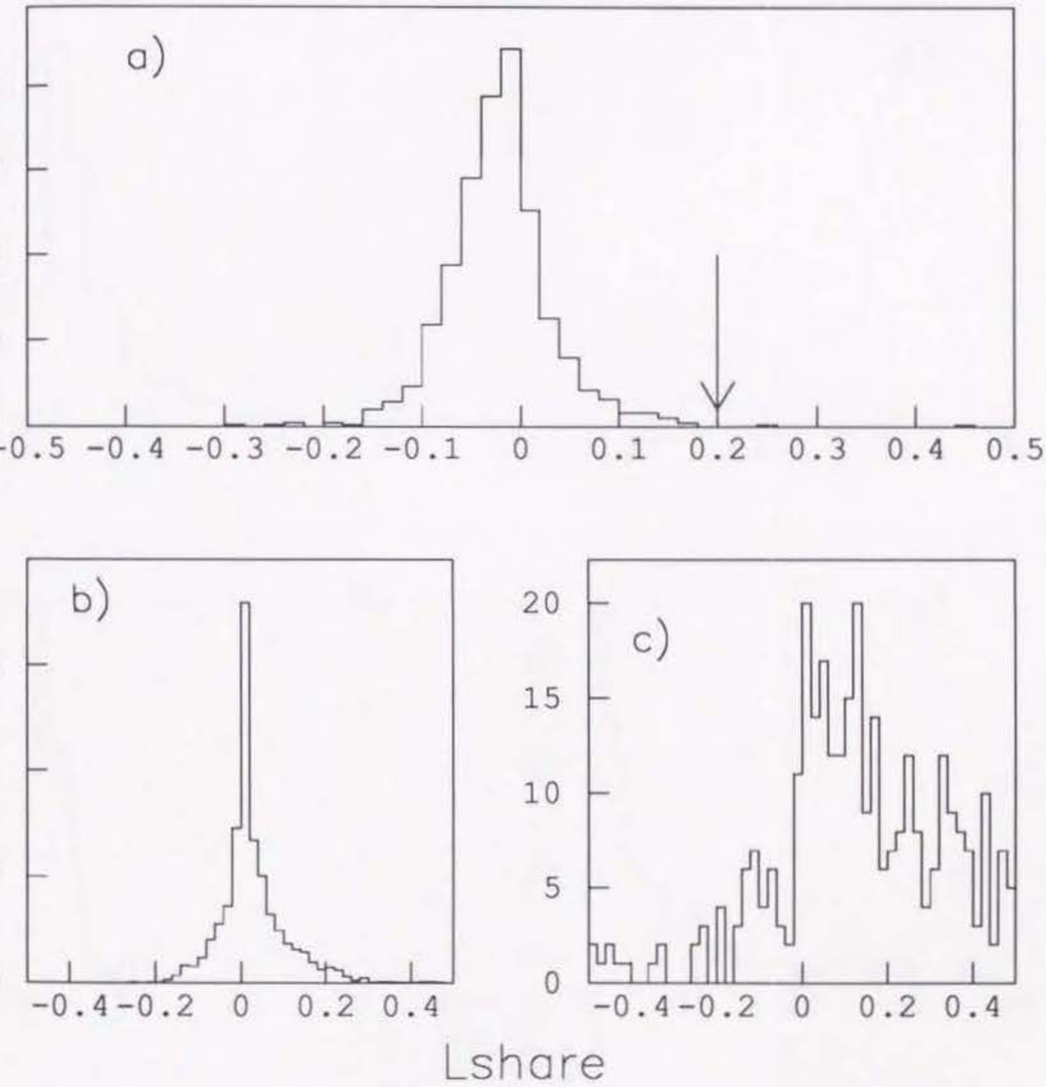

re 4.5: Lateral shower profile for electrons from a) $Z \to ee$ decays. Also shown are values of the cuts for the selection in the dilepton analysis. b) and c) are the same ble for electrons from the decays of W and from the decays of b, respectively in the te Carlo $t\bar{t}$ events.

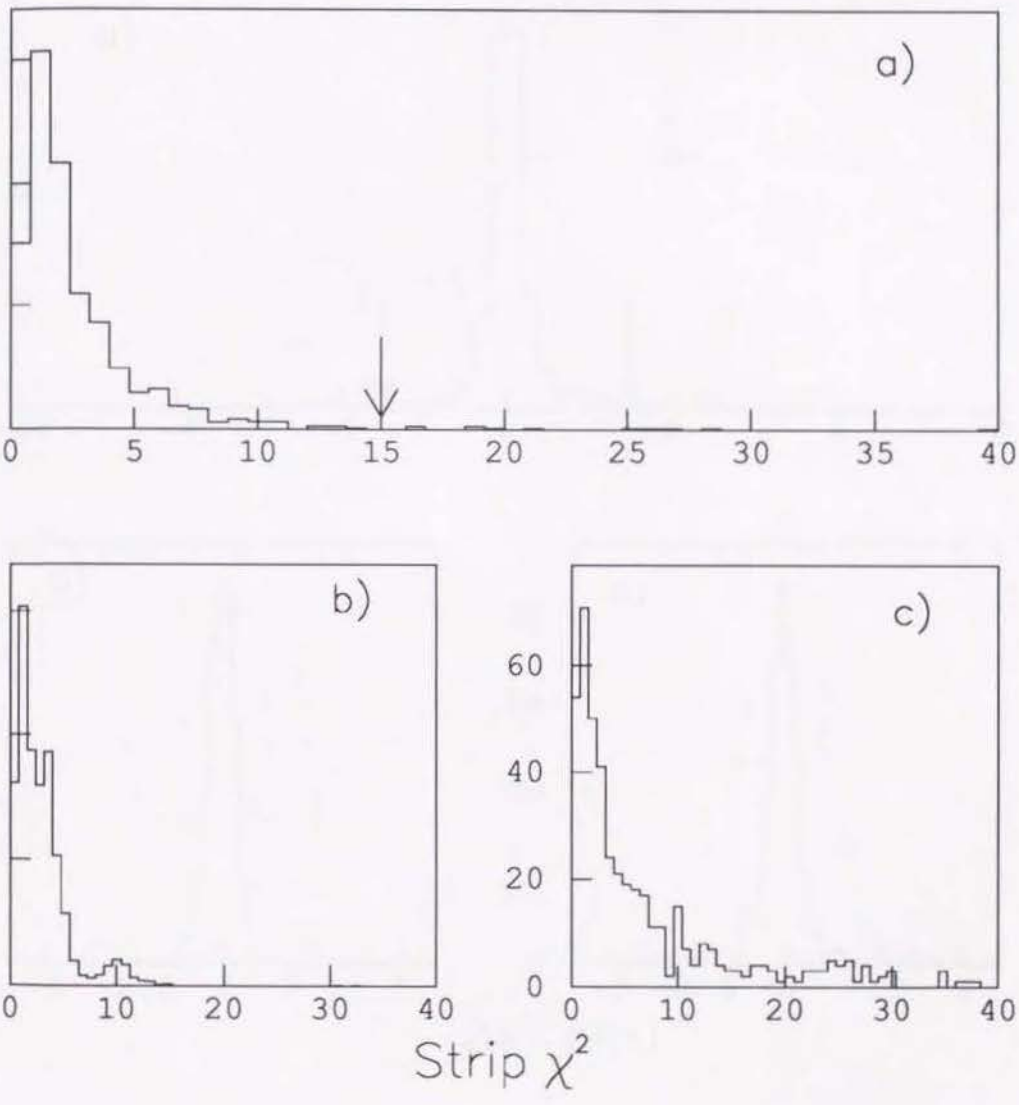

re 4.6: Distribution of χ^2_{strip} for a) $Z \to ee$ events. Also shown are the values of cuts for the selection in the dilepton analysis. b) and c) are the same distributions lectrons from the decays of W and from the decays of b, respectively in the Monte o $t\bar{t}$ events.

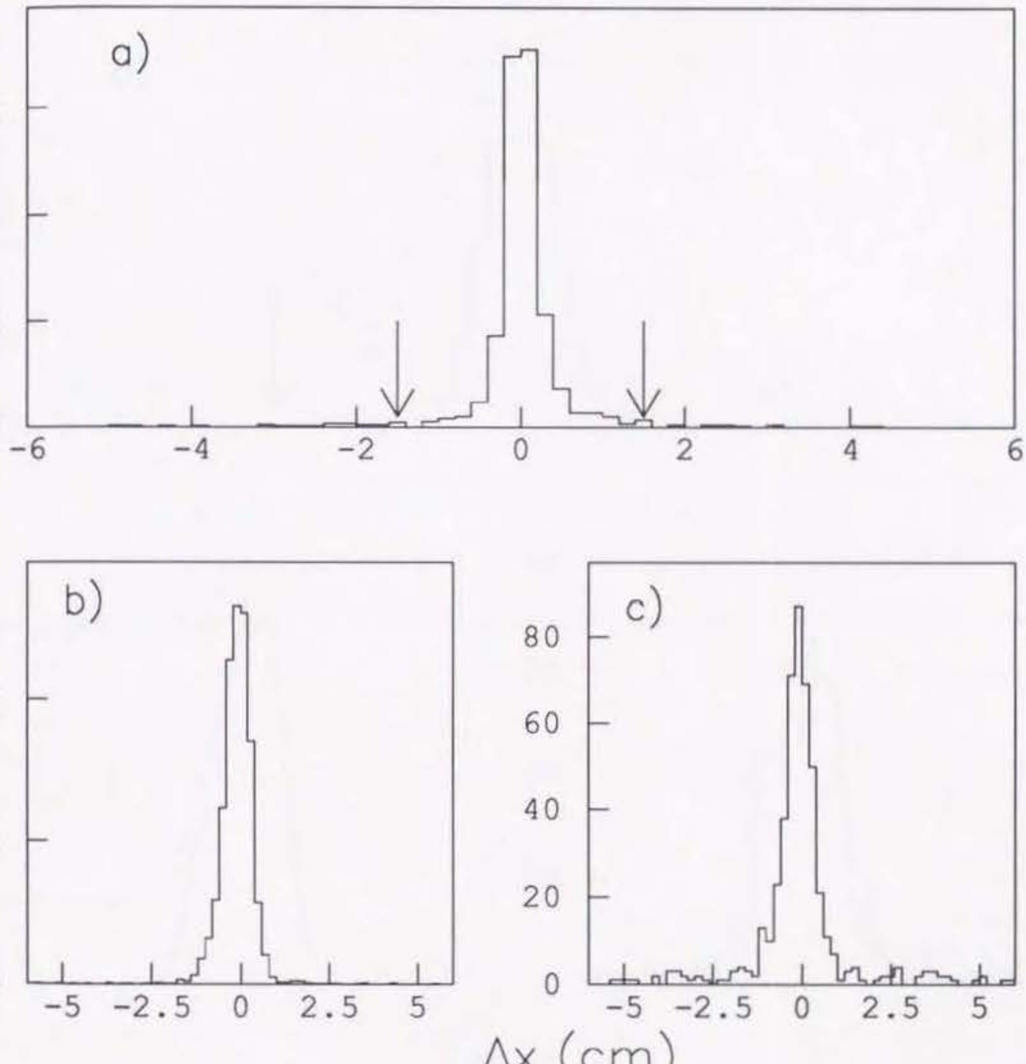

re 4.7: Distribution of match in the $R-\phi$ view between the track and the shower ion as measured in the strip chambers for a) $Z \rightarrow ee$ events. Also shown are the es of the cuts for the selection in the dilepton analysis. b) and c) are the same ributions for electrons from the decays of W and from the decays of b, respectively ie Monte Carlo $t\bar{t}$ events.

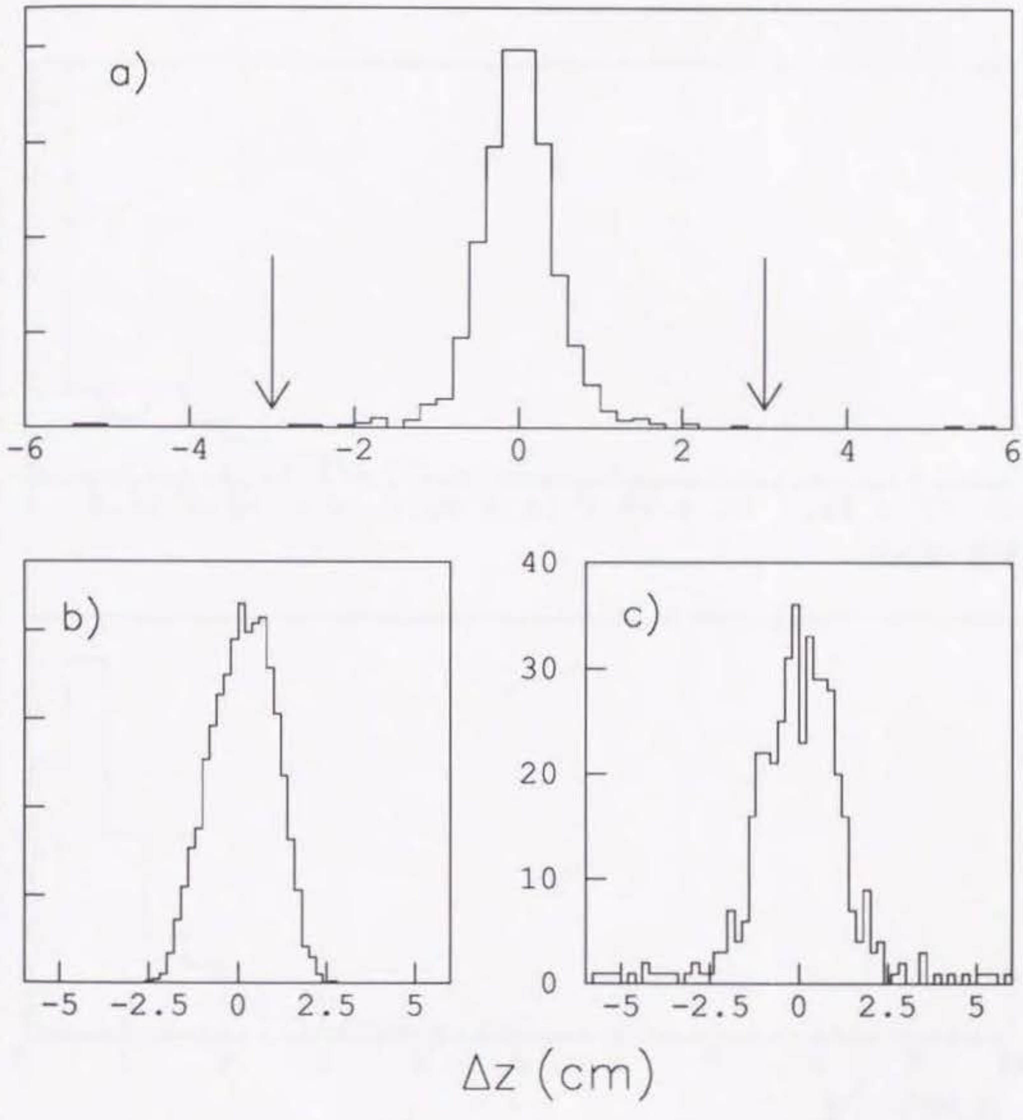

re 4.8: Distribution of match in the z view between the track and the shower position easured in the strip chambers for a) $Z \to ee$ events. Also shown are the values of cuts for the selection in the dilepton analysis. b) and c) are the same distributions lectrons from the decays of W and from the decays of b, respectively in the Monte o $t\bar{t}$ events.

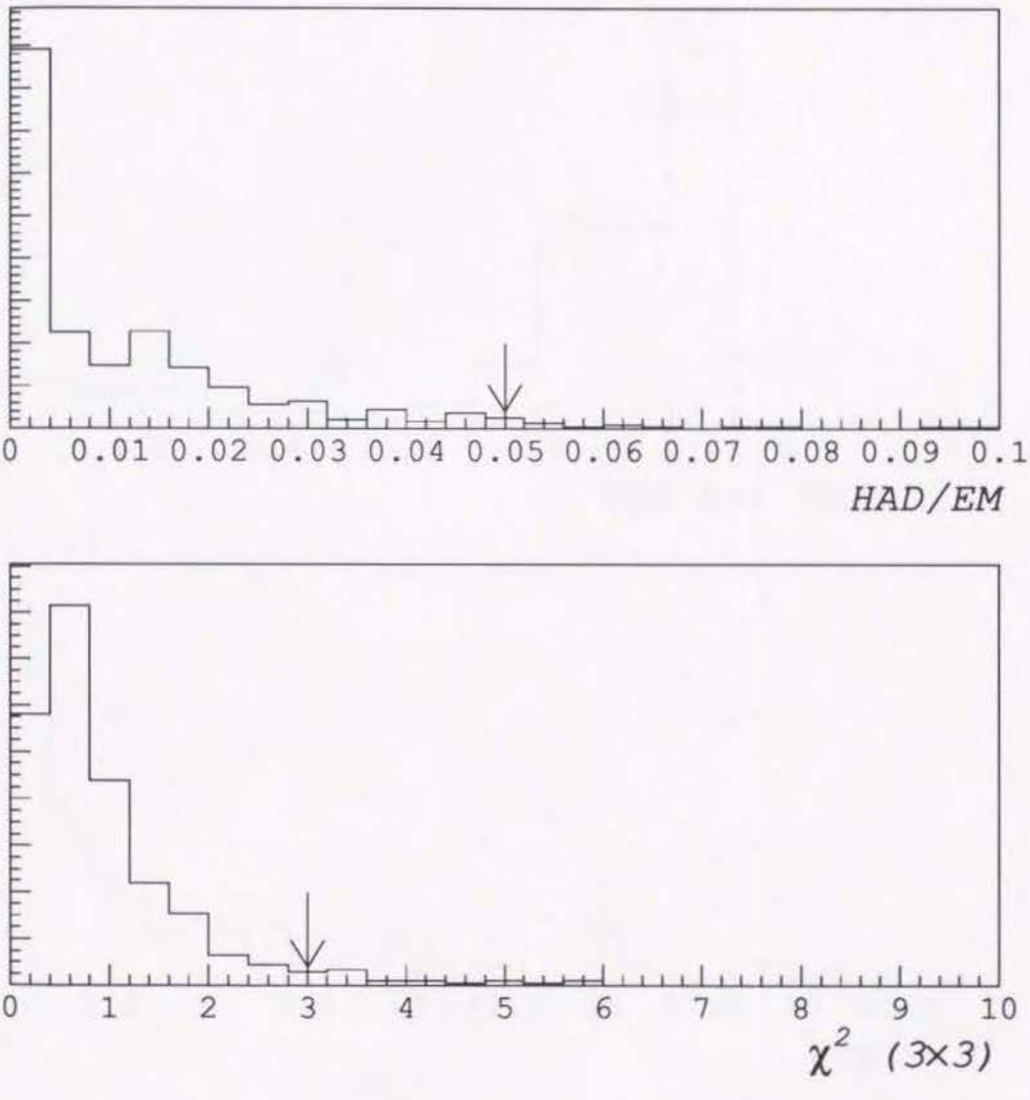

re 4.9: Plug electron quality variables for $Z \rightarrow ee$ events. Also shown are the values
e cuts for the selection in the dilepton analysis.

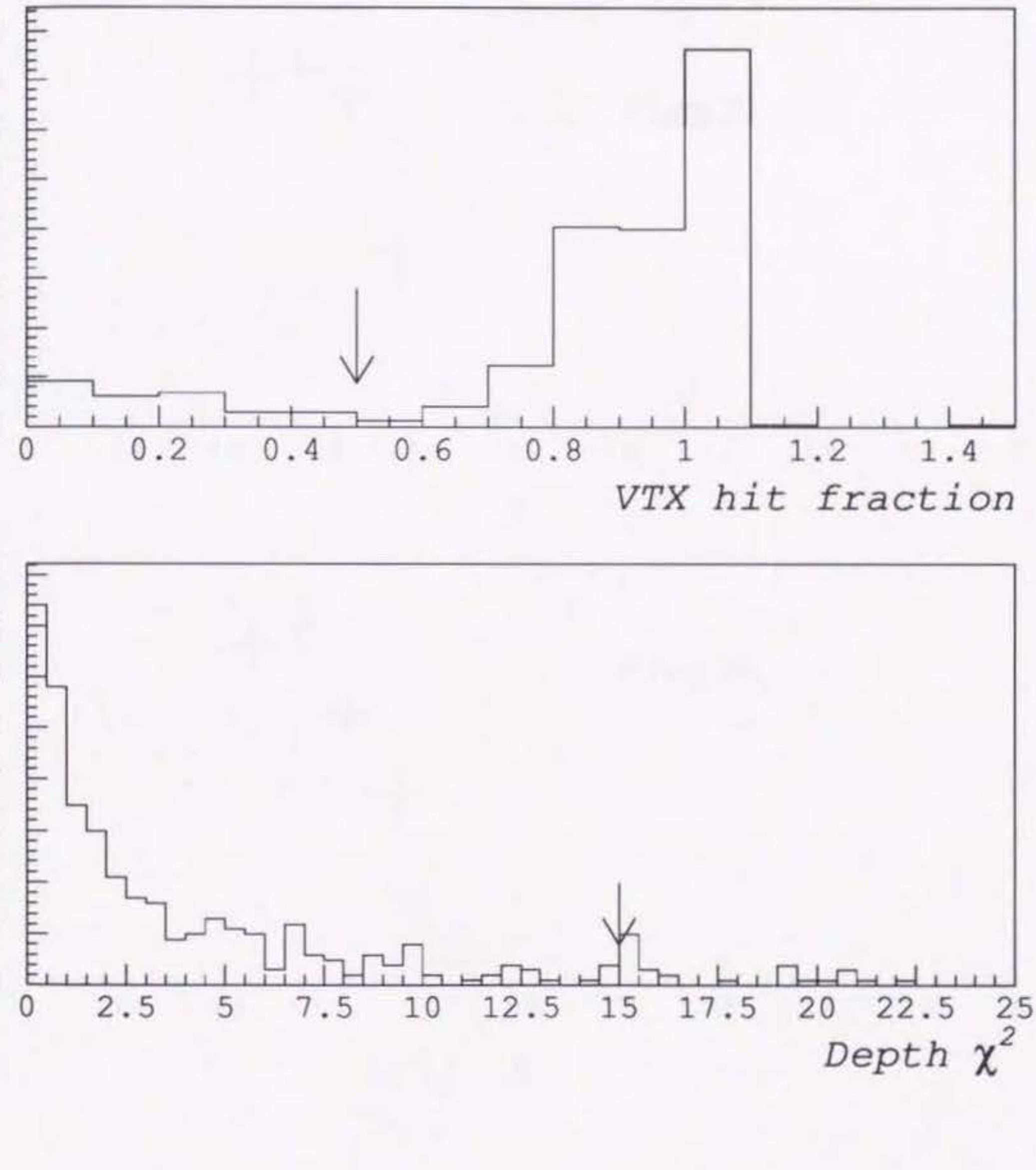

re 4.10: Plug electron quality variables for $Z \to ee$ events. Also shown are the es of the cuts for the selection in the dilepton analysis.

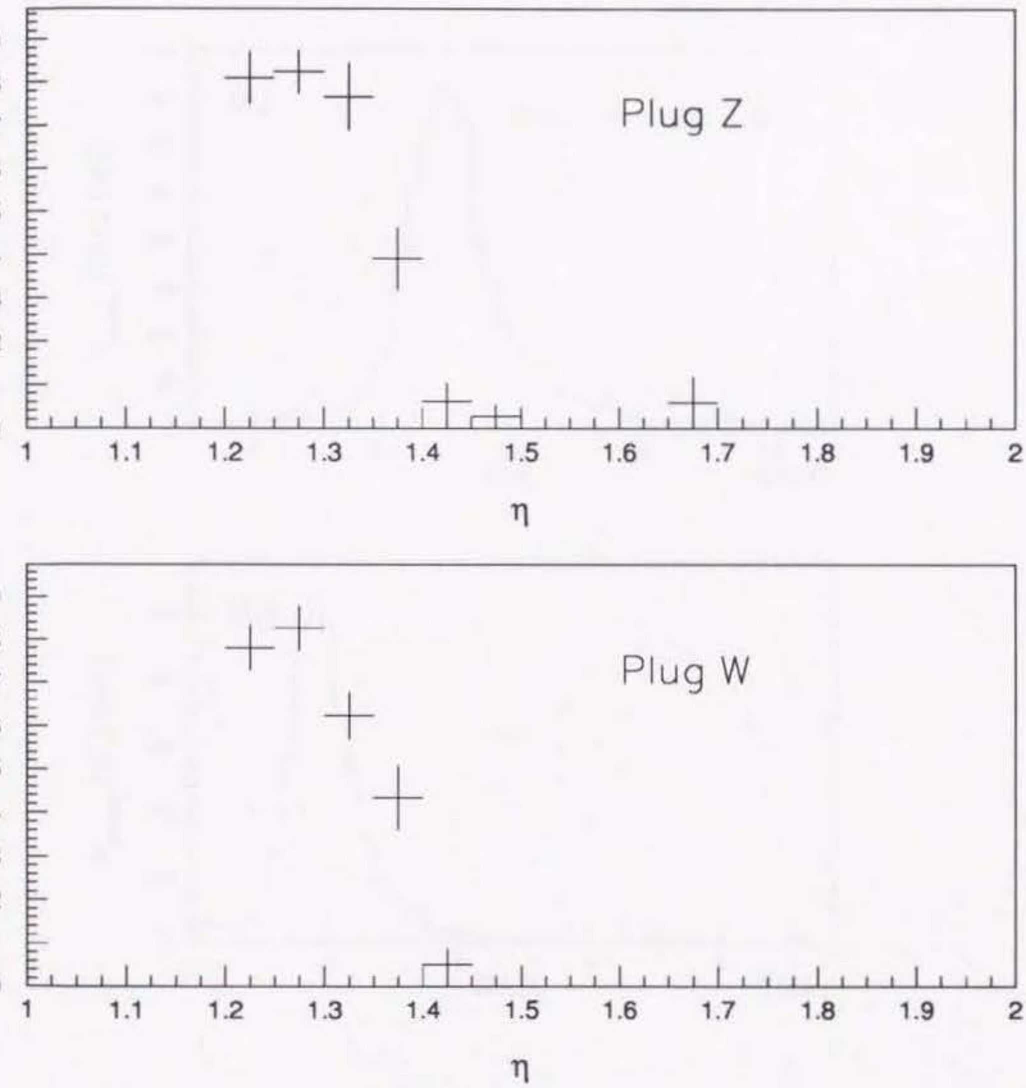

re 4.11: Effiicency for track requirement on plug electrons as a function of pseudo-
dity (η) measured using plug electrons from (a) Z decays and (b) W decays.

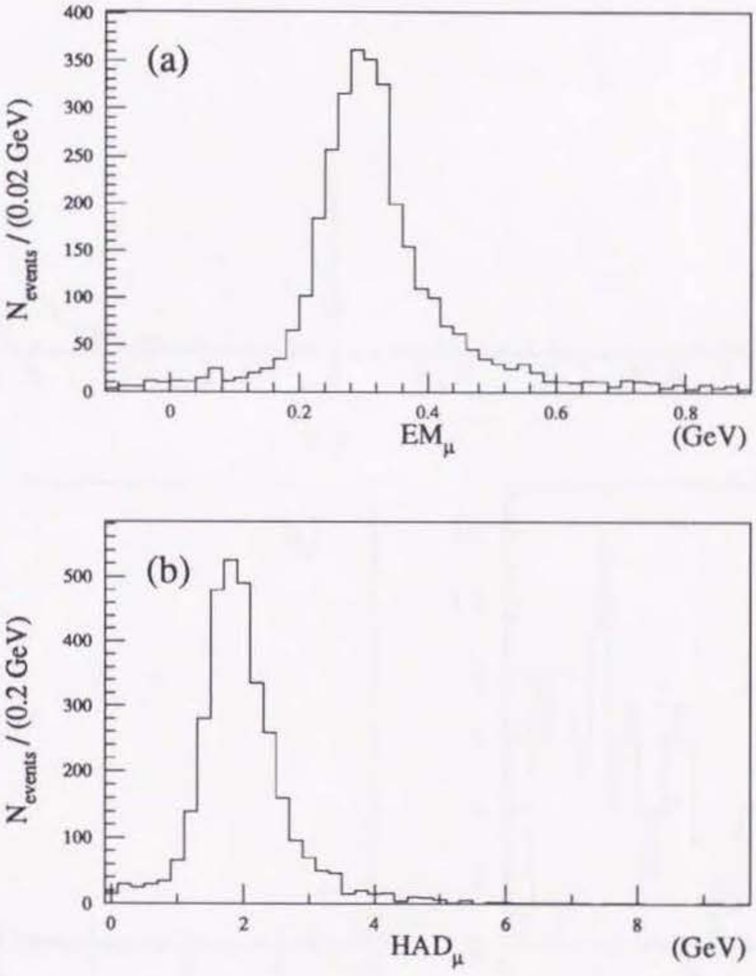

re 4.12: Energy deposited in the calorimeter by test-beam muons: a) electromag- : calorimeter and b) hadronic calorimeter.

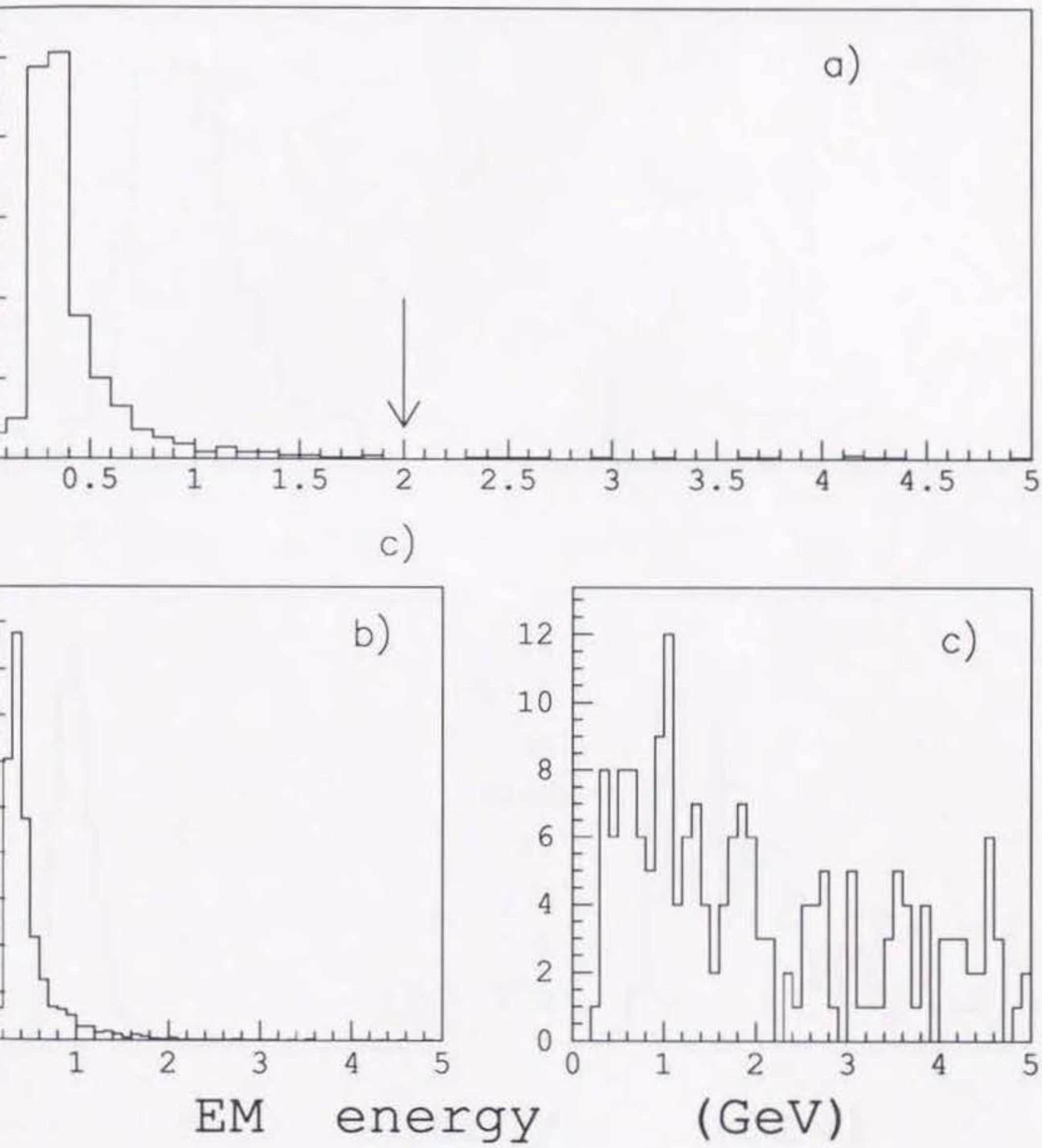

re 4.13: Energy deposited in the electromagnetic calorimeter by muons for a) $Z \rightarrow$ vents. Also shown are the values of the cuts for the selection in the dilepton analysis. d c) are the same distributions for muons from the decays of W and from the decays respectively in the Monte Carlo $t\bar{t}$ events.

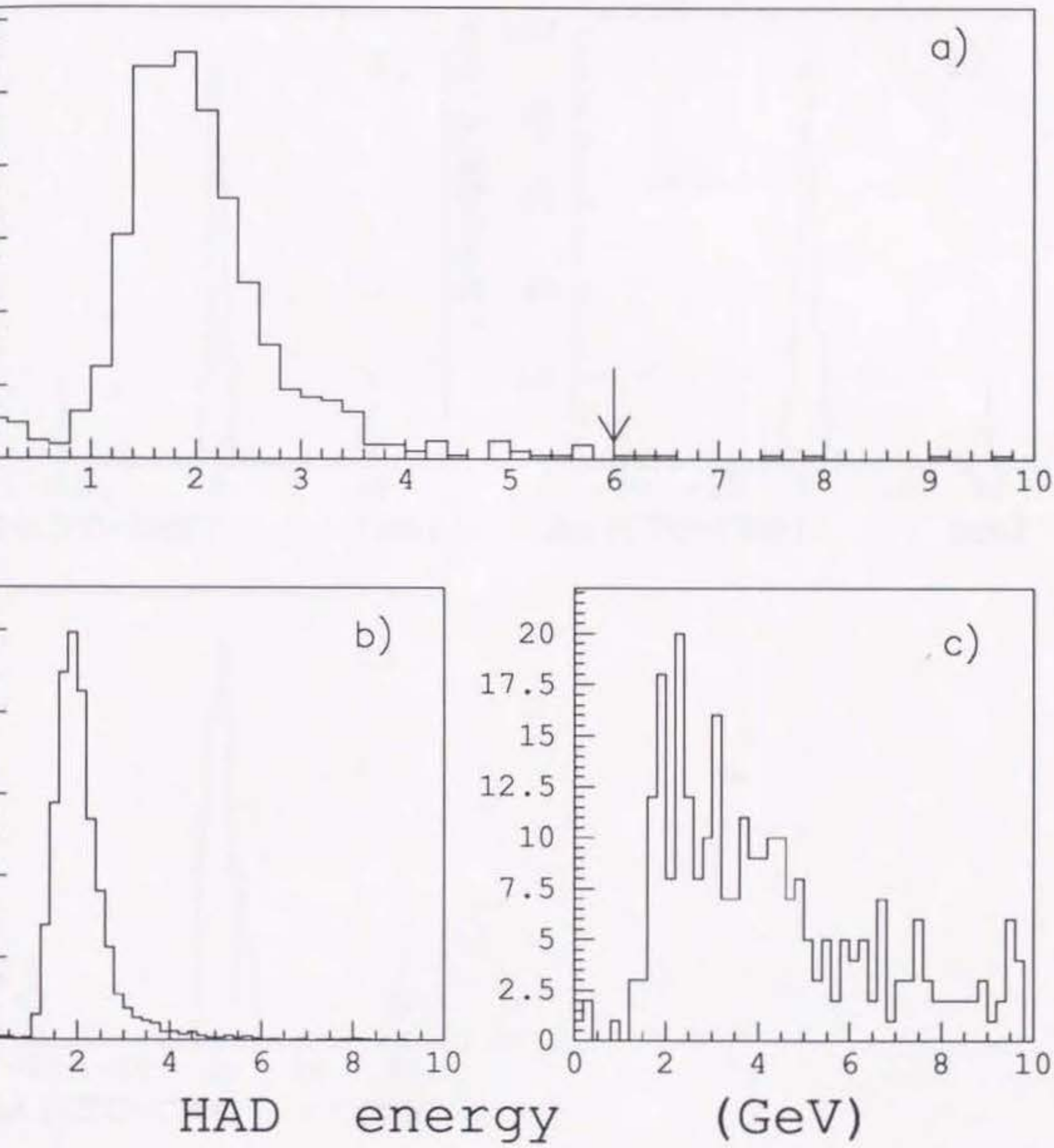

re 4.14: Energy deposited in the hadronic calorimeter by muons for a) $Z \to \mu\mu$ ts. Also shown are the values of the cuts for the selection in the dilepton analysis. d c) are the same distributions for muons from the decays of W and from the decays respectively in the Monte Carlo $t\bar{t}$ events.

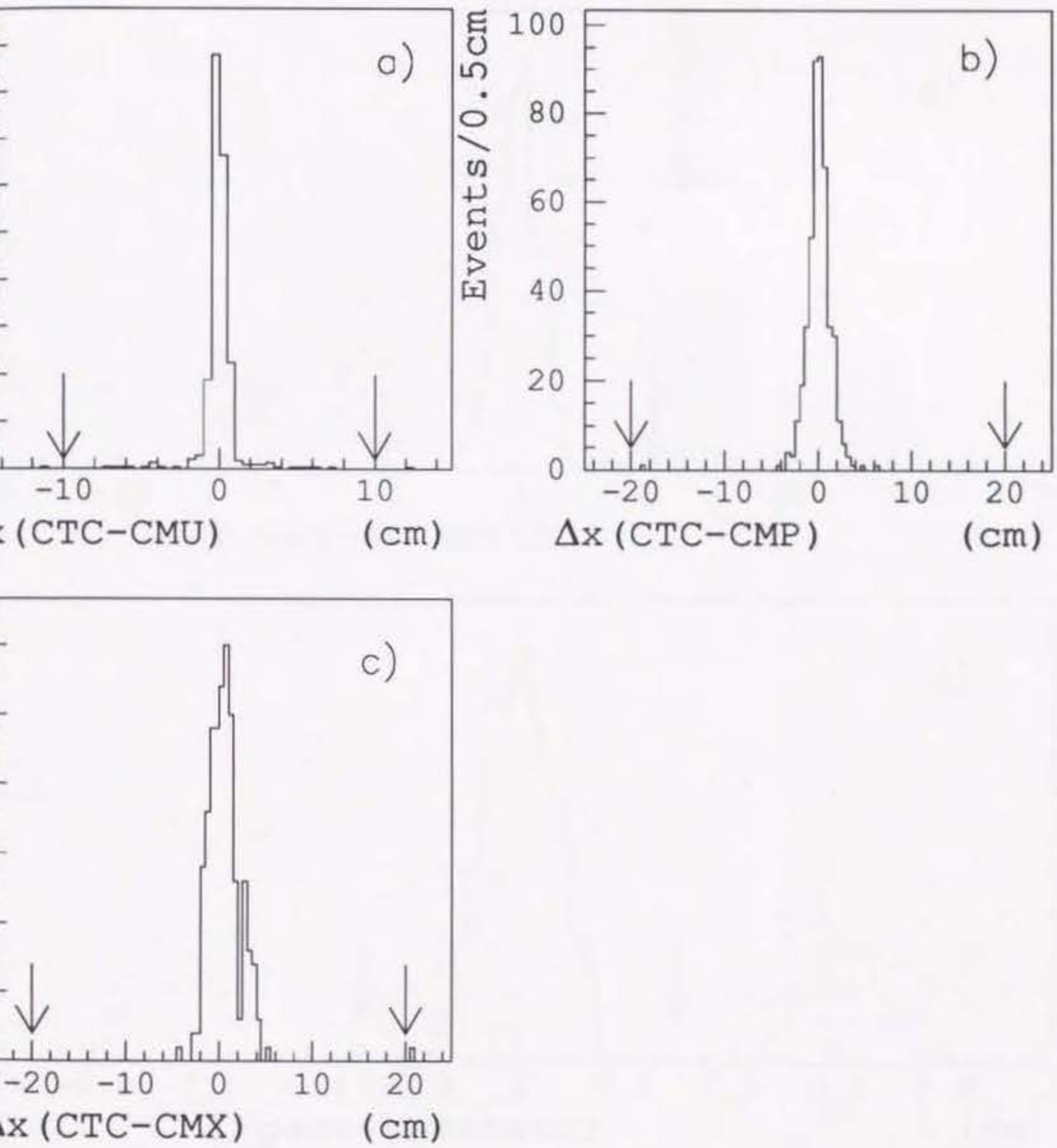

re 4.15: Match (Δ x) between the CTC track extrapolated to the lowest wire plane e muon chambers and the muon chamber track for a sample of muons from Z decays $_T$ >20 GeV/c.

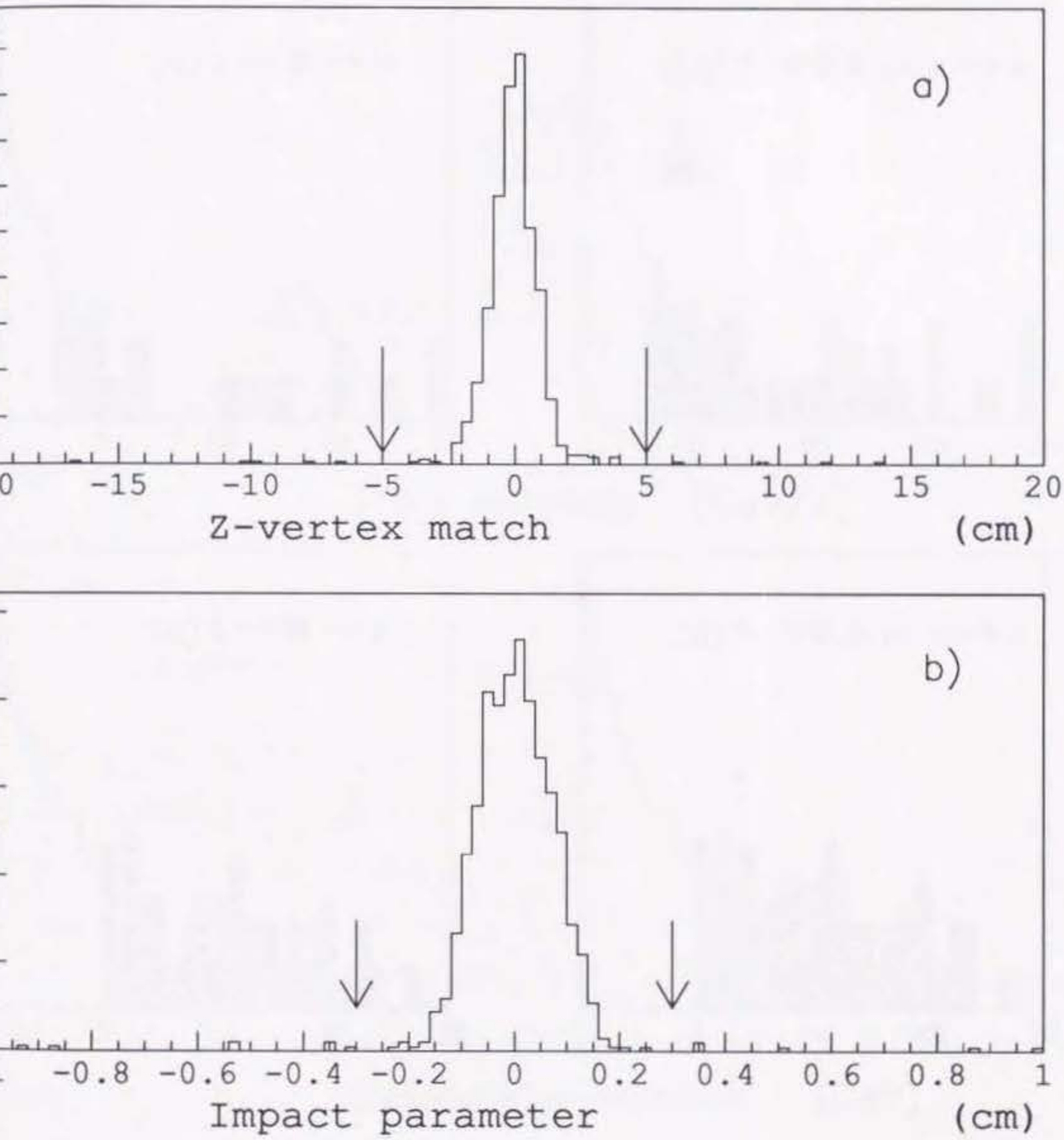

re 4.16: Variables for track quality cuts: a) the track-to-vertex distance along the nline ($Z_{track} - Z_{vertex}$) for muon tracks from the decays of Z. b) the impact parameter nuon tracks from the decays of Z of P_T >20 GeV/c.

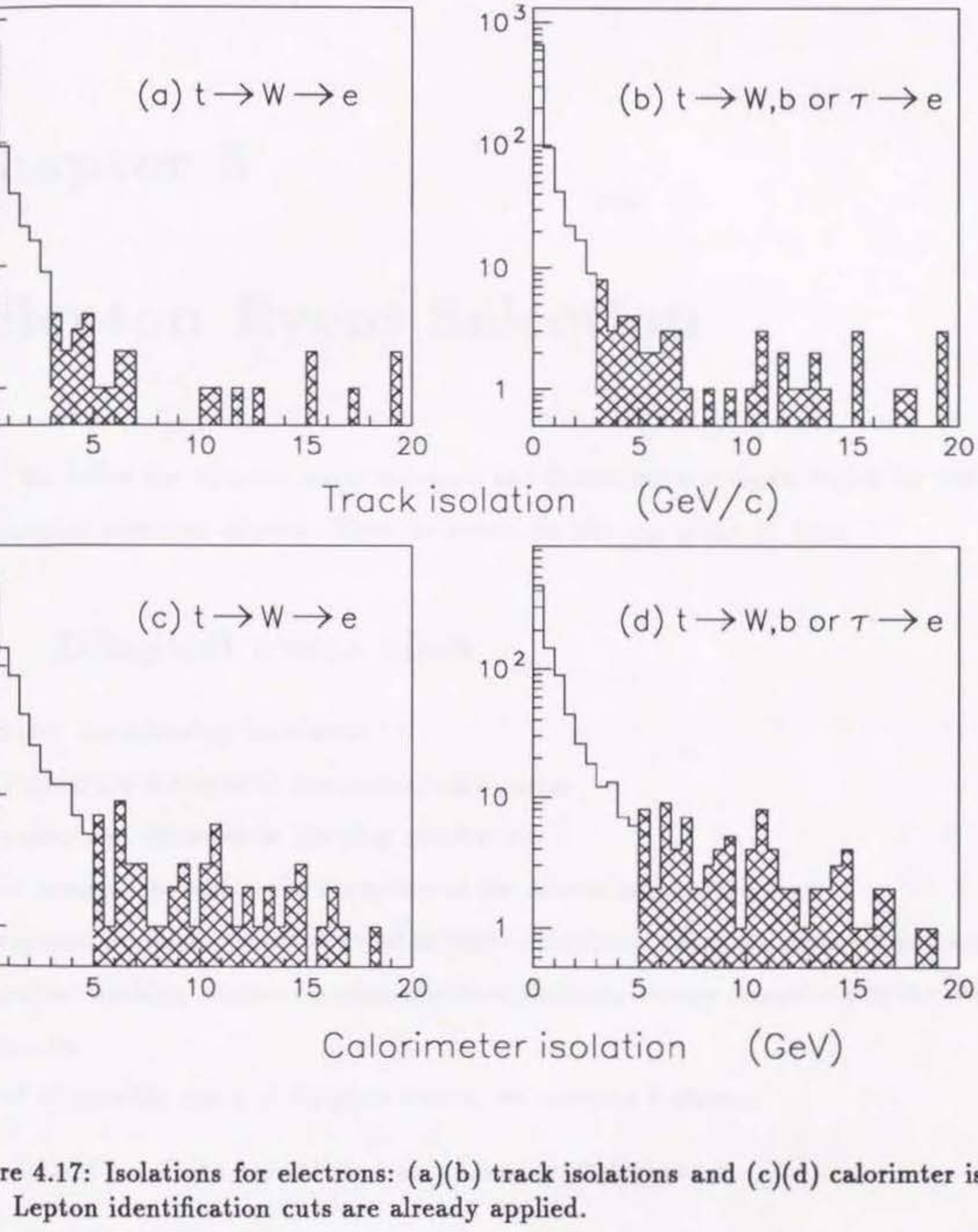

re 4.17: Isolations for electrons: (a)(b) track isolations and (c)(d) calorimter isola- Lepton identification cuts are already applied.

hapter 5

ilepton Event Selection

, we define the dilepton event category and determine our signal region by defining dilepton selection criteria. Then we search for the top quark in data.

Dilepton event class

define the following notations:

= electrons detected in the central calorimeter

= electrons detected in the plug calorimeter

= muons detected in the chambers of the central muon detector

= muons directed outside the central muon chambers, which are detected as tracks in central tracking chamber having minimum-ionizing energy deposition in the central imeter

of 10 possible clsses of dilepton events, we consider 8 classes:

CE-CE Tight central electron - Loose central electron

CE-PE Tight central electron - Plug electron

MU-MU Tight central muon - Loose central muon

MU-MI Tight central muon - Minimum ionizing track (CMIO)

CE-MU Tight central electron - Loose central muon

MU-CE Tight central muon - Loose central electron

CE-MI Tight central electron - Minimum ionizing track (CMIO)

PE-MU Plug electron - Loose central muon

PE-MI Plug electron - Minimum ionizing track (CMIO)

Ve require that there be at least one lepton in the central region, as a dilepton idate. Dilepton events consisting of two CMIO's (MI-MI) are not directly triggered nd hence are not used. PE-PE has not been include in the analysis, because a ion of having both electrons in the plug region is very small for $t\bar{t}$ events. (<1 % M_{top}=140 GeV/c^2.)

trigger path was not explicitly required when events were selected, however we checked that volunteers, which do not trigger on with the central or plug electron ntral muon paths, are amount to $\sim$ 1% of the dilepton events after the P_T cuts. ermore, we observed two candidate events in the signal region and verified that they in the proper trigger path.

n the following section, we define the signal region. The selection cuts we will use are n P_T, isolation cut, event topological cuts of the mass, missing E_T, and the two-jet We also require two leptons in the event must be oppositly-charged dilepton.

Lepton P_T cut

require that the transverse momentum (P_T) of both leptons be greater than 20 /c. Large P_T leptons provide a good signature, because a high P_T threshold sepa- the $t\bar{t}$ signal from $b\bar{b}$, Z$\rightarrow \tau\tau$, which concentrate at lower P_T and also can separate the fake lepton backgrounds. This can be seen from Figure 5.1. The acceptance to geometrical and P_T cuts varies from 34 to 63 % for a top quark mass from 100 0 GeV/c^2.

Lepton track isolation

op decay ($t \to Wb \to l\nu b$), the large top mass results in a large separation between epton and the bottom quark, yielding an isolated lepton. On the other hand, in om decay ($b \to l\nu c$), the lepton is much closer to the charm quark and thus less ted. The $b\bar{b}$ and fake lepton backgrounds are rejected by an isolation requirement.

s we saw in section 4.3, the track isolation variable has a better background rejection preserves much more $t\bar{t}$ events than using the calorimeter isolation variable.

Ve define the lepton track isolation to be the sum of all the CTC track transverse enta within a cone of radius $\Delta R = (\Delta\eta^2 + \Delta\phi^2)^{1/2} = 0.25$ around the lepton track, ding the lepton track itself. Here, η is the pseudo-rapidity and ϕ is the azimuthal measured in radians.

o keep more $t\bar{t}$ events, we always require at least one central lepton (e or μ) and this n must have a stiff isolated track pointing to cluster. We always impose calorimeter tion cut on PE and CMIO. In other words,

there are two central leptons, where central is CE,MU or MI, then we require at one of them (any one of them) to pass track isolation.

r PE+(CE, MU, or MI) we require the CE, MU, or MI to pass track isolation.

he efficiency of this requirement is about 95 %, independently of top mass.

Oppositely charged leptons

same-sign charged lepton pairs from $t\bar{t}$ must include one lepton from the decay of Since these leptons tend to be non-isolated (accompanied by nearby particles from hadronization and decay), they are less likely to pass lepton identification cuts. two leptons in the events are required to have opposite charges. This cut reduces grounds from lepton misidentification by a factor of two and $b\bar{b}$ by 30 %, while this oses 3 to 6 % of top signals.

M_{top} (GeV/c^2)	120	160
1) (W^+W^-)	81.9 ± 1.4	75.9 ± 1.5
2a) (Wb) ($b\bar{b}$) ($\tau^+\bar{b}$) (Opposite sign)	4.2 ± 0.8	6.5 ± 0.9
2b) (Wb) ($b\bar{b}$) (τ^- b) (Same sign)	3.4 ± 0.7	5.7 ± 0.8
3) ($\tau^+\tau^-$) ($W^+\tau^-$) ($W^-\tau^+$)	10.4 ± 1.1	11.7 ± 1.1

e 5.1: The fractions of $t\bar{t} \rightarrow ll + X$ having 1) both leptons coming directly from the quark decay, 2) at least one lepton coming from the decay of a bottom or charm k, and 3) one or both leptons coming from a τ decays. In category 2), frcations of opposite and same sign events are shown. Lepton identification cuts are imposed. umbers are percentages.

Z^0 removal

ts containing a Z^0 decaying into an e^+e^- ($\mu^+\mu^-$) pair give rise to high P_T elec- (muons), thereby contributing to the background to the top signal. We explicitly ved events that contain a lepton pair with a mass between 75 and 105 GeV/c^2. The ency for top events is 80% for M_{top}=140 GeV/c^2

Missing transverse energy

remaining backgrounds are $b\bar{b}$, $Z \rightarrow \tau\tau$ and lepton misidentification for $e\mu$ channel, ee and $\mu\mu$ events are expected to be dominated by the Drell-Yan events. None of events are expected to have significant missing E_T, while $t\bar{t}$ events contain at least energetic neutrinos, which results in large missing transverse energy. Figure 5.4 s the missing E_T distribution for $t\bar{t}$ events together with background processes of $\rightarrow \tau\tau$, and WW. We require that candidate events must have a missing transverse gy greater 25 GeV.

ote that we compute the missing E_T after correcting the jet energy scale, as dis- ed in section 4.5, The motivation is that the corrected missing E_T reject Drell-Yan ts better than using uncorrected missing E_T as shown in Figure 5.5(a). For $t\bar{t}$ events, hange was observed as shown in Figure 5.5(b).

n addition to the cut on the magnitude of the missing transverse energy, the Drell- and Z→ $\tau\tau$ backgrounds are further reduced by cuts on the direction of the missing sverse energy.

n principle no neutrinos are involved in the Drell-Yan events so that the missing E_T ie event is expected to be small. The significant missing E_T arises from jets when ge fluctuation in the calorimeter measurement occurs. In this case, the direction of ing E_T tends to lie along that of the jet. Figure 5.7 illustrates one of examples for e events. The missing E_T of this event is 50 GeV, but it can be seen that the missing s observed along a jet with a large E_T of 83 GeV. The mising E_T is considered to rised from mismeasurement of the jet. Hence, no energetic jets must be detected in direction of the missing transverse energy for candidate events. We show a plot of azimuthal difference between a missing E_T and a closest jet) versus a missing E_T igure 5.8. We require that the missing E_T direction be more than 20° away from closest jet. The cut value is chosen to achieve good rejection in a Drell-Yan control ple of Z + jets events[1] .

similar cut is imposed to minimize the background from $Z \rightarrow \tau\tau$. For Z→ $\tau\tau$ events nissing transverse energy originates from neutrinos, which are often aligned with the ged leptons. Because of the large mass of the top quark, neutrinos from top decay produced isotropic and are not aligned with the charged leptons. The backgrounds $Z \rightarrow \tau\tau$ are minimized by requiring that no energetic lepton be detected in the tion of the missing transverse energy. Figure 5.8 shows the azimuthal difference een a missing E_T and a closest lepton versus a missing E_T. We demand that the ing E_T direction be more than 20° away from the closest lepton.

n summary, we require that $\Delta\phi(\not{E}_T$, lepton) >20 ° and $\Delta\phi(\not{E}_T$, jet) >20 °, if $\not{E}_T$ GeV. Note that the cut is imposed in case that the missing E_T be less than 50

Ve estimate the background from Drell-Yan continuum using Z events in CDF data as we will s in Section 7.1

, otherwise the cut is not imposed. This condition is added in order to preserve $t\bar{t}$ events, since Monte Carlo study shows that these background events are less y to have a large missing E_T greater than 50 GeV, as illustrated in Figure 5.6. We show in Figure 5.10 the azimuthal separation between the missing E_T and a closest r lepton versus the missing E_T.

'he efficiency of this requirement for top events is 76% for M_{top}=140 GeV/c^2

Two jet cut for higher mass top search

arching for the higher mass top quark, it is difficult to achieve a good signal-to-ground separation, because $t\bar{t}$ production cross section becomes significantly smaller, also because the background from WW production becomes comparable with the $t\bar{t}$ l for a top mass above 150 GeV/c^2, As a result, we must rely on additional details e top signature to improve the signal-to-background ratio. One of methods is to ire the presence of jets in the events. This can be seen in Figure 5.11 which shows listribution of the jet multiplicity for WW and top Monte Carlo.

'igure 5.12 shows the leading and second leading jet E_T for the top masses of 100, and 160 GeV/c^2. For the top mass not much larger than the W mass, the b quark the top decay has a rather soft P_T spectrum and the efficiency for reconstructing s in the detector is low. For higher mass top, above 120 GeV/c^2, however, the two arks in the decay of the $t\bar{t}$ pair can have significant energy and are detected with efficiency as hadronic jets in the calorimeter. An additional two-jet requirement rves most of the $t\bar{t}$ signal for high mass top and reduces backgrounds, which contain tionally observed hadronic jets only through higher order processes. The $Z \rightarrow \tau\tau$, and WZ backgrounds can be reduced by a factor of about 6 by requiring two jets. efficiency for the two-jet requirement depends on the observed jet E_T and on the nass. We have investigated the fraction of events which pass the two-jet cut for $t\bar{t}$ WW events by varying the jet Et threshold. We used three set of cuts: E_T^{jet1}, E_T^{jet2}

,10), (15,15) and (20,10) GeV. The fractions are tabulated in Table 5.2. Figure 5.14 rates the two-jet cut efficiencies for the top quark as a function of its mass, together those for WW events.

or $t\bar{t}$ events with mass above 120 GeV/c^2, the efficiency is more than 63 %, while of WW events survives the cut by requiring two or more jets with observed E_T GeV.

n the case, we require two or more jets with observed transverse energy greater than eV. A cluster cone radius of 0.4 is used. Furthermore, because the pseudorapidity ibution of jets from ttbar production is narrower than that from other background ts, we require the jets to have $\mid \eta \mid < 2.4$. This cut was made on the pseudorapidity e jet as determined from the center of the detector to ensure that the jets are ained in the central or plug calorimeter, rather than the event origin.

M_{top} (GeV/c^2)	100	120	140	160	WW
>(10,10) GeV	$33.0 \pm 1.4\%$	$63.0 \pm 1.3\%$	$75.1 \pm 1.0\%$	$83.9 \pm 0.9\%$	13.7 ± 1.1
>(15,15) GeV	$22.2 \pm 1.3\%$	$45.9 \pm 1.4\%$	$62.3 \pm 1.2\%$	$74.5 \pm 1.0\%$	5.5 ± 0.7
>(20,10) GeV	$26.2 \pm 1.4\%$	$54.9 \pm 1.3\%$	$72.0 \pm 1.1\%$	$82.4 \pm 0.9\%$	10.9 ± 1.0

e 5.2: The efficiency of the two-jet cut of different jet E_T thresholds for top and Monte Carlo events.

Table 5.3: Summary of dilepton selection criteria

At least one central lepton isolated in the tracking chamber
Reject same sign dilepton events
$\not{E}_T$ >25 GeV
Reject 75 $<M_{ll}<$105 GeV/c^2 for ee and $\mu\mu$
$\Delta\phi(\not{E}_T, \text{jet}) > 20°$ and $\Delta\phi(\not{E}_T, \text{lepton}) > 20°$ if $\not{E}_T < 50$ GeV
Two or more jets with observed E_T >10 GeV

Data Analysis

ır data sample, 5 $e\mu$, 685 ee and 571 $\mu\mu$ events are left after the Lepton P_T, lepton :ification, isolation, and opposite charge cuts.

.1 $e\mu$

lepton P_T transverse momenta for the five electron-muon events are shown in 5.15, together with the prediction from $t\bar{t}$ Monte Carlo. The azimuthal angle differ- between the missing transverse energy and the closest lepton or jet for is plotted in 5.16 against the missing transverse energy. Two $e\mu$ events survive the final missing :ut, both its magnitude and direction cuts. The one of candidates has an isolated :al electron with E_T^e of 22.2 GeV and an opposite-sign muon with P_T^μ of 47.7 GeV/c a dilepton azimuthal opening angle of 18°. There are two large calorimeter clusters ıe central region with observed transverse-energy depositions of 108 and 44 GeV, :luster of 18 GeV in the forward region. Other characteristics of the event include presence of a second muon candidate with transverse momentum of 8.8 GeV/c in ıighest E_T jet. Another event contains an isolated central electron with E_T^e of 50.6 and an isolated opposite-sign muon in the CMX chamber with P_T^μ of 37.3 GeV/c three calorimeter clusters with observed E_T of 67, 14 and 11 GeV.

n these events, no energetic lepton or jet is detected in the direction of the missing Figure 5.20 - 5.23 show a tracking chamber and calorimeter displays for the idates. Some properties of two events are summarized in Table 5.5.

.2 ee and $\mu\mu$

dielectron and dimuon invariant masses are shown in Figure 5.17 and 5.18 for dielectron events and 571 dimuon events, respectively. Also shown in the plots are Monte Carlo predictions from ISAJET program. By removing the majority of Z^0 grounds, the data sample is reduced to 58 ee and 62 $\mu\mu$ events. The distribution in nissing E_T- $\Delta\phi(\not{E}_T$, lepton or jet) plane is shown in Figure 5.19 for CDF data. After sing the missing E_T requirement, no dielectron or dimuon events were observed.

summary of the numbers of events surviving different stage of cuts is shown in e 5.4.

e following two sections, we will determine the detection efficiency for the selection ria stated above, and estimate the expected number of backgrounds.

Cut	ee	$\mu\mu$	$e\mu$
P_T	702	588	8
Opposite-Charge	695	583	6
Isolation	685	571	5
Invariant Mass	58	62	5
$\not{E}_T$	0	1	2
$\not{E}_T$ direction	0	0	2
Two-jet	0	0	2

Table 5.4: Numbers of data events surviving various consecutive cuts.

	Event I				Event II			
	Charge	P_T (GeV/c)	η	ϕ (deg)	Charge	P_T (GeV/c)	η	ϕ (deg)
ctron	$-$	22.2	0.84	32	$+$	50.6	0.93	25
ion	$+$	47.7	0.17	14	$-$	37.3	-0.74	4
ion	$+$	8.8	0.18	352				
1		107.9	0.11	352		67.0	0.64	218
2		44.3	-0.54	215		13.6	-3.31	344
3		18.0	-2.94	112		10.7	1.34	344
ssing E_T		136.4		179		59.6		149
ϕ ($\not{E}_T$,ℓ)				147				124
ϕ ($\not{E}_T$,j)				36				68

e 5.5: Characteristics of the top-quark cndidate events. Observed calorimeter E_T is for jet clusters.

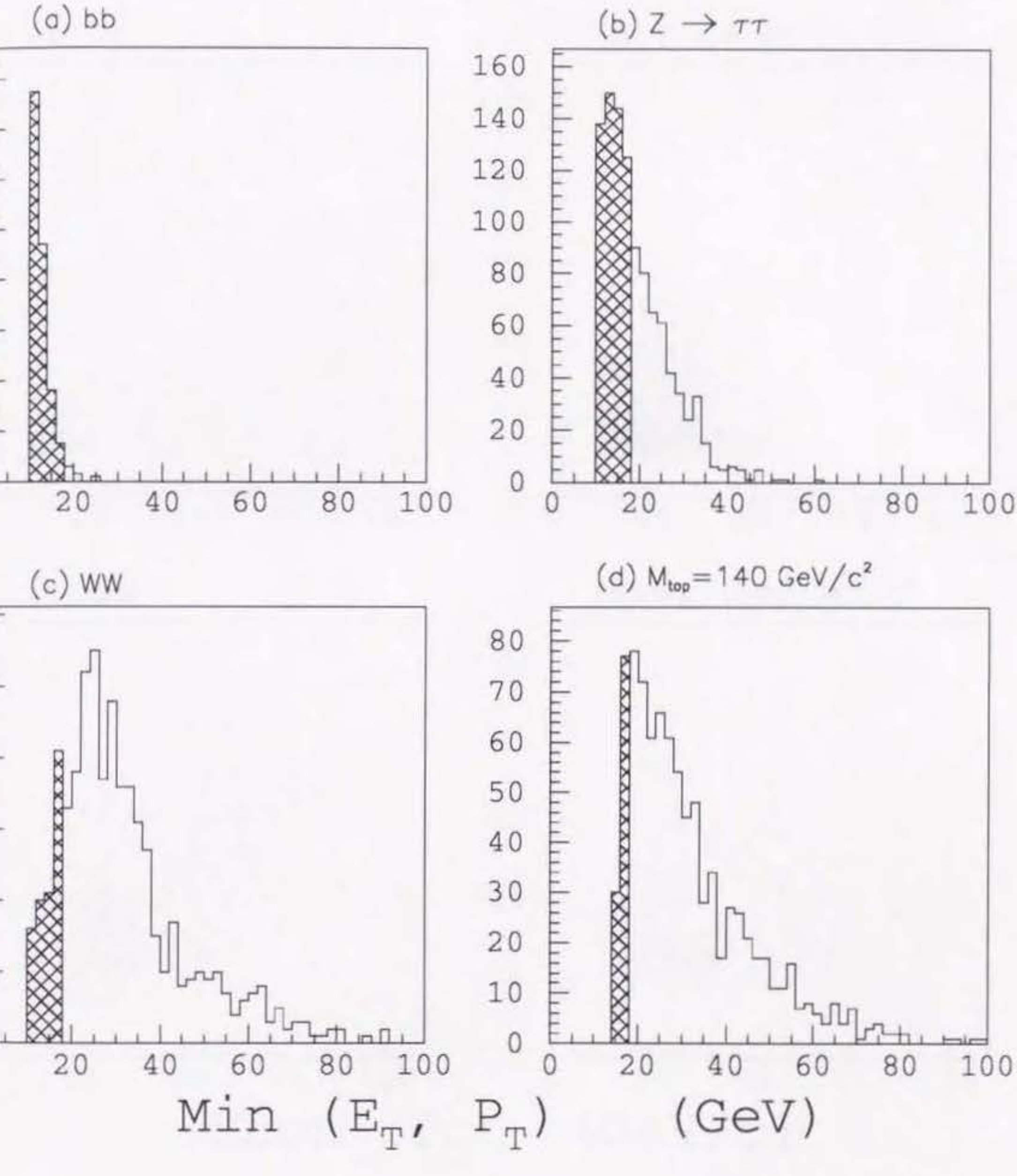

re 5.1: Minimum of E_T^e and P_T^μ for (a) $b\bar{b}$, (b) $Z \to \tau\tau$, (c) WW, and (d) $t\bar{t}$ Monte
o data (M_{top}=140 GeV/c^2) P_T >10 GeV is imposed on the Monte Carlo samples.
he $t\bar{t}$ events, P_T >15 GeV is imposed. The hatched area is rejected.

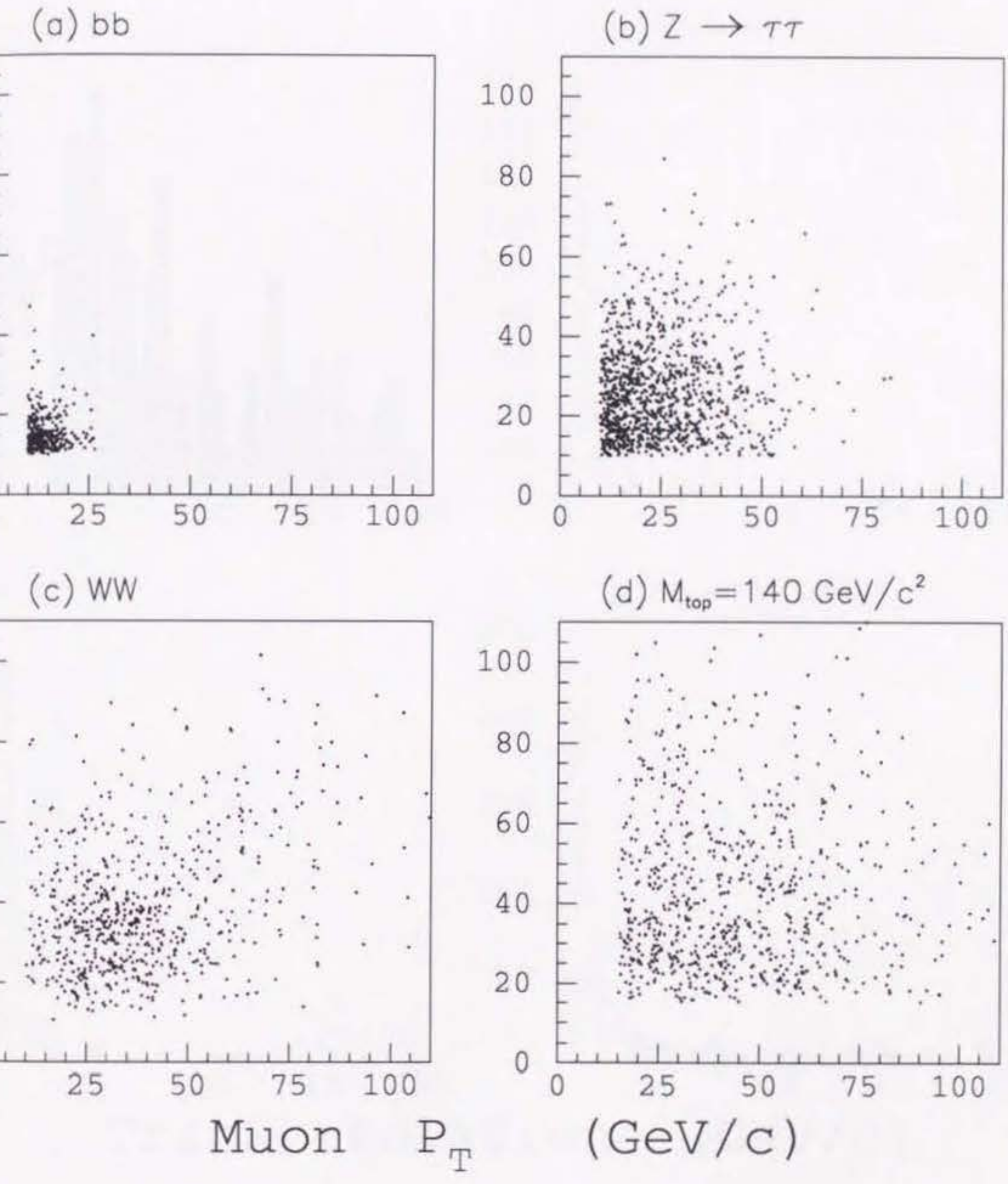

re 5.2: E_T^e versus P_T^μ for (a) $b\bar{b}$, (b) $Z \to \tau\tau$, (c) WW, and (d) $t\bar{t}$ Monte Carlo data
$_p$=140 GeV/c^2). $E_T^e(P_T^\mu)$ >10 GeV(/c) is imposed except for $t\bar{t}$ events.

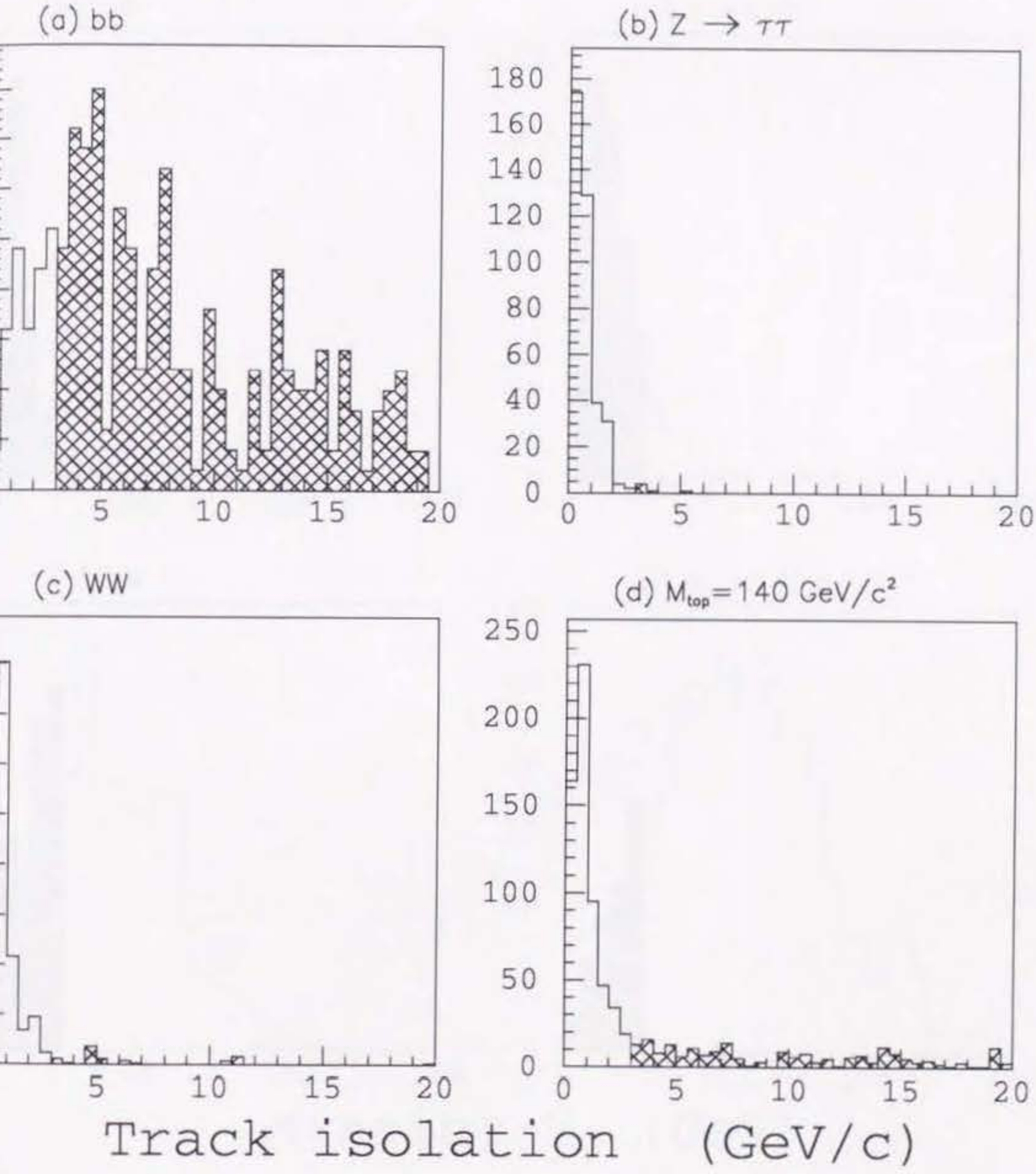

re 5.3: Track isoaltion of E_T^e and P_T^μ for (a) $b\bar{b}$, (b) $Z \rightarrow \tau\tau$, (c) WW, and (d) $t\bar{t}$:e Carlo data (M_{top}=140 GeV/c^2) The hatched area is rejected.

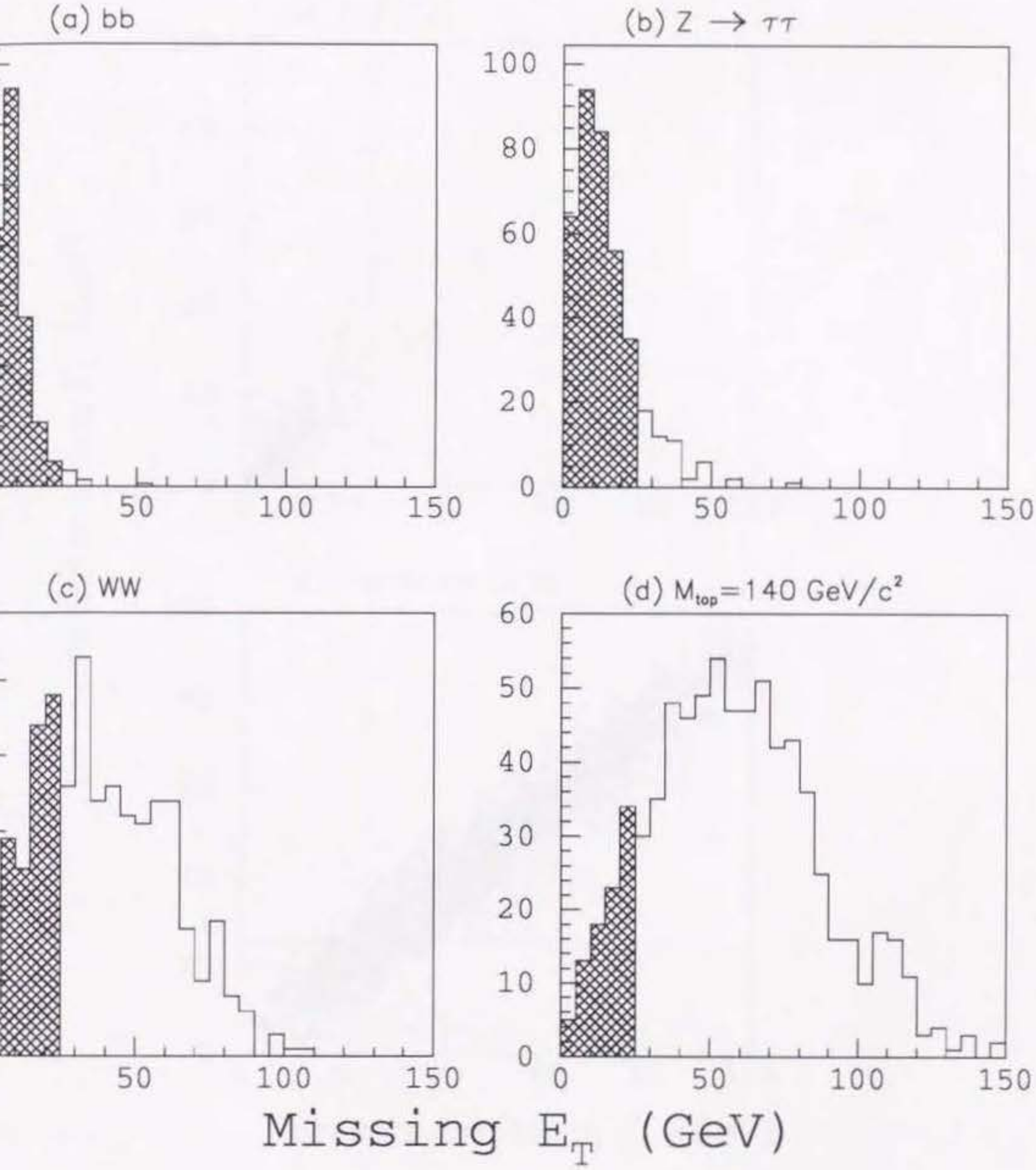

re 5.4: Missing transverse energy for (a) $b\bar{b}$, (b) $Z \rightarrow \tau\tau$, (c) WW, and (d) $t\bar{t}$ te Carlo data (M_{top}=140 GeV/c^2) The hatched area is rejected. The hatched area ected.

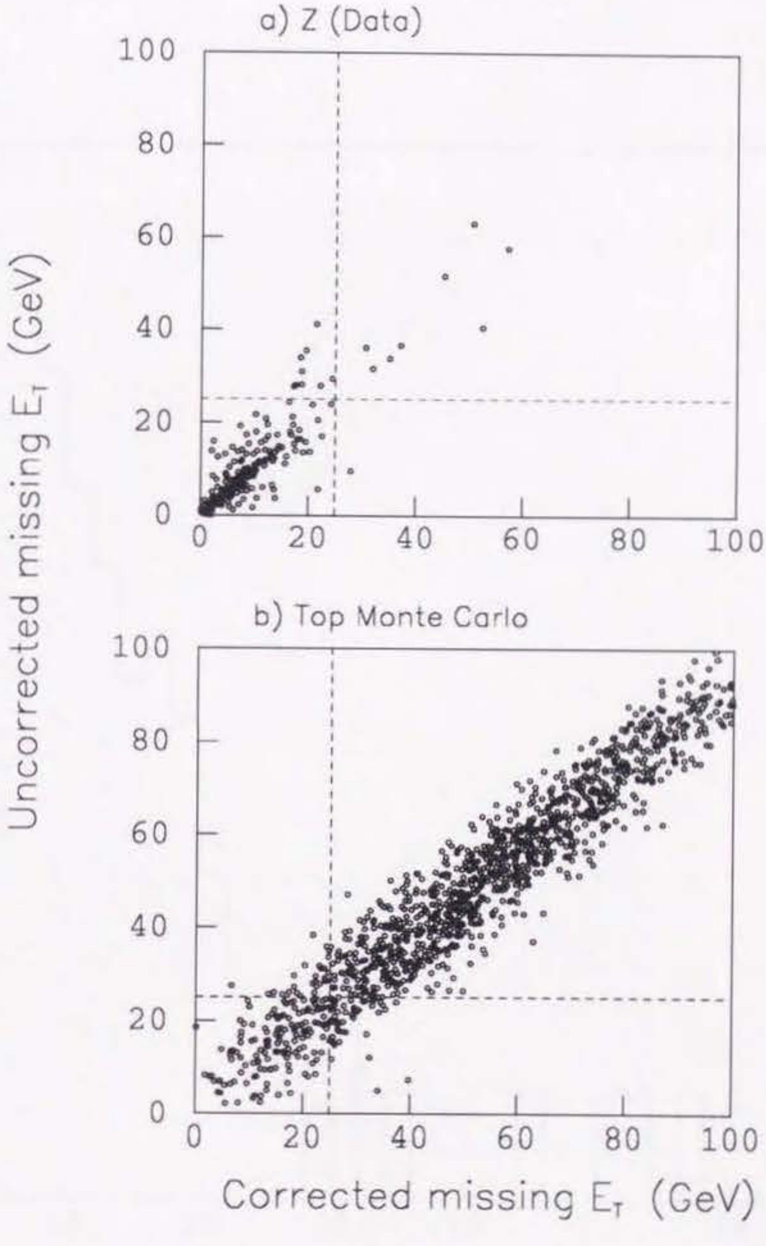

re 5.5: Raw missing E_T versus missing E_T corrected for jet energy scale a) for events the Z decays, and b) top Monte Carlo of 140 GeV/c^2. Note that the corrected tity has better background rejection near the missing E_T threshold.

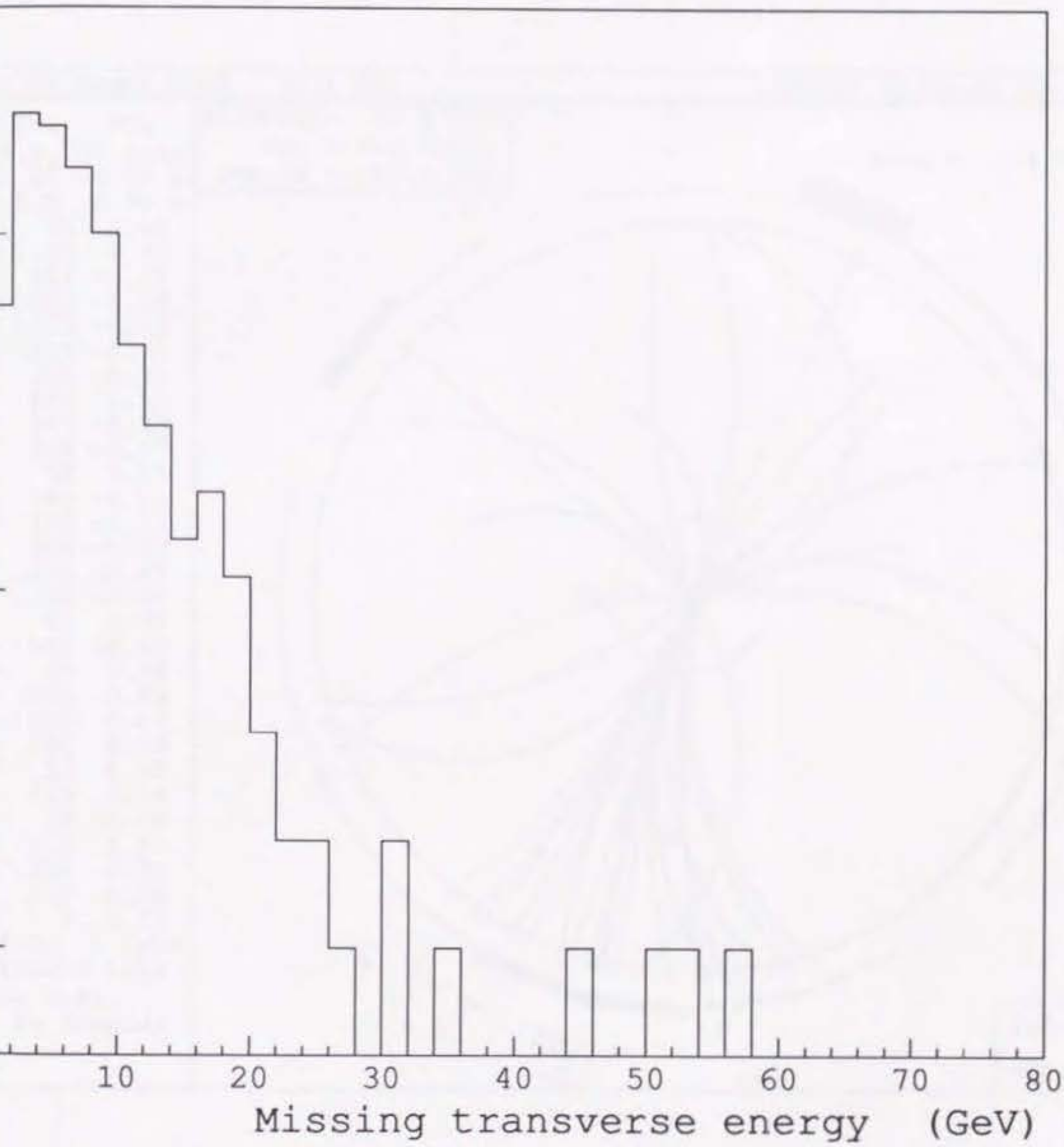

Figure 5.6: Missing E_T distribution for $Z \to ll$ decays from CDF data.

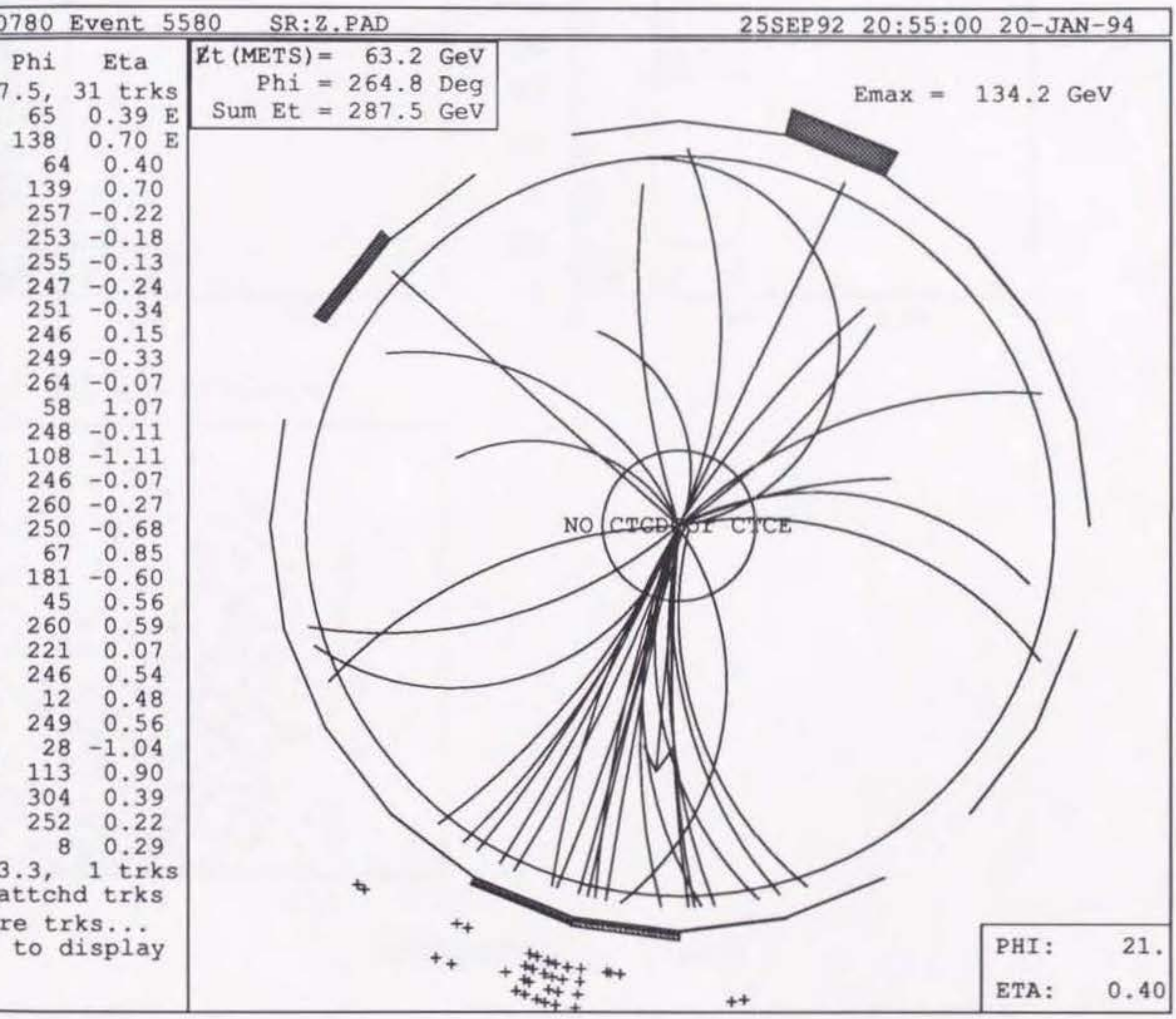

re 5.7: One event from $Z \to ee$ decays with the large missing E_T. The large missing rises from jet mismeasurement.

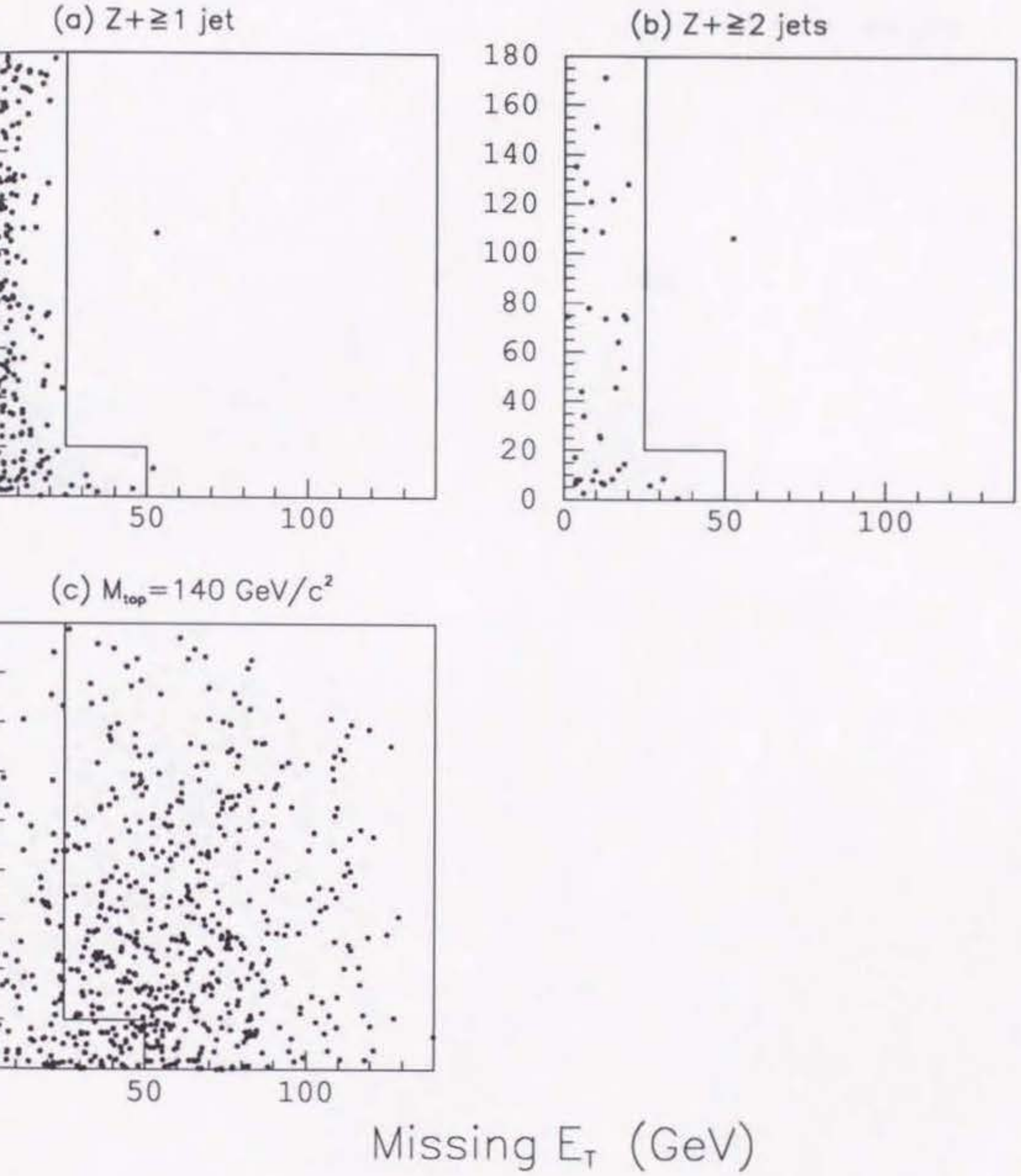

re 5.8: Azimuthal angle difference between the missing E_T and the closest lepton
is the missing E_T : dielectron and dimuon data from a Drell-Yan control sample of
+ $\geq$ 1 jet and b) Z + $\geq$ 2 jets. c) top Monte Carlo of 140 GeV/c^2.

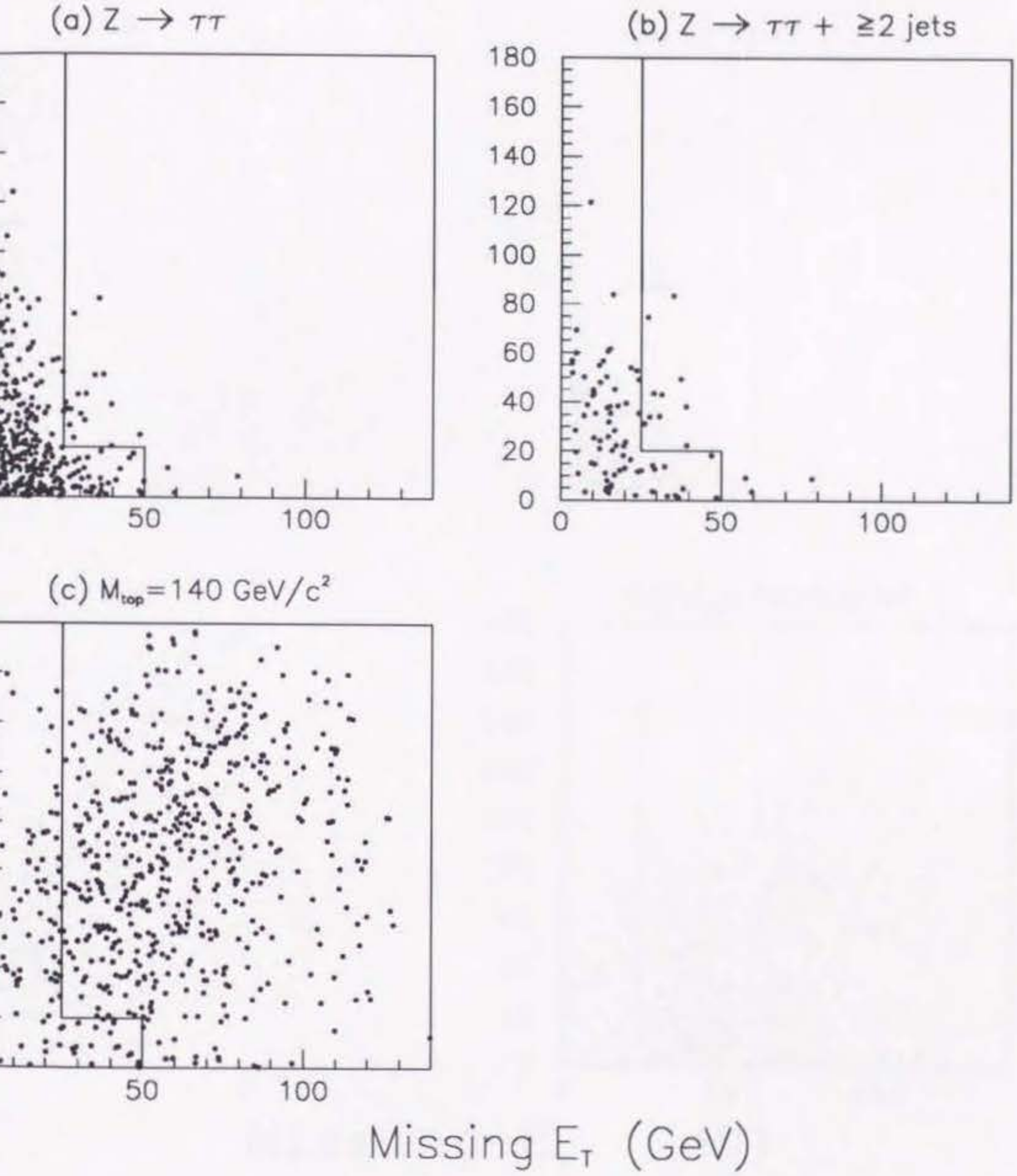

re 5.9: Azimuthal angle difference between the missing E_T and the closest jet versus nissing E_T. a) Z → ττ simulation, b) Z → ττ simulation with two-jet cut, and c) Monte Carlo of 140 GeV/c^2.

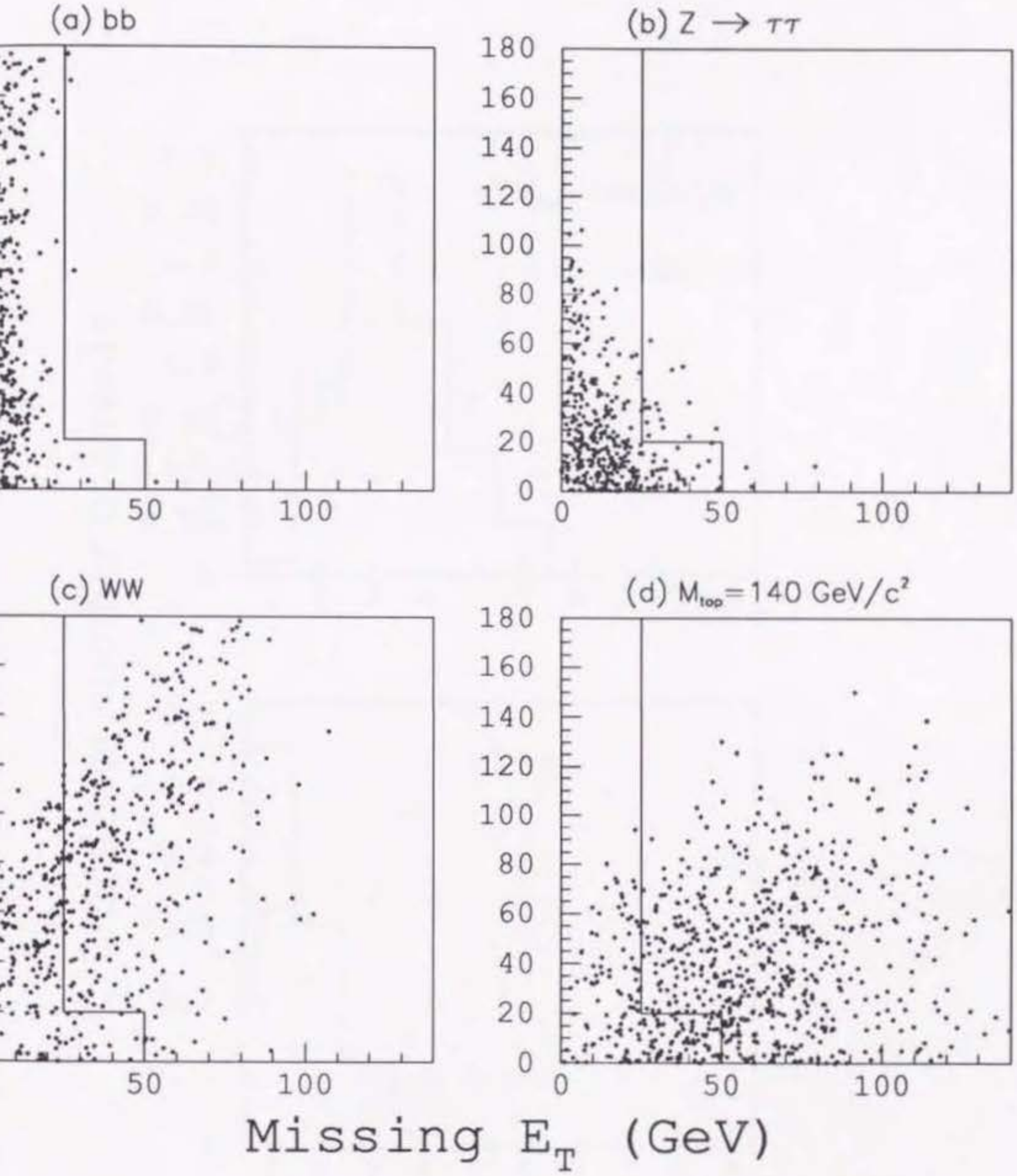

re 5.10: Azimuthal difference between the missing transverse energy and a closest n or jet for (a) $b\bar{b}$, (b) $Z \rightarrow \tau\tau$, (c) WW, and (d) $t\bar{t}$ Monte Carlo data (M_{top}=140 /c^2)

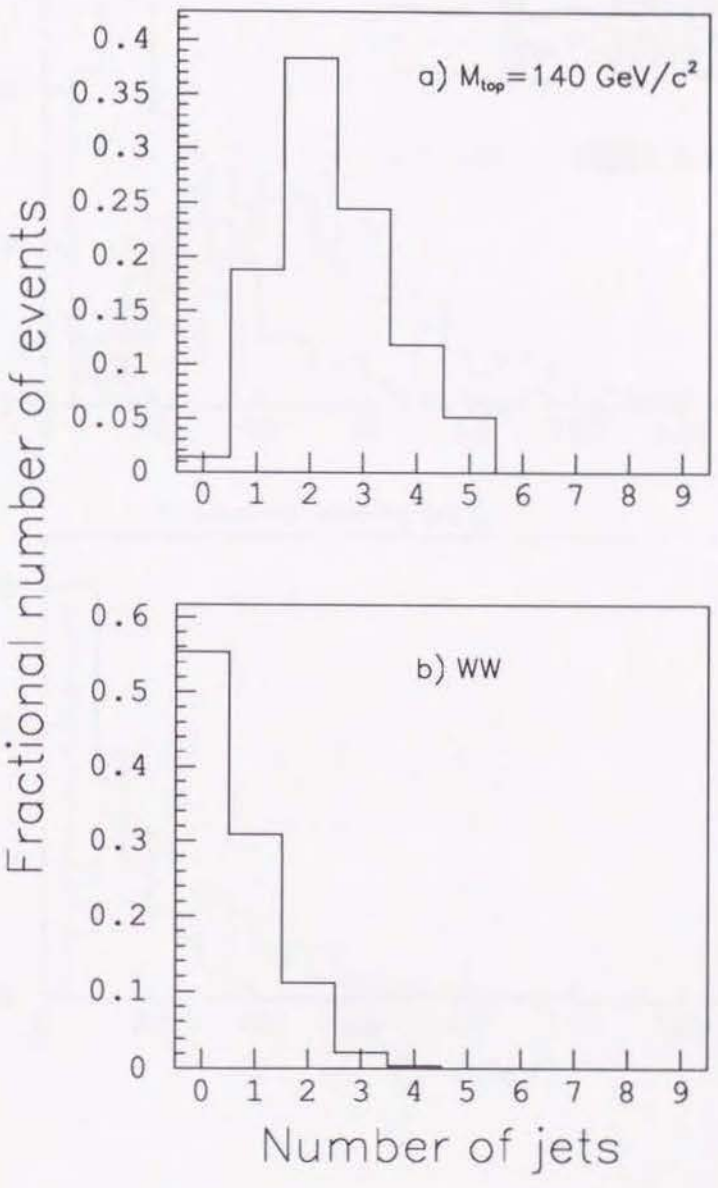

re 5.11: The number of jets for a) top Monte Carlo of 140 Gev/c^2 and b) WW s. The numbers are normalized by the total number of events.

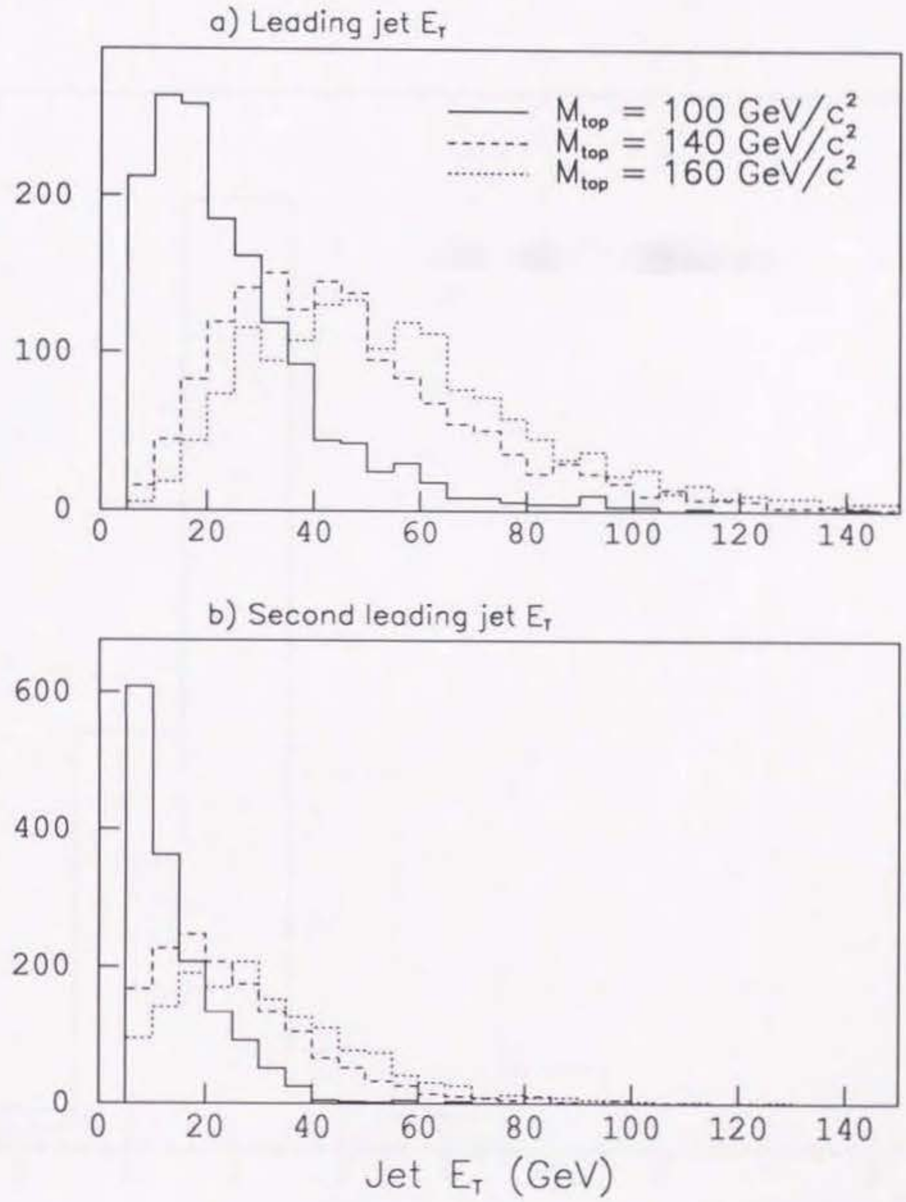

re 5.12: Jet E_T distribution for top Monte Carlo events: a) leading jet E_T and b) -to-leading jet E_T. Distributions are normalized to unity.

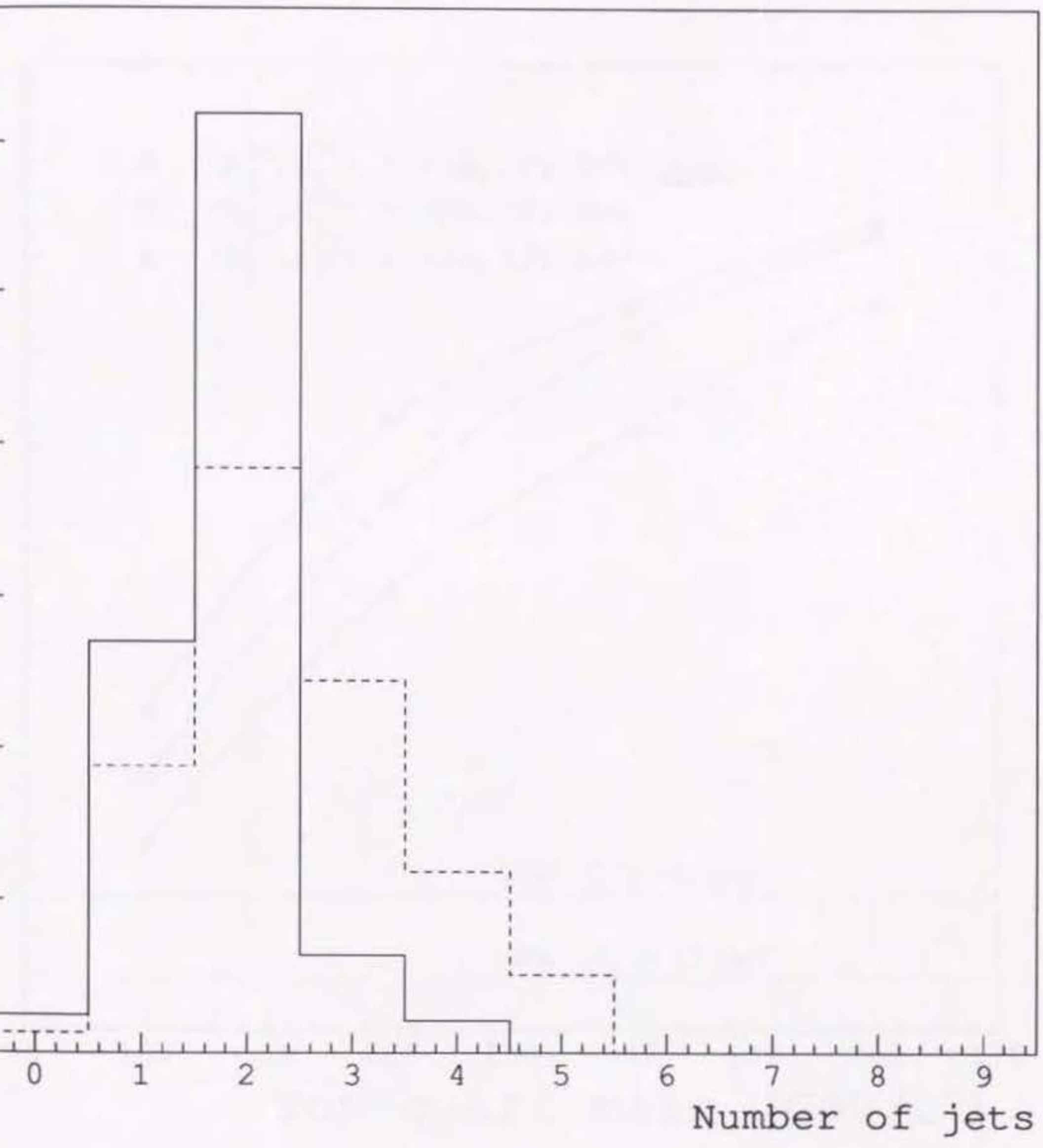

re 5.13: The number of jets for top Monte Carlo of 140 Gev/c^2 with gluon radiatopn ned line) and without gluon radiation (solid line). The numbers are normalized by otal number of events.

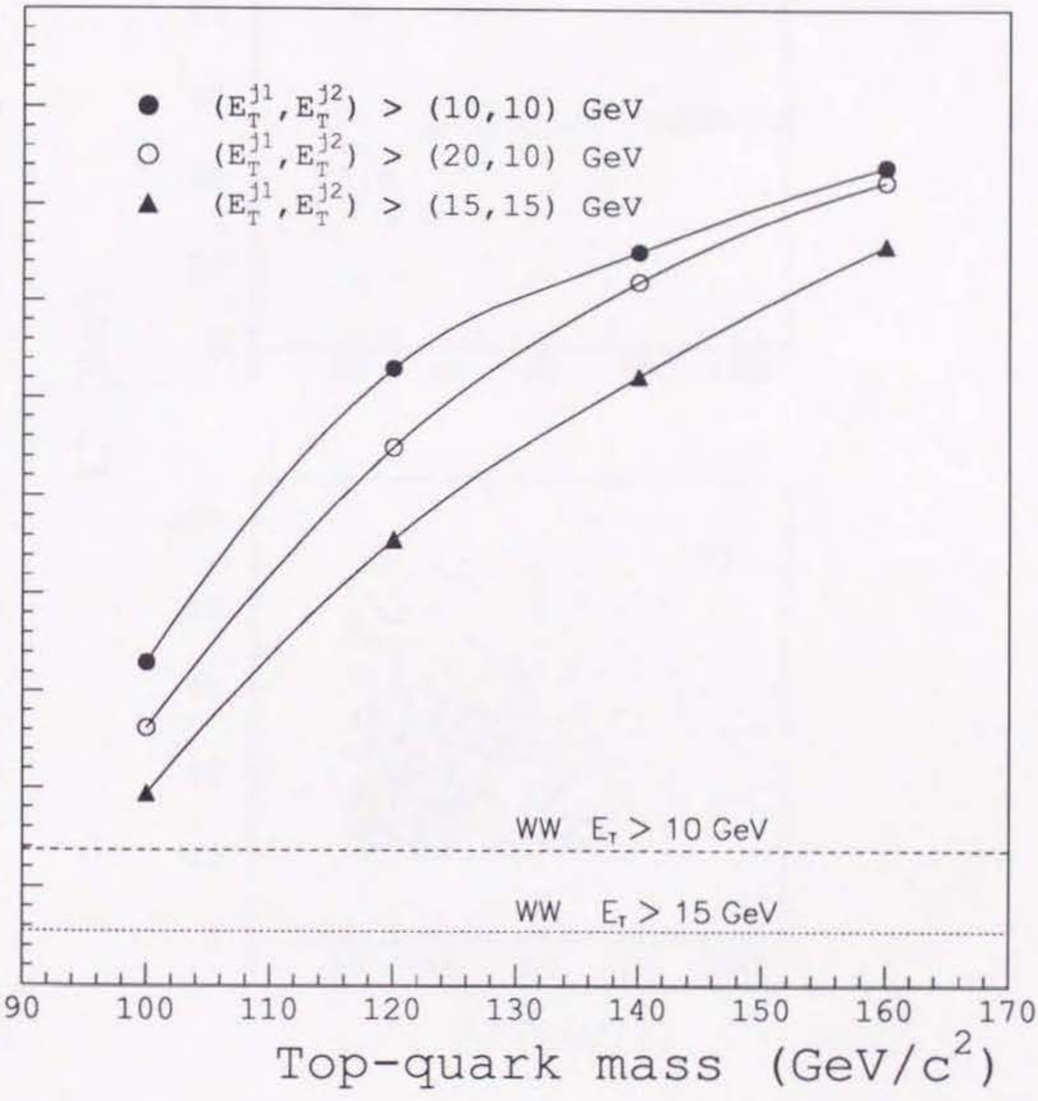

re 5.14: Two-jet cut efficiency for $t\bar{t}$ events as a function of a top-quark mass. Also
n are the efficiencies for WW Monte Carlo events with both E_T >10 and 15 GeV

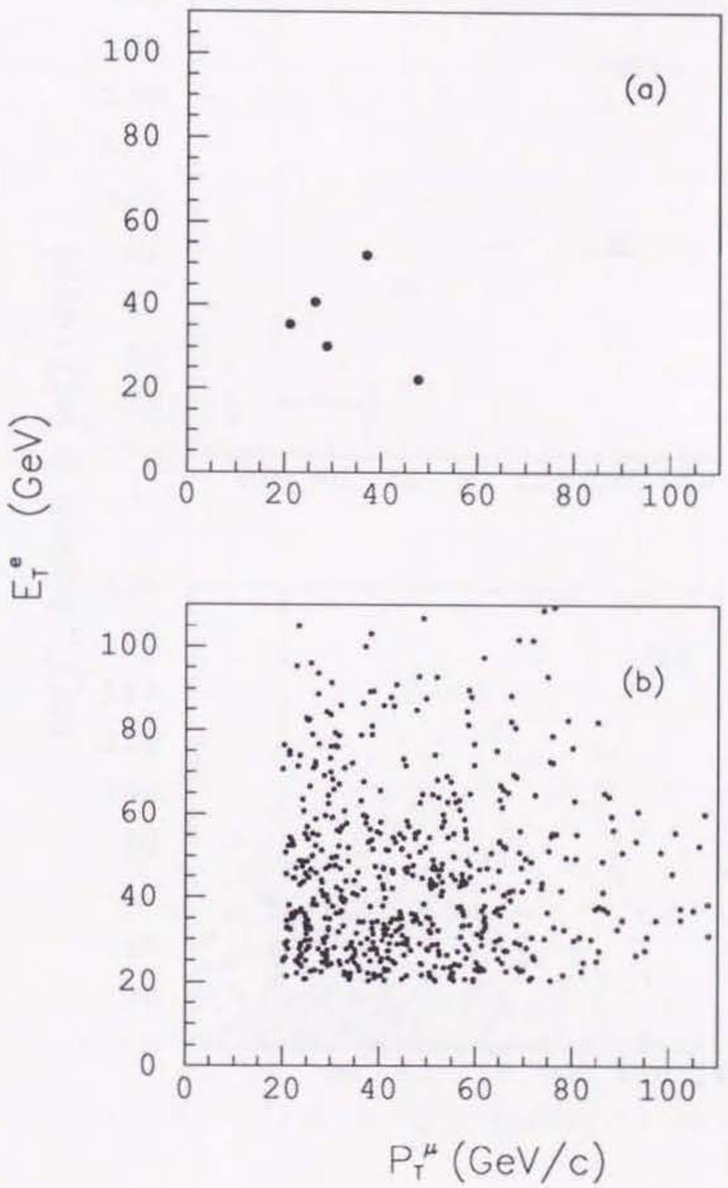

re 5.15: Electron transverse energy versus muon transverse momentum in CDF ron-muon data with integrated luminosity of 21.4 pb^{-1}, together with b) $t\bar{t}$ prediction (M_{top}=140 GeV/c^2).

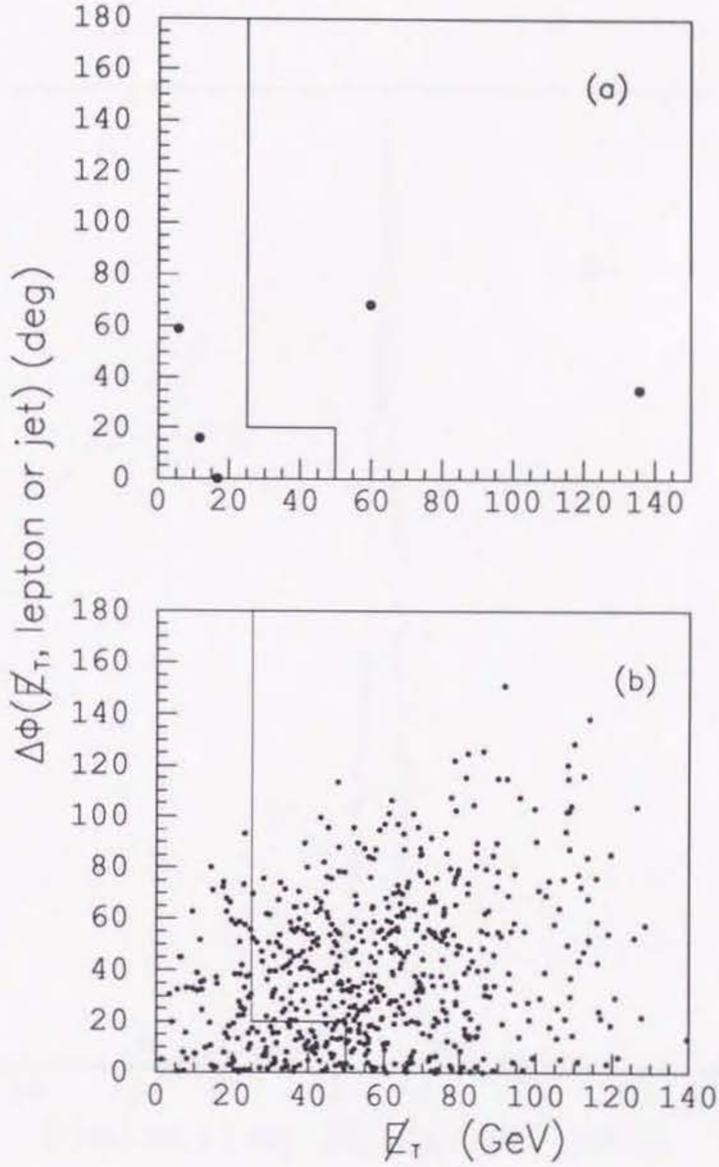

re 5.16: Azimuthal angle difference between missing E_T and the closest lepton or CDF electron-muon data with integrated luminosity of 21.4 pb^{-1}, together with prediction (M_{top}=140 GeV/c^2). The region to the left of the solid line is excluded e missing E_T requirement.

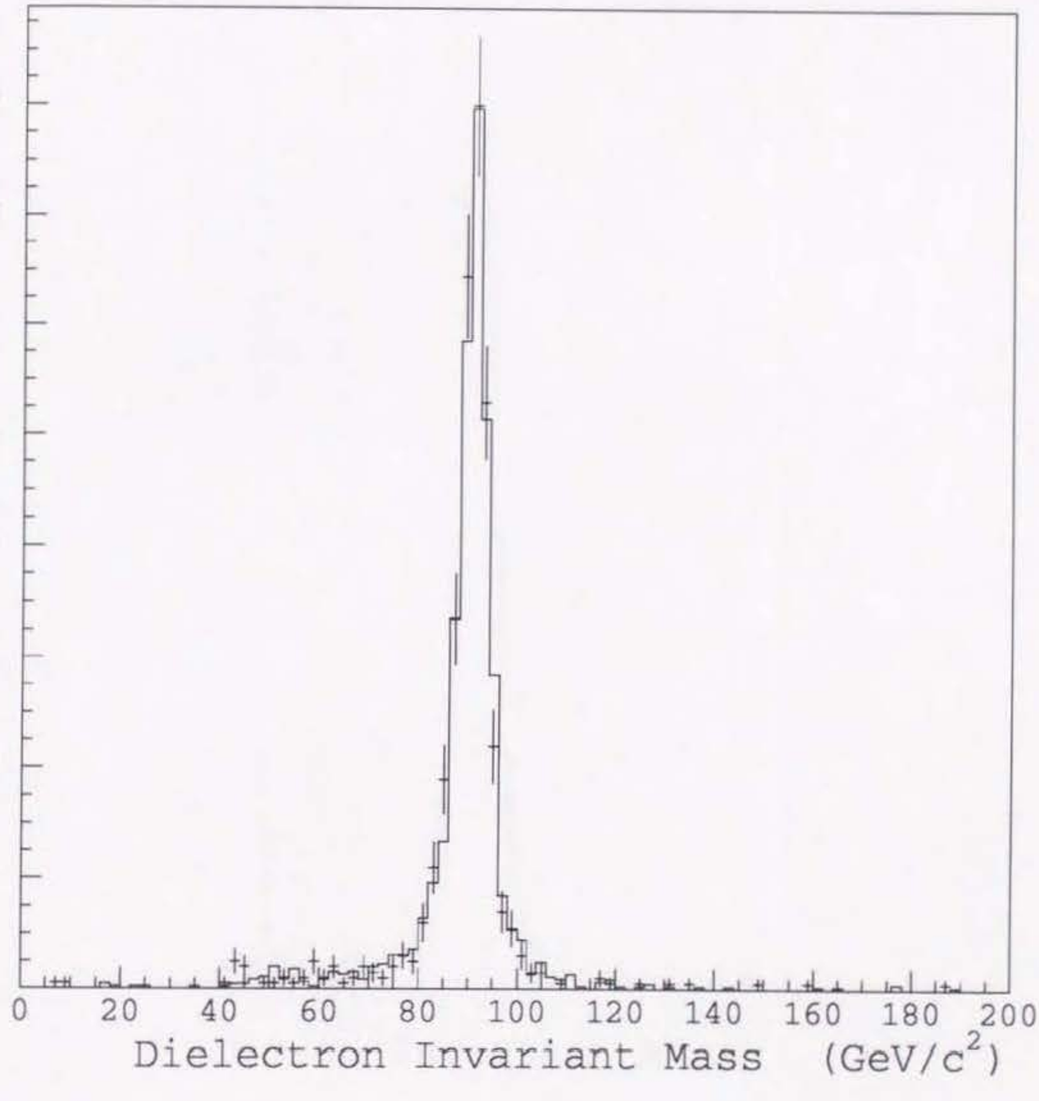

e 5.17: Dielectron invarianat-mass distribution of CDF data with integrated lu-
sity of 21.4 pb^{-1}(plotted). The histogram is a Monte Carlo Dreall-Yan prediction
alized to data.

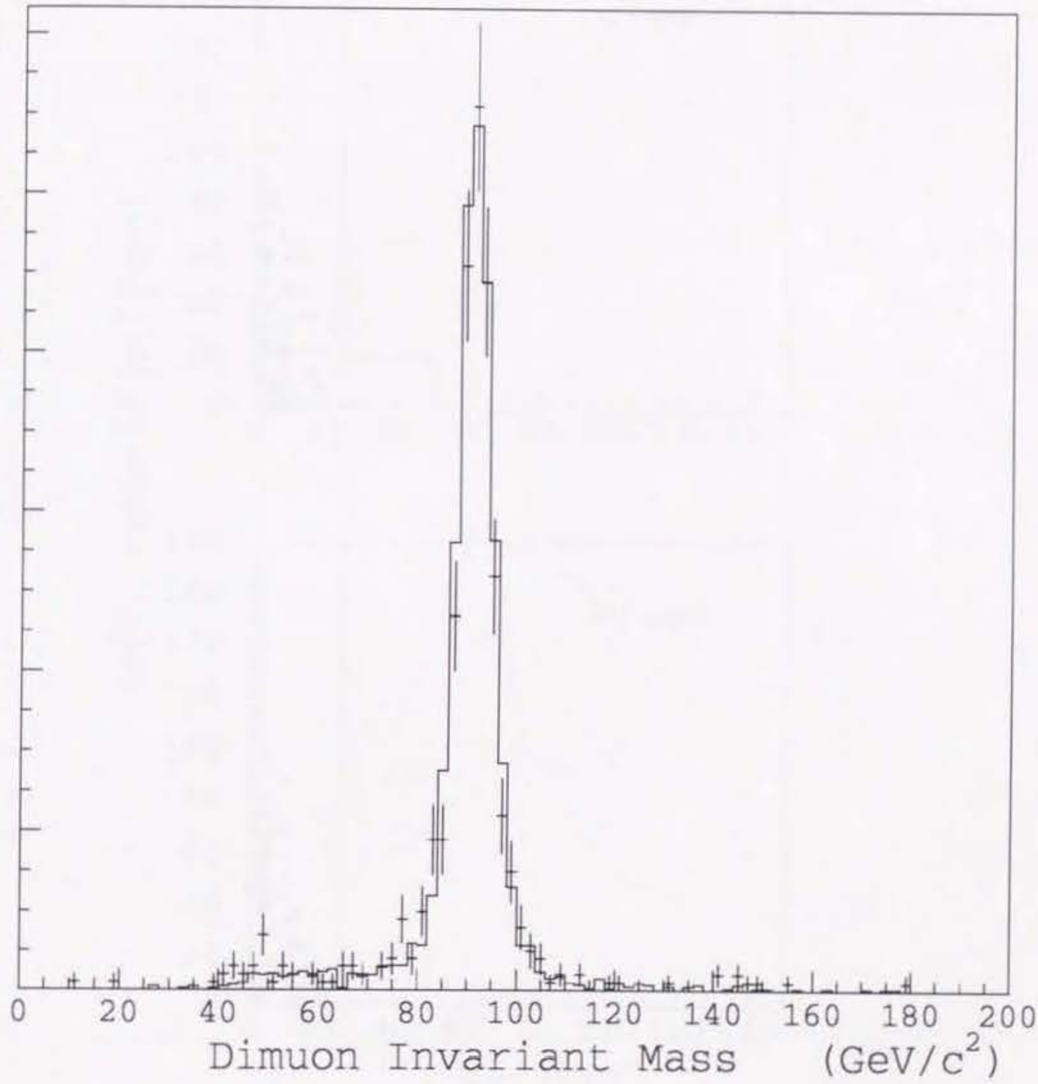

e 5.18: Dimuon invarianat-mass distribution of CDF data with integrated lumi-
y of 21.4 pb^{-1}(plotted). The histogram is a Monte Carlo Dreall-Yan prediction
alized to data.

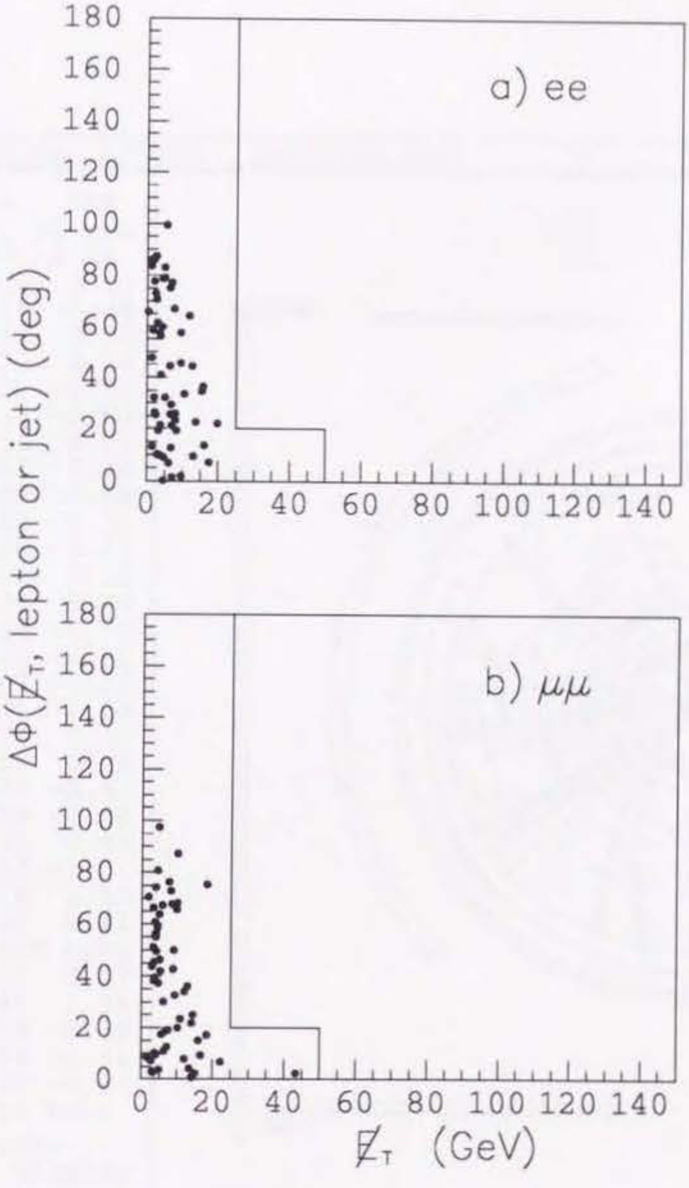

e 5.19: Distribution in the $\Delta\phi(\not{E}_T$, lepton or jet)-$\not{E}_T$ plane for CDF data with ated luminosity of 21.4 pb^{-1}. The solid line indicate the event toplogy cuts: ectron and b) dimuon events. Events with dilepton masees in the range 75 $< M_{ll}$ are not included in the figure.

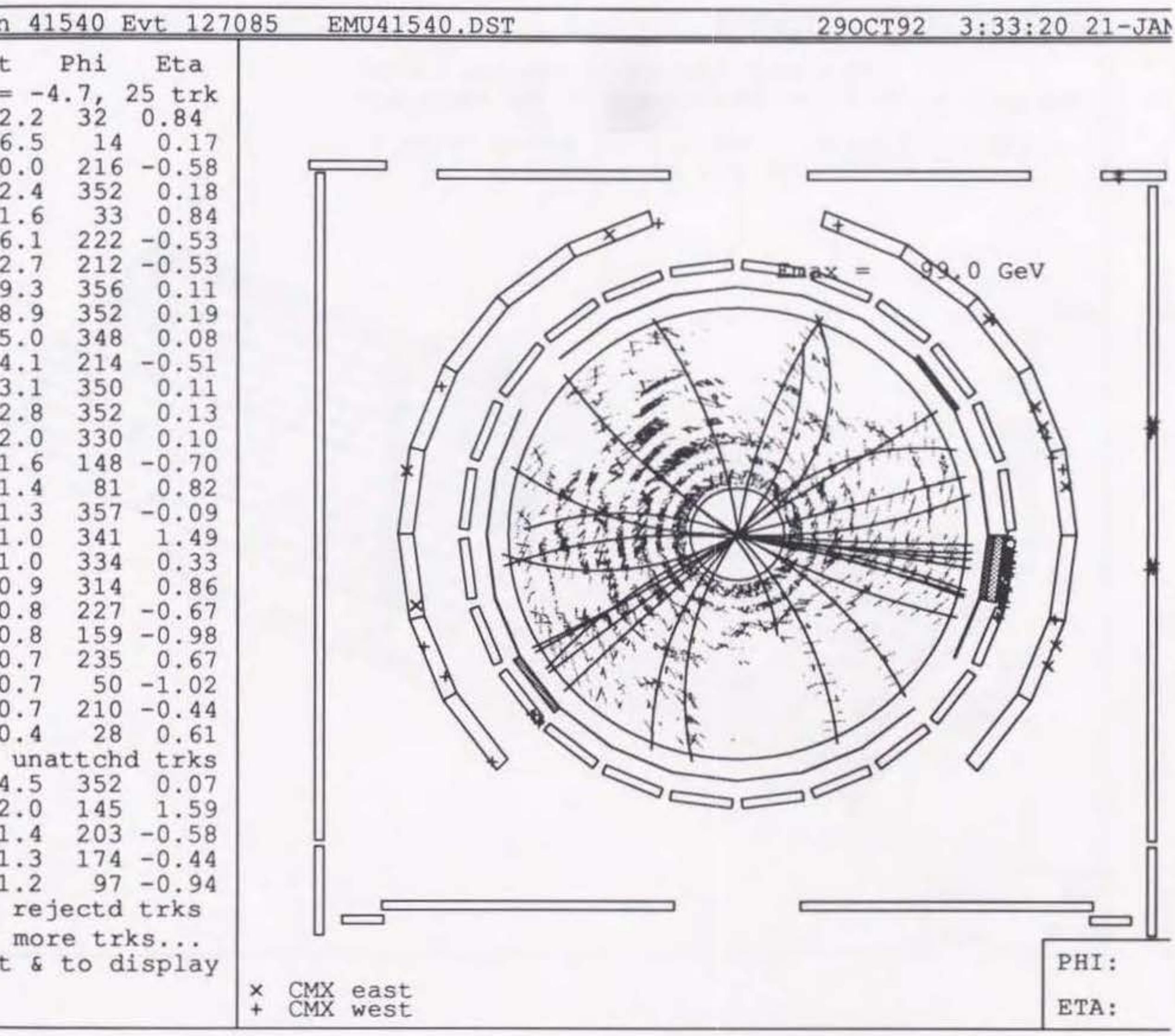

re 5.20: A display of the candidate events: Run 41540 Event 127085 view of the ing chamber in the transverse plane

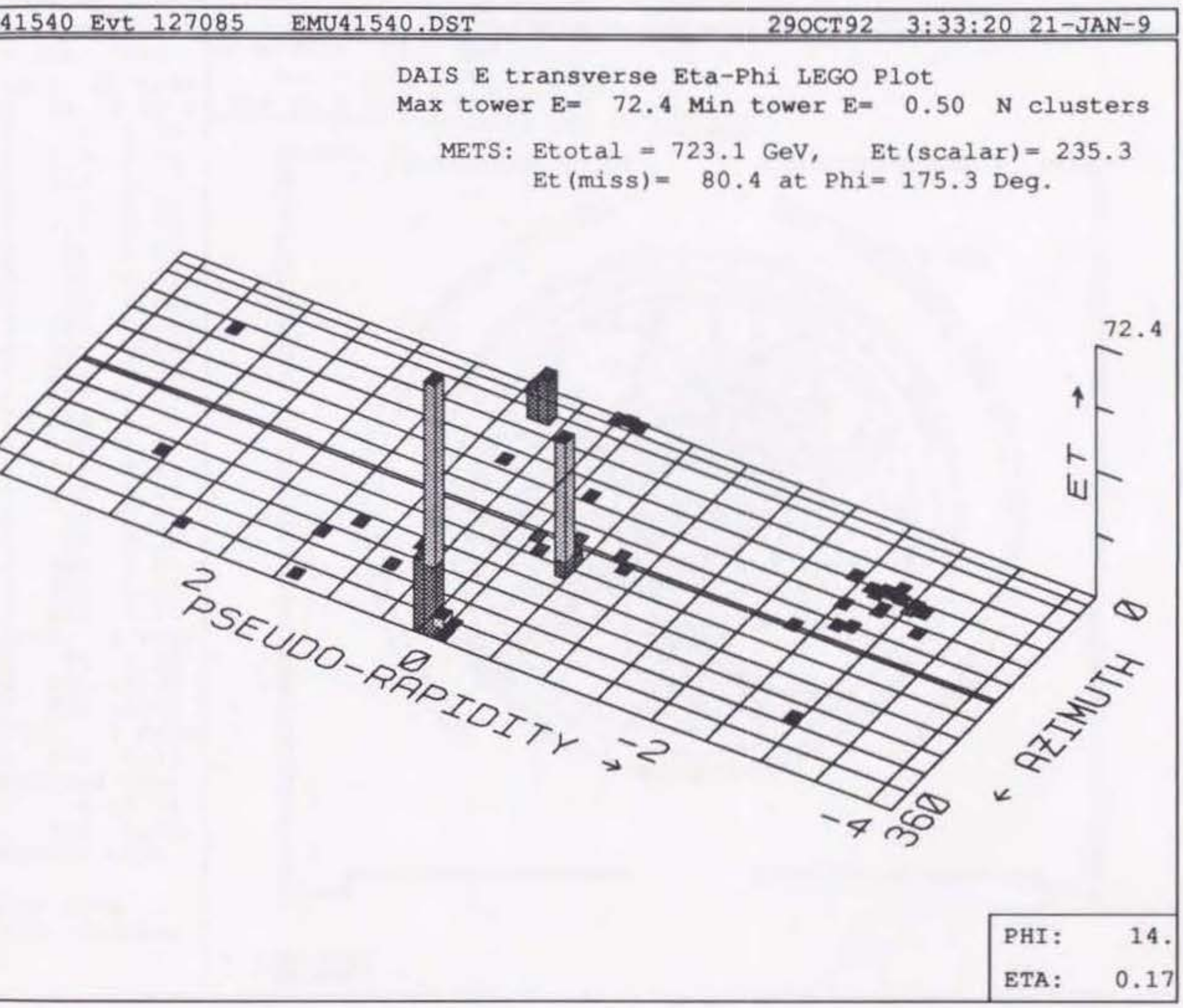

ure 5.21: A display of the candidate events: Run 41540 Event 127085 The cylindrical olimeter has been "unrolled" such that the axes of the grid the azimuthal angle und the beam line, and the peudorapidity, defined as $\eta = -log(tan(\theta/2))$, where θ is polar angle with respect to the beam line. The hight of each cell is proportional to transverse energy $E_T = Esin\theta$.

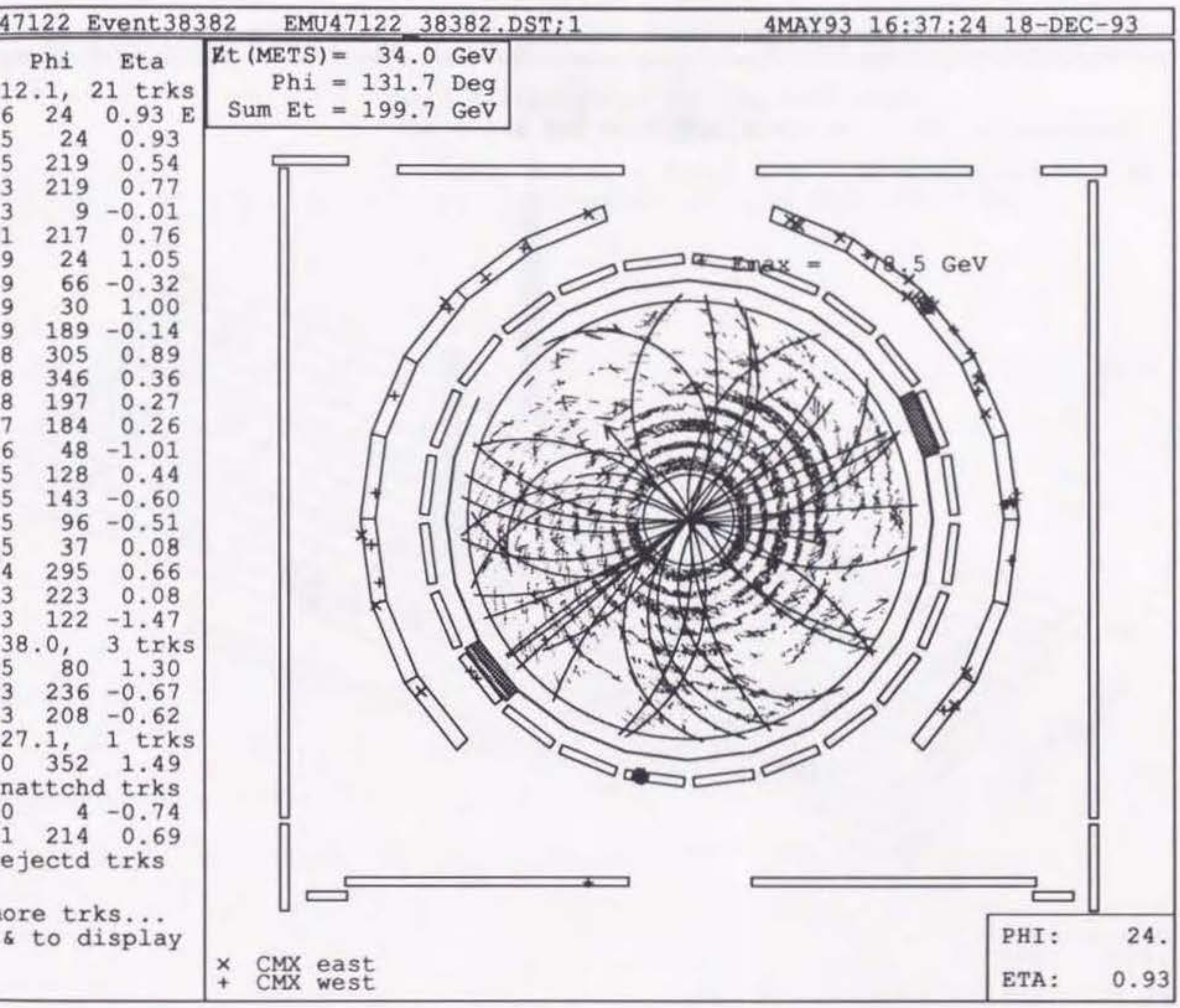

ure 5.22: A display of the candidate events: Run 47122 Event 38382 view of the
cking chamber in the transverse plane

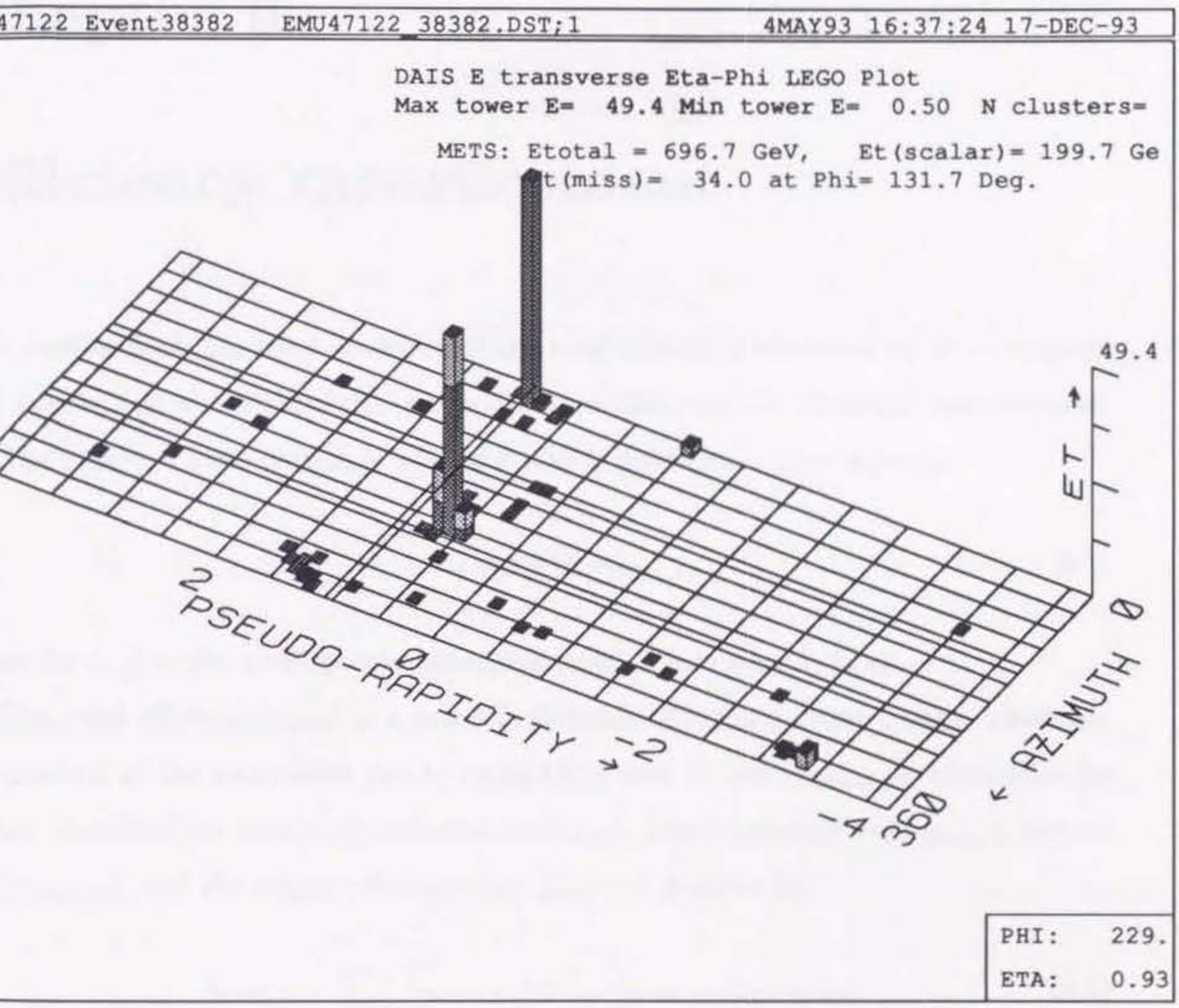

Figure 5.23: A display of the candidate events: Run 47122 Event 38382

Chapter 6

Efficiency measurement

s section describes the calculation of the total detection efficiency for $t\bar{t} \rightarrow$ dilepton events, and also discuss the systematic uncertainty on the efficiency measurement.

The observed cross section is related to the $t\bar{t}$ production cross section:

$$\sigma_{\rm obs} = \sigma_{t\bar{t}}\,{\rm Br}\,\epsilon_{\rm total} \tag{6.1}$$

ere Br $= \frac{4}{81}$ is the semileptonic branching fraction into ee, $\mu\mu$, or eμ.

The total efficiency(ϵ_{total}) is a sum of efficiencies for the 8 event classes, which are product of the acceptance due to geometrical and P_T cut ($\epsilon_{geom \cdot P_T}$), efficiencies for on identification cuts(ϵ_{ID}), isolation cut(ϵ_{isol}), event topology cut(ϵ_{Event}), two-jet ($\epsilon_{Two-jet}$), and the trigger efficiency ($\epsilon_{Trigger}$) and is given by

$$\epsilon_{\rm total} = \sum_{\rm event\ class} \epsilon_{\rm geom \cdot P_T}\,\epsilon_{\rm ID}\,\epsilon_{\rm Isol}\,\epsilon_{\rm event}\,\epsilon_{\rm two-jet}\,\epsilon_{\rm trigger} \tag{6.2}$$

arrangement of the factors on the right-hand side of equation (6.2) is meant to ne an order in our set of selection cuts. According to this order, the efficiency of a en cut is determined relative to a sample on which all the preceding cuts have already n applied.

In the following sections, we will describe the efficiency calculation for individual

s. We use the ISAJET Monte Carlo generator and a simulation of the CDF detector determine the geometric and kinematic acceptance and the efficiencies for lepton ntification cuts, lepton isolation cuts, the combined efficiency of the dilepton charge, ariant mass and missing E_T cuts, and the efficiency for the two-jet cut. The trigger ciencies are determined using data collected by independent triggers.

1 Geometric and kinematic acceptance

e acceptance due to geometrical and P_T cut is the fraction of $t\bar{t} \rightarrow$ dilepton + X nts (normalized to the double semi-leptonic brancing ratio of 4/81) inside the fiducial ıme of the detector and passing the P_T cuts. It should be noted that this definition in nciple allows efficiencies larger than 1.0. The double semi-leptonic decay of a $t\bar{t}$ pair h an assumed branching ratio of 4/81, *i.e.*, a lepton pair from WW, contributes most he signal, but the remaining contributions from sequential decays of a daughter b or uark or τ lepton are also take into account. Hence, the effective branching ratio is ger than 4/81. In Table 6.1, we show the contributions to the signal from the following on sources: (1) both leptons come directly from the W decay; (2) at least one lepton nes from the b decay[1] ; and (3) leptons coming from the decay of a tau (but no events h as $b - \tau$, since these events are counted in the category (2)). This is evaluated ıg ISAJET Monte Carlo generator and the CDF detector simulation. Leptons from quarks at the ISAJET generator level are related to the simulated lepton candidates examining the matching in $\eta - \phi$ space between both leptons. We looked at the ributions of the distance between them and required to be less than 0.04. Figure 6.1 strates the matching distribution for electrons coming from the decays of W and of tom. The efficiency of passing the matching cut is about 95 %.

After testing the matching cut, we counted the number of events which passes the on P_T and fiducial cuts described in section 4.1 and 4.2. In the calculation, track re-

[1] We also include the charm decay. By b, we mean both b and c quarks.

		100	120	140	160
1)	W^+W^-	82.2 ± 1.5	68.1 ± 1.6	55.0 ± 1.5	46.7 ± 1.4
2)	$Wb, \tau b$	9.2 ± 1.1	23.7 ± 1.5	38.4 ± 1.7	46.2 ± 1.6
3)	$\tau\tau$, $W\tau$	8.7 ± 1.1	7.9 ± 0.9	6.4 ± 0.8	6.7 ± 0.7

ble 6.1: Fractions of $t\bar{t} \rightarrow ll + X$ having 1) both leptons coming directory from the quark decay, 2) at least one lepton coming from the decay of a bottom or charm ark, and 3) leptons coming from other decays except 1) and 2). This was calculated he parton level using ISAJET Monte Carlo program.

M_{top}	100	120	140	160
CE-CE	0.064 ± 0.003	0.085 ± 0.004	0.112 ± 0.004	0.114 ± 0.005
CE-MU	0.131 ± 0.005	0.175 ± 0.005	0.218 ± 0.006	0.279 ± 0.006
CE-MI	0.039 ± 0.003	0.042 ± 0.003	0.054 ± 0.003	0.053 ± 0.003
CE-PE	0.011 ± 0.001	0.013 ± 0.002	0.014 ± 0.002	0.013 ± 0.002
MU-MU	0.055 ± 0.003	0.066 ± 0.004	0.089 ± 0.004	0.114 ± 0.005
MU-MI	0.019 ± 0.002	0.022 ± 0.002	0.038 ± 0.003	0.037 ± 0.003
MU-PE	0.013 ± 0.002	0.012 ± 0.002	0.017 ± 0.002	0.018 ± 0.002
PE-MI	0.004 ± 0.001	0.004 ± 0.001	0.004 ± 0.001	0.003 ± 0.001
Total	0.337 ± 0.012	0.419 ± 0.011	0.547 ± 0.010	0.632 ± 0.009

ble 6.2: Geometric and kinematic acceptances for the top mass from 100- 160 GeV/c^2.

rement on the plug electron is imposed. For the dimuon class, at least one triggerable on is required.

Table 6.2 summarizes the geometric and kinematic acceptance. The acceptance is reasing with the top mass (34 - 63 %) because the leptons are more likely to be in the tral region and have large P_T at higher top mass, and also because the contribution to acceptance from events with one or more leptons from the decay of b is increasing, n 24 % at M_{top}=120 GeV/c^2 to 46 % at M_{top}=160 GeV/c^2. However, note that contribution of leptons coming from b quarks are suppressed because they are less ated, and less likely to pass implicit isolation cuts such as HAD/EM and Lshr, than leptons directly coming from W, as we will see in the next section.

2 Lepton Identification

ere are 3 sources of top dileptons, as we have discussed in previous section. Leptons $t\bar{t}$ events have widely varying isolation characteristic, depending on whether their ent particle is W, bottom(charm) or tau, as shown in Figure 6.2. It is evident that tons from the decay of W's and τ's are well isolated but ones from the decay of b are isolated. Hence the efficiencies for lepton identification cuts are expected to vary ording to parentage. It also should be noted that the presence of jet activity in the events makes the detection efficiency less efficient than in Z^0 events. It can be seen the same figure (Figure6.2 (d)) that leptons from Z decays are more isolated than se from W-decays. It is not realistic to estimate the lepton detection efficiency using tons from the Z decay. Therefore, the efficiencies are extracted from the $t\bar{t}$ Monte lo. Before measuring the efficiency, it is important to check how well Monte Carlo ulates the lepton identification variables. From Figure 6.3 to 6.5, comparisons of ctron variables between data and Monte Carlo are made using central electrons from decay of Z. We have also included a small correction factor which account for the erence of identification efficiencies between Monte Carlo and data using Z events.

e correction ensures that the efficiencies for leptons from Z-decay measured in the a agree with those of simulated Z-decay leptons.

We compute the lepton selection efficiency as

$$\epsilon_{ID} = \sum_{i,j} f_{i,j}\epsilon_i \frac{\epsilon_Z^{Data}}{\epsilon_Z^{MC}}, \tag{6.3}$$

(i = lepton parentage, and j = lepton class).

s is the weighted average where $f_{i,j}$ is the fraction of leptons passing the P_T cut at ISAJET generator level[2] and ϵ_i is the efficiencies for leptons extracted from top nte Carlo. The summation runs over i's, three lepton origins which are W, b and τ l over j's, five lepton classes which are tight CE, loose CE, PE, MU and MI. The last n $(\epsilon_Z^{Data}/\epsilon_Z^{MC})$ is a correction factor to account for the difference between data and nte Carlo reconstruction. This ratio is determined from the Z decays to dileptons for h data and Monte Carlo events.

2.1 Lepton identification efficiency from Z events

st, we determine the lepton selection efficiency(ϵ_Z^{Data}) using a sample of leptons from decays in data. We select the sample of Z^0 events by requiring a lepton candidate sing the selection criteria and another cluster(or track for a muon) such that the on pair form a mass between 75 GeV/c^2 and 105 GeV/c^2. The efficiency is measured looking at whether the second lepton passes the cuts or not and the efficiency ratio lefined as r=(number of electrons passed cut) / (number of electron tested). For nts with two central electrons (CE-CE) and with two CMUO's (MU-MU), in order properly take into account the combinatorics, the effiiciency is $\epsilon = 2r/(1+r)$ as cribe below, wheres we have simply $\epsilon = r$ for the plug electron and the MI's.

The following efficiency calculations rely on a simple probability argument that lep-

[2] Strictly speaking, we took the matching in $\eta - \phi$ of particles between ISAJET generator level and ılated particle as mentioned in the previous section, but no lepton identification cuts were imposed.

s have two chances to pass the cuts, since real $Z \to l_1 l_2$ decays have two leptons. For ut efficiency of ϵ, then there are four cases:

- probability of both leptons pass the cut = ϵ^2

- probability of l_1 passes and l_2 fails the cut = $\epsilon(1-\epsilon)$

- probability of l_1 fails and l_2 passes the cut = $\epsilon(1-\epsilon)$

- probabilty of neither lepton passes the cut = $(1-\epsilon)^2$

Let N be the number of events inside the mass window with at least one tight elec- n, N1 the number of events with both leptons passing the tight cuts, N_i the number events in which both leptons pass the cut i. The number of Z events in the sample is oted by N_Z, which is unknown. We can express,

$$N = N_Z\epsilon(2-\epsilon) \tag{6.4}$$

$$N_1 = N_Z\epsilon^2 \tag{6.5}$$

$$N = N_Z\epsilon(2\epsilon_i-\epsilon) \tag{6.6}$$

ving these equations[3] ,

e efficiency for the individual cuts are

$$\epsilon_i = \frac{N_1+N_i}{N+N_1}$$

l the overall efficiency is

$$\epsilon_{all} = \frac{2N_1}{N+N_1}.$$

Eq. (1.6) can be obtainedas follows. The efficiency that a positron passes the individual cut i is essed as $\epsilon_i\,\epsilon\,N_Z$ and the efficiency for an electron is $\epsilon_i\,\epsilon\,N_Z$ in the same way. Here we should note the events which pass both electron and positron pass the cut i are counted twice ($=\epsilon^2 N$). Thus, btain $(2\times\epsilon_i,\epsilon - \epsilon^2)N_Z$.

e statistical error on this efficiency, given by binominal statistics, is

$$\delta\epsilon^i = \sqrt{\frac{\epsilon^i(1-\epsilon^i)}{N+N_1}}.$$

e efficiencies for the loose selection cuts are calculated similarly. Of course, the indi-
ual cut efficiencies remain the same if the cut is the same.; only the total efficiencies
nge.

ntral electrons

e efficiency is determined from a data sample of $Z^0 \to ee$. The event must contain one
it central electron which passes the electron identification cuts listed in Table 4.1 and
in side the fiducial region. In addition, a second central cluster is required to pass
s: E_T >20 GeV and a track pointing to it with P_T >10 GeV/c. There remains 509
nts. The sample contains 394 events which both electrons pass the tight cuts, and
he type tight-tight and 450 events which one pass tight and the other pass our loose
ction cuts. The central electron identification effiicencies for the different selections
summarized in Table 6.3. They are measured to be 87.3 ± 1.1 % and 93.8 ± 0.8 %
the tight and loose selection criteria, excluding about 4% loss of electrons associated
h the conversion removal.

ig electrons PE

e plug electron ID efficiency was measured using $Z^0 \to ee$, where one electron is in
central region satisfying with the tight selection criteria and the other in the plug
sfying E_T >20 GeV and the isolation measured in the calorimeter is less than 0.1.
r sample consists of 115 tight-loose Z's. For this sample, a three-dimensional track
uirement on plug electrons was imposed. Only about 1/3 of the total CE-PE Z events
s this requirement. The track requirement is taken as a fiducial cut, and absorbed
part of the geometrical acceptance in the calculation of the top detection efficiency.

Cut	N_i	ϵ_{Data}	ϵ_{MC}
(tight cut)			
HAD/EM < 0.05	484	0.972 ± 0.005	0.837
E/P < 2.0	478	0.966 ± 0.006	0.983
Δx < 1.5 cm	466	0.952 ± 0.007	0.990
Δz < 3.0 cm	500	0.990 ± 0.003	0.988
χ^2(Strip) < 15.	489	0.978 ± 0.005	0.994
L_{shr} < 0.2	504	0.994 ± 0.002	1.000
Total (tight)	394	0.873 ± 0.011	0.802
(loose cut)			
HAD/EM < 0.055 + 0.045E_T/100	504	0.994 ± 0.002	0.936
E/P < 4.0	509	1.000 ± 0.000	0.998
Δx < 1.5 cm	466	0.952 ± 0.007	0.998
Δz < 3.0 cm	500	0.990 ± 0.003	0.988
L_{shr} < 0.2	504	0.994 ± 0.002	1.000
Total (loose)	450	0.938 ± 0.008	0.909

ble 6.3: Central electron selection efficiency from $Z \to ee$ in data. Both tight and se selection efficiencies are listed. Efficiencies calculated from Z Monte Carlo are also wn in the last column

e plug electron isolation efficiency for the top quark is estimated from the $t\bar{t}$ Monte rlo. The efficiencies are summarized in Table 6.4 and the overall efficiency is found be 85.2 ± 0.03 %.

	Cut	Npass	ϵ		
HAD/EM	< 0.05	113	0.983	±	0.012
χ^2(3x3)	< 3.	111	0.965	±	0.017
N(VTPC)	> 0.5	109	0.948	±	0.021
χ^2(depth)	< 15.	109	0.948	±	0.021
Combined		98	0.852	±	0.033

Table 6.4: Plug electron selection efficiency

ntral muons MU

m a sample of $Z^0 \rightarrow \mu\mu$ events, the efficiencies for the minimum ionizing and a match ween the CTC track and the muon chamber track was determined. The number of nts in the sample is 394 events. The efficiency is summarised in Table 6.5 and the rall selection efficiency is estimated to be 92.6±0.1%. The efficiency of the track lity requirement is measured to be 0.99±0.1% using a sample of electron tracks from $\rightarrow e\nu$ decays. Since the matching between a CTC track and a muon segment track is te efficient(>0.99), the selection efficiency for CMIO is almost equal to the one for UOs. The CMIO efficiency can be obtained from table 6.5 by removing the Δx cut. We also calculated the muon selection efficiency for Monte Carlo events and results shown in Table 6.5.

.2 Efficiency calculation from top Monte Carlo

this point we calculated the lepton selection efficiencies using Z events. We can npute the correction factor in eq. 6.3. Next step is to extract lepton identification

cut	N_i	ϵ_{Data}	ϵ_{MC}
EM	368	0.965 ± 0.007	0.996
HAD	385	0.993 ± 0.005	0.982
EM+HAD	392	0.997 ± 0.002	1.000
dX	393	0.999 ± 0.001	1.000
	340	0.926 ± 0.010	0.977

le 6.5: Central muon selection efficiency from $Z \rightarrow \mu\mu$. Efficiencies from Z Monte lo are also shown.

ciencies from the top Monte Carlo events. Distributions for identification variables e shown in Figure 4.3 - 4.8.

	ϵ_W	ϵ_b	ϵ_τ	ϵ_{total}
CE(tight)	0.794 ± 0.009	0.114 ± 0.016	0.822 ± 0.036	0.670 ± 0.014
CE(loose)	0.872 ± 0.006	0.156 ± 0.017	0.854 ± 0.028	0.739 ± 0.014
PE	0.627 ± 0.022	0.092 ± 0.051	0.454 ± 0.122	0.520 ± 0.022
MU	0.924 ± 0.003	0.213 ± 0.020	0.885 ± 0.020	0.775 ± 0.015
MI	0.893 ± 0.010	0.131 ± 0.043	0.829 ± 0.064	0.732 ± 0.018

le 6.6: Single lepton identification efficiency extracted from top Monte Carlo. Errors statistical only.

In Table 6.6 we give the single lepton efficiencies (ϵ_i in Eq. 6.3) of the 3 sources and asses of leptons[4] for M_{top}=140 GeV/c^2 for instance to illustrate how the efficiencies calculated. The fractions f_W, f_b and f_τ depend slightly on the top mass and on the idity of the leptons considered. For M_{top} = 140 GeV/c^2 and for central electrons, fractions are f_W=0.767±0.013, f_b=0.185±0.012, and f_τ=0.049±0.007. The efficiency the single central electron is calculated using these fractions and the first row in

Correction factors to account for the difference between Monte Carlo and real data are already ıded in these numbers.

ble 6.6 as follows:

$$
\begin{aligned}
& f_W\,\epsilon_W + f_b\,\epsilon_b + f_\tau\,\epsilon_\tau \\
= \;& 0.767 \times 0.794 + 0.207 \times 0.114 + 0.049 \times 0.822 \\
= \;& 0.670
\end{aligned}
$$

ilarly, the fractions for the muons are f_W=0.746±0.013, f_b=0.207±0.012, and f_τ=0.048±0.007. e efficiencies ϵ(class,W), ϵ(class,b) and ϵ(class,τ) include a small correction factor ch accounts for the difference between real data and Monte Carlo. We find the ratios $^{ata}/\epsilon_Z^{MC}$) to be 1.04, 0.99, 1.08, and 0.95 for the tight CE, loose CE, PE, and MU/MI on classes, respectively. In addition, central electron efficiencies have been degraded 4% to account for losses due to the conversion cuts.

The total lepton identification efficiency in dilepton events is obtained by summing r the eight dilepton categories. It is given in table 6.7. The entries in table 6.7 products of the single lepton efficiencies of table 6.6, except for the CE-CE case ere the formula $\epsilon = \epsilon_{\rm tight}\,(2\,\epsilon_{\rm loose} - \epsilon_{\rm tight})$ was used to take into account correlations ween tight and loose central electron cuts. Figure 6.7 shows the plot of the lepton ntification efficiency as a function of top mass. It can be seen that the efficiency onstant, as we expect, if we count only leptons coming from the decay of W. The ciency is decreasing, if we count all the lepton contributions to the efficiency, because fraction of having leptons from b-decays is increasing as a function of the top mass, also because leptons from b-decay are less likely to pass identification cuts.

In table 6.6, the MI efficiency is low by two sigma (4%) compared with the muon(MU), ough these efficiencies are expected to be equal. We believe this could be a statistical tuation, with negligible effect in the overall detection efficiency.

	ϵ_{ID}			
M_{top}	100	120	140	160
CE-CE	0.625 ± 0.017	0.577 ± 0.019	0.494 ± 0.014	0.441 ± 0.013
CE-MU	0.657 ± 0.017	0.612 ± 0.019	0.519 ± 0.015	0.463 ± 0.013
CE-MI	0.631 ± 0.018	0.596 ± 0.022	0.490 ± 0.016	0.451 ± 0.014
CE-PE	0.451 ± 0.020	0.438 ± 0.027	0.341 ± 0.016	0.333 ± 0.016
MU-MU	0.782 ± 0.018	0.724 ± 0.019	0.601 ± 0.016	0.550 ± 0.014
MU-MI	0.751 ± 0.020	0.705 ± 0.023	0.568 ± 0.018	0.536 ± 0.016
MU-PE	0.537 ± 0.023	0.518 ± 0.031	0.394 ± 0.019	0.396 ± 0.019
PE-MI	0.516 ± 0.023	0.505 ± 0.032	0.372 ± 0.019	0.386 ± 0.019

ble 6.7: The lepton selection efficiency for the top mass from 100-160 GeV/c². Errors statistical only.

3 Isolation

e dilepton isolation efficiencies shown in table 6.8, are the fractions of dilepton events sing the P_T and lepton ID cuts, which also pass the isolation cuts. The isolation cut is y efficient because we require only one central isolated lepton in the tracking chamber the CECE,CEMU,MUMU categories, which account for 82% of the acceptance for $_{p}$ = 140 GeV/c^2. In addition to requiring at least one CE, MU or MI isolated in tracking chamber, for the CE-MI, CE-PE, MU-MI, MU-PE, and PE-MI categories % of the acceptance), the PE or MI leg is required to be isolated in the calorimeter, ılting in a lower isolation efficiency for these categories.

4 Event toplogy cuts

e efficiency for event topology cuts (ϵ_{event}) is the fraction of dilepton events passing P_T and isolation cuts which also pass the following cuts combined: opposite-sign, ariant mass, and missing E_T (both magnitude and direction). See table 6.9. For M_{top} 60 GeV/c^2, the efficiencies of the opposite-sign and missing E_T cuts are 94% and

	$\epsilon_{\rm Isol}$			
$M_{\rm top}$	100	120	140	160
CE-CE	0.989 ± 0.008	0.973 ± 0.011	0.984 ± 0.008	0.988 ± 0.007
CE-MU	0.989 ± 0.005	0.986 ± 0.005	0.980 ± 0.006	0.975 ± 0.006
CE-MI	0.812 ± 0.036	0.830 ± 0.032	0.839 ± 0.030	0.782 ± 0.033
CE-PE	0.889 ± 0.105	1.000 ± 0.000	0.867 ± 0.088	0.842 ± 0.084
MU-MU	0.979 ± 0.009	0.982 ± 0.008	0.980 ± 0.008	0.988 ± 0.006
MU-MI	0.880 ± 0.036	0.856 ± 0.037	0.875 ± 0.029	0.831 ± 0.035
MU-PE	0.955 ± 0.044	0.824 ± 0.092	0.704 ± 0.088	0.926 ± 0.050
PE-MI	0.875 ± 0.117	1.000 ± 0.000	0.875 ± 0.117	1.000 ± 0.000
Total	0.959 ± 0.006	0.955 ± 0.006	0.951 ± 0.006	0.947 ± 0.006

le 6.8: Isolation cut efficiency for the top masses:100-160 GeV/c^2. Errors are statis-
l only.

%, respectively. The invariant mass cut applied in the ee and $\mu\mu$ channels is 80% cient. The combined efficiency of the three cuts on dileptons is $\epsilon_{\rm event} = 69\%$.

5 Two-jet cut

investigated the efficiency for the two-jet cut in section 5.7 to determine the jet E_T esholds. The reasult was tabulated in Table 5.2. Jet multiplicity and E_T spectrum affected by Monte Carlo assumptions about gluon radiation. ISAJET $t\bar{t}$ Monte lo generator includes radiation of gluons from the initial- and final-state partons. misions of these gluons increases the jet multiplicity and therefore increases the ciency of the number-of-jets requirement. For M_{top}=120 GeVc^2, approximately 30 % he jets passing the selection cuts are due to gluon radiation.

To get around the problem of the poorly known effects due to the gluon radiation, calculated the efficiency ($\epsilon_{\rm Two-jet}$) listed in Table 5.2 in the following manner.

$$\epsilon_{\rm Two-jet} = 1/2\ (\epsilon^{\rm ON}_{\rm Two-jet} + \epsilon^{\rm OFF}_{\rm Two-jet}), \tag{6.7}$$

	100	120	140	160
CE-CE	0.52 ± 0.04	0.55 ± 0.03	0.59 ± 0.03	0.57 ± 0.03
CE-MU	0.73 ± 0.02	0.71 ± 0.02	0.75 ± 0.02	0.75 ± 0.02
CE-MI	0.71 ± 0.05	0.67 ± 0.04	0.78 ± 0.03	0.71 ± 0.04
CE-PE	0.50 ± 0.18	0.59 ± 0.12	0.69 ± 0.13	0.50 ± 0.13
MU-MU	0.61 ± 0.03	0.61 ± 0.03	0.54 ± 0.03	0.58 ± 0.03
MU-MI	0.60 ± 0.06	0.58 ± 0.06	0.50 ± 0.05	0.55 ± 0.05
MU-PE	0.71 ± 0.10	0.64 ± 0.13	0.89 ± 0.07	0.76 ± 0.09
PE-MI	0.71 ± 0.17	0.86 ± 0.13	0.86 ± 0.13	1.0 ± 0.00
Total	0.659 ± 0.014	0.662 ± 0.013	0.690 ± 0.012	0.688 ± 0.012

le 6.9: The combined efficiency of the dilepton charge, invariant mass, and missing cuts for top masses from 100-160 GeV/c^2. Errors are statistical only.

ere $\epsilon^{ON}_{Two-jet}$ is the two-jet cut efficiency with the default ISAJET, and $\epsilon^{OFF}_{Two-jet}$ is nputed by disabling gluon radiation in ISAJET. Thus, we define the efficiency as a an value of both numbers. We have also checked the jet multiplicity using HERWIG nte Carlo generator [49] and found that 73.9 ± 2.8 % of top Monte Carlo events of GeV/c^2 were satisfied with the two-jet requirement. This result is consistent with ISAJET average of 75.1 ± 1.0 %.

6 Trigger

ciencies of single electron or muon triggers are calculated as shown in Table 6.10 n data using independent triggers [42].

Trigger	Electron	Muon
Level 1	99.2 ± 0.08	$94.99^{+0.74}_{-0.82}$
Level 2	93.5 ± 0.3	$93.68^{+1.27}_{-1.52}$
Level 3	97.4 ± 0.2	97.7 ± 0.6

Table 6.10: Single lepton trigger efficiency at each trigger level

Dilepton events are collected with two of any high P_T single lepton triggers. The ger efficiency for dilepton events is evaluated using the trigger efficiency for inclusive :on trigger. The trigger effficiency for the dilepton events is calculated as is $1\text{-}f_1 \cdot f_2$, ere ff_1 and f_2 are the separate probabilities for failing the first and second triggers, pectively. In case of having no trigger for one of two leptons, for instance for CMIO, set to be 1. A summary of dilepton trigger efficiencies is shown in Table 6.11.

	$\epsilon_{\text{trigger}}$			
M_{top}	100	120	140	160
CE-CE	0.993	0.993	0.993	0.993
CE-MU	0.989	0.989	0.989	0.989
CE-MI	0.916	0.916	0.916	0.916
CE-PE	0.983	0.983	0.979	0.983
MU-MU	0.983	0.983	0.983	0.983
MU-MI	0.869	0.869	0.869	0.869
MU-PE	0.973	0.974	0.967	0.973
PE-MI	0.797	0.803	0.745	0.797
Total	0.972	0.974	0.972	0.976

Table 6.11: Trigger efficiency

7 Total detection efficiency

le 6.12 shows the detection efficiency as a function of top mass for each dilepton egory. The sums over dilepton categories are also provided. Efficiency plots before :he two-jet cut, and b) after the additional two-jet cut, are shown in Figures 6.10 6.11. respectively. In table 6.13 a rundown is given of all the individual efficiencies ch contribute to the total detection efficiency for a top mass of 140 GeV/c^2.

The total detection efficiency as a function of the top mass remains relatively constant he top mass increases because the decrease in the the lepton detection efficiency with ss is compensated by the rising acceptance due to geometrical and P_T cuts.

	ϵ_{total}				
M_{top}	100	120	140	160	180
CE-CE	0.007	0.016	0.024	0.024	0.028
CE-MU	0.020	0.047	0.062	0.078	0.080
CE-MI	0.004	0.008	0.012	0.010	0.011
CE-PE	0.001	0.002	0.002	0.002	0.002
MU-MU	0.008	0.018	0.021	0.029	0.032
MU-MI	0.002	0.004	0.006	0.007	0.010
MU-PE	0.002	0.002	0.003	0.004	0.005
PE-MI	0.000	0.001	0.001	0.001	0.001
Total	0.044	0.098	0.132	0.154	0.169
Total(no jet cut)	0.135	0.156	0.175	0.184	0.192

Table 6.12: Total efficiency

	$\epsilon_{geom \cdot P_T}$	ϵ_{ID}	ϵ_{Isol}	ϵ_{event}	$\epsilon_{two-jet}$	$\epsilon_{Trigger}$	ϵ_{total}
CE-CE	11.2	54.1	98.8	59.1	75.1	99.3	2.6
CE-MU	21.8	51.9	98.3	75.1	75.1	98.9	6.2
CE-MI	5.4	49.0	84.6	78.3	75.1	91.6	1.2
CE-PE	1.4	34.1	85.7	66.7	75.1	97.9	0.2
MU-MU	8.9	60.1	98.4	54.0	75.1	98.3	2.1
MU-MI	3.8	56.8	87.7	50.2	75.1	86.9	0.6
MU-PE	1.7	39.4	79.5	87.1	75.1	96.7	0.3
PE-MI	0.4	37.2	91.7	90.9	75.1	74.5	0.1
Total (%)	54.7	52.8	95.4	69.4	75.1	97.3	13.4

Table 6.13: Dilepton efficiency for a top mass of 140 GeV/c^2

8 Systematic uncertainties

describe systematic uncertainties of the dilepton analysis in this section. The basic a to estimate these errors are to compare the different generator or simulator and to asure the variation by chaanging the parameters.

Acceptance due to geometrical and P_T cuts

e, one source of systematic uncertainty is the modeling of initial state radiation. ial state radiation affects the motion of the $t\bar{t}$ system and hence the rapidity and nsverse momentum distributions of the top quark decay products. This effect can be died by turning on and off gluon radiation in ISAJET. Another systematic uncertainty ilts from the choice of structure functions. Our estimate is 3% for the total systematic ertainty on the geometrical and kinematical acceptance.

Lepton identification

extracted the lepton identification efficiencies from the $t\bar{t}$ Monte Carlo, together h Z events in data to correct for the difference between data and Monte Carlo. certainties depend largely on how the Monte Carlo models the $t\bar{t}$ production and ay. Detector simulation affects lepton identification. Here, we take half the difference ween the result obtained from two different simulations of the CDF detector; this is . The modeling of gluon radiation affects the isolation properties of the leptons, hence their identification efficiency. We studied this effect by turning on and off on radiation in ISAJET, and taking half the difference in the corresponding lepton ntification efficiencies as systematic uncertainty. This gives 2.4%. Since these two tributions are clearly independent, the systematic uncertainty on lepton identification .4% $\oplus$ 5% = 6%.

Isolation

technique for determining the systematic uncertainty on lepton isolation is the same or lepton identification. The effect due to gluon radiation and detector simulation both 1 %. Hence the combined systematic uncertainty is conservatively 1% $\oplus$ 1% = . We have also investigated the uncertainty due to the fragmentation model ISAJET gments quarks according to the Peterson fragmentation function:

$$D(z) = 1/z \times (1 - 1/z - \epsilon/(1-z))^{-}2$$

ere z is the fraction of the quark momentum carried by the particle (usually a meson) t contains the quark. The parameter ϵ for top qurk in ISAJET defaults to 0.5. We e changed ϵ to 0.2 and 1.5 and generated samples of top Monte Carlo with M_{top}=140 V/c^2. As a result, no significant change was observed.

Trigger

ors of each single lepton trigger efficiency are propagated to the total detection effi- icy, which result in observation of less than 1%.

Jet

case of requiring the two-jet cut, we have to take into account systematic uncertainty to jets and this arises the largest contribution.

Uncertainties in the understanding of the jet energy scale and the gluon radiation reflected in an uncertainty in the total detection efficiency in case of requiring the -jet cuts in the analysis, where we require that there are at least two jets with E_T) GeV. The energy scale is estimated to be $\pm$ 10% for jets of E_T near 10 GeV. A $\pm$ % uncertainty in the jet energy scale, which depends on M_{top}, results in the change letection efficiency by $\pm$ 1.3(M_{top}=160 GeV/^{2}) - 5.0(M_{top}=100 GeV/^{2}).

The ISAJET Monte Carlo generator includes radiation of gluons from the initial- final state-partons. These radiations increases the jet multiplicity, which results in reasing th efficiency of the number-of-jet requirement. We estimate that $\sim$ 20 - 30% ets in the $t\bar{t}$ eventscoming from gluon radiation. Disabling gluon radiation in ISAJET reases the efficiency of the jet multiplicity requirement by 6.4% for M_{top}=140 GeV^2.

Others

measure some of the efficiencies, we depend much on Monte Caro. This is about 3

We also take the 10% uncertainty in luminosity measurement.

Table 6.14: Summary of uncertainties in the acceptance calculation.

Uncertainty source	No jet cut
Geometrical and P_T cuts	3%
Lepton detection	
(a) gluon radiation	2.4%
(b) simulation	5 %
Isolation	
(a) gluon radiation	1 %
(b) simulation	1 %
Calorimeter(jet) energy scale on the missing E_T	2 %
MC statistics	3%

To obtain the error in the expected number of events we have added the statistical or in quadrature with the systematic error. A systematic error of 13% is used except the calculation of the two jet efficiency cut. The later systematic error depends two factors the gluon radiation and the jet energy scale. The error due to gluon iation is obtained by turning off the gluon radiation in ISAJET. We use half the erence between on and off as the sigma for the gluon radiation. By changing the jet rgy scale by ± 10% we determine the systematic error in the jet energy scale. The tematic error is a function of the top quark mass and is given in table 6.15.

Systematic error in ϵ_{total} (%) 13% error in quadrature with error on jets				
M_{top}	100	120	140	160
Gluon radiation	36.3	12.1	6.4	2.9
Energy scale	5.0	3.6	2.2	1.3
Other from table above	8	8	8	8
total	38	15	10	9

Table 6.15: Systematic uncertainty in the two-jet cut

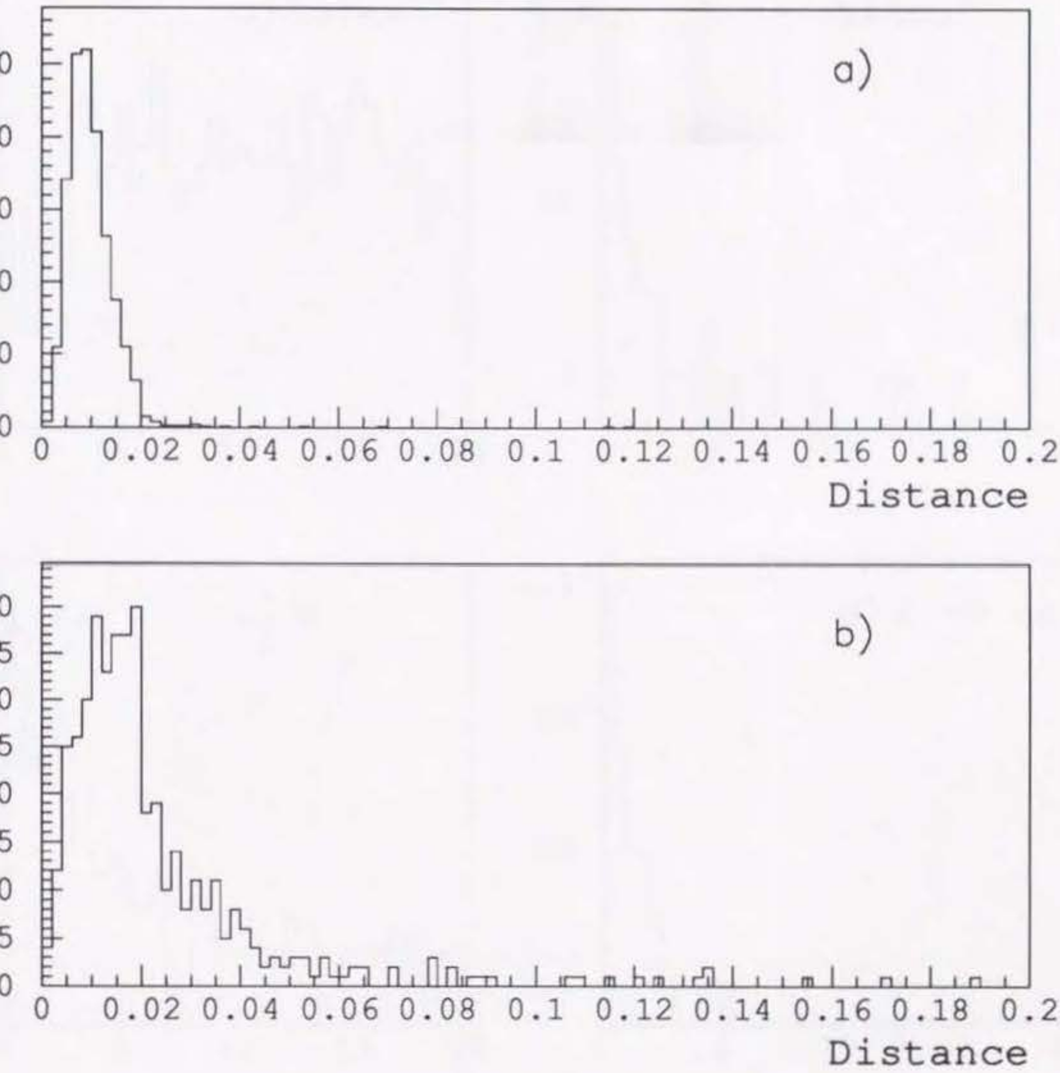

ure 6.1: A matching in $\eta - \phi$ between reconstructed electron and electron before ulation. Electrons from a) W decays and b) bottom decays in $t\bar{t}$ events. The top ss is 140 GeV

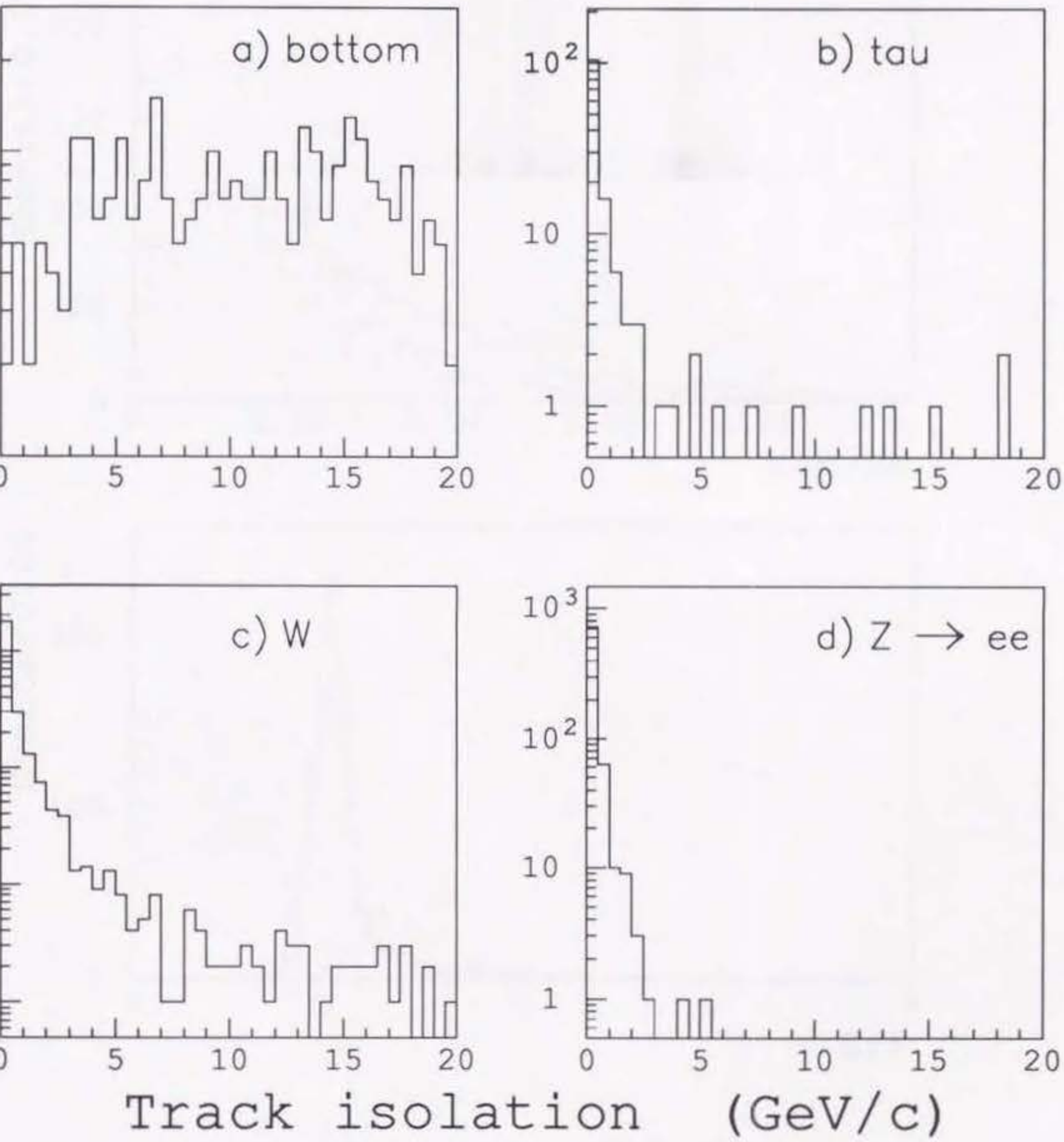

ure 6.2: Track isolation distributions from top Monte Carlo ($M_{top} = 140$ GeV/c^2) for ons from a) b decays, b) τ decays, and c) W decays. Also shown in d) is the track ation for electrons from Z decays.

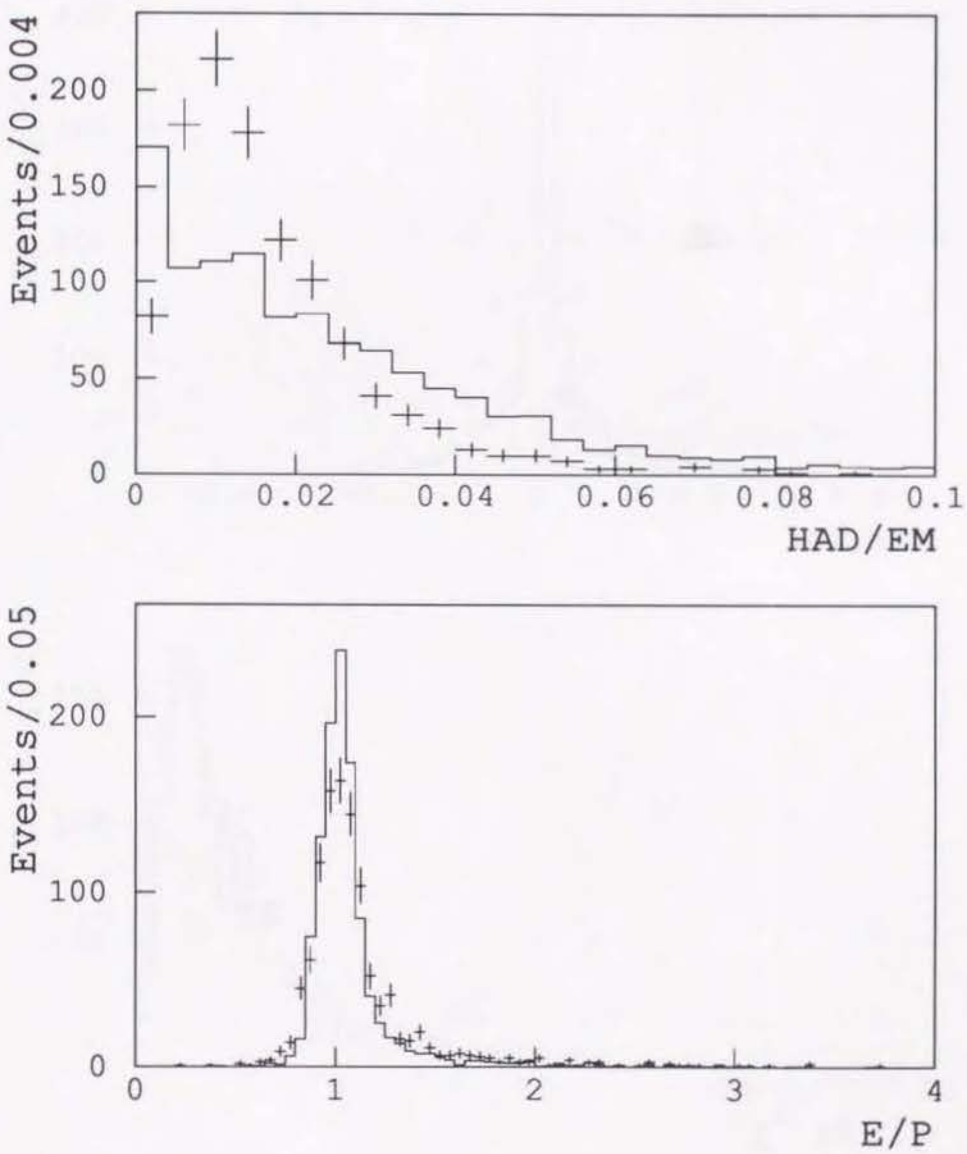

ure 6.3: Central electron quality variables: HAD/EM and E/p. The full histogram responds to the distribution from ISAJET Monte Carlo $Z \to ee$ events, and points $Z \to ee$ events from CDF data.

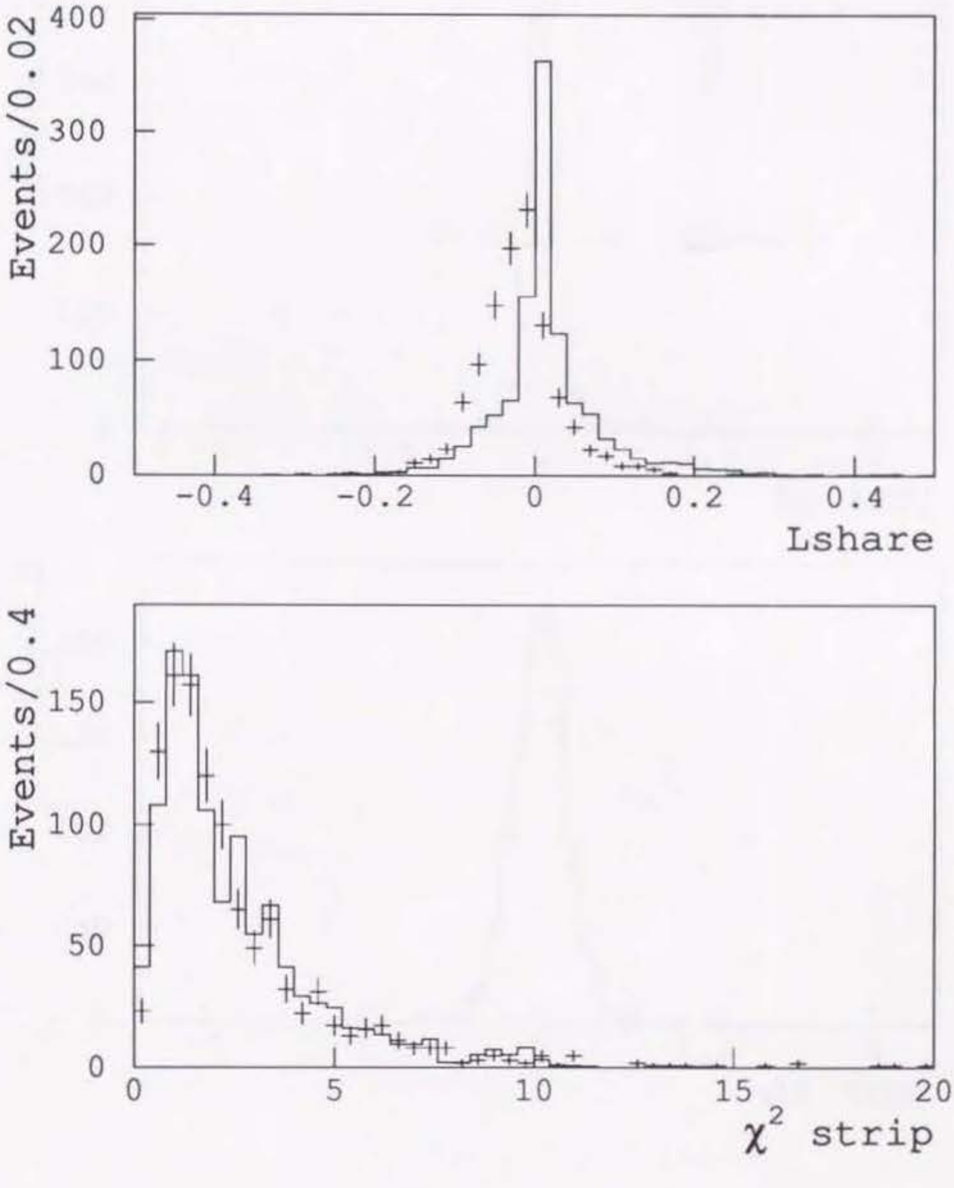

ure 6.4: Central electron quality variables: Lshare and χ^2. The full histogram cor-
ponds to the distribution from ISAJET Monte Carlo $Z \rightarrow ee$ events, and points for
$\rightarrow ee$ events from CDF data.

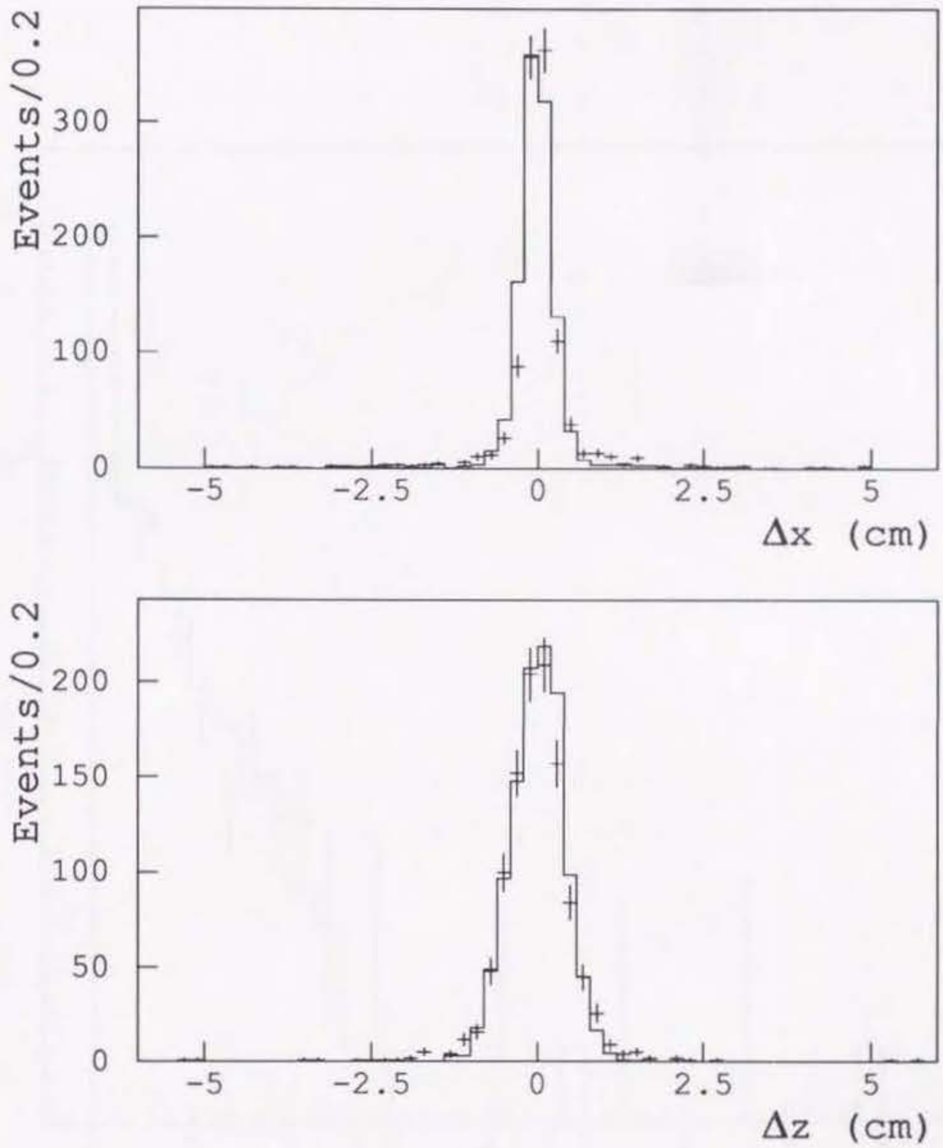

ure 6.5: Central electron quality variables: a) match in the $R\phi$ view between the ck and the shower position as measured in the strip chamber and b) match in the iew between the track and the shower position as measured in the strip chamber. e full histogram corresponds to the distribution from ISAJET Monte Carlo $Z \rightarrow ee$ nts, and points for $Z \rightarrow ee$ events from CDF data.

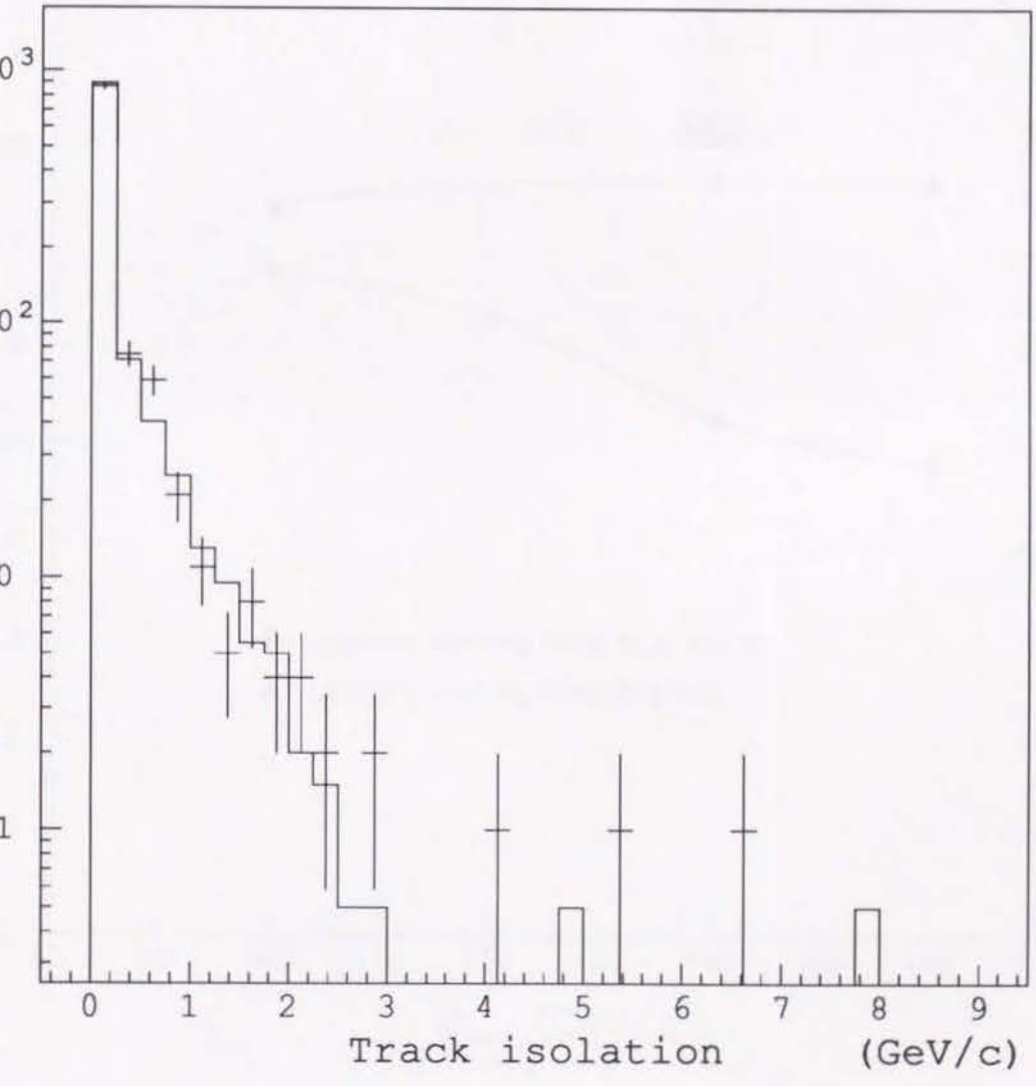

ure 6.6: Track isolation distribution of the Z decay into ee from CDF data is shown ints), and the histogram corresponds to track isolation distribution from ISAJET nte Carlo, together with a simulation of the CDF detector.

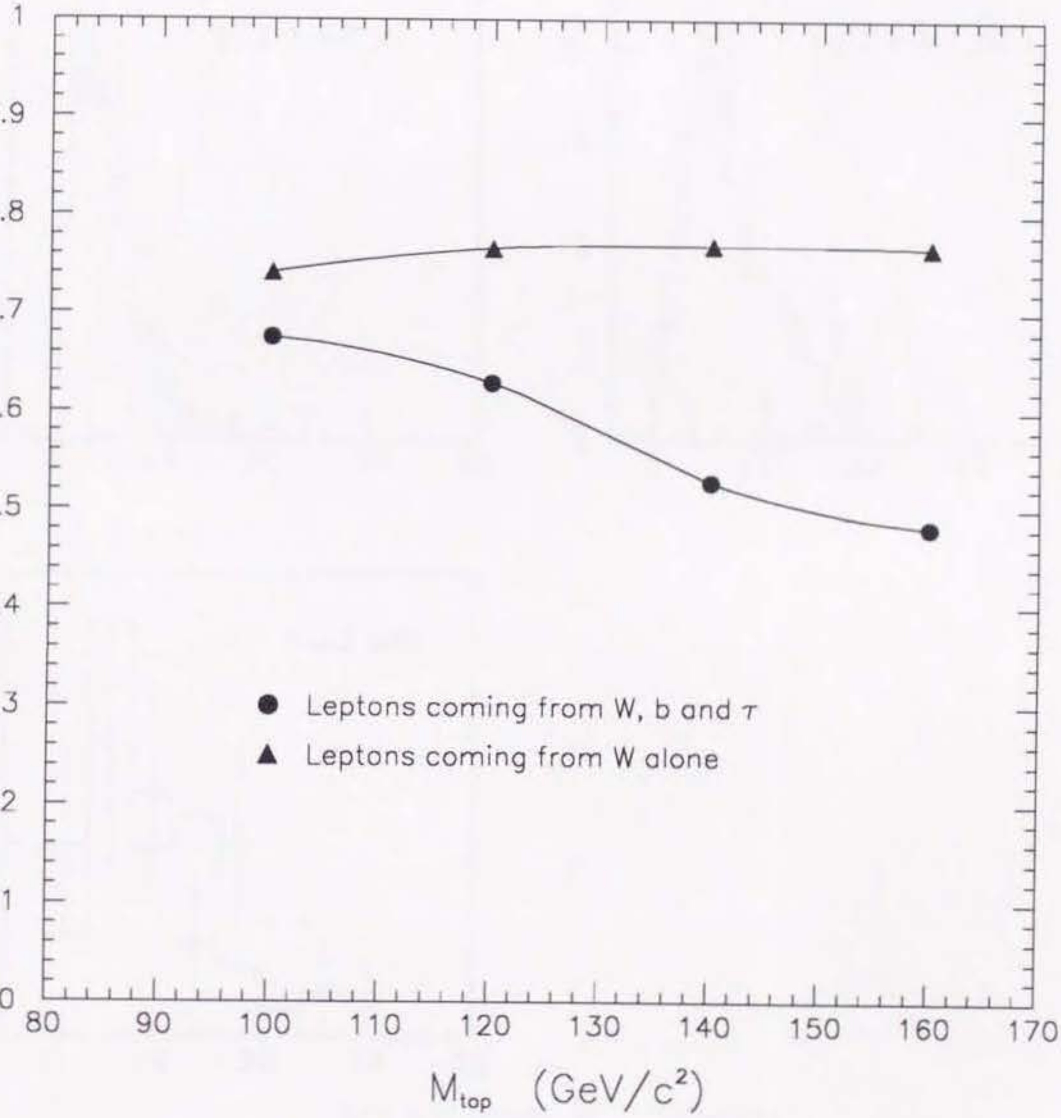

ure 6.7: Lepton detection efficiency as a function of top quark mass. Two curves ws efficiencies of leptons coming from WW only and all the lepton contribution from bottom or τ.

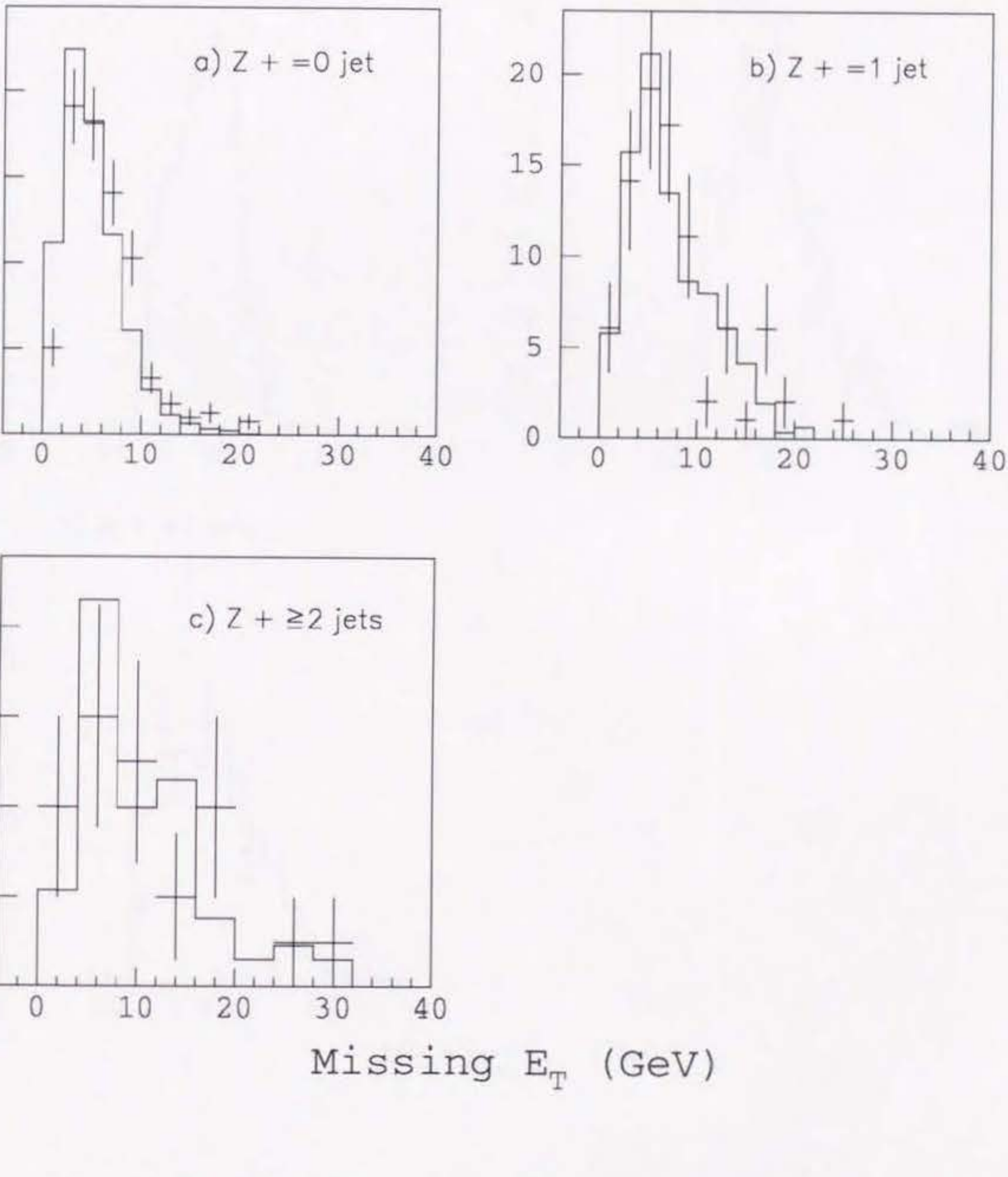

ure 6.8: Distributions of the missing transverse energy of Z → ee events. The ogram is the Monte Carlo prediction and the overlay is from data: a) Z + 0 jet, b) 1 jet and c) Z + ≥ 2 jets.

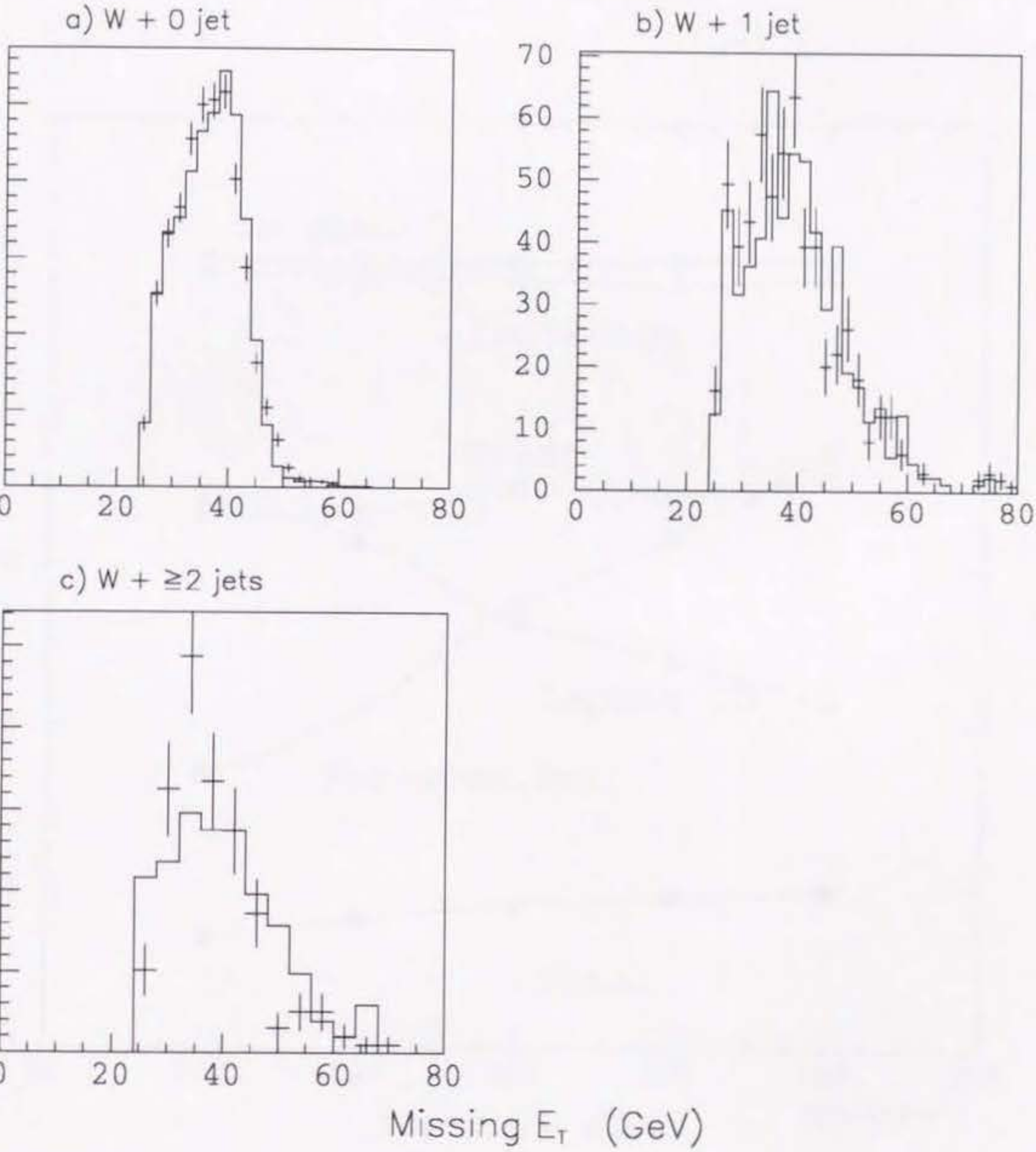

ure 6.9: Distributions of the missing transverse energy of W $\rightarrow e\nu$ events. The ogram is the Monte Carlo prediction and the overlay is from data: a) W + 0 jet, b) + jet, c) W + $\geq$ 2 jets.

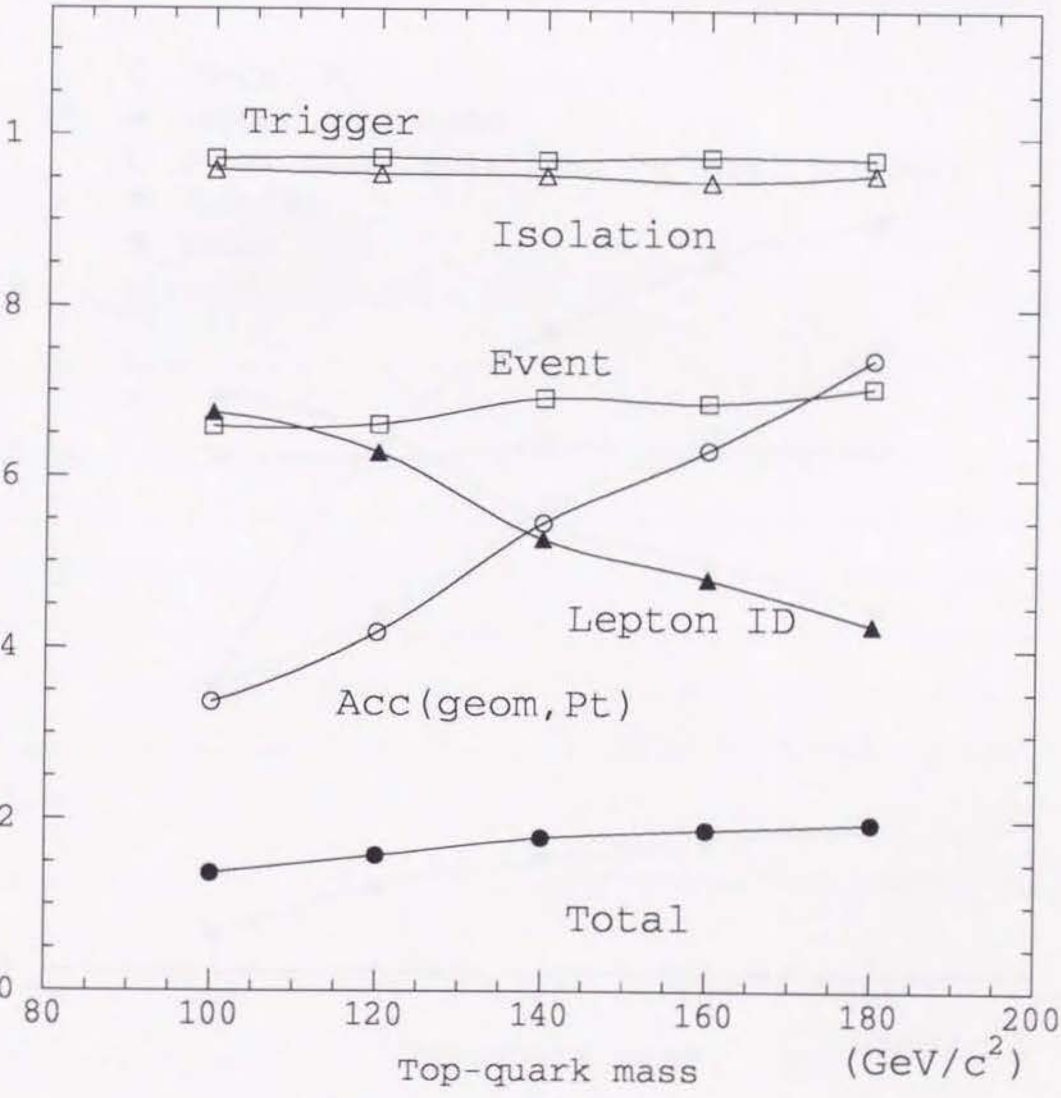

ure 6.10: Dilepton efficiency as a function of top quark mass without the two-jet cut

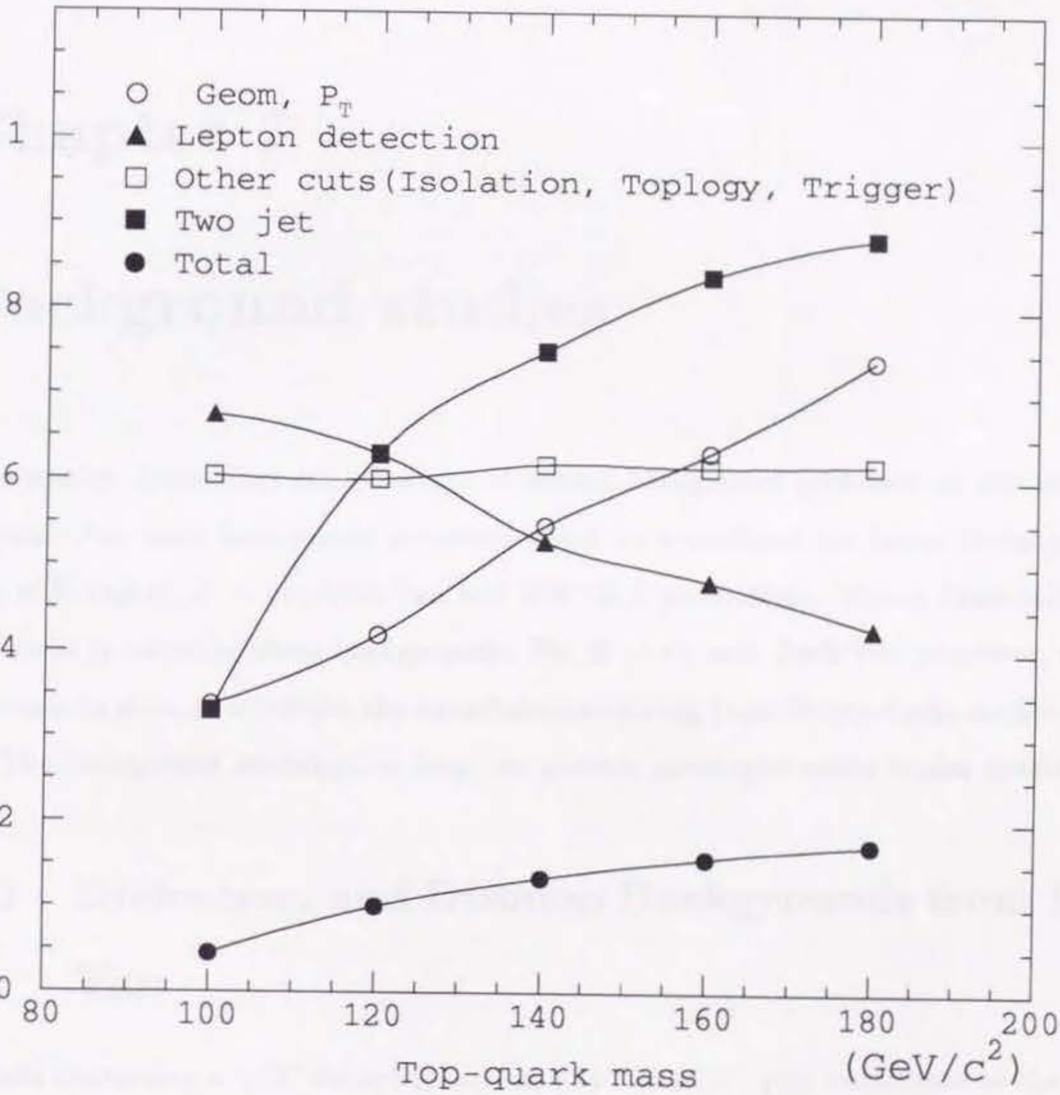

ure 6.11: Dilepton efficiency as a function of top quark mass with the two-jet cut. efficiencies for isolation, event toplogy cut and trigger are combined in the plot.

hapter 7

ackground studies

s section determines contributions of several background processes to our selection eria. The main background processes which we considered are heavy flavor production of $b\bar{b}$ and $c\bar{c}$, $Z \to \tau\tau$, Drell-Yan and WW/WZ productions. Monte Carlo technique used to estimate these backgrounds. For $Z \to \tau\tau$ and Drell-Yan processes, we use vents in data to minimize the uncertainties coming from Monte Carlo modeling.

The background contribution from the particle misidentification is also considered.

1 Dielectron and Dimuon Backgrounds from Drell-Yan

nts containing a γ/Z^0 decaying into an e^+e^- or $\mu^+\mu^-$ pair contribute to the backund to the top signal. Although events in the Z mass window between 75 and 105 $/c^2$ are explicitly removed from the signel region, Drell-Yan continuum events out- the window are potential backgrounds.

We use the observed $Z^0 \to$ ee, and $\mu\mu$ distributions to estimate the background from continuum. Since the modeling of the tail of the P_T distribution is important, it is rable to be independent of the Monte Carlo prediction. Our initial assumption is the P_T^{γ,Z^0} distributions inside and near the Z^0 region are similar. Figure 7.1 shows

	Cut	Number of Events	Fraction
a)	Z events	1151	100%
b)	$\not\!\!E_T$ (uncorr) > 20GeV	32	2.8%
c)	$\not\!\!E_T$ (corr) > 20GeV	27	2.3%
d)	$\not\!\!E_T$ (uncorr) > 25GeV	16	1.4%
e)	$\not\!\!E_T$ (corr) > 25GeV	9	0.8%
f)	e) + $\Delta\phi(\not\!\!E_T$,jet) cut	4	0.3%
g)	f) + $\Delta\phi(\not\!\!E_T,l)$ cut	3	0.3%
h)	g) + 1 or more jets w/ E_T>10	3	0.3%
i)	g) + 2 or more jets w/ E_T>10	1	0.1%

Table 7.1: Cut rejections. Each line is an independent cut.

P_T^{γ,Z^0} distribution from ISAJET Monte Carlo[1] for near Z mass peak (75 $<M_{l^+l^-}$ or $<M_{l^+l^-}$) and inside Z mass region. ISAJET Monte Carlo predicts that there is a ht stiffening with increasing mass in the $P_T^{\gamma,Z}$ which could lead to an overestimate of background. When looking at $P_T^{\gamma,Z}$ in data, it turns out that the $P_T^{\gamma,Z}$ distribution no mass dependence inside and outside Z mass region as shown in Figure 7.2, and our umption is verified. We also note that the ISAJET Monte Carlo does not reproduce jet multiplicity in Z events as shown in Figure 7.3. For these reasons, Drell-Yan kground is estimated from Z events in data rather than using Monte Carlo. The thod consists of (1) the determination of the rejection factors, which are applied to Drell-Yan events outside the Z-window, for the missing E_T and jet cuts obtained n Z events; follwed by (2) applying a small Monte Carlo correction to account for mass dependence of the P_T and jet activity.

We exploited in section 5.6 that both the magnitude and direction of the missing E_T the useful variables. We require that the missing E_T must be greater than 25 GeV, also that the direction of the missing E_T must be separated from a jet by more than , if the missing E_T is less than 50 GeV. Table 7.1 summarizes how the events inside nass region (1151 events) are reduced by each selection cut. In the table, fraction

[1] We have used version 6.36 of ISAJET Monte Carlo to generate the Drell-Yan process.

M^{ll}(GeV)	$P_T>$ 15GeV ($\times 10^{-2}$)	$P_T>$ 20GeV ($\times 10^{-2}$)	$P_T>$ 30GeV ($\times 10^{-3}$)
40.0	1.832	0.992	2.824
60.0	2.500	1.184	3.947
80.0	3.133	1.533	5.533
100.0	3.333	1.594	5.217
120.0	3.889	1.944	5.833
200.0	5.6		
300.0	8.5		

ole 7.2: Efficiencies of having two or more jets with different parton P_T threshold h Drell-Yan masses.

passing different missing E_T cuts are shown and the missing E_T corrected for jets es better rejection by a factor of two in case of the missing E_T >25 GeV. The latter helps reduce Drell-Yan background since the large missing E_T often arizes from measurement of hadronic jets.. The definition of the cut was chosen from looking Figure 5.9 (a) and (b) for Z + 1 jet events. Also shown in the table is the rejection or for the jet requirement.

Next, the missing E_T and jet rejection factors obtained from Z events are corrected mass dependence due to small changes in P_T and jet activity. We use two-jet cut ciencies as a function of mass from a boson+2 jet matrix element Monte Carlo [43]. ole 7.2 tabulates the fraction of γ/Z^0 events with two jets of P_T larger than the icated value. Note that these are parton P_T's. The 15 GeV column corresponds to GeV jets before correction. We find that for our cuts, using the jet activity from events and assigning it to events outside the Z^0 mass window requires a correction or[2] of 0.87. Even though we only use the mass dependence, and not the absolute diction of Mangano's boson + 2 jet matrix element Monte Carlo, it is interesting to

Using the first column of Table 7.2, we calculate the correction factor as follows. For a 20 GeV on P_T cut, 88 events have a mass less than 75 GeV and the average mass for these events is 56 GeV h corresponds to $\epsilon_1 = 2.35\%$, 35 events have a mass above 105 GeV and the average mass for these ts is 133 GeV which corresponds to $\epsilon_3 = 4.1\%$, and events inside Z mass region correspond to $\epsilon_2 =$ 5. So $\epsilon_1 : \epsilon_2 : \epsilon_3 = 0.7 : 1.0 : 1.3$ and the correction is $(88\times0.7 + 35\times1.3)/(88 + 35) = 0.87$.

Lepton P_T cut	Before two-jet	E_T^{jet} >10 GeV
(15,15)	0.46 ± 0.27	0.15 ± 0.15
(20,20)	0.28 ± 0.17	0.10 ± 0.10

Table 7.3: Number of events expected from Drell-Yan background.

e that the values predicted are somewhat low. In fact, only about 3.2% of Z events predicted to have two jets with P_T >15 GeV at the generator level. After simulation reconstruction this would translate into 2% or less for an uncorrected jet threshold 0 GeV, to be compared with 4.1±0.6% in Z data.

The backgrounds before the two-jet cut are based on the three events left in our se-ion criteria. Only one of these events satisfies the two-jet requirement. The numbers vents expected from the Drell-Yan background in 21.4 pb^{-1} are listed in Table 7.3. different choices of P_T cut and two-jet cut. The correction factor is applied.

After the signal cuts, including the two-jet cut, there is one event in the Z-region. en scaled back, this gives a background expectation of 0.10 ± 0.10 events in the top pton signal region.

2 $Z^0 \rightarrow \tau\tau$

her than using a Monte Carlo to estimate the $Z^0 \rightarrow \tau\tau$ background, we have used data sample of 1113 $\gamma/Z^0 \rightarrow e\,e$ events.A sample of $Z \rightarrow \tau\tau$ [44] was simulated as ows: In each event we remove the two electrons from the event and then replace each tron with a τ which has the same momenta and energy as the electon removed. The are then decayed semileptonically and simulated with the CDF detector simulation. ally we merge the reconstructed τ's to the underlying event which is the original nt with the two electron removed. We repeated this procedure 80 times for 1113 nts to get a better statistics.

ISAJET Monte Carlo together with a simulation of the CDF detector was used to

Cut	Mass window	$\not{E}_T$	Two-jet
Our sample	0.89	0.15	0.31
ISAJET QTW=0	0.97	0.11	0.67
ISAJET QTW=3-200	0.93	0.06	0.67
ISAJET QTW=7-200	0.96	0.11	0.69

le 7.4: Event topology cut efficiencies for the $Z^0 \rightarrow \tau\tau$ background with a (20,20) cut.

Lepton P_T	E_T^{jet}	eμ	ee, $\mu\mu$	Total
20 GeV		0.22±0.04	0.20±0.04	0.42±0.08
20 GeV	>10 GeV	0.07±0.02	0.06±0.02	0.13±0.04
15 GeV		0.56±0.08	0.55±0.07	1.11±0.15
15 GeV	>10 GeV	0.17±0.04	0.17±0.04	0.34±0.07

le 7.5: Number of events expected from the $Z \rightarrow \tau\tau$ background in 21.4 pb^{-1} with erent lepton P_T, and with and without the two-jet requirement. Errors are statistical y.

erate three set of samples with different values of the ISAJET parameter QTW[3] which erns the transverse momentum of the Z. These samples were used for comparison with results.

The event topology cut efficiencies extracted from these simulation sample are given able 7.4. In order to reduce the $Z \rightarrow \tau\tau$ background, we have developed the similar as used for the Drell-Yan process. As discussed in Section 5.6, the missing E_T ction must be more than 20° away from a lepton, since it is expected to be aligned h one of leptons as illustrated in Figure 5.9 (a) and (b). In addition, if we require or more jets, this background can be further reduced by a factor of three or more. fractions are shown in Table 7.4.

The overall yields were normalized by taking the $Z \rightarrow \tau\tau$ cross section to be equal he $Z \rightarrow ee$ cross section measured at CDF [45], and a branching fraction of the τ into dileptons $B = (0.178 \times 2)^2 = 0.127$. The number of events we expect in 21.4 $^{-1}$ is given in table 7.5.

3 Background from WW and WZ

detection efficiency was calculated in the same way as was done for the $t\bar{t}$ signal, ch is described in Chapter 6. As before, ISAJET Monte Carlo generator together with mulation of CDF detector was used to determine the geometrical and kinematical eptance, the efficiency of the lepton isolation cuts, and the efficiency of the combined sing E_T, invariant mass, and two-jet cuts. We used lepton identification efficiencies n Z and trigger eficiencies measured in data collected with independent triggers. se efficiencies are shown in Table 7.6

The cross sections used to normalize the diboson expectations are taken from Ref-

The ISAJET parameter QTW selects Z Pt limits for Z and γ. A choice of QTW equal to 0 would t lowest order Drell Yan process with the parent γ or Z Pt originating from initial state radiation. oice of a non-zero QTW select next-to-leading order Drell-Yan processes to generate the parent γ P_T.

Efficiency (%)	Geom· P_T	ID	Isol	Event	Two-jet	Trigger	Total($\epsilon_{\rm Total}$)
WW	26.3	98.9	76.3	60.5	13.1	97.1	1.5±0.6
WZ	25.3	99.4	76.3	13.2	13.1	97.3	1.3±0.5

Table 7.6: Detection efficiency for WW and WZ with a two-jet requirement

Lepton P_T thresh.	Jet E_T thresh.	eμ	ee, $\mu\mu$	Total
20 GeV	None	0.74±0.22	0.43±0.13	1.17±0.35
20 GeV	10 GeV	0.097±0.041	0.057±0.024	0.15±0.06
15 GeV	None	0.86±0.26	0.51±0.15	1.37±0.41
15 GeV	10 GeV	0.11±0.05	0.07±0.03	0.18±0.08

Table 7.7: Number of WW events expected in 21.4 pb^{-1}.

ace [47]: 9.5 pb for WW and 2.5 for WZ. We assigned a 30% of uncertainty due to oretical uncertainties in the cross section. The cross section of background events, , is given by:

$$\sigma_{\rm obs} = \sigma_{\rm Theory} \times Br \times \epsilon_{\rm Total},$$

ere $\sigma_{\rm Theory}$ is the theoretical cross section and $\epsilon_{\rm Total}$ is the total detection efficiency ed in Table 7.6.

Contributions of WW background to the selection criteria are 1.17±0.35 and 0.15±0.06 nts before and after the two-jet requirement. The number of WW background events ected for different lepton P_T and the jet E_T is summarized in Table 7.7.

Our estimation using ISAJET Monte Carlo predicts that the 13 % of WW events tain two or more jets with the observed E_T with 10 GeV. Since the ISAJET pre- ption for gluon radiation is esentially unconfirmed, we checked the two-jet rejection or by examining a matrix element Monte Carlo [43], as was done for the Drell-Yan kground. It can be seen from Table 7.2 that the efficiency of the two-jet requirement uld be approximately 2.7 times higher at typical WW subprocess energies of 300 GeV n at subprocess energies of 90 GeV. We can use this Monte Carlo shape for the mass ation and we can use Z data at 90 GeV for calibration. The data show that 4.1 ± % of Z events have two jets above 10 GeV. Therefore the two-jet cut efficiency for V can be estimated as 2.7×4.1%=11%. Since the agreement between this estimate ISAJET is good, we simply use the ISAJET two-jet cut efficiency and assign a 30% ematic uncertainty on it.

4 Background from heavy flavor production ($b\bar{b}$)

vy flavor backgrounds, mostly $b\bar{b}$, have been studied using ISAJET Monte Carlo gram to model the production processes, together with the CLEO Monte Carlo to del b quark decays, as briefly described in section 3.1. An integrated luminosity of 67.5 ^{1} of $b\bar{b}$ Monte Carlo samples have been generated for studies of high P_T leptons from ecays as a background in top searches [46]. Basic idea to estimate $b\bar{b}$ backgrounds is t we obtain the rejection factor due to event topology and two jet requirement using mple of dilepton events with P_T >15 GeV/c, which has a higher statistics, and that number of events with P_T >20 GeV/c is used to determine the normalization.

The reduction factors for each cuts was determined as follows. At first, the reduction or for the missing E_T requirement(>25 GeV) is 0.14±0.06. The correlation between and lepton P_T was checked by varying the P_T of one of the leptons to 17, 19, and GeV/c. A 30% change was observed and this contributes the major part of the ertainty assigned to the rejection factor for $\not{E}_T$. The azimuthal angle requirement uce the events further by 0.56±0.12. No strong correlation was observed between lepton P_T and the azimuthal angle separation between the missing E_T and a closest on (or jet). Another additional rejection was obtained by requiring two or more jets he events and this was 0.43±0.10.

To determine the number for 21.4 pb^{-1} of data, we choose to normalize the number μ events that pass the (15, 5) cuts with no isolation requirement in 16.3 pb^{-1} of nte Carlo and 13.1 pb^{-1} of data. Such data are dominated by $e\mu$ events from $b\bar{b}$

rces and hence they provide a better normalization than using the Monte Carlo cross ions. In doing this Monte Carlo to data luminosity normalization, we are taking into ount possible effects not considered by the Monte Carlo, such as trigger efficiencies. uncertainty on lepton ID efficiencies is reduced to variations of data to Monte Carlo o as a function of lepton P_T. There are 184 $e\mu$ events found in 13.1 pb^{-1} of data and events in 16.3 pb^{-1} of Monte Carlo. In last run's low P_T $e\mu$ analysis, background in data was determined to be $20 \pm 10\%$. At higher P_T, the background fraction should lower since QCD process in general have a softer P_T spectrum than heavyflavor duction. To be conservative, we use a background fraction of $20 \pm 20\%$ in this study. normalization factor is therefore 0.94 ± 0.19. This factor must be divided by 90% ccount for the inefficiency of the cut in the Monte Carlo generation on b quark P_T 5 GeV, which keeps 90% of the daughter leptons with $P_T \geq 15$ GeV. Combining this the above background estimate, we obtain the background expected in 21.4 pb^{-1} lata as given in the following tables.

The number of background events expected in our data sample is given in table 7.8.

	P_T cut at (15,15)	P_T cut at (20,20)
P_T, Iso, Opp-Sgn Cuts	24 ±5	2.8 ±0.6
Additional Missing E_T Cut	1.91 ± 0.96	0.22 ± 0.12
Additional Two-Jet Cut	0.83 ± 0.43	0.10 ± 0.05

Table 7.8: Number of events expected from $b\bar{b}$ background for a run of 21.4 pb^{-1}.

5 $Z^0 \to b\bar{b}$

JET Monte Carlo generator together with the CDF detector simulation was used to mate the $Z^0 \to b\bar{b}$ background. The total of 740 K were generated corresponding to integrated luminosity of 841 pb^{-1}. No events were found in the signal region when nominal cuts (no two jet cut) were applied. This gives a limit of less than 0.025 nts for a run of 21.4 pb^{-1}. If the two jet cut reduces this by a factor of 3, as it s for $Z^0 \rightarrow \tau\tau$[4] , then this background is less than 0.01 events. We therefore do not sider this background further.

6 $Wb\bar{b}, Wc\bar{c}$

have looked at the background from production of W's in association with heavy rk pairs ($Wb\bar{b}, Wc\bar{c}$) via the gluon splitting processes. An integrated luminosity of 0 pb^{-1} of events were generated with the leading-order matrix element calculation cribed in [48] and the HERWIG Monte Carlo generator [49] together with the CDF ector simulation. This sample was used to compute the contribution of these events he signal region. The cross section, according to ref [48], is 5.4pb. Figure 7.5 shows lepton P_T distribution from the $Wb\bar{b}$ events. It is obvious that a leading P_T lepton nes from the decay of W and that a second one with soft P_T comes from the decay . Most of $Wb\bar{b}$ backgrounds are rejected using large P_T.

No events survived our selection cuts without the two jet cut. This gives us the t of the number of events expected in 21.4 pb-1 and it is less than 0.006. The nple contains only events with the decay of W into the central electron. So, we need ake into account events of the W decay into plug electrons and muons. Using W nte Carlo, the ratios of W decaying into central electron(CE), plug electron(PE) and on(MU) were calculated to be CE : PE : MU = 1 : 0.07 : 0.80. Thus we would ect less than 0.011 $Wb\bar{b}$ events ($= 0.006\times(1+0.07+0.80)$) We conclude that this kground contribution to the signal region is neglegibly small.

[4] 31% of events have two or more jets as seen in section 7.2

7 Fake dilepton background

consider the "fake dilepton" background: (1) events from ordinary QCD jet or -jets with at least one misidentified lepton[5], (2) conversion electron, and (3)muon n hadronic decay in flight. These events may also have large missing $\not{E}_T$, and maybe icult to distinguish kinematically from top events. The procedure employed for esti- ting the background is to a) estimate the probability of a jet to fake a lepton, b) find many events with lepton+jet would be in the signal region if the jet faked a lepton, c) multiply the number of events found in b) by the fake rates found in a).

The "fake probability" per lepton is obtained from a background sample of events ected with a jet trigger with an E_T threshold for the jet of 20 GeV. Central and plug tromagnetic clusters, and 1muon' candidate tracks are selected with minimal cuts. probability to pass the standard electron and muon identification is then measured. fake rates are determined separately for central isolated and non-isolated tracks or ters. This separation is necessary because in the dilepton selection, all events are uired to have at least one central(CE, MU or MI) isolated lepton. Fake rates are ulated in Table 7.9.

When looking through the jet data for jets which fake leptons, we will also find some leptons from b decay. The effect of this is to increase the fake probability we would from light quark jets alone. It is desirable to use fake probabilities which have the tributions from b quarks subtracted. To accomplish this, we refer to a study [50] ch estimates the b fraction of ELES banks which pass our tight central electron cuts e 46% ± 8%. We use this number both to scale back the fake probabilities for central trons, and also as an indicator of the number of CMUO banks we should expect from in the jet data. We multiply the number of central electrons we expect from b decay he ratio of acceptances for CMUO muons and central electrons, and use this as our mate of the number of CMUO muons we expect from b in the jet data. We do not

[5] One of the partons fragmenting into an electromagnetic rich jet is identified as an electron (or stiff k, for muons)

Type	Iso?	P_{fake} before b subtraction	P_{fake} after b subtraction
CE(tight)	yes	.075±.028	.059±.028
CE(tight)	no	.035±.011	.012+.013−.012
CE(loose)	yes	.150±.041	.132±.040
CE(loose)	no	.063±.015	.038±.017
MU	yes	.121±.067	.111±.066
MU	no	.009±.007	.004+.007−.004
MX	yes	.333±.219	.310+.315−.310
MX	no	.071±.055	.052+.055−.052
MI	yes	.048±.029	.048±.029
MI	no	<.013	<.013
PE	yes	<.013	<.013

Table 7.9: Fake rates for each lepton category ,before and after b subtraction.

form the b subtraction for plug electrons or CMIO muons because we expect the rimeter isolation cuts on these categories to reduce the b contamination. We don't ly the 2 jet cut and opposite sign cuts when counting events which have one good on and one lepton bank passing the relaxed cuts. Assuming the relaxed lepton track om a hadron, we expect its sign to be uncorrelated with the sign of the good lepton. therefore count both opposite sign and same sign events, and divide by 2 to get the ectation for opposite sign alone. There are 15 opposite sign events and 10 same sign nts. The statistics suffer badly when the 2 jet cut is applied. We have looked at -jet events to find the rejection factor of the 2 jet cut after the other topology cuts applied, and we use this rejection factor to obtain the number of events we expect he signal region. Tables 7.10 and 7.11 show the expected numbers of background nts for 15-15 and 20-20 lepton Pt cuts, before and after the 2-jet cut is applied.

Fake Background in 21.4 pb^{-1} Before 2-jet Cut		
Category	15 GeV Lepton P_T Cuts	20 GeV Lepton P_T Cuts
CE-CE	.339±.168	.169±.111
CE-PE	<.034	<.033
MU-MU	.140+.257−.140	.073+.238−.073
MU-MI	.091±.064	.022+.038−.022
CE-MU	.385±.300	.111+.240−.111
CE-MI	.148±.102	.061±.051
PE-MU	<.023	<.023
PE-MI	<.028	<.028
TOTAL	1.10±.41	.436±.292
SS Data	1	0

ble 7.10: Expected background due to hadron misidentification for 15 GeV and 20 V lepton P_T cuts. All cuts except for the 2-jet cut are applied. Also shown are the nber of same-sign events found in the data for these cuts.

Fake Background in 21.4 pb^{-1} After 2-jet Cut		
Category	15 GeV Lepton P_T Cuts	20 GeV Lepton P_T Cuts
CE-CE	.056±.028	.028±.018
CE-PE	<.006	<.005
MU-MU	.023+.042−.023	.012+.039−.012
MU-MI	.015±.010	.004+.006−.004
CE-MU	.063±.049	.018+.039−.018
CE-MI	.024±.017	.010±.008
PE-MU	<.038	<.038
PE-MI	<.005	<.005
TOTAL	.181±.068	.072±.048
SS Data	0	0

ble 7.11: Expected background due to hadron misidentification for 15 GeV and 20 V lepton P_T cuts after the 2-jet cut is applied. Also shown are the number of same- events found in the data for these cuts.

8 Background Summary and Checks

: number of background events contributed to our selection criteria is summarized in le 7.12. The total background is 0.56±0.14 events after all cuts and the data yield is rents. When releasing the two-jet requirement, we expect 2.5±0.5 events and observe : same) 2 events.

A better statistics check was done in the $e\mu$ channel by lowering the P_T threshold to GeV and comparing the background prediction with the number of events observed he data after isolation cuts. The dilepton+0 jet sample should be dominated by kground. Our ability to calculate the size of this background is an important check the analysis. Our results are shown in table 7.13. There is agreement between the kground prediction and the data. As an additional check of the reliability of our kground predictions, we compared the number of same-sign events observed in the a with a P_T threshold of 15 GeV after isolation cuts, with predictions from fakes and We find that the sum of the $b\bar{b}$ and fake predictions is 19.8 ± 4.0, compared to 10 ie-sign events observed in the data. Again the agreement is good, although there is m to believe that our backgrounds could be somewhat overestimated and therefore servative.

	Without $\not{E}_T$ and two-jet cuts	Without two-jet cut	All cuts
eμ			
WW	1.1	0.74	0.10±0.04
$Z \to \tau\tau$	3.7	0.22	0.07±0.02
$b\bar{b}$	1.2	0.10	0.04±0.03
Fake	1.2	0.19	0.03±0.03
Total background	7.2	1.25	0.24±0.03
CDF data	5	2	2
ee, μμ			
WW	0.6	0.43	0.06±0.02
$Z \to \tau\tau$	3.0	0.20	0.06±0.02
$b\bar{b}$	1.6	0.12	0.05±0.03
Fake	1.7	0.25	0.04±0.03
Drell-Yan	113	0.28	0.10±0.10
Total background	120	1.28	0.31±0.11
CDF data	120	0	0

ble 7.12: Number of background events expected 21.4 pb^{-1} and the number of events erved in the data.

	$P_T > 15$ GeV/c, Isolation, and opp.-charge requirement
$e\mu$	
WW	1.2±0.4
Z $\rightarrow \tau\tau$	8.3±0.5
$b\bar{b}$	10±2
Fake	5.9±1.8
Total background	25±3
CDF data	18

le 7.13: Number of $e\mu$ background events expected in 21.4 pb^{-1} and the number pposite-charge dilepton events observed in the data after isolation cuts and a P_T eshold of 15 GeV/c.

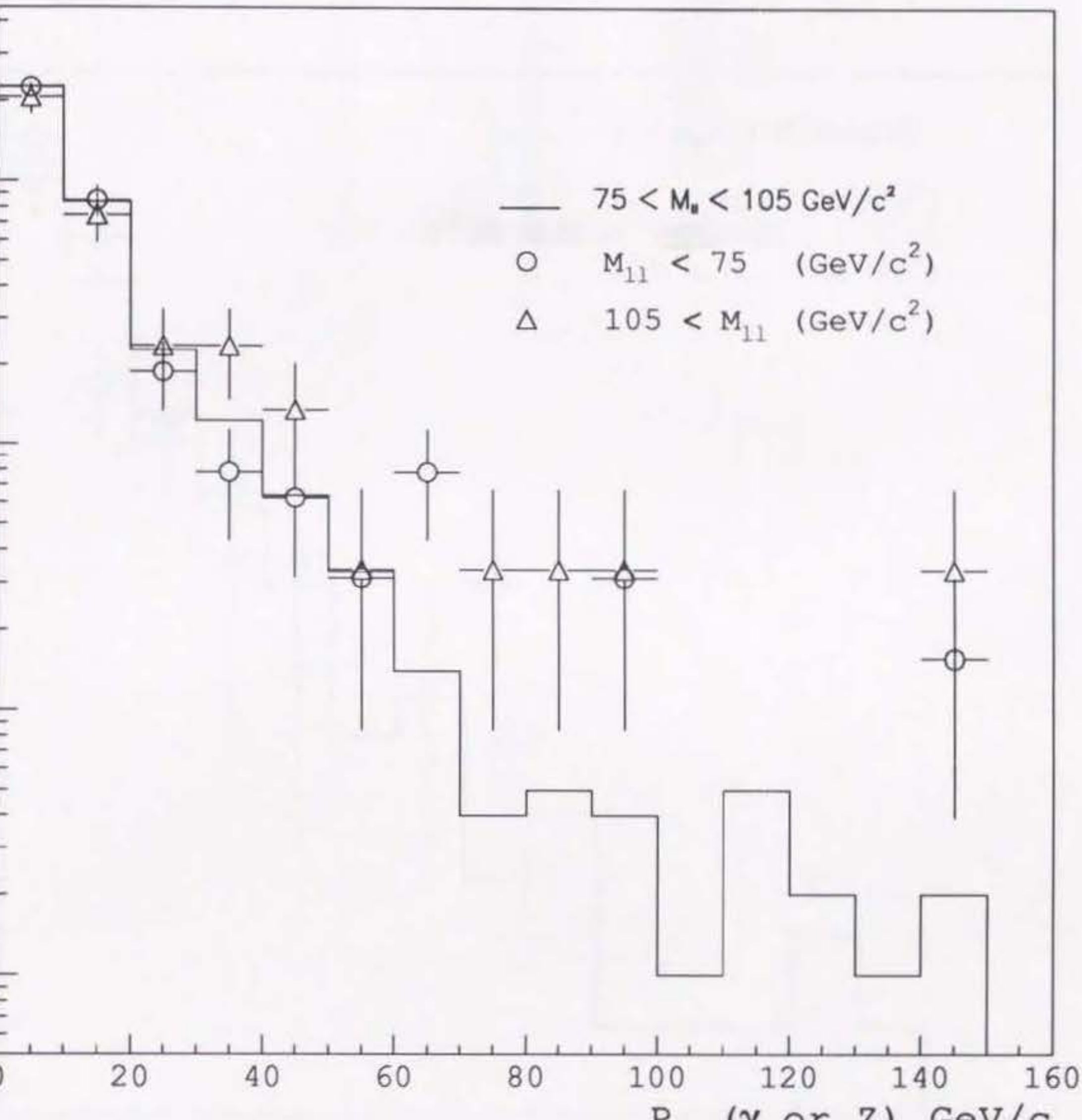

ure 7.1: ISAJET Monte Carlo $P_T(\gamma, Z)$ distribution in three mass region: 30-75 V/c, 75-105 GeV/c and above 105 GeV/c. The distributions are normalized to the nber of events inside the Z mass region.

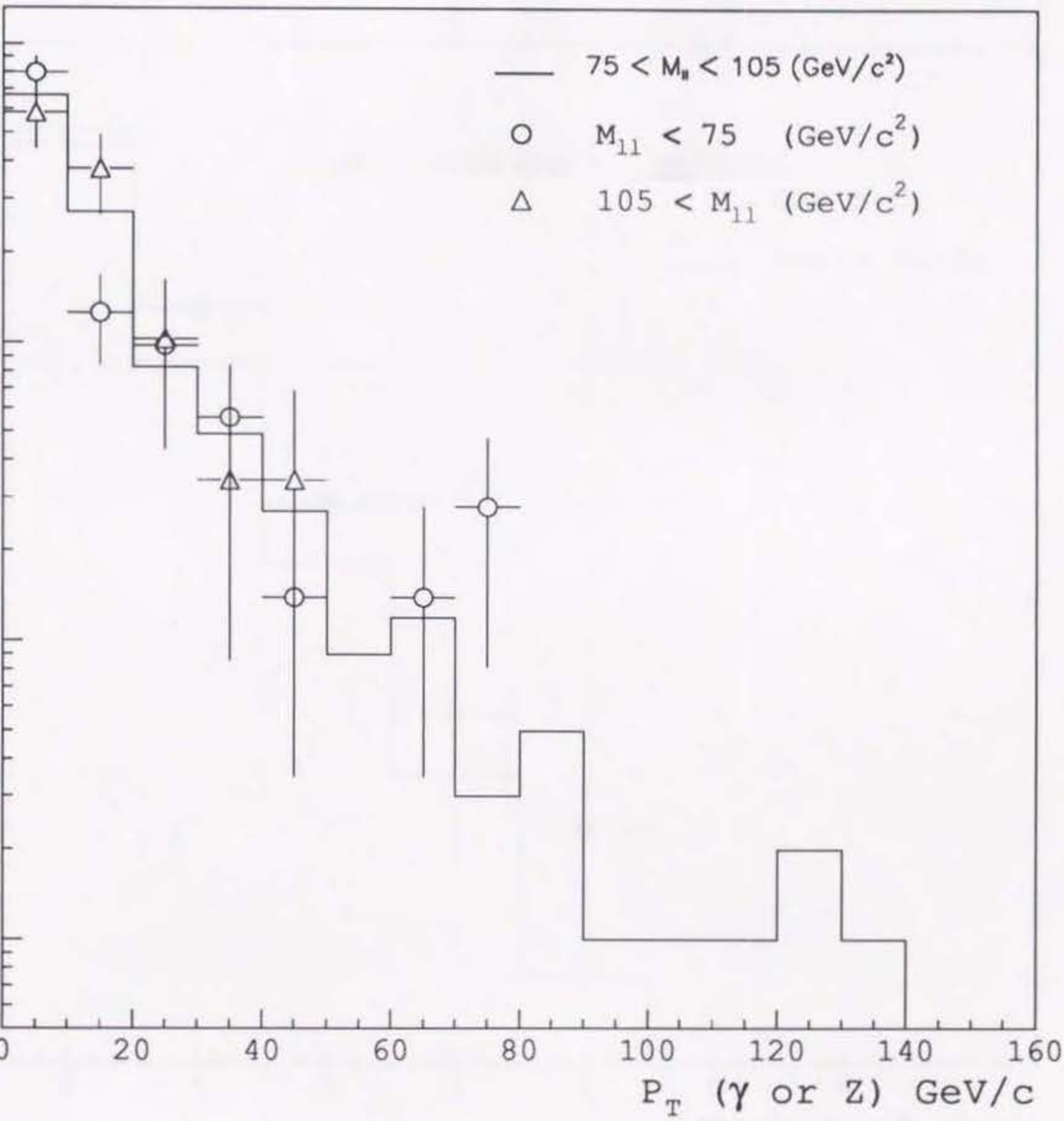

ure 7.2: $P_T(\gamma, Z)$ distribution from data in three mass region: 30-75 GeV/c, 75-105 V/c and above 105 GeV/c. The distributions are normalized to the number of events de the Z mass region.

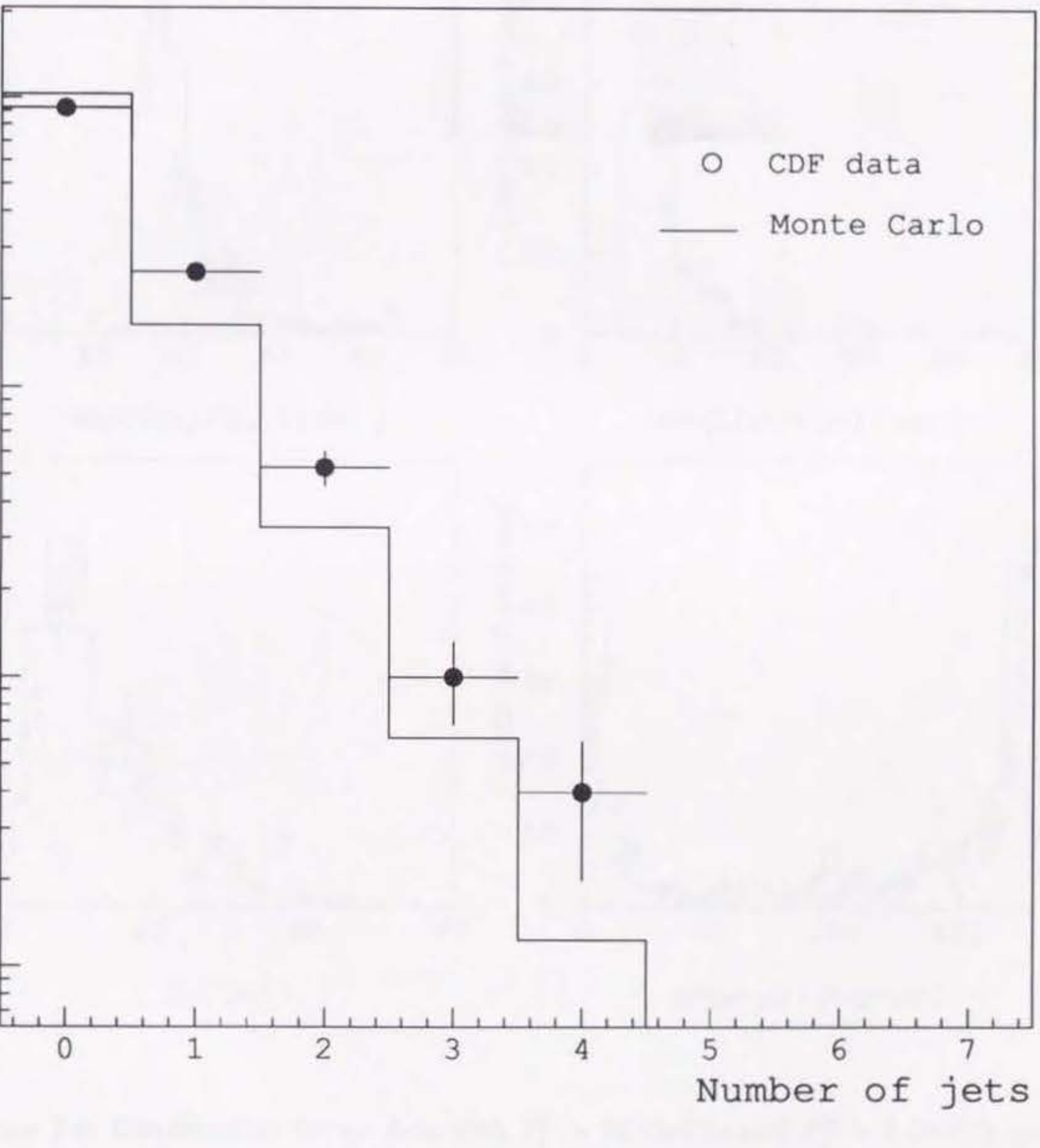

Figure 7.3: The number of jets for Z events from CDF data and Monte Carlo.

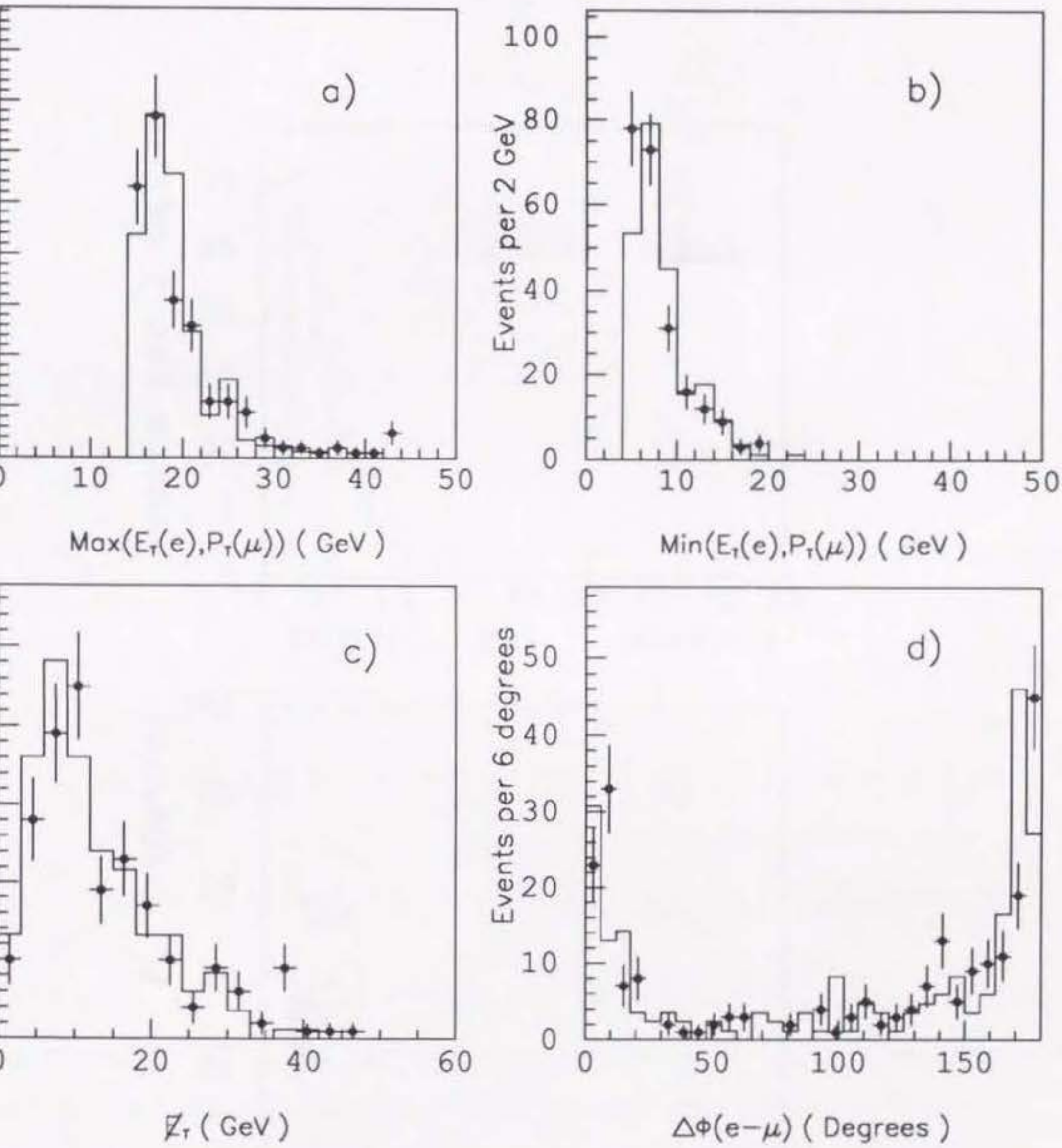

ure 7.4: Distributions for $e\mu$ data with $P_T^{l_1} > 15$ GeV/c and $P_T^{l_2} > 5$ GeV/c (points) pared to expectations from the ISAJET Monte Carlo (histograms). a) P_T spectrum he leading lepton. b) P_T spectrum of the second lepton. c) Missing E_T distribution. ilepton azimuthal angular separation.

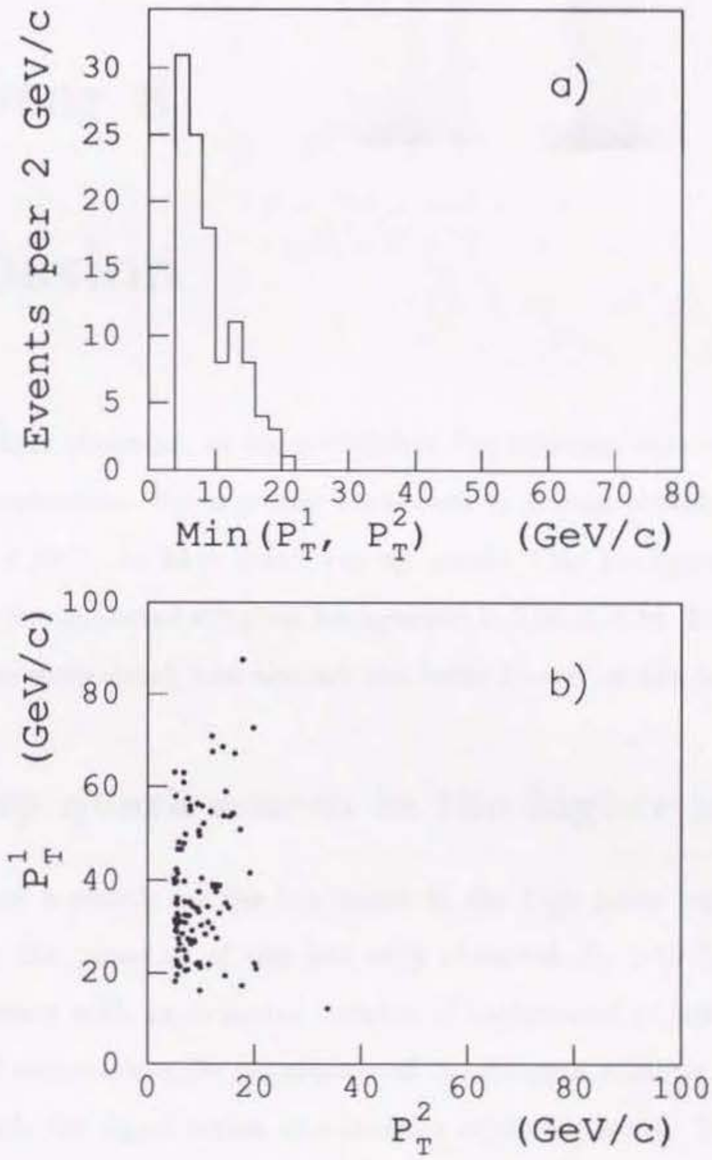

Figure 7.5: $Wb\bar{b}$ Monte Carlo events: (a) Minimum of lepton P_T. (b) P_T^{l2} versus P_T^{l1}.

hapter 8

iscussion

ie last three chapters, we have exploited the selection cuts to improve the signal to
round separation. By imposing these cuts on a data sample of an integrated lumi-
ty of 21.4 pb^{-1}, we have found two $e\mu$ events. Our background study in Chapter 7
ed that the expected dilepton background is 0.56 ± 0.14. In this section we discuss
results in some detail and also set the lower bound on the top quark mass.

Top quark search in the higher mass region

performed a search for the top quark in the high mass region above 120 GeV/c^2
equiring the presence of two jets with observed E_T >10 GeV. We found two $e\mu$
lidate events with an expected number of background of 0.56 ± 0.14 events.

Table 8.2 summarizes the acceptance of the dilepton analysis and the expected num-
of events in the signal region as a function of the top mass. To compute the expected
ber of events, we used the theoretical central values with the next-to-next-leading
r calculation. The uncertainties are the sum in quadrature of the statistical uncer-
y on the number of observed events, the systematic uncertainty on the acceptance
nction of top mass), and the uncertainty on the luminosity (10%)

We see the excess of events over expected backgrounds. Estimation of the probability

the expected background has fluctuated up to the number of candidate events seen
reater is 10.9 %. This is evaluated using Poisson statistics convoluted with a Gaussian
aring of the mean number of backgrounds expected.

M_{top} (GeV/c^2)	100	120	140	160	180
$\sigma_{t\bar{t}}^{Theory}$	102	38.9	16.9	8.16	4.21
$\epsilon_{total} \cdot Br$ (%)	0.22	0.49	0.66	0.78	0.86
$N_{expected}$	4.9	4.1	2.4	1.4	0.8

le 8.1: Theoretical prediction of $t\bar{t}$ cross section from Ref [26]. Efficiency × branching
o and expected number of events in 21.4 pb^{-1}, as a function of top mass.

2 Low mass top search and limits on $t\bar{t}$ production

previous publication [7], based on a data sample of 4.1 pb^{-1} collected by CDF in
-89, we reported a lower bound of 85 GeV/c^2 on M_{top} from the dilepton channel
e. When combined with the results from the lepton + jets, where the b was tagged
ugh its semileptonic decay into muons, we obtained an improved limit of 91 GeV/c^2
e 95 % confidence level. In the dilepton search with the two-jet cut, we concentrate
op mass above 120 GeV/c^2 where the event selection is reasonably efficient. This
es a hole between our previously published mass limit of 91 GeV/c^2 and 120 GeV/c^2.
his section we describe a search for the top quark in this relatively lower mass region
we extract a new lower bound on the top mass using the 21.4 pb^{-1} data sample from
1992-93 run and the 4.1 pb^{-1} from the 1988-89 run. First of all, it should be noted
for top masses close to the previous lower limit of 91 GeV/c^2, the b quarks are
luced near our jet E_T threshold, and hence most $t\bar{t}$ dilepton events will not have two
rvable jets above 10 GeV in the calorimeter. For a search in this low mass region,
emove the the two-jet requirement.

The search without the two-jet cut results in two candidate events passing our $t\bar{t}$ ction criteria. These two events are the same as those passed the two-jet cut. With events detected we can place upper limits on the $t\bar{t}$ production cross section, using theoretical calculation for this cross section. We can also derive a limit on the top rk mass.

The 95%-confidence level (C.L.) upper limits on the cross section is given by

$$\sigma_{t\bar{t}} < \frac{N_{top}}{\int \mathcal{L}dt \; a_{top}} \tag{8.1}$$

re N_{top} is the 95%-C.L. upper limit on the number of expected events, and $\int \mathcal{L}dt$ is integrated luminosity of the experiment, and a_{top} is the acceptance of our analysis $\bar{t}$ events, normalized to assumed branching ratio. Since a_{top} varies slightly with the mass, the limit on $\sigma_{t\bar{t}}$ will also be a a function of the top mass.

The systematic uncertainties in a_{top} and $\int \mathcal{L}dt$, which we discussed in Section 6.8, e listed in Table 6.14. The total uncertainty for the number of events predicted in data timated to be 13 % without the two-jet requirement. This systematic uncertainty is l as the standard deviation of a Gaussian distribution convoluted with the Poisson istical probability. The resulting distribution is used to obtain the 95%-C.L. upper t on the number of events expected as a function of the top mass. (The method we l to take uncertainties into account is explained in Aappendix 9). Given that two nts were observed and without the subtracting the backgrounds, we find an upper t of N_{top}=6.54. (If ignoring the effects of syetematic uncertainties, 6.30 would be l.) The 95%-C.L. upper limit on is 33 pb for M_{top}=120 GeV/c^2.

Using the theoretical predictions for $\sigma_{t\bar{t}}$ the limits on the cross section can be trans- d into a lower limit on the mass of the top quark. Figure 8.1 shows the upper ts on the $t\bar{t}$ cross section as a function of the top mass together with the theoretical ulation of the cross section from Reference [26].

To set a lower limit on the top mass, we find the point at which the $\sigma_{t\bar{t}}$-limit curve ses crosses the lower (more conservatively) bound of the theoretical prediction. At

% C.L. we obtain M_{top} >116 GeV/c^2, based on the analysis using a data sample from 92-93 collider run alone.

We also combine the 1988-89 data sample with 1992-93 data sample. By adding in 1988-89 data, the integrated luminosity becomes 25.5 pb^{-1}, the number of events served remains 2, which is the same events found in this analysis using the 1992-93 data nple. One $e\mu$ events in the previous analysis [7] fails the missing E_T requirement added the $e\mu$ channel in the 1992-93 analysis to reduce backgrounds expected in the larger ninosity data sample. The expected background becomes $(2.5 \pm 0.5) + (0.5 \pm 0.3) =$ $0 \pm 0.6)$ events. To calculate upper limits with the combined 1988-89 and 1992-93 a sets, we used the following formula:

$$\sigma_{t\bar{t}}^{\text{upper limit}} = \frac{\text{N}^{\text{upper limit}}}{(\int \mathcal{L}_{89}\,\text{dt}\;\epsilon'_{89} + \int \mathcal{L}_{93}\,\text{dt}\;\epsilon_{93})\;\cdot\;\text{Br}} \tag{8.2}$$

ere ϵ_{93} is the acceptance of the 'new' analysis with the 'new' detector, whereas ϵ'_{89} the acceptance of the 'new' analysis with the 'old' detector. We believe that ϵ'_{89} omewhat larger than ϵ_{93}, because of the reduced 1993 muon trigger acceptance (the 93 muon trigger requires a CMU-CMP coincidence in the ϕ regions where CMP covers IU). This only affects dimuon events (electron-muon events come in with the electron), so that the difference between the two acceptances should not be more than a few We made the conservative choice of setting $\epsilon'_{89} = \epsilon_{93}$; this slightly increases the upper its on the cross section. For each of these upper limits, we have calculated 95%-C.L. ver limits on the top mass as the intersection of the experimental upper limit with theoretical lower limit to be M_{top} >120 GeV/c^2. Thus, we conclude that the top ss region between 91 and 120 GeV/c^2 is excluded[1]. For comparison with previously blished results, we use the same theoretical cross section with the next-to-leading

[1]The D0 Collaboration recently reported the lower bound on the top quark mass of 131 GeV/c^2 at 95%-C.L., assuming the Standard Model branching fractions. Our limit from this analusis is lower n the limit from D0 measurement, although they used the same method as this analysis, because limit was calculated by combining four decay modes of $t\bar{t} \to e\mu + jets, ee$+jets, e+jets andμ+jets heir measurement.

er calculation to obtain a lower bound on M_{top} of 115 GeV/c^2.

M_{top} (GeV/c^2)	100	120	140	160
$\sigma_{t\bar{t}}^{Theory}$	102	38.9	16.9	8.16
$\epsilon_{total} \cdot Br$ (%)	0.68±0.05	0.78±0.06	0.88±0.07	0.93±0.07
$N_{expected}$	14.8	6.5	3.2	1.6
$\sigma_{t\bar{t}}$ (pb) at 95%-C.L.	38.3	33.3	29.5	28.2

le 8.2: Theoretical prediction of $t\bar{t}$ cross section from Ref [26]. Efficiency × branching o and expected number of events in 21.4 pb^{-1}, as a function of top mass.

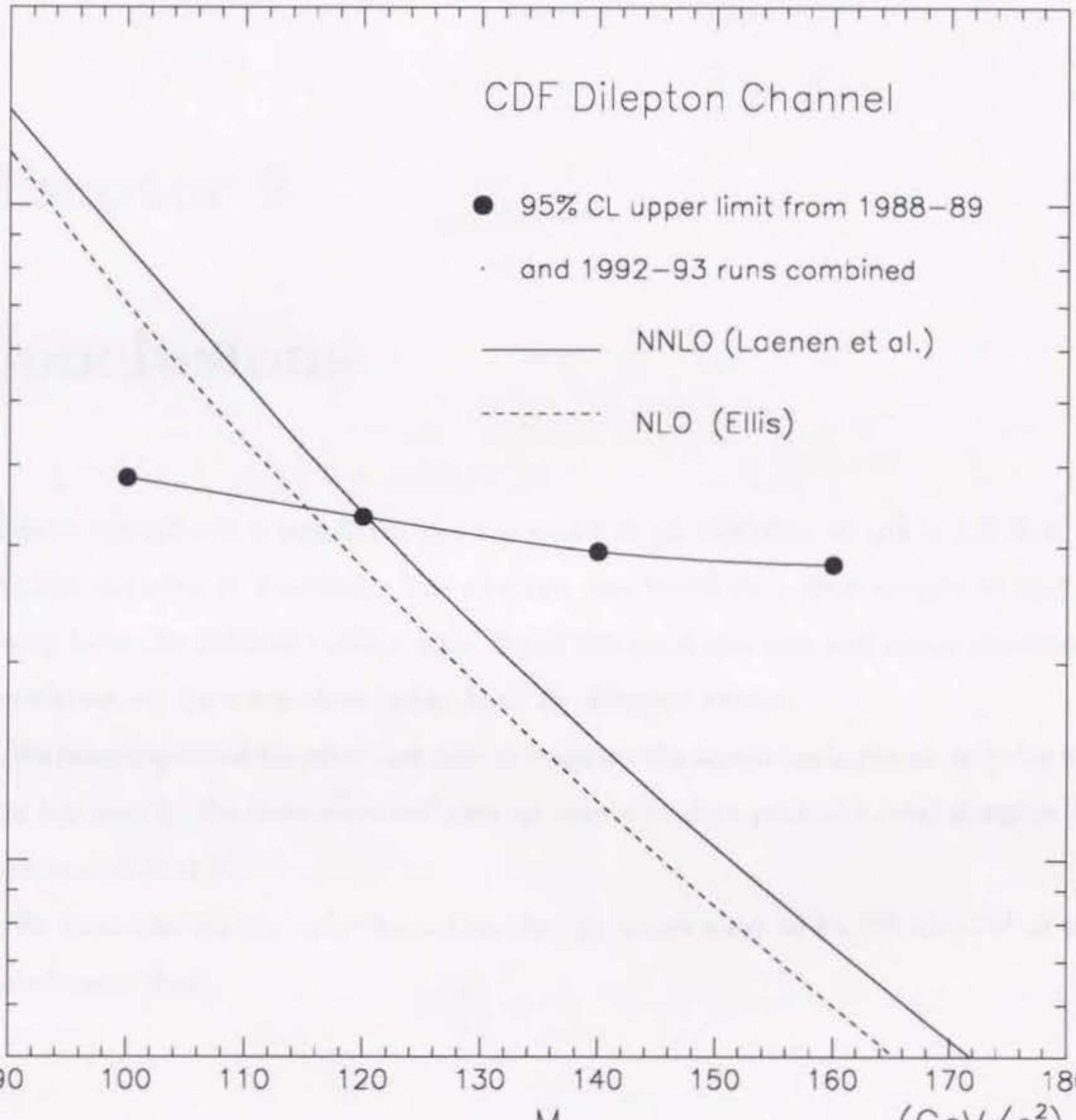

ure 8.1: The 95-% C.L. on $\sigma_{t\bar{t}}$ compared with the theoretical lower bound of a next-next-to leading order (NNLO) calculation from Ref. [26] and the theoretical lower und of a next-to-leading order calculation from Ref. [25]

Chapter 9

Conclusions

have carried out a search for the top quark in $p\bar{p}$ collisions at $\sqrt{s} = 1.8$ TeV using CDF detector at Fermilab. The analysis was based on a data sample of 21.4 pb^{-1} ning from the 1992-93 collider run. Using the good electron and muon identification abilities, we have searched in the high P_T dilepton events.

We have exploited the selection cuts to improve the signal-background ratio for higher ss top quark. We have observed two $e\mu$ events in data with the total dilepton backunds of 0.56 ± 0.14.

We have also set the lower bound on the top quark mass to be 120 GeV/c^2 at the 95 confidence level.

ppendix A

alculation of Upper Limits on oisson Processes

his appendix we briefly present and justify the equations we used to calculate upper ts on the $t\bar{t}$ production cross section. In section A.1 we describe the calculation of er limits in the simplest case, namely when there are no no systematic uncertain- Next we consider the case where there is background, and in the final section we rporate the effect of systematic uncertainties.

1 Upper limits without systematic uncertainties

stematic errors are negligible in a counting expeeriments, the results of the counting stributed according to the Poisson distribution:

$$P(\mu : n) = \frac{e^{-\mu}\mu^n}{n!},$$

re the mean μ is the average number of observeed events over a large number of eriments.

Confidence levels for Poisson distributions are usually defined in terms of quantities ed 'upper limits':the C.L. associated with a given upper limit N and an observed e n_0, is the probability that $n > n_0$. if the mean of th distribution is $\mu = N$. In other ls, if the mean of the Poisoon distribution is greeater or equal than the upper limit hen the probability of observing n_0 or fewer events is lower than or equal to 1-C.L..

2 Upper Limits with systematic uncertainties

ematic uncertainties are incorporated with the help of Gaussian smearing functions. σ_B be the uncertainty on the expected background μ_B, σ_S the *fractional* uncertainty he expected signal μ_S, and define:

$$G(x;\mu,\sigma) = A(\mu,\sigma)\, e^{\frac{-(x-\mu)^2}{2\sigma^2}} \tag{A.1}$$

e A is a normalization factor:

$$A(\mu,\sigma) \int_0^\infty G(x;\mu,\sigma)\, dx = 1 \tag{A.2}$$

important to realize that this normalization condition defines A as a *function* of μ σ. Upper limits are obtained by solving the following equation for N:

$$1 - \mathrm{CL} = \int_0^\infty P_\mu(n)\, G(x;\mu,\sigma)\, dx \tag{A.3}$$

ibliography

S.L. Glashow, Nucl. Phys. 22, 579(1961)

S. Weinberg, Phys. Rev. Lett. 19, 1264 (1967)

A. Salam, "in Elementary Particle Theory", edited by N.Svartholm (Almqvist and Wiksell, Sweden, 1968), p.367

S. Abachi et al.(D0 Collaboration), FERMILAB-Pub-94/004-E (1994).

C. Arbajar et al.(UA1 collab.), Z.Phys.C48(1990) 1.

T. Akkeson et al.(UA2 collab.), Z.Phys.C46(1990) 179.

F. Abe et al. (CDF collab.), Phys. Rev. Lett. 64(1990)142. and 147.

F. Abe et al. (CDF collab.), Phys. Rev. Lett. 64 147(1990)

F. Abe et al. (CDF collab.), Phys. Rev. Lett. 68, 447(1992)

F. Abe et al. (CDF collab.), Phys. Rev. D45, 3921 (1992)

W. Bartle et al., Phys. Lett. 146B, 437 (1984)

U. Amardi et al., Phys. Rev. D36 (1987) 1385.

G. Costa et al., Nucl. Phys. B297, 244(1988)

J. Ellis and G.L. Fogli, Phys. Lett. B213, 526(1988) and B232, 139(1989)

J. Ellis and G.L. Folgi, Phys. Lett. B232 139 (1989)

P.Langacker, Phys. Rev.Lett. 63 1920 (1989)

J. Ellis and G.L. Folgi, Preprint CERN-TH. 5817/90 (1990)

W. Hollick, Proceedings of the XVI international Symposium on Lepton-Photon Interactions, 10-15, August 1993, to be published.

W. Bartel et al., CLLEO collab., Phys. Lett., 146B 437 (1984)

G.L. Kane and M. Peskin, Nucl. Phys. B195, 29 (1982)

A. Bean et al.(CLEO), Phys. Rev. D35 3533 (1987)

H. Arbrecht et al., ARGUS Collab., Phys. Lett., 192B 245 (1987)

C. Albajar et al., Phys. Lett. B186 247(1987)

I.I. Bigi and A.I.Sanda Phys. Rev. D29 1393(1984)

B. Adeva et.al., Phys. Lett. 241B, 416(1990)
D.Decamp et. al., Phys. Lett. 244B, 551(1990)

F. Abe et al., CDF collab., Phys. Rev. Lett. 69, 28 (1992)

W.J. Marciano and A. Sirlin, Phys. Rev. D29, 945(1984)

C. Albajar et al.(UA1 Collaboration), Z.Phys. C37, 505(1988)

A.D. Martin, R.G. Roberts, W.J. Stirling, Z. Phys. **C42**, 277 (1989)

Alterelli, M.Diemoz, G. Martinelli and P.Nason, Nucl. Phys.

G. Alterelli, M.Diemoz, G. Martinelli and P.Nason, Nucl. Phys. B308, 724 (1988)

P. Nason, S. Dawson and R.K. Ellis, Nucl.Phys. B303, 607(1988).
R.K. Ellis, FERMILAB-Pub-91/30-T, 1991.

E. Laenen, J. Smith, and W.L.van Neerven, Nucl. Phys. B369 543(1992); Fermilab-Pub-93/270-T

V. Barger and R. Phillips, Collider Physics, Collider Physics, Addison-Wesley Publishing Company (1987).

F. Abe et al., CDF collab., Nucl. Instr. Meth. A271, 387(1988)

K .Hara et al. "Cosmic-Ray Test of the CDF Central Muon Upgrade Chambers", CDF internal note 1513 (1992)

F. Paige and S.D. Protopopescu, BNL Report No.BNL 38034, 1986 (unpublished)

E.J. Eichten, I.Hinchliffe, K.D. Lane C. Quigg, Rev.Mod.Phys. 56 579 (1984)

G.C Fox and S. Wolfram, Nucl. Phys. B 168 (1980) 285;
T. Sjostrand, Phys. Lett. B157 (1985) 321

C. Peterson, D.Schlatter, I.Schmitt, and P.Zerwas Phys. rev. D27 105(1983)

P. Avery, K. Read, and G. Trahern, Cornell Internal Note CSN-212 (1985) Unpublished.

R. G. Wagner (unpublished), based on calculations by F. Berend et al., Z. Phys. C27, 155 (1985)

J. Proudfoot, CDF internal note 935 (1989)

R.M. Harris, CDF internal note 1329.

M. Miller CDF internal note 1086

F. Abe et al. Phys. Rev. D44 29 (1991)

A. Gordon, D. Kestenbaum, M. Franklin and P. Hurst, CDF internal note 1811

L. Keeble and B. Flaughter, CDF internal note 1513

S. Kopp, CDF internal note 1942 J. Konigsberg and A.Gordon, Private communication.

T. LeCompte, T. Liss and A. Martin, CDF internal note 2367

Private communication.

J.Wang and M. Contreras, CDF internal note 2108

F. Abe et al., Phys. Rev. D44, 29(1991)

L. Song et al., CDF internal note 2106

J. Ohnemus, Phys.Rev. D44, 1403(1991)

J. Ohnemus, Phys. Rev. D44, 3477(1991)

M.L Mangano, Nucl. Phys. B405, 536(1993)

G.Marchesini and B.R Webber, Nucl.Phys. B310, 461(1988)

G.Marchesini et al., Comput.Phys.Comm. 67, 465(1992)

S.Kopp, CDF internal note 2391

T.Han and S. Parke, Phys. Rev. Lett. 71 1494 (1993)